# THE URBAN SURFACE ENERGY BUDGET AND MIXING HEIGHT IN EUROPEAN CITIES: DATA, MODELS AND CHALLENGES FOR URBAN METEOROLOGY AND AIR QUALITY

Final Report of Working Group 2 of COST-715 Action

R2 Time Series from 131941 of the 26th to 130000 of the 27th of June 2002

EDITORS: Martin Piringer and Sylvain Joffre

COST – the acronym for European **CO**operation in the field of **S**cientific and **T**echnical Research – is the oldest and widest European intergovernmental network for cooperation in research. Established by the Ministerial Conference in November 1971, COST is presently used by the scientific communities of 35 European countries to cooperate in common research projects supported by national funds. The funds provided by COST – less than 1% of the total value of the projects – support the COST cooperation networks (COST Actions) through which, with only around € 20 million per year, more than 30.000 European scientists are involved in research having a total value which exceeds € 2 billion per year. This is the financial worth of the European added value which COST achieves. A "bottom up approach" (the initiative of launching a COST Action comes from the European scientists themselves), "à la carte participation" (only countries interested in the Action participate), "equality of access" (participation is open also to the scientific communities of countries not belonging to the European Union) and "flexible structure" (easy implementation and light management of the research initiatives) are the main characteristics of COST. As precursor of advanced multidisciplinary research COST has a very important role for the realisation of the European Research Area (ERA) anticipating and complementing the activities of the Framework Programmes, constituting a "bridge" towards the scientific communities of emerging countries, increasing the mobility of researchers across Europe and fostering the establishment of "Networks of Excellence" in many key scientific domains such as: Physics, Chemistry, Telecommunications and Information Science, Nanotechnologies, Meteorology, Environment, Medicine and Health, Forests, Agriculture and Social Sciences. It covers basic and more applied research and also addresses issues of pre-normative nature or of societal importance.

COST-715 Action
Final Report of Working Group 2

Cover
LIDAR scans of the backscatter from the atmosphere on 26 June 2002. The measurements are performed in Basel during the BUBBLE experiment. The mixing heights as determined from the derivative of the range-corrected signal are indicated by crosses. *Courtesy V.Mitev, R. Matthey and G. Martucci, Observatory of Neuchatel, Switzerland.*

THE URBAN SURFACE ENERGY BUDGET AND MIXING HEIGHT IN EUROPEAN CITIES: DATA, MODELS AND CHALLENGES FOR URBAN METEOROLOGY AND AIR QUALITY

*Final Report of Working Group 2
of COST-715 Action*

EDITORS: Martin Piringer and Sylvain Joffre

Lead Authors:
Alexander Baklanov, Jerzy Burzynski, Andreas Christen, Marco Deserti, Koen De Ridder, Stefan Emeis, Sylvain Joffre, Ari Karppinen, Patrice Mestayer, Douglas Middleton, Martin Piringer, and Maria Tombrou

Contributions by:
Kathrin Baumann-Stanzer, Giovanni Bonafè, Angela Dandou, Sylvain Dupont, Nicola Ellis, Sue Grimmond, Emmanuel Guilloteau, Alberto Martilli, Valéry Masson, Tim Oke, Victor Prior, Mathias Rotach, and Roland Vogt

THE URBAN SURFACE ENERGY BUDGET AND MIXING HEIGHT IN EUROPEAN CITIES: DATA, MODELS AND CHALLENGES FOR URBAN METEOROLOGY AND AIR QUALITY

EDITORS: Martin Piringer[1] and Sylvain Joffre[2]

Lead Authors:

Alexander Baklanov[3], Jerzy Burzynski[4], Andreas Christen[5], Marco Deserti[6], Koen De Ridder[7], Stefan Emeis[8], Sylvain Joffre[2], Ari Karppinen[2], Patrice Mestayer[9], Douglas Middleton[10], Martin Piringer[1], Maria Tombrou[11]

Contributions by:

Kathrin Baumann-Stanzer[1], Giovanni Bonafè[6], Angela Dandou[11], Sylvain Dupont[12], Nicola Ellis[10], Sue Grimmond[13], Emmanuel Guilloteau[14], Alberto Martilli[15], Valéry Masson[16], Tim Oke[17], Victor Prior[18], Mathias Rotach[19], Roland Vogt[5]

1. Central Institute for Meteorology and Geodynamics, A-1190 Vienna, Austria
2. Finnish Meteorological Institute, FIN-00101 Helsinki, Finland
3. Danish Meteorological Institute, DK-2100 Copenhagen, Denmark
4. Institute of Meteorology and Water Management, Regional Office, PL-30215 Krakow, Poland
5. Institute of Meteorology, Climatology & Remote Sensing, Univ. Basel, CH-4055, Basel, Switzerland
6. Agenzia Regionale Prevenzione e Ambiente dell'Emilia Romagna – Servizio Idro Meteorologico, I-40122 Bologna, Italy
7. VITO-TAP, B-2400 Mol, Belgium
8. Institut für Meteorologie und Klimaforschung – Atmosphärische Umweltforschung – IMK-IFU Forschungszentrum Karlsruhe GmbH, D-82467 Garmisch-Partenkirchen, Germany
9. Equipe Dynamique de l'Atmosphere Habitee, Laboratoire de Mecanique des Fluides (UMR CNRS 6598), Ecole Centrale de Nantes, F-44321 Nantes, France
10. Meteorological Office, Exeter, EX1 3PB, United Kingdom
11. Dept. of Applied Physics, Univ. of Athens, GR-157 84, Athens, Greece
12. Unité de Recherche EPHYSE, INRA, F-33883 Villenave d'Ornon, France
13. Dept. of Geography, Indiana University, Bloomington, IN, USA
14. ALSTOM Transport, F-59494 Valenciennes, France
15. Univ. of British Columbia, Vancouver, B:C., Canada V6T 1Z4
16. CNRM Meteo France, F-31057 Toulouse, France
17. Dept. Geography, Univ. of British Columbia, Vancouver, B.C., Canada V6T 1Z2
18. Instituto de Meteorologia, P-1749-077 Lisbon, Portugal
19. MeteoSwiss, CH-8044 Zürich, Switzerland

LIST OF CONTENTS

1. Introduction

Urban areas are the site of most anthropogenic pollutant emissions and where the vast majority of Europeran citizens live (ca. 70%). Consequently, there is a strong scientific, governance and societal need for accurate and effective assessments and forecasts of air pollution in urban areas. Urban meteorology and pollution are characterised by a number of fundamental parameters and their evolution in time, which all have specific problems as to their monitoring, representativeness, parameterisation and modelling. Within the joint European project COST-715[1] (Urban Meteorology Applied to Air Pollution Problems; COST-715, 2004), its Working Group 2 (WG2) addressed the specific problems of determining and simulating the surface energy balance and the mixing height, which are critical components in many algorithms and/or numerical models. The surface energy balance together with the surface temperature and heat fluxes determine the hydrostatic stability conditions in the lower atmosphere, which regulate the mixing of pollutants, whereas the mixing height parameter determines the available volume for pollutant mixing.

WG2 addressed these issues along the following lines:

- To review relevant theoretical concepts of the structure of the urban boundary layer.

- To review and assess pre-processors, schemes and models for determining the mixing height, the surface energy budget and the stability, which are available to the participants.

- To identify and review suitable data sets within and outside the group that could be used to test and validate the pre-processors and models.

- To carry out inter-comparisons and to summarise comparisons of different schemes against each other and against data under specific conditions.

- To assess the influence of certain specific effects such as complex topography, strong heterogeneity, slope effects and canopy trapping on surface properties and fluxes.

- To assess the suitability of remote sensing tools to estimate canopy characteristics and surface fluxes and the mixing height.

- To provide recommendations for the improvement of existing pre-processors and models and for the development of new schemes.

- To provide recommendations for planning and conducting field campaigns in order to fill the important existing gaps for empirical data of key parameters for urban air pollution.

---

[1]COST is an acronym for co-operation in the fields of science and technology

- To provide recommendations for developing meteorological monitoring able to representatively describe various fields and processes under urban conditions.

- To promote co-ordination of related activities in Europe of presently scattered works, objectives, and responsibilities.

In the course of this COST-Action, the working group participated in several experiments and organised 3 open workshops with external experts:

1. Surface energy balance in urban areas, Antwerp, Belgium, 12 April 2000 (COST-715, 2002a),

2. Urban boundary layer parameterisations, Zurich, Switzerland, 24-25 May 2001 (COST-715, 2002b),

3. Mixing height and inversions in urban areas, Toulouse, France, 3-4 October 2001 (COST-715, 2002c).

During this COST-715 Action (1998-2004), in parallel and beyond the scientific work *per se*, the participating groups had the possibility to compare their respective experience and gaps in data or models. Consequently, it was possible to bring together various expertise and tools in order to promote, coordinate and optimise intra-European synergy through cooperation between national research activities. This was a major benefit offered by the COST framework, which is the oldest (funded in 1971) and widest (including 35 Member States) European intergovernmental network (see `http://ue.eu.int/cost/default.asp` or `http://cost.cordis.lu/src/home.cfm`). This report does not aim to be exhaustive but is primarily related to activities of WG2 Members, the outcome of these workshops and recent experiments and includes also findings from the literature. It complements the COST 715 Final Report (COST-715, 2004) in which the overall picture of urban air pollution meteorology from the point of view of science and air quality applications is addressed.

The present report is structured in the following way: after a short description of the basic concepts and issues in Section 2, Section 3 introduces some of the methods treating the surface energy budget for urban conditions, Section 4 the methods available to determine the mixing height. Section 5 describes some of the major European campaigns for urban meteorology, Sections 6 and 7 show the empirical and numerical results for the surface energy balance and the mixing height, respectively. Section 8 describes the use of remote sensing methods in urban studies, and finally Section 9 presents conclusions and recommendations based on the previous findings.

2. The specific problems of urban meteorology

2.1. Characteristics of the urban canopy

There is a strong body of knowledge and understanding of the classical homogeneous atmospheric boundary layer (ABL). In contrast the urban boundary layer (UBL) is more complex due to several specific features and processes but has recently started to receive more attention for characterising and understanding its structure and behaviour. The main disturbing features of the urban environment are the buildings, of different heights and shapes, extending well into the classical homogeneous surface layer, where otherwise the Monin-Obukhov similarity theory (MOST) applies. The buildings introduce a large amount of vertical surfaces, high roughness elements, artificial materials, and impervious surfaces.

The urban canopy is defined as the layer between ground and approximately the roof level, where most of the pollutant sources and receptors (humans, vegetation and materials) are located. The urban canopy layer (UCL) is composed of individual street canyons and other building arrangements of high elevation, from a few metres to several tens of metres. The array of streets induces partial channelling of the lowest level flow while high roughness elements induce the occurrence of a thick roughness sub-layer (Fig. 2.1) above the UCL.

The roughness sub-layer (RS) of height z^*, with a much larger vertical extent than found in classical boundary layers, occupies the first tens/hundreds of meters above the surface. An important practical consequence is that the MOST is not valid within the horizontally and vertically inhomogeneous RS, where turbulent fluxes of momentum, energy, moisture and pollutants are height dependent (e.g., Rotach, 2001). Above the inhomogeneous RS is the remainder of the surface layer, i.e., the inertial sub-layer where vertical turbulent fluxes are roughly constant with height. Only in the upper part of the surface layer (i.e., the inertial sub-layer), contributions from individual surface roughness elements are blended into possibly representative averages (Taha and Bornstein, 2000). Yet in certain circumstances the existence of the inertial sub-layer is questionable.

The building and ground covering materials have radiative properties such as albedo and emissivity different from the natural grounds and vegetation. In addition, they have not only horizontal but also vertical and/or slanted orientations, which strongly alter radiative transfers and the energy budget.

Also, the urban surfaces react to precipitation and evaporation quite specifically since many of them are impervious (roofs) and connected to drainage systems and some are semi-impervious over soils that have been disturbed or reshaped to improve drainage of the ground upper layers. As a consequence, the horizontal water flows within the

ground are different from their counterparts in natural grounds. In densely built districts, the vegetation is scarce, thus reducing the evapo-transpiration.
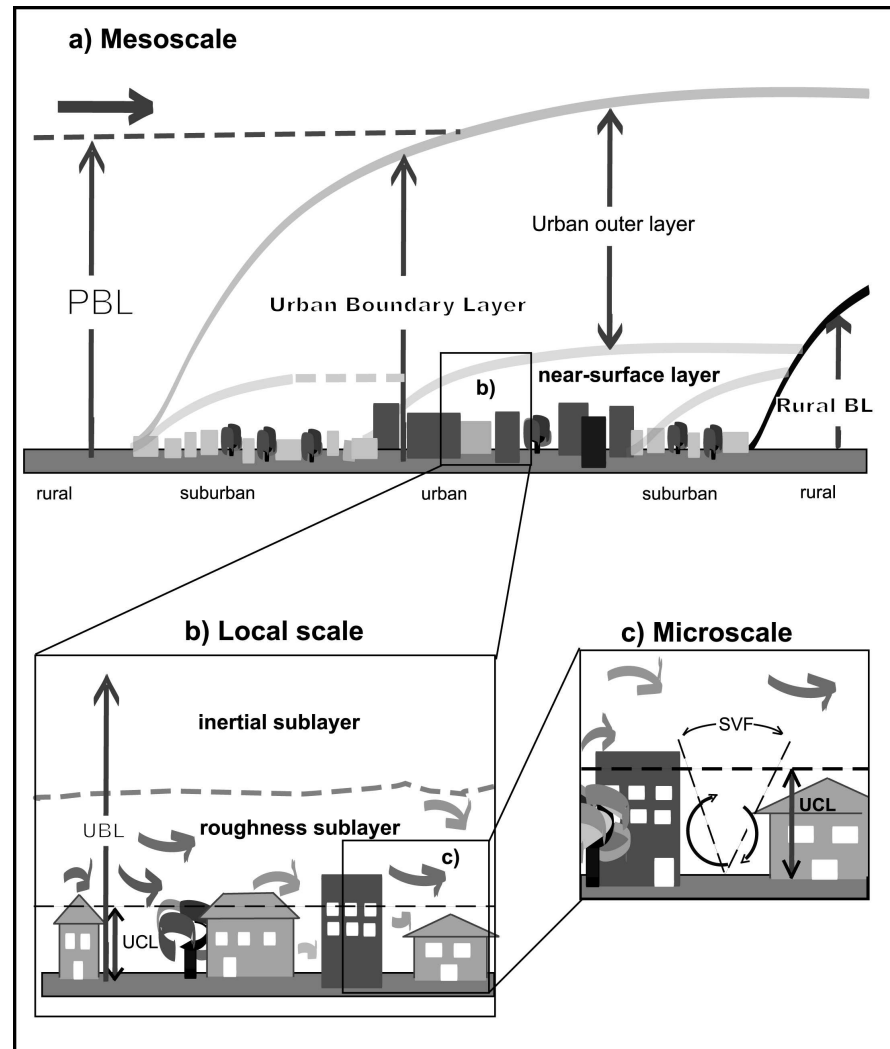
Figure 2.1: Sketch of the urban boundary layer structure indicating the various (sub)layers and their names (from Rotach et al., 2004a; modified after Oke, 1987).

The horizontal heterogeneity of the districts, at the kilometre scale, with sometimes strong roughness and/or temperature transitions, may generate a series of internal boundary layers (IBL). Their superposition increases the vertical heterogeneity of the lower surface layer.

Another source of horizontal heterogeneity is the presence of strong point sources of heat and water vapour in the middle of otherwise dry grounds, e.g., power plants and industrial areas. Urban areas therefore include very heterogeneous sensible and latent heat sources from surface transfers (ground and buildings), diverse low level point sources (household heating, automobiles), and elevated point sources (stacks). This is also the case for pollutant sources, where point and line sources (e.g., stacks and street traffic) differ largely from the surface and dispersed sources.

The structure of the UBL has a series of physical consequences that are well recognised, although not always quantitatively assessed. The urban heat island (UHI) is the temperature distribution at ground level with higher temperatures at the city centre that is evidenced predominantly at night and also in the long term statistics. The series of dynamic and thermal internal boundary layers destroy the UBL wind fields equilibrium, generate local flows between the city centre and its outskirts and between the various districts (quarter breezes), as well as thermal convection. The presence of the city also enhances fog and precipitation, probably due to the increase in cloud condensation nuclei (CCN) from particulate pollution. The influence of the city may be observed not only in the atmosphere above the city itself but also downwind where an "urban plume" is generated by the city disturbances; its vertical extension is limited by the ABL top which in turn limits the dilution of the pollutants, and the urban plume may be observed at large distance from the city (Changnon, 1981; Piringer and Baumann, 1999b).

Meteorological stations in urban areas should be sited so that their data reflect the characteristic meteorological state of the urban environs (district/quarter) under consideration, excluding localised influences. For surface energy balance observations, instruments must be placed above the RS. This height, z^*, is usually expressed as a function of the roughness element separation and/or the mean building height h_r. As a rule-of-thumb, z^* is somewhere between $2 - 5\ h_r$ (see Fig. 2.1 b-c). With instruments mounted at such heights, the area for which the measurements are representative (the flux footprint), typically is of the order of $10^2 - 10^4$ m^2. The exact dimensions and area of influence will vary with the exact height of measurements and roughness of the surface, as well as with wind speed, direction and atmospheric stability. The area of influence is much greater at night, a factor that must be considered when interpreting surface controls on urban energy balance fluxes through time. If large observational heights are necessary, the foot-print of the observation may become very large and represent inhomogeneous surface covers. Achieving uniform upwind fetch may be difficult to meet in parts of typical European cities.

The WMO-guideline for rural stations declares wind measurements as representative if placed 10 m above ground without close obstacles; temperature and humidity measurements have to be conducted at 2 m. For urban areas, no guidelines for proper siting exist, although this issue is presently under review by WMO (Oke, *pers. comm.*, 2004). This difficult issue is related to the vast amount of morphometric parameters characterising surface properties.

Surface characteristics like albedo, thermal properties, roughness, or moisture availability significantly control the surface energy balance partitioning of any surface. Therefore, detailed surface information is needed when modelling or estimating the surface energy balance. In contrast to most natural surfaces, urban landscapes show a much larger bandwidth and variability of surface characteristics. It is not possible to present universal "urban" surface values, which are valid for all types of urban neighbourhoods worldwide.

By defining distinct **categories** of urban neighbourhoods, typical surface characteristics can be attributed to each of these categories. A classification can be done based on maps or aerial photos. Digital land-use classification datasets often provide different urban classes, and are a source of increasing importance, e.g., the BDTopo dataset by IGN France was analyzed for the derivation of surface parameters in Marseille (Long *et al.* 2003). Unfortunately, most land-use classifications are classified by *functional* aspects (residential, industrial) and not by surface morphometry or surface cover. Focussing on meteorological aspects, Ellefsen (1991) classifies North American cities by building contiguity, construction, and materials into 17 Urban Terrain Zones (UTZ). On the other hand, the new WMO guideline on urban observations suggests seven Urban Climate Zones (UCZ) (Oke, *pers. comm.,* 2004). Fehrenbach *et al.* (2001) have automated the classification of urban climatological neighbourhoods by satellite image analysis. However, no universal classification scheme exists. Historical development results in a huge variety of urban neighbourhood types worldwide. The more complete a description scheme is, the more it is restricted to a specific (historical) region, e.g., UTZs are difficult to apply to non-North-American cities because typical morphometry and building materials do not correspond.

An appropriately chosen set of **surface parameters** can be related to physical processes. For example, it is not surprising that the area covered by vegetation drives the magnitude of the latent heat flux, or that morphometric parameters help to describe the roughness and turbulence characteristics over a particular urban surface. Therefore, one can outline the most important characteristics as follows:

Urban Cover

Two dimensional plan aspect ratios describe the two dimensional surface fraction of a particular surface type per total plan area (as viewed from above). They are also known as "plan area fractions". Plan aspect ratios can be easily retrieved from maps, geographic information systems, aerial photos, or from high resolution satellite images. Table 2.1 lists the most often used plan aspect ratios, which are sometimes further divided into subcategories. Figure 2.2 shows the surface fractions from 20 European and North American neighbourhoods where urban surface flux experiments were carried out in the last 20 years. It also illustrates worldwide sets of typical "suburban" and "urban" surfaces clusters.

<u>*Three dimensional structure*</u>

Three dimensional (3D) morphometric parameters describe the configuration of urban buildings (and sometimes include vegetation). They are often used in parameterisations to describe drag and turbulence production or to model storage heat flux densities and surface temperatures. Grimmond and Oke (1999b) review methods to deduce aerodynamic properties from a set of morphometric parameters. Table 2.1 also lists the most important morphometric parameters used in urban meteorology. For more and more cities, authorities provide digital 3D building data sets, which are a powerful tool for the analysis of urban surface forms (Fig. 2.3). Such high resolution models can provide detailed measures of three dimensional parameters, and additionally vertical profiles e.g. of building volume density and sky view factors.

<u>*Urban materials*</u>

They are of great importance especially for the estimation of radiative properties and the determination of storage heat flux densities, construction materials of the buildings (roofs, walls). Detailed analysis of aerial photos or field surveys can provide the necessary information.

Table 2.1: Parameters used to describe properties of urban surfaces and the range of typical values for suburban, urban, and high-rise neighbourhoods. The range of values given for the three dimensional structure (b) does not take vegetation into account. The typical values are taken from the experiments listed in Fig. 2.2.

(a) Urban Cover				
λ_P	Plan area ratio of buildings		Describes the plan area covered by buildings per total plan area.	Urban: $35 - 65\%$ Suburban: 15 - 40%
λ_V	Plan area ratio of vegetation		Describes the plan area covered by vegetation (and sometimes also unmanaged bare soil) per total plan area.	Urban: $0 - 35\%$ Suburban: $35 - 70\%$
λ_I	Plan area ratio of impervious surfaces		Describes the plan area covered by impervious surfaces, which are not buildings (e.g. streets, parking lots, pavements) per total plan area.	Urban: $20 - 50\%$ Suburban: $10 - 40\%$
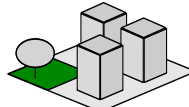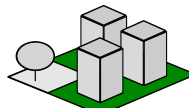
(b) Three dimensional structure

z_H	Mean building height		The (area-weighted) average height of all buildings.	Suburban: $4 - 8$ m Urban: $8 - 20$ m High-rise: > 20 m
λ_F	Frontal aspect ratio (or frontal area index)		Ratio of the total projected frontal area of buildings to the total plan area. Including vegetation λ_F can be increased by a factor up to 4.	Suburban: $0.1 - 0.3$ Urban: $0.1 - 0.6$ High-rise: > 0.4
λ_C	Complete aspect ratio (or surface enlargement)		Ratio of the complete 3-D surface area per total plan area (Voogt and Oke, 1997).	Suburban: $1.3 - 1.8$ Urban: $1.5 - 2.0$ High-rise: > 2
V_P	Normalized building volume		$\lambda_P \cdot z_H$. Building volume per total plan area.	Suburban: $1 - 3$ m^3 m^{-2} Urban: $3 - 15$ m^3 m^{-2} High-rise: > 15 m^3 m^{-2}
D_x	Characteristic inter-element spacing $^{(a)}$		The distance between building centroids in ideal arrangements (wind tunnel). For real urban surfaces the characteristic spacing between buildings. $D_x = L_x + W_x$	
W_x	Characteristic canyon width $^{(a)}$		The distance in between buildings in ideal arrangements (wind tunnel). For real urban surfaces the average width of free space in between buildings (and therefore including backyards and open areas).	
λ_S	Canyon aspect ratio (or canyon height to width ratio		A widely used ratio between the average building height z_H and the characteristic canyon width W_x.	Suburban: $0.1 - 0.5$ Urban: $0.5 - 2$ High-rise: > 2
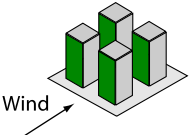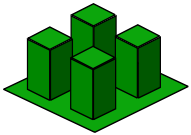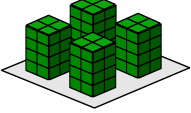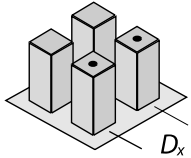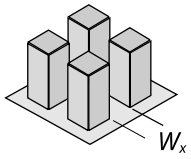
L_x	Characteristic building breath [a]		The breadth of buildings in ideal arrangements (wind tunnel). For real urban surfaces the average breadth of buildings.	
λ_B	Building height to width ratio		z_H / L_x. The ratio between the average building height z_H and the characteristic building breath L_x. Often used in wind tunnel or numerical studies.	Suburban: < 1 Urban: $1 - 3$ High-rise: > 2
ψ_S	Sky view factor		For a particular point, the sky view factor defines the fraction of the sky directly seen in to the total of the upper hemisphere. ψ_{S0} is the spatial average sky view factor at ground level (outside buildings). For an idealized infinite long canyon, the average ψ_{S0} in the canyon is related to λ_S by $\lambda_S = 0.5 \tan(\cos^1(\psi_{S0}))$ (Oke, 1981).	Suburban: $0.6 - 0.9$ Urban: $0.3 - 0.6$

[a] Usually, D_x, W_x and L_x are given for the along wind direction in a wind tunnel, and a separate set of D_y, W_y and L_y describe the building arrangement in the direction perpendicular to the mean wind. However, for real cities integral information over all wind direction is given.
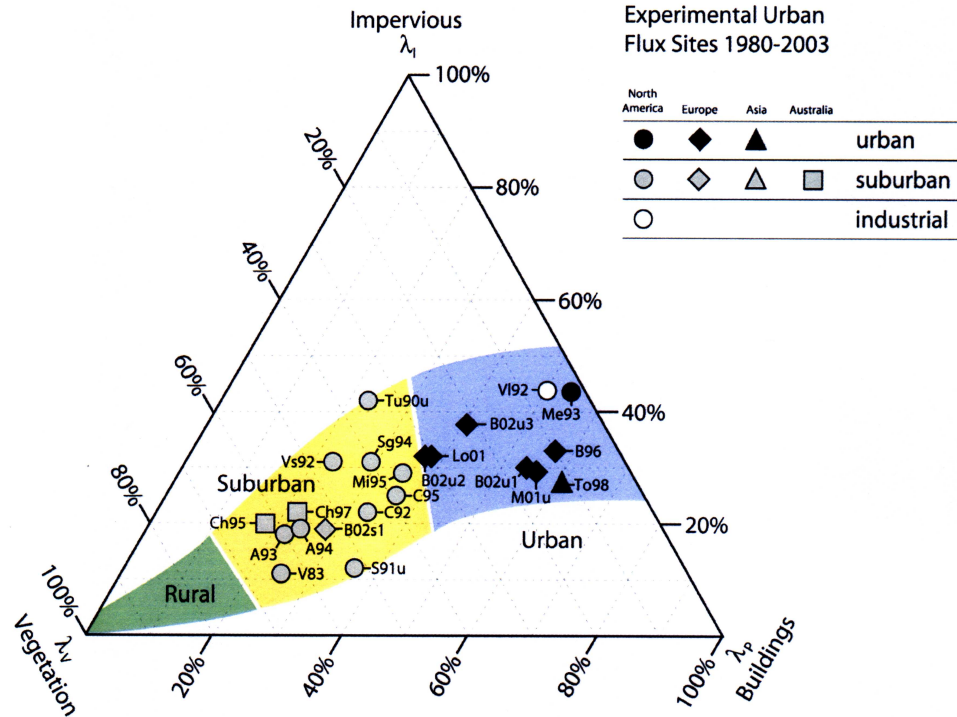
Figure 2.2: *Plan aspect ratios of neighbourhoods around experimental urban flux sites. All surfaces are classified into three categories: Plan aspect ratios of buildings λ_P, plan aspect ratio of vegetation λ_V (including unmanaged land, bare soil and open water) and plan aspect ratio of impervious surfaces λ_I. The labels refer to experimental sites and the numbers to the year of the measurement campaign. Sources: V83: Vancouver, Canada (Cleugh and Oke, 1986). Tu90u: Tucson, USA; S91u: Sacramento, USA; C92: Chicago, USA (all Grimmond and Oke, 1995). Me93: Mexico City, Mexico (Oke et al., 1999). Vs92, Vl92: Vancouver, Canada; A93, A94: Los Angeles, USA; Sg94, San Gabriel, USA; Mi95, Miami, USA; C95: Chicago, USA (all Grimmond and Oke, 1999a ˚). Ch95, Ch97: Christchurch, New Zealand (Spronken-Smith, 2002). B96: Basel, Switzerland (Feigenwinter et al., 1999). To98: Tokyo, Japan (Kanda et al., 2002). Lo01: Lodz, Poland (Offerle et al., 2003). M01u: Marseille, France (Mestayer et al., 2004). B02u1, B02u2, B02u3, B02s1: Basel, Switzerland (Christen et al., 2003).*
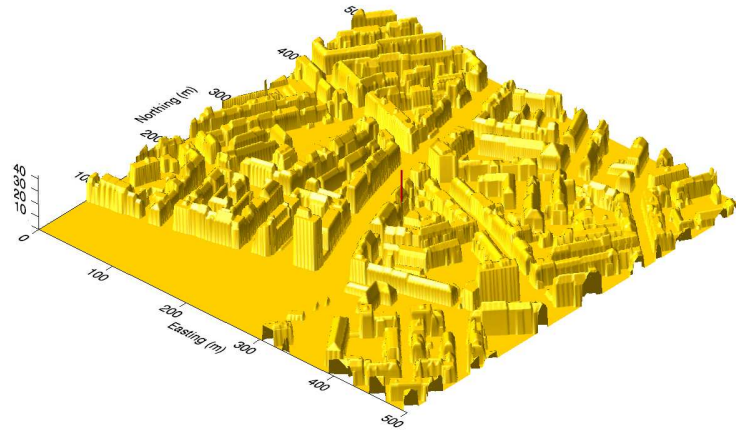
Figure 2.3: *The visualization shows a 1 m digital building model for the surrounding of the urban long-term flux site "Basel-Spalenring" in Basel, Switzerland (© GVA Basel-Stadt).*

2.2. Practical modelling applications

The basic problem at hand is to be able to represent and forecast adequately meteorological and pollution fields, especially their diurnal evolution, over urban areas. The quality of urban air pollution forecasts and Urban Air Quality Information and Forecasting Systems (UAQIFS) critically depends on: (i) the mapping of emissions, (ii) the urban air pollution (UAP) models, and (iii) the meteorological fields in urban areas. The main issue in forecasting UAP is the prediction of episodes with high pollutant concentration in urban areas where most of current/common methods and models, based on in-situ meteorological measurements, have difficulties to realistically reproduce the meteorological input fields for the UAP models.

UAP models in operational UAQIFSs, as a rule, use simple in-situ meteorological measurements which are fed into meteorological pre-processors (Fig. 2.4). These pre-processors do not achieve the potential of numerical weather prediction (NWP) models in providing all the meteorological fields needed by modern UAP models to improve urban air quality forecasts as they lack an adequate description of physical phenomena and the complex data assimilation and parameterisations of numerical weather prediction models. On the other hand,

during the last decade, substantial progress in the description of urban atmospheric processes and in NWP modelling was achieved (see Sections 3.2 and 3.5).

Nevertheless, in recent years, a number of boundary-layer parameterisation schemes has been developed to estimate the components of the surface energy balance (net radiation, sensible heat flux) and other UBL parameters (wind, temperature and turbulence profiles, the mixing height) on a routine basis from hourly standard meteorological data. For the former terms, the most referred ones are the method of van Ulden and Holtslag (1985) and of Berkowicz and Prahm (1982). COST-710 (1998) reviewed and performed inter-comparisons of these methods against rural data. Possible errors and differences between methods used in this pre-processing can be of comparable or even greater importance to errors occurring in the dispersion modelling itself. Most of these models were developed and validated using data from flat, grass-covered environments. These approaches are therefore limited to horizontally quasi-homogeneous conditions, which is seldom the case in urban conditions (see above).
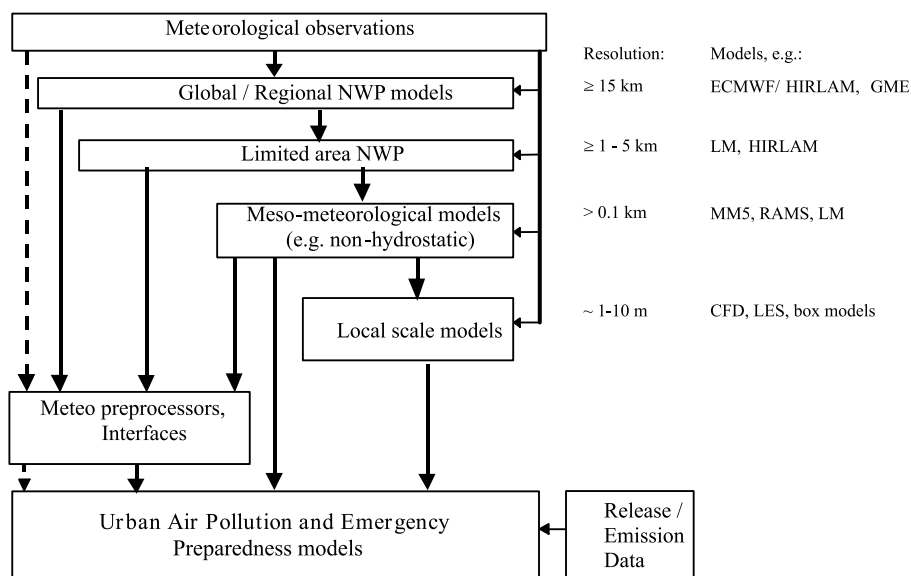
Figure 2.4: Current regulatory (dash line) and suggested (solid line) ways for systems of forecasting of urban meteorology for UAQIFSs.

3. Pre-processors, schemes and models for the surface energy budget

3.1. The urban surface energy budget

The surface energy balance (SEB) is the key component of any model aiming to simulate dynamical and thermodynamical patterns above the surface (e.g., Kallos, 1998; Mestayer, 1998). For a rural environment with a low plant cover the surface radiation budget and SEB are written:

$$Q^* = K \downarrow - K \uparrow + L \downarrow - L \uparrow = Q_H + Q_E + Q_G \quad [\text{W m}^{-2}] \qquad (3.1)$$

where Q^* is the net all-wave radiation; $K \downarrow$ the incoming shortwave radiation; $K \uparrow = \alpha_0.K \downarrow$ the outgoing, reflected shortwave radiation where α_0 is surface albedo; $L \downarrow$ the incoming long-wave radiation from the sky and surrounding environment 'seen' from the observation point; $L \uparrow = \varepsilon_0 \sigma T_s^4 + (1 - \varepsilon_0)L \downarrow$ the outgoing long-wave including both that emitted from the surface consistent with its emissivity ε_0 and absolute surface temperature T_s, and the reflected incoming long-wave; Q_H the turbulent sensible heat flux; Q_E the turbulent latent heat flux; and Q_G the soil heat flux.

For a city, additional sources of energy need to be considered in theory, the fluxes of heat due to combustion of fuels (Q_F) by:

— the traffic, at ground level,

— the domestic heating, through wall heat transfers and direct release from chimneys,

— the similar heat releases of small dispersed industries,

— elevated point sources of warm discharges (high stacks),

thus, yielding:

$$Q^* = K \downarrow - K \uparrow + L \downarrow - L \uparrow = Q_H + Q_E + Q_G + Q_F \quad [\text{W m}^{-2}] \qquad (3.2)$$

The anthropogenic energy sources that must be introduced in the models depend on their use and on the definition of the "surface" in this context. In the

case when a SEB model is used as a pre-processor for an atmospheric/meteorological numerical model, the surface is the lower limit of this model's computational domain: its elevation defines which energy sources must be taken care of by the SEB model and which ones must be modelled as elevated sources within the second, or higher, computational grid level. The "surface" may thus be high above the canopy in meso-scale simulations, or just millimetres above ground when the canopy layers are within the simulation domain (Martilli *et al.*, 2002; Dupont *et al.*, 2004). Most often, the "surface" is conceptually that of the top of the urban canopy, i.e., the mean roof-level when it may be recognised without ambiguity.

In experimental data analysis, when measurements have been performed above the roofs, the urban SEB is made up of directly measured terms, each one including automatically part of the energy released by combustion:

$$Q^* = K \downarrow -K \uparrow +L \downarrow -L \uparrow = Q_H + Q_E + \Delta Q_S \quad [\text{W m}^{-2}] \qquad (3.3)$$

where the imbalance term ΔQ_S includes the storage heat flux in the urban fabric, the ground and the air layer, which extends from the surface to a level where the vertical heat exchange divergence is negligible (constant flux layer). This balance (3.3) therefore applies to the top of the urban canopy plus a substrate volume (see Oke, 1988). The form of these three equations assumes that the surface is of sufficient horizontal extent (fetch) that advection can be considered negligible. However, this assumption is often not well verified in urban areas due to strong horizontal contrasts in temperature and heat sources.

When comparing urban to rural conditions, the following general statements can be made regarding the components of the SEB:

- The **radiation budget** does not differ significantly for urban and rural surfaces, as the increased loss of net thermal long-wave radiation is partly compensated by a gain in net shortwave radiation due to a lower albedo.

- The **turbulent fluxes of sensible and latent heat**, as well as their ratio ($\beta = Q_H/Q_E$, the Bowen ratio) are variable, depending in particular on the amount of rainfall that fell during the previous hours or days. However, the impermeability of urban surfaces generally reduces the availability of soil moisture for evaporation after a few rainless days, generally leading to high values of the Bowen ratio.

- The **storage heat flux** is usually significantly higher in urban areas compared to densely vegetated surfaces.

- The **anthropogenic heat flux** is a most typical urban energy component as it is generally absent over rural or natural surfaces.

As to the parameters that characterise the surface, the difference between urban and rural environments can be summarised as follows:

- The **albedo** (hemispheric reflectivity) is variable for both urban and rural surfaces, though urban surfaces may be darker.

- The **emissivity** of rural surfaces is often quoted to be close to 0.98, whereas for urban surfaces one encounters lower figures, mainly in the range 0.85-0.95.

- The aerodynamic surface **roughness** of cities (one to a few metres) is at the high side of the spectrum for continental surfaces (see Mestayer and Bottema, 2002 in COST-715, 2002b).

- A typically urban feature is the large momentum to heat **roughness lengths ratio** z_0/z_{0t}. This is caused by the presence of so-called bluff elements, i.e., solid rather than permeable obstacles (see Garratt, 1992).

- **Moisture availability** in cities is generally rather low due to the presence of impermeable surfaces and the relative absence of vegetation. It should be noted, though, that immediately after rain, a city may be wetter than its rural surroundings. The term "moisture availability" is a vague concept; physical parameters closely related to this quantity are vegetation fraction cover and volumetric soil moisture.

- **Thermal inertia** (also referred to as thermal admittance, defined as $(k_s \rho_s c_s)^{1/2}$, with k_s the thermal conductivity, and $\rho_s c_s$ the specific heat capacity of the soil substrate) is marginally higher for urban surfaces: around 1800 compared to rural values of 1500 J m^{-2} s$^{-1/2}$ K^{-1}.

3.2. Preprocessors and models

In the following Sections 3.2.1-5, examples of models and pre-processors with urban parameterisations that require standard meteorological observations as

well as numerical models with detailed surface exchange parameterisations are given to show the range of procedures available today.

3.2.1. Local-scale Urban Meteorological Pre-processing Scheme (LUMPS)

Grimmond and Oke (2000, 2002) developed a linked set of equations to calculate heat fluxes, and in turn atmospheric stability, specifically designed for the urban environment. The scheme is basically an urban-specific modification of the approach of Holtslag and van Ulden (1983). This pre-processor scheme (LUMPS – **L**ocal-scale **U**rban **M**eteorological **P**re-processing **S**cheme) makes use of parameterisations that require standard meteorological observations, supplemented by basic knowledge of the surface character of the target urban area.

Ideally LUMPS is forced by observed short- or net radiation data, but these fluxes also can be modelled. Heat storage in the urban fabric, including hysteresis, is parameterised from the radiation and surface cover information using the objective hysteresis model (OHM; Grimmond *et al.*, 1991; Grimmond and Oke, 1999a):

$$\Delta Q_S = \sum_{i=1}^{n}(\lambda_i \alpha_{1i})Q^* + \sum_{i=1}^{n}(\lambda_i \alpha_{2i})\partial Q^*/\partial t + \sum_{i=1}^{n}(\lambda_i \alpha_{3i}) \quad [\text{W m}^{-2}] \qquad (3.4)$$

where the λ_i are the plan fractions of each surface type in the area of interest and the $\alpha_{\text{xtzg}\iota}$ are the corresponding empirical coefficients. These αtcoefficients have been deduced from a re-analysis of the Multi-city Urban Hydrometeorological Database (MUHD, see also Section 6.1.1) obtained from ten sites in seven North American cities.

The turbulent sensible and latent heat fluxes are calculated using the available energy and a simplified Penman–Monteith/Priestley–Taylor type of equation using a measure of the surface moisture status, given by the fraction of the surface covered by vegetation, and temperature. LUMPS has been shown to perform well when evaluated using data from North American cities. The MUHD database is currently extended to include experimental data from European urban sites (Grimmond, *personal communication*, 2004).

3.2.2. The Town Energy Balance (TEB) scheme

The Town Energy Balance (TEB) scheme of Masson (2000; see also COST-715, 2002a) is one of the most detailed parameterisations of urban effects within current numerical models with an explicit consideration of the effects of buildings, roads, and other anthropogenic building materials on the urban surface energy budget.

The TEB scheme is built following the canyon approach, generalised in order to represent larger horizontal scales. The physics treated by the scheme is relatively complete. Due to the complex shape of the city surface, the urban energy budget is split into three surface energy budgets separately for roofs, roads, and walls, respectively. Orientation effects are averaged for roads and walls. Up to two energy budgets are added for snow when it is present on roofs or roads. Some of the physics was derived from the literature (long-wave radiation or thermal conduction through surfaces), since they are classically assumed to estimate temperatures in conditions without feedback towards the atmosphere (during nights with calm wind). However, most parts of the physics need an original approach (short-wave radiation, thermodynamical and anthropogenic flux treatment, rain and snow), since they occur when interaction with the atmosphere is strong.

TEB therefore uses the following original city representation:

1. Within the model mesh, all buildings have the same height and width, with the roof level at the surface level of the atmospheric model.

2. The buildings are located along identical roads, the length of which is considered far greater than their width; the space contained between two facing buildings is defined as a canyon.

3. Any road orientation is possible, and all exist with the same probability. This hypothesis allows the computation of an averaged forcing for road and wall surfaces. In other words, when the canyon orientation appears in a formula (with respect to the sun or the wind direction), it is averaged over 360°. In this way, no discretisation is performed on the orientation. The radiative trapping is the subject of an original development, including estimation of the solar flux received either by the walls or the roads accounting for the shadow effects, scattered solar radiation reflections with sky-view factors resolving a geometric system for an infinite number of re-

flections, and the trapping of long-wave radiation by the canyon surfaces computed with one re-emission.

The TEB model does not use one urban surface temperature (representative of the entire urban cover), but three surface temperatures, representative of roofs, roads and walls. To treat the conduction fluxes to or from the building interiors (roof, wall) or the ground (road), each surface type is discretised into several layers, typically 3 layers. The heat fluxes between the surfaces and the canyon are computed using a resistance approach, with transfer coefficients using a parameterised canyon ventilation wind speed. The turbulent heat fluxes to/from the roofs are also recovered from classical boundary-layer laws, because the roof heights are supposed uniform, using a roughness length of 0.15 m.

3.2.3 The Finite Volume Model (FVM) urban module

A detailed surface exchange parameterisation scheme has been developed by Martilli *et al.* (2002, see also COST-715, 2002a) in the meso-scale FVM model to simulate semi-explicitly the canopy layers with the "porosity-drag" approach.

The lowest model level is at the physical ground. The city is characterized by an array of buildings of the same width located at the same distance from each other (canyon width W) but with different heights z_H, with a probability $P(z_H)$ to have a building height z_H. The street-canyon length is equal to the horizontal grid size.

Roofs, walls, and the canyon floor are considered as active surfaces. For the exchange of momentum, horizontal and vertical surfaces are treated separately. Two different roughness lengths are defined for the roof and canyon floors, respectively. The momentum sink from friction on horizontal surfaces is vertically distributed in all the model levels within the urban canopy.

The contribution of the walls is parameterised with a porous drag force approach as usually adopted in vegetation canopy models:

$$\boldsymbol{F}\boldsymbol{u}_j^v = -\rho C_{\text{drag}} \quad |\boldsymbol{U}_j^{\text{ort}}|\boldsymbol{U}_j^{\text{ort}}S_j \tag{3.5}$$

where $\boldsymbol{U}_j^{\text{ort}}$ is the horizontal wind speed component, orthogonal to street direction at level j, and ρ is the density of air, C_{drag} a drag coefficient of a square cylinder (≈ 0.4), and S_j the total surface of walls at level j. In the turbulent

kinetic energy (TKE) equation of the k-l closure model, a source of TKE by building wakes is added while the mixing length l is modified to account for the building-induced eddies in the canopy layers which are assumed to be of the same size as the buildings.

The sensible heat fluxes are determined as a function of the difference between the air temperature and the corresponding surface temperature. The short and long wave radiative fluxes are computed by taking into account the shadows and multiple reflection effects of the street canyon element with a unique street direction per grid-mesh. The urban latent heat fluxes are neglected in the original formulation.

3.2.4. The SM2-U soil model

The "soil model for sub-mesoscale urban", SM2-U, is based on the force-restore model of Noilhan and Planton (1989) for the transfers between the atmosphere, one vegetation layer, and three soil layers in its most recent version, ISBA-3L (Boone *et al.*, 1999). It keeps the principal characteristics of this "soil" model and was developed as a pre-processor for fine resolution sub-mesoscale simulations. The surface dynamic influence is represented through roughness lengths and displacement heights. Except for radiation reflections and water runoff from saturated surfaces, the horizontal exchanges inside the urban canopy are not explicitly simulated, considering that the effects of wind advection between urban surfaces is accounted for by the atmospheric model above, due to the fine spatial resolution of the computational grid (100-1000 m).

SM2-U separates 8 types of surfaces (see Figure 3.1), namely: bare soil without vegetation (denoted "*bare*"), bare soil located between sparse vegetation elements (*nat*), vegetation over bare soil (*vegn*), vegetation over paved surfaces (e.g., trees on the road side: *vega*), paved surfaces located between the sparse vegetation elements (*pav*), paved surfaces located under the vegetation (*cova*), building roofs (*roof*), and water surfaces (*wat*). Three soil layers are considered: a surface layer for the natural surfaces (nat+vegn and bare), allowing evaluation of the evaporation fluxes from the bare soils; a root zone layer representing the influence area of the vegetation roots; and a deep soil layer used as a water reservoir for dry periods. Roof surfaces are considered fully impervious while paved surfaces are semi-impervious, letting water infiltrate downwards but not upwards. The model includes the constants for 11 soil classes, 11 vegetations, 3 water bodies, 4 roof materials, and 2 paved surface materials.

In each cell, the model solves equations for surface temperature T_{si}, specific humidity q_{vsi}, and energy fluxes for each of the 8 surface covers i, as

$$\partial T_{si}/\partial t = C_{Ti}Q_{Gi} - (2\pi/\tau)(T_{si} - T_{\text{soil}}) \qquad (3.6)$$

for $i \in \{\text{bare, nat, pav, vega, vegn}\}$, where τ is the day duration, $C_{Ti}(= \rho_s c_s)$ the surface layer heat capacity, T_{soil} the underlying soil layer temperature obtained from its own heat budget, and Q_{Gi} is the heat storage computed as the imbalance in the i's SEB (see Eq. 3.2). In this budget the anthropogenic heat flux Q_F may include contributions from vehicles and heat flux through building roofs.

The three-dimensional structure complexity of the **urban canopy** is not explicitly simulated at the sub-grid scale: the horizontal effects are expected to be taken into account by the fine resolution of the computational grid, but the canopy vertical dimension influence is accounted for by parameterisation relationships. The building walls are integrated in the paved surface temperature and energy budget equations. Schematically, this consists in solving the energy budget of a street canyon (Fig. 3.1) instead of paved horizontal surfaces alone. Thus, $T_{s\ pav}$ corresponds to an effective average temperature of street canyon surfaces while the heat stored by walls and the radiative trapping, which are the principal effects of the canopy thickness, are integrated in the paved surface energy budget. The building walls are actually considered in three ways: first by modifying the surface atmospheric resistance to the heat flux (to account for heat stored by walls); second by modifying the energy budget to include the heat flux through the walls; third by considering the radiative trapping inside the streets by means of a corrective factor to the paved surface albedo, called street canyon effective albedo.

This effective albedo depends on the individual wall and paved surface albedos, the street aspect ratio, and the sun position with respect to the average street axis direction. The computation of the street canyon effective albedo is similar to Masson's (2000) as shown by Dupont *et al.* (2003). The effective emissivity of the street canyon is that of the paved surfaces.

SM2-U has been implemented in SUBMESO, a high-resolution atmospheric model developed on the basis of the Advanced Regional Prediction System (ARPS) Version 3 (Xue *et al.*, 2000, 2001) by Dupont (2001) and in MM5 by Otte *et al.* (2003). Its transposition, implementation and test with other NWP models is part of the EU-project FUMAPEX (see Sections below).
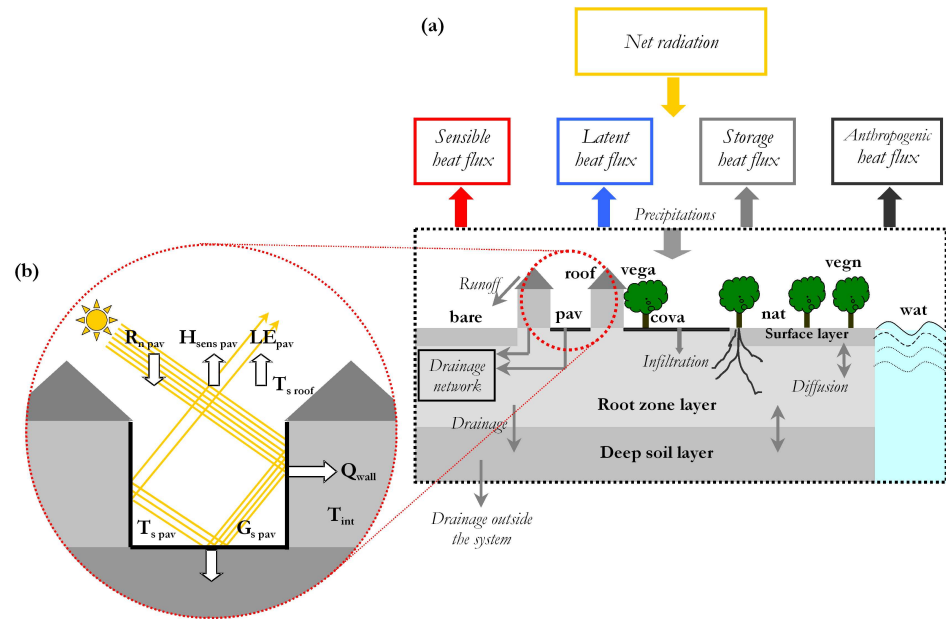
Figure 3.1: (a) Scheme of the SM2-U energy and water budget models with 8 surface types (pav, cova, bare, nat, roof, vega, vegn, wat) and 3 soil layers; (b) Energy budget of paved surfaces.

3.2.5. Urban parameterisations in the Advanced Regional Prediction System (ARPS)

The Advanced Regional Prediction System (ARPS) is a non-hydrostatic meso-scale meteorological model developed at the Center for Analysis and Prediction of Storms (CAPS) at the University of Oklahoma (Xue *et al.*, 2000, 2001). An advanced land surface scheme (De Ridder and Schayes, 1997) was incorporated in ARPS Version 4 to study the impact of land use changes on atmospheric circulation and pollutant dispersion (Lefebre *et al.*, 2004). The surface scheme calculates the interactions between the land surface and the atmosphere, including the effects of vegetation using the big-leaf approach, partitioning the net radiation between the sensible and latent heat turbulent fluxes and the storage heat flux. Sub-grid terrain heterogeneity is accounted for by separately calculating energy fluxes for bare soil and vegetation, obtaining a grid-average flux weighted with fractional occurrences.

Turbulent heat fluxes at the land surface are treated by means of bulk formulas derived from the Monin-Obukhov similarity theory (MOST). Using the resistance formalism, the sensible heat flux can be written as:

$$(Q_H/\rho c_p) = (T_0 - T_a)/(r_a + r_b) \tag{3.7}$$

where c_p is the heat capacity of air at constant pressure, T_o is the aerodynamic surface temperature (i.e., the temperature of air in contact with the surface) and T_a the air temperature at the first level of the model. It should be noted that for urban areas, the definition of T_o, and that of the surface, is not unambiguous (see Section 8.3). The aerodynamic and laminar resistances are given by the following expressions:

$$r_a = (\kappa^2 U_a)^{-1} \ln(z_a/z_0)^2 F(Ri_B); \quad r_b = \kappa u_* \ln(z_0/z_{0t}) \tag{3.8}$$

where κ is von Kármán's constant, U_a the wind speed at level z_a in the surface layer, z_0 and z_{0t} are the roughness lengths for momentum and temperature, F is a stability function based on the bulk Richardson number Ri_B, and u_* is the friction velocity.

In the context of urban air quality modelling studies, the land surface model was upgraded to better represent urban areas. In this approach, cities were represented as bare soil, though with appropriate values for albedo, thermal admittance, and roughness. Furthermore, urban surfaces were considered impermeable for rainfall. However, the most fundamental change consisted in the incorporation of Brutsaert's (1975, 1982) temperature roughness parameterisation for a surface consisting of bluff-rough (solid) elements representative of building arrays, as opposed to permeable-rough (porous) obstacles that are associated with vegetation, and reads as follows:

$$z_{0t}/z_0 \approx 7.4 \exp(-2.5 Re_*^{1/4}) \tag{3.9}$$

where $Re_* = u_* z_0/\nu$ is the roughness Reynolds number, with ν the kinematic viscosity of air. The choice for this particular parameterisation was made following experimental work by Voogt and Grimmond (2000), who obtained a fair agreement between measured and estimated sensible heat fluxes when the estimation was done using measured radiative surface temperatures in combination with a bulk formula for sensible heat based on Brutsaert's expression.

Inserting typical values in the above expression, it is readily found that for cities, values of z_0/z_{0t} may become more than an order of magnitude larger than the value of 10 which is generally cited for vegetation (Garratt, 1992). The resulting extremely small values of z_{0t}, combined with relatively low wind speeds generally found over cities (owing to the high momentum roughness), lead to a very high resistance for turbulent heat exchange, thus strongly inhibiting the latter. As a consequence, cities tend to store incoming radiant energy in the soil and building substrate rather than to convert it to atmospheric heating, which is normally the dominant mode. Heat storage in cities occurs in vast amounts during the day, to be released again during the night. Thermal inertia, though often cited as a cause of the observed large values of the storage heat flux in cities, is less important in this respect as urban and rural thermal admittance values do not differ by much.

This urbanised land surface scheme remains simple and does not require information on the vertical structure within the urban canopy. It gives an aggregated representation of some key processes of urban surface-atmosphere exchanges. However, in cases where the focus is on the effect of cities on the atmosphere more than on the details of in-canopy processes themselves, the scheme described here could be a valuable alternative. Moreover, it is easy to incorporate into existing schemes, requiring modification of only a few lines of computer code.

3.3. Effect of strong heterogeneity on surface properties and fluxes

3.3.1. Effective roughness

In a general manner, the roughness length concept assumes that the surface is relatively homogeneous and can be characterised by a single value of z_0 (Fiedler and Panofsky, 1972). A review of urban roughness and of assessment methods can be found in Mestayer and Bottema (2002, in COST-715, 2002b).

Over urban areas, the ABL is strongly influenced by the roughness heterogeneity of a patchwork of urban blocks, especially at the city boundaries. In numerical simulations the vertical momentum transfer is most commonly parameterised by a grid-cell averaged roughness length, while the urban roughness lengths may vary by several orders of magnitude from one grid mesh to the next one. Therefore, it is not enough to calculate the roughness parameters for urban

areas according to classical methods, but rather the concept of an effective roughness to treat urban areas in NWP and meso-meteorological models can be considered. There are several publications introducing and testing such an effective roughness for different types of heterogeneous terrains, e.g., for forest-grass canopies, land-sea interaction, etc. (Taylor, 1987; Gutman and Ignatov, 1998; Hasager *et al.*, 2003; De Ridder, 2003; Schlünzen and Katzfey, 2003; De Ridder *et al.*, 2004).

The influence of strong roughness changes on the simulation of a neutrally stratified ABL was explored by Mestayer *et al.* (2003), with a view of optimising the geographical representation of the aerodynamic characteristics of urban quarters in high resolution numerical simulations using an advanced 3D atmospheric model. At first, the influence of isolated, strong transitions was assessed for 2D and 3D geometries. This showed that the structure of the developing internal boundary layer (IBL) after an isolated roughness step embedded a new constant flux layer extending only about one tenth of the IBL height, thus inducing a strong momentum variation in the transition layer above, with this momentum excess still noticeable several kilometres downstream from the step. Roughness strips had much more influence on the turbulent fields than on the mean wind field; their perturbations extended over several kilometres downstream and a few tens of metres upwards. Besides, perturbations generated by the transitions, through the pressure field equilibrium loss, were larger by a factor of 2-3 than if the equilibrium with the new roughness would have been reached immediately. The perturbations generated by an array of high and low roughness patches are less intense than by the equivalent crosswind strips, but they do not extend much in the lateral direction.

3.3.2. Flux aggregation technique for urban areas

So, it is reasonable to simulate the effective roughness fields for a considered city separately for different situations (e.g., for different seasons, wind directions) and to build a kind of effective roughness maps library. For such a strategy, a new flux aggregation technique suggested by Hasager *et al.* (2002, 2003) was installed in the DMI-HIRLAM model but, for the moment, only for non-urban areas. Figure 3.2 gives a schematic structure of the surface flux microscale aggregation model where the upper panel illustrates a simple version "H" according to Hasager and Jensen (1999), while the bottom panel represents a more advanced version "z_{0t}" following Hasager *et al.* (2002).

A short description of the algorithms presented in Fig. 3.2 is the following. The inputs are wind speed (U), air temperature (T_a) at the computational level and maps of surface temperature, land cover classes and leaf area index (LAI) from satellite. The aerodynamic roughness map (z_0) is generated from a roughness index derived from the land cover classes except for water bodies. The index and an equation for the temperature roughness z_{0t} are prescribed for each land cover class to provide the z_{0t} map. The model runs within the dotted red box of Fig. 3.2. The atmospheric flow equations are linearised and solved by the Fast Fourier Transform (FFT) scheme. The output maps are the friction velocity (u_*), the temperature scale (θ_*), the roughness map (z_0), and the temperature roughness map (z_{0t}), all of which are found through iteration (indicated by the green curved arrows). The iteration is due to the stability correction to the profiles. The final output is a map of the sensible heat flux Q_H.

Using maps of the effective roughness length, satellite-based sea surface temperature and albedo in the DMI-HIRLAM-E model makes it possible to treat the urban area in-homogeneities with more detailed structure and specific effects. It is planned to extend this approach to the urban canopies as well. However, adequate experimental data are needed to verify the parameterisations for urban areas and to check the applicability of the linear approximation in the model for urban conditions.

3.3.3. Flux divergences

Urban heterogeneity in roughness and thermodynamic properties generates horizontal and vertical flux divergences. The flux footprint is a function of the measurement height; especially its size and distance grow with the measurement height. Vice versa, the fluxes at different heights above an urban district are generated by different footprints, inducing a height dependence of fluxes at heights where otherwise the constant flux MOST would be expected. As a consequence, in the heat and humidity budgets, vertical advection, horizontal advection, and time variations may be of the same order of magnitude and non negligible. Additionally, in the heat budget this may also be the case for the radiative flux divergences, generated by varying surface temperatures and atmospheric compositions. The influence of this breakdown of the MOST assumptions requires further assessment study.
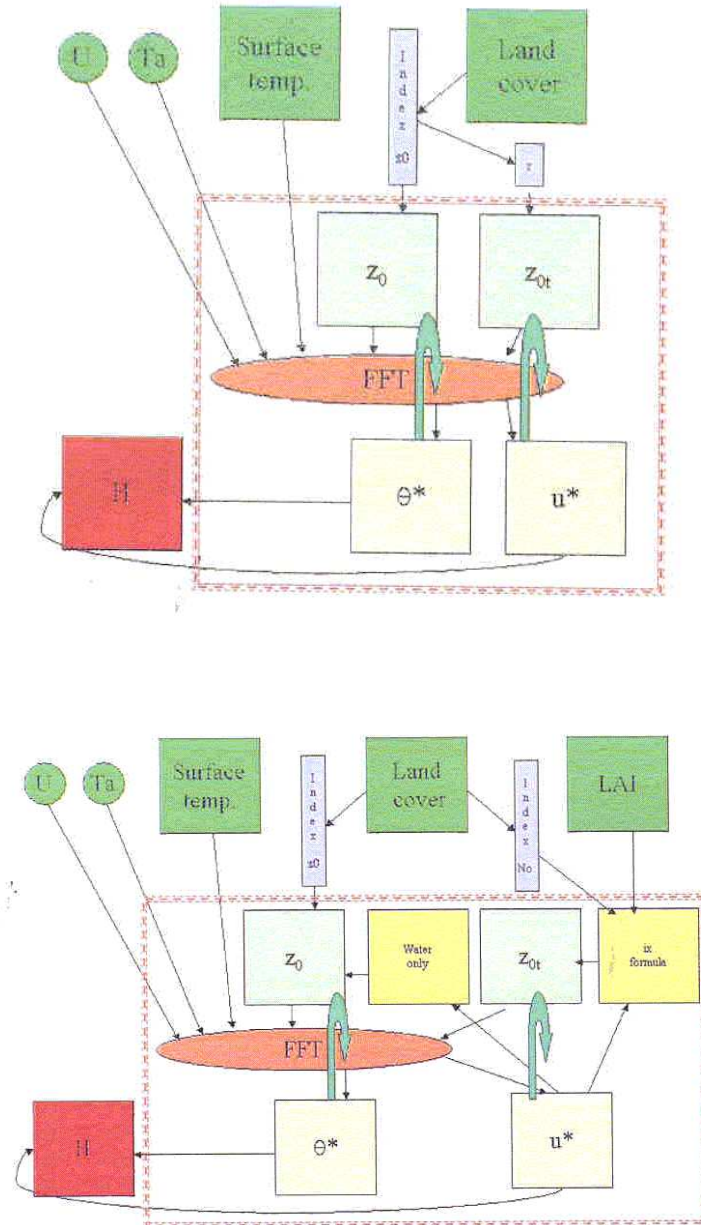
Figure 3.2: New flux aggregation technique suggested by Hasager et al. (2002): version "H" (upper panel) and version "z_{0t}" (lower panel).

3.4. Temperature roughness

The determination of the turbulent fluxes of momentum, heat and moisture in NWP models by way of bulk transfer equations requires the specification of the aerodynamic roughness length z_0 (for momentum) and the scalar roughness lengths for temperature, z_{0t}, and for moisture, z_{0q}. Most of the NWP and meso-meteorological models for surface layer profiles consider z_{0t} and z_{0q} equal to z_0. However, numerous experimental data (Garratt, 1992; Mahrt and Ek, 1993; Mölder and Lindroth, 1999) and theoretical calculations (Guilloteau, 1998) show that, especially for very rough surfaces such as urban canopies and forests, this approximation can lead to quite erroneous results for the heat and moisture fluxes. Measurements indicate values for z_0/z_{0t} of about 10 for natural vegetation (Garratt, 1992) and up to 50 and more for urban surfaces (see also Section 3.2.5).

Theoretical studies (Zilitinkevich, 1970; Brutsaert, 1975; Jensen *et al.*, 2002) suggest that the ratio z_0/z_{0t} is a function of the roughness Reynolds number $Re_* = (u_* z_0)/\nu$. However, in general this ratio is relevant mostly for moderately rough surfaces and has not been verified for urban conditions.

In the flux aggregation technique of Hasager *et al.* (2002) presented in Chapter 3.3, the following equation for z_{0t} is suggested for use in the case of a rough surface (including urban areas):

$$z_{0t}/z_0 = \exp(-23.1 u_*^{1/2}) = 7.4 \exp(-23.1 u_*^{1/2} - 2) \tag{3.10}$$

However, it is necessary to mention that the above formulation was not verified for urban conditions versus city area measurements and could be problematic for very rough urban areas.

Voogt and Grimmond (2000) studied the sensible heat fluxes over a light industrial area in Vancouver, British Columbia, Canada, from observed tower and modelled fluxes using a bulk heat transfer approach. Sensitivity analyses of the various surface temperature estimates were performed. Estimates of z_0/z_{0t} generally agreed for this area with theoretical estimates for bluff rough surfaces and were larger than those documented for vegetated and agricultural surfaces. Back-calculated values vary depending on the method used to determine surface temperature, but even more with the time of the day. Empirical relations de-

rived previously for vegetated surfaces were shown to agree well with the results for a dry urban environment, but approaches based on micro-scale variability (for different surface fractions, e.g., roofs, sunlit streets, shaded streets, different direction walls, etc) in temperature fields were problematic. So, following previous studies of Brutsaert (1975, 1982) and Brutsaert and Sugita (1996), they suggested using the following formulation for bluff-rough situations:

$$z_{0t}/z_0 = 7.4 \exp(-2.46 Re_*^{1/4}) \tag{3.11}$$

Joffre (1988a) modified one fluid dynamics assumption of Brutsaert's model concerning the level under which the log-profile is not valid by using the Reichardt's profile that has the merit to cover the full structure from the surface through the transitional layer up to the log-layer above. This yields a modification of one numerical constant in Brutsaert's model, after which the new formula perfectly fits (Joffre, 1988b) the compilation of observations of Garratt and Hicks (1973) for various bluff types of roughness over a wide range of the roughness Reynolds number ($0.1 \leq Re_* \leq 100$). This modification yields

$$z_{0t}/z_0 = 20 \exp(-7.3\kappa a_c Re_*^{1/4} Sc^{1/2}) \;\; \text{for} \;\; Re_* > 0.15 \tag{3.12}$$

where a_c is the inverse turbulent Schmidt number ($=K_H/K_M$ for z_{0t} and K_E/K_M for z_{0q}) and Sc the Schmidt number ($=\nu/D_c$, where D_c is the molecular diffusivity of the property, i.e., heat, moisture but also gaseous compounds). Thus, compared to Brutsaert's original formula with a coefficient 7.4 (Eq. 3.11), the new formulation has instead a coefficient of 20 in the first term of the right-hand side and is valid for $Re_* > 2$ (rough case only). Equation (3.12) matches the corresponding expression (3.13) valid for aerodynamically smooth case at $Re_* = 0.15$, i.e.:

$$z_{0t}/z_0 = 30(\nu/u^*) \exp(-13.6\kappa a_c Sc^{2/3}) \;\; \text{for} \;\; Re_* < 0.15 \tag{3.13}$$

A series of sensitivity studies was performed (see Section 3.2.5) using the ARPS model to evaluate the impact of the above parameters on the urban SEB. The main conclusion of this analysis is that the large ratio of the roughness length for momentum versus heat characterising cities may be the main cause of the observed high values for the heat storage flux: on the one hand, momentum

roughness is high, resulting in comparatively low wind speeds close to the urban surface, whereas on the other hand, these low wind speeds, combined with the extremely low values of the heat roughness, result in a very high resistance inhibiting turbulent heat fluxes.

Thus, it appears important to assess separately the aerodynamic roughness length, z_0, and the scalar roughness lengths for temperature, z_{0t}, and for moisture, z_{0q}, in city-scale models.

3.5. Urbanisation of NWP models for urban air pollution forecasting

A palette of urban SEB schemes and models is now available, although they are not all in the same state of validation. They range from simple transformations of some key coefficients in exchange schemes developed for the ABL over natural ground to detailed schemes computing quasi-explicitly the radiative and turbulent energy exchanges of each building element category, e.g., ground, walls and roofs, treated in groups by type. Additionally, even more detailed models and softwares are available, that compute the thermo-radiative budgets of, or interactions with, elemental building surfaces. These tools may be used to analyse experimental data from validation campaigns, to run numerical experiments on urban areas, or to perform sensitivity analysis studies. Some of the developments in the above SEB models were derived from these tools or studies, such as SOLENE (Groleau *et al.*, 2003), POV RAY (Lagouarde *et al.*, 2002; see also `www.povray.org`), and DART (Gastellu-Etchegorry *et al.*, 2004).

The development and the validation of these SEB models brought to light and helped to quantify several characteristics of the urban canopy energetics:

- A net radiation varying in time at the local scale with solar orientation and in space with district morphology, which is not much different from its rural counterpart, on average;

- A low but highly variable latent heat flux;

- A large heat storage in building materials, rather than in the ground, as a function of building density and morphology;

- A large but highly variable sensible turbulent heat flux diurnal cycle, highly dependent on district structure, often positive at night. In the

dense city centres, this flux is limited by a strong aerodynamic resistance (high z_0/z_{0t} roughness length ratio), favouring the heat storage;

- A hysteresis in the diurnal cycles, with phase lags between the energy budget components due to heat being diverted from the budget and provisionally stored in the building materials in the morning at the expenses of the sensible heat, while the stored heat is released in the evening and at night.

Modern nested NWP models utilise land-use databases down to hundred metres resolution or finer, and are approaching the necessary horizontal and vertical resolution to provide weather forecasts for the urban scale. In combination with recent scientific developments in the field of urban sub-layer atmospheric physics and the enhanced availability of high-resolution urban surface characteristics, the capability of NWP models to provide high quality urban meteorological data will therefore increase.

Despite the increased resolution of existing operational NWP models, urban and non-urban areas mostly contain similar sub-surface, surface, and boundary layer formulations. These do not account for specific urban dynamics and energetics or for their impacts on the simulation of the ABL and its various characteristics (e.g. internal boundary layers, urban heat island, precipitation patterns). Additionally, NWP models are not primarily developed for air pollution modelling and their outputs need to be designed into suitable inputs for urban and meso-scale air quality models. Therefore, a revision of the traditional approach to urban air pollution forecasting is required. The main objectives are to improve meteorological forecasts for urban areas, to connect numerical weather prediction models to urban air pollution and population exposure models, to build improved Urban Air Quality Information and Forecasting Systems (UAQIFS), and to demonstrate their application in cities subject to various European climates.

A proposal (Integrated Systems for Forecasting Urban Meteorology, Air Pollution and Population Exposure FUMAPEX) for an EU-project was initiated by COST-715 and accepted for funding (2002-2005). The scheme developed within FUMAPEX for the improvements of meteorological forecasts in urban areas, interfaces and integration with urban air pollution and population exposure models for an UAQIFS is presented in Fig. 3.3 (Baklanov, 2003). In order to achieve the innovative goal of establishing and implementing an improved new UAQIFS to assist sustainable urban development, the following steps will have

to be achieved:

1. Improve predictions of the meteorological fields needed by UAP models by refining resolution, developing specific parameterisations of the urban effects in NWP models, and adapting advanced turbulence schemes and sub-grid-scale models,

2. Develop suitable interfaces or meteorological pre-processors from NWP to UAP models,

3. Validate improvements in NWP models and meteorological pre-processors by evaluating their effects on the UAP models against urban measurement data,

4. Apply improved meteorological data to UAQIFS, emergency preparedness and population exposure models and verify results, and

5. Establish links between NWP modellers, urban air pollution scientists and the 'end-users' of UAQIFS.

In conclusion, the improvement of urban meteorological forecasts will also provide information to city management regarding additional hazardous or stressing urban climate (e.g. urban runoff and flooding, icing and snow accumulation, high urban winds or gusts, heat or cold stress in growing cities and/or a warming climate). Moreover, the availability of reliable urban scale weather forecasts could be of relevant support for the emergency management of fires, accidental toxic emissions, potential terrorist actions, etc.
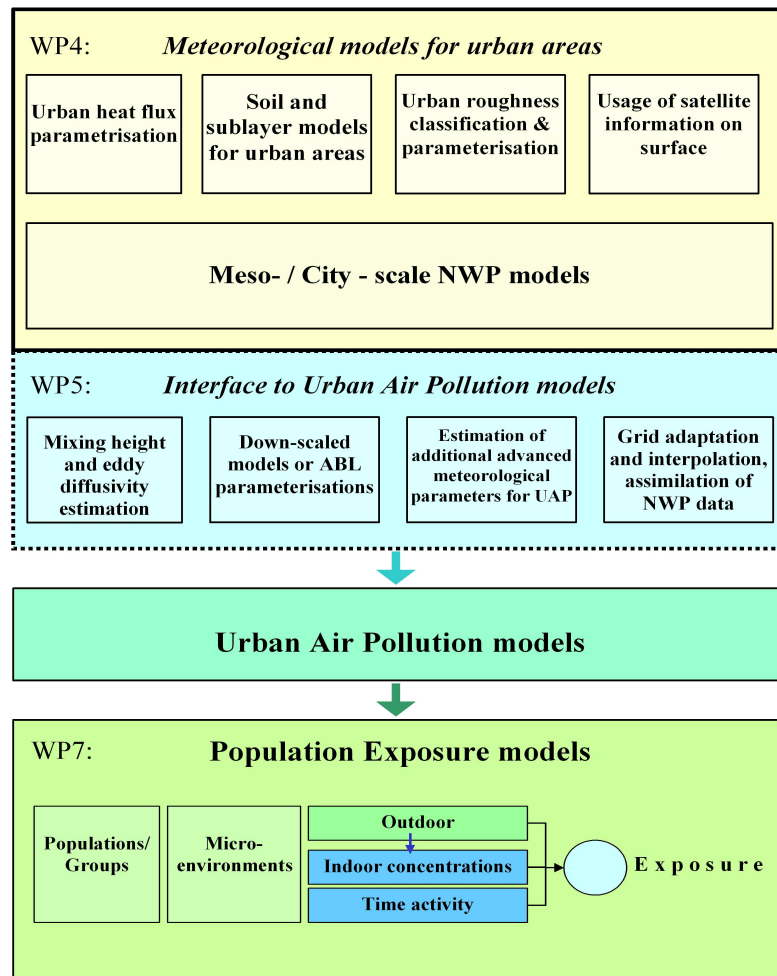
Figure 3.3: FUMAPEX scheme for the improvements of meteorological forecasts (NWP) in urban areas, interfaces and integration with urban air pollution (UAP) and population exposure models for Urban Air Quality Information and Forecasting Systems (UAQIFS).

4. Pre-processors, schemes and models for determining the mixing height

Most dispersion models require an estimate of the MH so that any effective limit on the vertical spread can be modelled. Its effect is most important when it is shallow, whereby low lying plumes may be trapped near to the ground, leading to high local concentrations, while at the same time elevated plumes might be unable to reach the ground. MH-estimates may be input to models, or calculated by specific routines within models. Both regulatory models based on traditional Gaussian plume models and new Lagrangian models for evaluating dispersion characteristics also encounter the problem of non-homogeneity over urban surfaces. Despite progresses in numerical turbulent modelling during the last decades, the MH is still one major uncertainty for most air quality models. Though no specific evaluation of the MH is necessary regarding the dispersion of traffic-originated pollution within the roughness sub-layer (e.g., within a street canyon), on the other hand, the MH is an important parameter for practically all air pollution applications at the urban and meso-scale.

4.1. Specificities of the urban boundary layer

The atmospheric boundary layer[2] (ABL) is the layer near the surface in which heat, momentum, moisture and other compounds are exchanged between the Earth and the atmosphere. The turbulent properties of this layer (diffusivity, mixing, and transport) will rule whether pollutants are dispersed and diluted or whether they build up and lead to pollution episodes. Thus, the ABL height

---

[2]In the atmosphere, vertical temperature gradients enhance or suppress turbulence formation. Convective Boundary Layer (CBL) is the layer of the atmosphere most directly influenced by solar heating of the surface: The CBL height is the height of convection during the day, where convective plumes meet a strong temperature gradient at the inversion. Acoustic echoes from the interface at the top of convection show vertical undulations and small scale features, see Caughey (1982, p.110). A Stable Boundary Layer SBL develops when buoyancy forces act to suppress turbulence; wave motion can be supported, and waves and turbulence may co-exist, a complicated situation (ibid, p. 139). A long time may be needed to approach equilibrium in SBL. Terrain slope may influence the mean winds. SBL height is the depth of significant turbulent exchange, which is increasingly restricted to a shallow layer near the ground as the inversion strength increases. Internal waves may locally produce and decay patches of turbulence, contributors to turbulent exchange. An empirical SBL height in field trials was the height at which heat flux fell to 5% of the surface flux, (ibid, p. 139). The SBL height may be less than the depth of the surface inversion.

or the mixing height (MH) will determine the volume available for pollutant dispersion and depends on basic meteorological parameters, surface turbulent fluxes and physiographic parameters, and follows a diurnal cycle. The MH cannot be observed directly by standard measurements, so that it must be parameterised or indirectly estimated from profile measurements or simulations.

The MH depends on the vertical variation of temperature in the atmosphere, and a particular type of situations are temperature inversions, which can have a significant influence on air quality such as ground-based inversions, and elevated inversions above the ABL. Inversions can be caused by several atmospheric mechanisms, such as subsidence, fronts, radiation and advection. Episodes of bad air quality are most frequently connected to radiational and advective inversions. The interdependence of mixing heights and temperature inversions was discussed during a Workshop organised jointly by the Working Groups 2 and 3 of COST-715 (COST-715, 2002c).

COST-710 (Seibert *et al.*, 1998, 2000) performed a comprehensive review of different definitions and practical determinations of the MH from measurements, by modelling and parameterisation, but only involving rural conditions and data. During the last decades, however, several experimental studies of the UBL were realised for urban areas (Baklanov, 2002). COST-715 has analysed the specificities of the urban MH and verified different methods for estimating the MH against measurements (remote sensing devices and diagnostic evaluation methods for radiosonde profiles) for several types of urban areas. COST-715 organised a Workshop to assess various parameterisation schemes to determine the urban MH (COST-715, 2002b; Rotach *et al.*, 2002). Additionally, statistical surveys of the UBL were performed as to its basic characteristics (e.g., height, inversion strength) and behaviour (e.g., growth and extent). More extended discussions of COST-715 results concerning the MH will be reported in Baklanov *et al.* (2004).

We analyse here the effects of urban characteristics for determining the MH, and assess different methods and models for estimating the MH versus new measurement data sets representing several types of urban conditions that are typical in Europe. Against the backdrop of the specificities of urban areas, the important questions to be addressed for analysing the urban MH are the following:

1. How much does the MH in urban areas differ from the rural MH?
2. How does the temporal dynamics of the MH in urban areas differ from

the rural MH?

3. What is the spatial and temporal scale of urban effects and how far downwind the 'urban plume' affects the MH?

4. How important are internal urban boundary layers in forming the urban MH?

5. What methods for estimating the MH are most suitable for urban conditions?

The urban boundary layer (UBL), in comparison with 'rural' ABLs, is characterised by greatly enhanced mixing, resulting from both the large surface roughness and increased surface heating, and by enhanced horizontal in-homogeneity of the MH and other meteorological fields due to variations in surface roughness and heating from rural to central city areas. So, it is reasonable to consider the UBL as a special case of the ABL over a very non-homogenous terrain with specific characteristics. This relates, first of all, to abrupt changes of the surface roughness and the urban surface heat fluxes at the micro-scale. A simplified sketch of the vertical structure of the UBL is presented in Fig. 4.1.
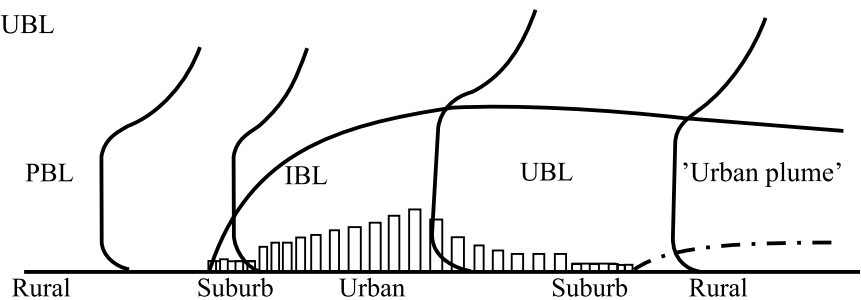
Figure 4.1: A simplified sketch of the vertical structure of the urban boundary layer with typical potential temperature profiles: a) daytime UBL, b) nocturnal UBL.

As a result of the specific features of urban areas, several issues should be taken into account for the analysis of the urban MH, i. e.:

(i) The development of an internal urban boundary layer (IBL), at the rural/suburban transition, and the so-called 'urban roughness island',

(ii) The presence of an elevated nocturnal inversion layer,

(iii) Ubiquitous strong horizontal non-homogeneity and temporal non-stationarity,

(iv) Identification of the zero-level of the urban canopy, and non-similarity between momentum and scalar exchanges ($z_0 \neq z_{0t}$),

(v) Anthropogenic heat fluxes from the street to city scale,

(vi) The downwind 'urban plume' and the spatial and temporal scale of urban effects,

(vii) Calm weather situation simulation with roughness elements channelling the flow,

(viii) Non-local character of urban MH formation,

(ix) Effect of water vapour fluxes.

In the following, we consider the various empirical, analytical, and numerical methods used to assess the MH.

4.2. Experimental methods for estimating the urban MH

As a general manner, the MH can be estimated experimentally from measured vertical profiles by several means or criteria, e.g.:

- The level where turbulence or the heat flux diminishes to, say, ∼5%, of its surface value;

- A level of discontinuity in the wind/temperature/dew point profiles (from radiosonde data);

- The level of strong back-returns from thermal discontinuities (inversions) or of strong decay of back-returns from thermal fluctuations (top of turbulent layer), such as sodars and windprofilers/RASS (Radio Acoustic Sounding System);

- The level of strong decay of aerosol back-scatter signal from lidar probing or ceilometer;

- The level of decay in turbulent motions as measured by pulsed Doppler lidars.

4.2.1 Diagnosing MH from radiosonde data

Radiosoundings are in principle relevant for estimating the MH (including operational modelling) but sounding stations are usually located outside urban areas. However, in many European countries, they are getting ever closer to or inside growing urban agglomerations and therefore, for many cities, it is becoming reasonable to analyse radiosonde data for urban MH estimation by selecting wind direction sectors downwind of the city (see Section 7.2).

Under unstable conditions, the MH is often identified as the base of an elevated inversion or stable layer[3]. Heffter (1980) formulates a criterion to analyse potential temperature profiles for such "critical" inversion height, whereby the MH is the level within the lowest layer with a potential temperature lapse rate equal to or larger than 5 K km^{-1}, where the temperature is 2 K higher than at the inversion base. Seibert *et al.* (2000) found the parcel method (e.g., Holzworth, 1967) to be the most reliable in convective situations. It is based on following the dry adiabat[4] from the measured surface temperature (or an expected maximum temperature) to its intersection with the temperature profile of the associated radiosounding. Thus, the MH is taken as the equilibrium level

---

[3]The temperature inversion will limit the ascent of thermals from the surface and is a good marker for the depth of the daytime boundary layer. Holzworth (1964, 1967) in the USA proposed that ascending air in convective conditions will usually obey a dry adiabat. Consequently the mixing depth can be determined by the height where a dry adiabat from the surface meets the environmental profile of temperature. Holzworth's method has been widely used in the USA. Holzworth had to adjust his method because the radiosonde ascents do not routinely coincide with the minimum or maximum boundary layer depths. Also the ascents are often at sites outside the cities, and some adjustment for urban heating was desired. Holzworth therefore added 5 C to the morning surface temperature.

[4]A dry adiabat Γ_d follows the decrease in temperature with height (9.8 C per km) using Poisson's equation for dry adiabatic expansion, (cf. Sutton, 1953; page 9-10.).

of an air parcel with this temperature, but depends on the surface temperature and the existence of a pronounced inversion at the top of the CBL. This method was refined by Garrett (1981), Stull (1991) and Wotawa *et al.* (1996) by adding an excess temperature at the surface ("advanced parcel method"). In the CBL, the MH is sometimes identified as the height of a significant reduction of air moisture, often accompanied with wind shear (e.g., Lyra *et al.*, 1992). A decrease of the mixing ratio of more than 0.01 g kg^{-1} m^{-1} with height is interpreted as a signal for the top of the mixing layer from day-time profile data only. This method is called the "humidity-jump" method.

A standard generic method for estimating MH is based on the **Richardson number approach**. This approach includes several variants differing in the formulation, choice of the levels over which the gradients are determined and in value of the critical Richardson number, Ri_c. It tends however to underestimate the SBL (Stably-stratified Boundary Layer) height (Seibert *et al.*, 1998; Baklanov, 2001). Following Zilitinkevich and Baklanov (2002), we can distinguish four different Ri-methods.

1. The <u>Gradient Richardson number.</u> Infinitesimal disturbances in a steady-state homogeneous stably stratified sheared flow decay if the gradient Richardson number Ri exceeds a critical value Ri_c,

$$Ri \equiv \frac{\beta\left(\partial\theta_v/\partial z\right)}{\left(\partial u/\partial z\right)^2 + \left(\partial v/\partial z\right)^2} > Ri_c, \qquad (4.1)$$

where $\beta(=g/T_0)$ is the buoyancy parameter (g is the acceleration due to gravity and T_0 a surface temperature). Accordingly, the MH is deduced from the inequalities $Ri < Ri_c$ at $z <$MH and $Ri > Ri_c$ at $z >$MH. The critical value Ri_c is derived from the perturbation analysis and generally taken as 0.25 (Taylor, 1931). This method is used in the NAME model (see Section 4.5.1) when conditions are not convective and the parcel ascent is inappropriate.

2. The <u>Bulk Richardson number.</u> An alternative, widely used method of estimating the MH employs, instead of the discrete gradient Richardson number, the bulk Richardson number, Ri_B, across the whole PBL, i.e.,

$$Ri_B \equiv \frac{\beta\Delta\theta_v h}{U_h^2} \quad \Rightarrow \quad h = \frac{Ri_{Bc}U_h^2}{\beta\Delta\theta_v} \qquad (4.2)$$

where $U_h = \sqrt{u^2(h) + v^2(h)}$ is the wind velocity at the upper boundary of the layer, and $\Delta\theta_v = \theta_v(h) - \theta_v(0)$ the virtual potential temperature increment across the whole layer. The mixing height is determined as the height where the Bulk Richardson number becomes equal to or larger than a critical Richardson number value Ri_{Bc} often taken as 0.25 by analogy with the previous approach, but other values have been suggested by different authors (between 0.1 and 3, see Table 2 in Zilitinkevich and Baklanov, 2002).

According to Vogelezang and Holtslag (1996), the bulk Richardson number method can be used both in convective conditions and in mechanical turbulence. In situations dominated by mechanical turbulence, the bulk Richardson number approach was found to be the most appropriate, whenever temperature and wind profiles are available (Seibert *et al.*, 2000). The technique is used in different models, e.g., in the DERMA model (Sørensen *et al.*, 1996).

3. The <u>finite-difference Richardson number.</u> The idea is to exclude the lower portion of the SBL, where the vertical temperature gradient is strong and critically depends on the surface value, and to determine a "finite-difference Richardson number", Ri_F, on the basis of increments $\delta\theta_v = \theta_v(h) - \theta_v(z_1)$ and $\delta U = U(h) - U(z_2)$ where $U = \sqrt{u^2(z) + v^2(z)}$ over the height intervals $z_1 < z < h$ and $z_2 < z < h$. Assuming the existence of its standard critical value, Ri_{Fc}, the equilibrium SBL height formulation becomes:

$$h \approx \frac{(h_{-}z_2)^2}{h_{-}z_1} = \frac{Ri_{Fc}(\delta U)^2}{\beta\delta\theta_v} \tag{4.3}$$

4. The <u>modified Richardson number method</u>. The above-mentioned broad variation of the SBL critical bulk Richardson number was analysed by Zilitinkevich and Baklanov (2002), who showed that Ri_{Bc} is not a constant but apparently increases with increasing free flow stability expressed through the Brunt-Väisälä frequency N (see Sections 4.3.1-2) and most probably depends also on the surface roughness length, the Coriolis parameter and the geostrophic wind shear in baroclinic flows. The Richardson-number-based calculation techniques can be recommended only for rough estimates of the SBL height. For practical use, Zilitinkevich and Baklanov (2002) recommended to use a function for the critical bulk Richardson number, e.g.:

$$Ri_{Bc} \approx 0.1371 + 0.0024\frac{N}{|f|} \tag{4.4}$$

The effect of surface roughness on the critical Richardson number is discussed in Gryning and Batchvarova (2002, 2003). They argue that the Richardson number is a function of the surface roughness, a small surface roughness is associated with a small critical Richardson number. For the marine boundary layer a value 0.03 gave overall best fit when using the method of Sørensen (1998) and 0.05 for Vogelezang and Holtslag (1996).

Another simple method is the method used routinely at the Finnish Meteorological Institute (FMI) for stable mixing height calculation (Karppinen *et al.*, 1998) that uses only the potential temperature gradient to estimate the stable mixing height h(e.g. it makes the strong assumption that the stable mixing height is directly proportional to the inversion height). Calculations are based on mast measurements from the suburban site of Helsinki/Kivenlahti and radiosoundings from the rural site of Jokioinen.

$$ h = \frac{4.5}{g_1 + 0.005}; \quad g_1 = \frac{(\theta_2 - \theta_1)}{(z_2 - z_1)}; \quad g_1 > 0.01 \text{ °K m}^{-1} \quad (4.5) $$

where θ_1 and θ_2 are the potential temperatures measured at two levels z_1 and z_2.

4.2.2 MH interpreted from sodar/lidar/radar/ceilometer

Radiosondes may be restricted by air traffic control requirements near cities. The different types of vertical profilers (sodars, lidars, radars, ceilometers, etc) have the potential to provide better and continuous information on the vertical structure of the ABL and to estimate the MH than radiosondes. Their main weaknesses arise from the limitation on their use in urban areas (e.g. due to noise) and the need of expert personnel so that usually they are not in operational use. However, for some specific problems (e.g. for nuclear emergency preparedness systems, wind energy and other research purposes) they are permanently used and could be used for the MH estimation in urban or semi-urban areas.

The **sodar** records the intensity of acoustic backscatter of the air S, which is proportional to the structure parameter of the acoustic refractive index C_N^2, which in turn mainly depends on the temperature structure parameter C_T^2. The measurement fails in case of stronger rain or snow, perfect adiabatic conditions due to strong thermal mixing, and large noise from the surroundings. Only in-

homogeneities in the temperature field in the order of half of the wavelength of the sound waves from the sodar contribute to S. Normally this is within the 'inertial sub-range' of the turbulence spectrum. Therefore S contains information on the structure of the turbulence in the boundary-layer, but not on the sign of the vertical temperature gradient. In case of a vanishing vertical gradient of potential temperature the backscatter intensity of the air is low even if there is still turbulent motion. During weather situations with weak winds and strong thermal inversions the contribution of the mean vertical temperature gradient to S can be at least as large as the contribution from the turbulent motion (Beyrich, 1997). This allows the detection of stable layers at night. The range of the instrument with respect to sound reflectivity is usually larger than with respect to the identification of a Doppler shift.

For sodars, the MH can be deduced from the vertical profile of the echo intensity or from a spectral analysis of the vertical velocity. Methods based on the former have been summarised by Beyrich (1997). The mechanical MH at night is associated with the height of the largest gradient in the nocturnal echo profile. After sunrise, the upper boundary of the growing mixing layer often coheres with the height of the echo intensity maximum in the vertical profile. The "echo intensity" method is however restricted by the vertical range of the sodar (at most 500 m). There are sodars that deliver acoustic backscatter information from larger heights, e.g., the sodar used in Hannover, Germany (Sections 5.10 and 7.3.1) recorded the acoustic backscatter up to 1200 m. Sodar manufacturers sometimes offer internal routines for MH determination (e.g., REMTECH, 1994), whereby the characteristic frequency scale of the most energetic eddies is deduced from the power spectrum of the vertical velocity distribution. Multiplying this value with the wind speed scale yields an estimate for the MH. With such a method, a mixing height can be estimated even if it is well above the maximum range reached by the sodar. Baumann and Piringer (2001) compared the two approaches for a REMTECH PA2 sodar and found no correlation using a two-year data set. Kuchin and Baklanov (2002) also found that the REMTECH factory routines for MH determination based on σ_w were not suitable for SBL conditions in the Arctic. Piringer and Baumann (1999a) found a better statistical agreement when sodar MH determined from the power spectrum of the vertical velocity instead of those derived from the echo method is compared to MH determined with a meteorological pre-processor and to those diagnosed from radiosoundings. The only existing long-term sodar study on the MH over cities was undertaken by Lokoshchenko (2002) for Moscow.

a   b
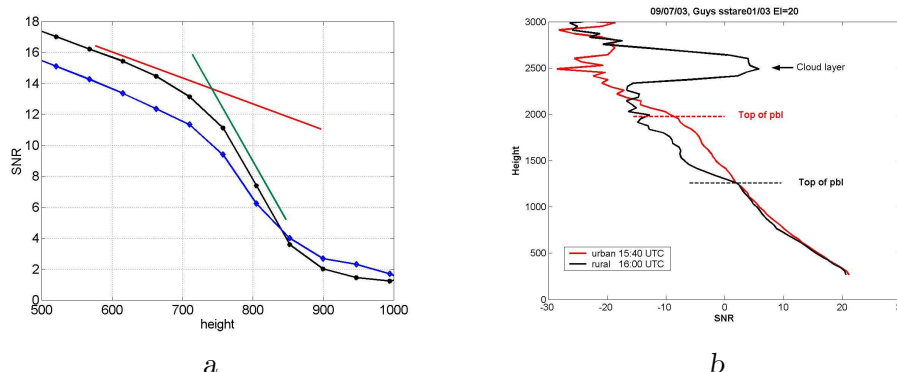
Figure 4.2: The signal-to-noise ratio (SNR) profiles from the lidar data: (a) SNR
profiles from QinetiQ data on 18th March 2003 at 16:00 (black) and at 18:50
(blue). The red and green lines denote the slopes of the SNR due to atmospheric
attenuation and the top of the boundary layer, respectively (from Davies et al.,
2003); (b) Comparative vertical structure (m) of SNRs (dB) on 9th July 2003
and possible interpretation of the MH for the urban and rural conditions (from
Middleton and Davies, 2004).

The ABL height can be derived from **lidar** data in various ways. The lidar
may measure both Doppler wind velocity and back-scatter intensity. The back-
scatter intensity is a function of the system properties, atmospheric attenuation
(due to the atmospheric water vapour content), the returned power (and thus
the measurement range) and the aerosol loading of the atmosphere. In urban
regions, where atmospheric aerosol concentrations are high, there is a large
back-scatter signal in most meteorological conditions.

At the top of the ABL, the temperature inversion traps pollutants within the
boundary layer. Above the top of the boundary layer, aerosol concentrations are
generally a few orders of magnitude lower. This drop in aerosol concentrations
reduces the back-scatter intensities measured with the lidar and can be used to
infer the height of the ABL top. The loss of lidar signal intensity and drop in
SNR (signal-to-noise ratio), or decrease in turbulence, are markers for the MH,
as follows below.

A pulsed lidar receives back the Doppler shifted velocities from the backscat-
tering particles, dust, aerosol, or cloud droplets. A spectrum of velocities is
obtained, corresponding to the motions of the particles. Return signal power di-
minishes rapidly with increasing range, following the radar equation. In cleaner
air, as above the polluted mixing layer, the number of back-scattering particles

diminishes. This reduces the return power and increases SNR (in dB). A graph of signal to noise ratio versus range or height for a beam inclined above horizontal, will drop as a smooth curve due to the radar range effect and attenuation by humidity. Additionally, more erratic changes in SNR occur as the number of scatterers in each sample of the atmosphere varies. The SNR method is essentially relying on the assumption that there are much less scattering polluting particles above the boundary layer top. Thus, the data interpretation must be done with care and experience, as other complicating factors may arise, depending on prevailing conditions. For example, cloud droplets may allow partial penetration, or complete blocking of the beam; the useful working range may decrease as cloud passes overhead and SNR rises rapidly once there is no useable signal strength.

Davies *et al.* (2003) and Middleton and Davies (2004) used pulsed Doppler lidars to simultaneously monitor profiles of turbulent fluctuations (velocity variance) and the aerosol back-scatter intensity with height. The lidar orientation is kept stationary for a period in order to accumulate turbulence statistics, before scanning to a new direction. The work compares the decay in turbulent motions with the decay in signal intensity (from SNR). The aerosol, largely concentrated in the ABL, can be employed to detect the MH. Figure 4.2 illustrates how the change in SNR from the usual rate of attenuation to the loss of signal on leaving the ABL can be seen as a change in gradient. The SNR profile from the lidar data in Figure 4.2a shows two gradients: normal atmospheric attenuation (red) and a sharper cut off caused by the attenuation due to the boundary layer top (green). The top of the boundary layer can be estimated from the height at which the gradient changes. The blue line in the figure is the SNR profile on the same day but after sunset. In this case the gradient change is not so well marked. Figure 4.2b demonstrates the comparative vertical structures of SNRs on 9th July 2003 for the urban and rural conditions and possible interpretations of the MH (Middleton and Davies, 2004). These plots illustrate the possibilities of the method in seeing differences of the MH over rural and urban landscapes.

Further work is in hand (Davies *et al.*, 2004) to compare various measures of MH and other dispersion parameters at an urban site in West London, UK, including use of the back-scatter coefficient. The advantage with these pulsed Doppler lidars is that both criteria, the turbulence and the signal strength, may be evaluated and compared when determining ABL height. A disadvantage is that the equipment is complex and needs experienced personnel and care in interpretation. Since the instruments have a scanning capability and a range of several kilometres according to conditions, it is possible to orient the beams

over a city, then over the approach fetch, to attempt urban-rural comparisons (Collier *et al.*, 2004; Middleton and Davies, 2004). They are thus powerful research tools; Davies *et al.* (2003) discuss dispersion parameters via lidar data.

During the BUBBLE experiment in Basel (see Section 5.1), urban Aerosol Mixed Layer (AML) heights were determined from the derivative of the logarithm of the range-corrected lidar signal. In this approach, a given level is identified as the AML height, if it exhibits the lowest substantial gradient (i.e., a local minimum in the derivative) with an additional constraint of continuity in time. Steyn *et al.* (1999) have fitted an idealized profile to lidar back-scatter data to determine the MH and entrainment zone thickness.

If the convective boundary layer is physically well defined, **wind profiler radars** (WPR) can find the mixing height from the reflectivity (roughly the product of humidity gradient and turbulence intensity) profiles. Several examples of the MH estimation by wind profiles in different meteorological conditions are presented by Angevine (2003). He concludes that WPRs are very useful in the determination of the MH but other instruments (e.g., ceilometers, etc.) greatly help in the interpretation, since simple automatic procedures are expected to work in only very simple situations. The profilers give very good information of the morning transition of the boundary layer (nocturnal stable to convective) whereas in the afternoon, the reverse transition (from convective to stable) is much more difficult to track with profilers, whence the residual inversion often shows stronger reflectivity maxima, leading easily to erroneous interpretation. However, spectral width profiles can be used to distinguish between active turbulent regions from developing residual layers.

The radio acoustic sounding system (**RASS**) is an extension to a coherent radar that allows for the measurement of the virtual temperature profile above the radar. It uses an acoustic source to generate a vertically propagating sound wave in the radar's scattering volume. This sound wave can either be a short pulse or a band-limited frequency-modulated continuous wave. RASS temperature retrievals are sensitive to the wind component parallel to the sound beam and the humidity. The influence of the wind on the measurements can be used to retrieve profiles of the horizontal wind components. RASS can be used as an extension of wind profiler radar (WPR) or Doppler sodar. The achieved height range depends not only on the system but also on a suite of atmospheric conditions, which include temperature, wind, humidity and turbulence. According to the COST-76 (2003) results, a vertical range of 2000 to 3000 m can be achieved

with a 482 MHz WPR/RASS, while with a 1235 MHz WPR/RASS, about 1000 m can be reached. The vertical range of a 1290 MHz Doppler RASS is limited to several 100 m. It seems that so far no systematic evaluation of RASS virtual temperature measurements for longer periods is available, as RASS has been used primarily for research programs. An example of RASS measurements will be given in Section 7.5.2.

Electromagnetic backscatter is generally the best option for determining the (high) afternoon CBL heights. Among this category, the **ceilometer** is found to be a very useful instrument in clear sky conditions as it is the only instrument (compared to RASS/sodar) which gives directly the vertical aerosol profile. Ceilometers originally designed just for cloud base height measurements have become available also for atmospheric profiling (Rogers *et al.*, 1997; Räsänen *et al.*, 2000; Münkel *et al.*, 2002). They have an improved vertical resolution (now about 15 m) and a much smaller lower detection range limit (now about 30 m above ground) (Emeis *et al.*, 2004). In the project VALIUM, Emeis *et al.* (2004) utilised different remote sensing instruments, including ceilometer, in a measurement campaign in 2002 in the city of Hannover. Their results showed that sodars are able to follow the CBL development only during the first half of the day: the afternoon CBL is either too high for the sodar range, or the potential temperature gradients are not strong enough to reflect sound waves.

Ceilometer is also by far the most "low cost"/"easily handled" remote sounding equipment considered here (its potential being similar to single-frequency lidar), and its vertical range (from the lowest range gate of 15 m up to 2-3 km) is well-suited for ABL studies.

4.2.3. Commercial aircraft measurements / AMDAR Data Processing

New opportunities for estimation of the MH and profiles of potential interest to the air pollution meteorologist have recently arisen from the AMDAR (Aircraft Meteorological Data Reporting) communication system (AMDAR, 2003) and a joint European EUMETNET-AMDAR project (E-AMDAR, 2002) looking at the use of data from civil aircraft, to complement to existing radiosoundings. This EUMETNET AMDAR system uses the aircraft sensors for measuring wind speed and direction, air temperature, altitude, a measure of turbulence and the aircraft position. Data are archived by meteorological services alongside more traditional synoptic observations and yield profiles of temperature and wind near airports close to most of the European large cities. Data processing yields

meteorological measurements representative of the free air-stream in the vicinity of the aircraft. Errors in reported wind and temperatures are comparable with those of radiosonde systems.

AMDAR data were retrieved from the UK Met Office archives (MetDB) to plot the profiles of potential temperature for the days of the urban lidar study cited in the previous Section (Middleton and Davies, 2004; Davies *et al.*, 2003). In order to do this, the altitude must be converted back to a pressure estimate, with allowance for the altimeter corrections applied by pilots. Useful profiles for the ABL can be generated every day near London (where many civil aircraft are present and data available for much of the day, but not at night due to noise restrictions on night flights). They replace the gap left when radiosoundings ceased in the London area in the 1990's.

Figure 4.3 plots the AMDAR profiles of the potential temperature θ versus altitude z for the morning and afternoon of 18 March 2003 for aircraft near Birmingham airport. They show clearly a mixed region up to 450 m in the morning, or 600 m in the evening. The discontinuity in potential temperature is very clear to see on this day. Some issues need further consideration, including improvements in processing, the evaluation of AMDAR data relative to other observations/model products, and the usefulness (or otherwise) of the AMDAR information for air quality studies. Their use and validity for dispersion studies is still under investigation, and there may be further refinements and developments to the AMDAR data processing program. Thus, in the absence of radiosonde ascents over cities or at trials sites, the AMDAR data offer useful profiles in the lower atmosphere. Standard objective methods for the determination of the MH from profiles (e.g., parcel ascent, Ri-number) may then be applicable to the AMDAR data.

4.2.4. Mixing heights deduced from tracer data

Natural earth radioactivity can be used as an indicator characterising the processes occurring in the ABL. The main source of radon ^{222}Rn in the atmosphere is radon escaping from the soil. This isotope is a noble gas and its half-life is equal to 3.82 days. Radon ^{222}Rn is a product of the decay of radium ^{226}Ra isotope which is a member of the uranium ^{238}U series. Radon is an unstable gas and does not accumulate and cannot be found in larger amounts in the rock. One can thus assume that the "age" of the radon does not exceed a few days. Radon abundance in soil depends on geological composition, geochem-
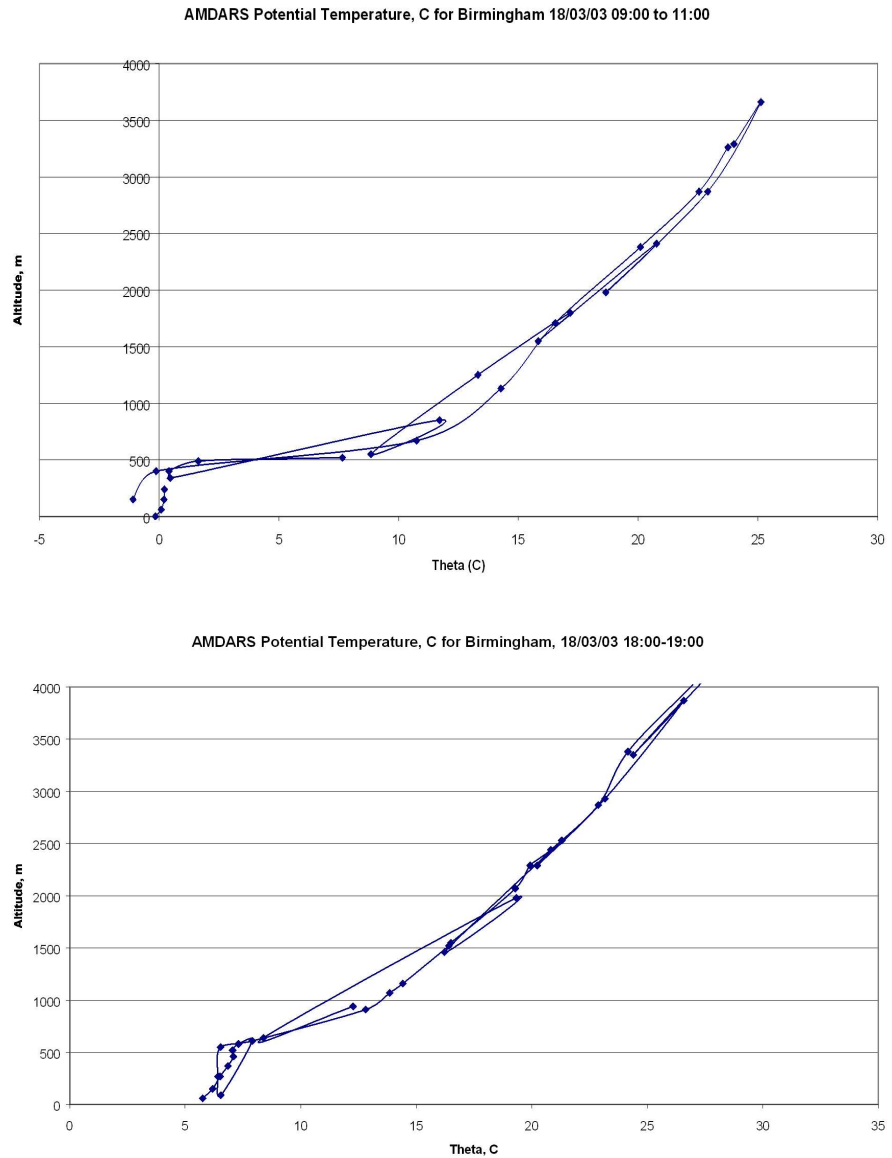
Figure 4.3: AMDAR profiles of θ versus altitude z for aircraft at the Birmingham airport for the morning (left) and afternoon (right) of 18 March 2003 (from Davies et al., 2003).

istry and geodynamic phenomena influencing the concentration of this gas in the atmosphere. Radon ^{222}Rn accumulated in the air decays producing radioactive isotopes of polonium, lead and bismuth: ^{218}Po, ^{214}Pb, ^{214}Bi, ^{214}Po. The first one has a half-life of 3.05 min.; this half-life is very short in relation to radon. Therefore these two isotopes, radon ^{222}Rn and polonium ^{218}Po, are close to the equilibrium state (their activity concentrations are almost equal).

In ambient air, gaseous radon undergoes dispersion and dilution. Measurement of radon ^{222}Rn concentrations and its short-lived daughter is thus one possibility to obtain information on the dynamics of the lower boundary layer (Fujinami and Esaka, 1988; Porstendörfer *et al.*, 1991; Allegrini *et al.*, 1994; Kataoka *et al.*, 1998). Radiometric methods with radon were mainly used so far to evaluate the mixing height (Guedalia *et al.*, 1974; Allegrini *et al.*, 1994; Kataoka *et al.*, 1998). On the other hand, radon is a water soluble gas and radon decay products adhere to water vapour molecules, gases and atmospheric dust forming clusters, free fractions and radioactive aerosols (Nazaroff, 1988, 1992). Thus, when high air humidity occurs near the surface layer, the measured radon concentration can be underestimated. Therefore, measuring ambient polonium ^{218}Po concentrations instead might be more relevant. Immediately after the decaying of radon, about 80-82% of ^{218}Po occurs as positive ions that are attached to air gas molecules and water particles within 10^{-7}second. This formation is called clustering (free atoms and clusters are called unattached fraction). Then the clusters can generate bigger particles called attached fraction.

The dependence of polonium ^{218}Po activity on the vertical thermal stratification shows up in the increased accumulation during steady equilibrium (nocturnal layer of ground temperature inversion) and in the decrease of activity when the atmosphere becomes unstable. Thus, an empirical simple power law formulation based on measurements, can be assumed to describe the relationship between polonium concentration (C_{P_0}) in air and an "equivalent mixing layer height" ($h_{eq_{mix}}$).

$$h_{eq_{mix}} = \frac{B}{\sqrt{C_{P_0}}} \qquad (4.6)$$

where the constant B depends on meteorology and specific local features of the radon release (Osrodka *et al.*, 2003).

The method can reflect the inertia of polonium concentration changes in relation

to changes of the MH $h_{eq_{mix}}$. The correlation coefficient improves when the height of the mixing layer is averaged over a period longer than 1 hour. The following relation was developed to take into account the time delay (ΔT – in hours) between polonium concentration and the MH evolution $C_{P_0}(t + \Delta T) = \alpha \left[h_{eq_{mix}}(t) \right]^{\beta}$. After appropriate conversion, the following differential equations are obtained:

$$h'_{eq_{mix}}(t) = \xi \frac{C'_{P_0}(t + \Delta T)}{C_{P_0}(t + \Delta T)} h_{eq_{mix}}(t)$$

$$h_e(t) = h_e(t - \Delta t) \left(1 - \xi \frac{C_{P_0}(t + \Delta T) - C_{P_0}(t + \Delta T - \Delta t)}{C_{P_0}(t + \Delta T)} \right)^{-1}$$

(4.7)

where α, β and ξ are empirical coefficients. These equations describe the diurnal variation of the height of the mixing layer as a function of the polonium concentration in air. Consequently, the MH can be calculated for any time knowing its value and polonium concentration for the time specified (Krajny *et al.*, 2004). However, one should notice that such type of model is not calibrated and is strongly site-specific, so that it cannot be widely recommended.

During the period 2000-2003, measurements of polonium isotope ^{218}Po in two cities (Cracow and Katowice) in southern Poland were used for the assessment of the MH (see Section 7.6). These experiments were performed when the height of the mixing layer was well defined, i.e., summertime, anticyclonic and sunny weather, with clear skies and light winds (see Section 5.5).

4.3. Mixing height parameterisations and pre-processors

The most common approach used in dispersion models to get MH values is its calculation from specific parameterisations and pre-processors. This approach is suitable to the use of *in situ* measurements or NWP-derived profiles. So far, parameterisations of the MH have been developed and validated mostly using rural homogeneous conditions, so that their applicability to urban conditions should be verified. Some authors have suggested specific methods for MH determination in urban areas. They can be classified in two main categories: (i) using a local correction to the heat fluxes and roughness to incorporate urban effects and, (ii) estimating the internal boundary layer (IBL) height growth as

the flow moves over a city. We address in this Section the first category, usually based on classical methods for homogeneous terrain, but using urban values for the heat flux and roughness. The second category is based on the general methods for the growth of the IBL height following an abrupt change of surface roughness and will be addressed in Section 4.4.

4.3.1. Classical ABL formulae

For the estimation of the MH in urban areas, most authors use a standard 'rural' diagnostic method for stable conditions and a prognostic equation for unstable conditions, but without any corrections for urban features (e.g., Seibert *et al.*, 1998). The most commonly used diagnostic formulae are listed in Appendix 1. The properties of the ABL are primarily described within the theoretical framework of similarity relations by which the variability of the structure of the ABL can be explained by the variation in the scales of the phenomena. The general similarity theory (Zilitinkevich and Deardorff, 1974) relates the surface turbulent fluxes to the bulk ABL structure in terms of observational variables.

The basic internal scaling quantities are the friction velocity u_*, the temperature scale T_*, and three length scales: the Monin-Obukhov-(MO) length L, the vertical height z and the ABL height h. The friction velocity acts as a scaling velocity under most conditions except strong convective conditions when the mean horizontal wind decays and the convective velocity $w_* = (\beta Q_0 h)^{1/3}$ becomes the relevant scale ($Q_0 = Q_H/\rho c_p$ is the kinematic heat flux). Under unstable conditions (but not free convection), when both mechanical and buoyant production of turbulence are active, u_* should be complemented by w_* through a linear combination (Driedonks and Tennekes, 1984). Under extreme stable conditions, when turbulence is intermittent and the wind field is undetermined, u_* might also be inapplicable, but there is no theoretical scale to replace it. When the surface heating/cooling is non-zero, the surface heat flux Q_0 is the other driving force setting up the structure of the boundary layer and yielding the temperature scale $T_* = -Q_0/u_*$. ABL meteorology has traditionally combined the effect of momentum and heat flux through the MO length scale $L = -u_*^3/\beta\kappa Q_0$ (β is the buoyancy parameter and κ the von Karman constant). The dimensionless parameters z/L and h/L act as stability parameters (determining whether the ABL is stably, neutrally or unstably stratified) in the surface layer and the whole ABL, respectively. These parameters have supplemented or replaced the empirical Pasquill classes in state-of-the-art dispersion models or procedures.

Additionally, the ABL structure is determined by the following external parameters: (i) the wind velocity at the top of the layer (or the geostrophic wind speed G), (ii) the Coriolis parameter f arising from Earth's rotation, (iii) the roughness of the surface described by the roughness length z_0, a measure of the height of typical surface irregularities, and (iv) the Brunt-Väisälä frequency N ($N^2 = \beta\gamma$, with γ the potential temperature gradient above the ABL), representative of the background stratification into which the ABL evolves (see next Section 4.3.2). In uniform, homogeneous, steady conditions, the ABL structure and variability is expressed as a combination of dimensionless ratios of these scales.

If these parameters are to be useful for the description of the ABL structure and pollutant dispersion in a practical way, they must be available at any site. Estimates of the friction velocity u_* can also be made routinely from the near ground wind, if the surface roughness conditions are well characterised. However, this is seldom the case in urban conditions. A number of different methods have been proposed and used to determine the surface heat flux on a routine basis. The most referred ones are the method of van Ulden and Holtslag (1985) and of Berkowicz and Prahm (1982). COST-710 (1998) reviewed and tested some of them based on rural data. Possible errors and differences between methods used in this pre-processing can be of comparable or even greater importance to errors occurring in the dispersion modelling itself. The Coriolis parameter f is fixed by the latitude of the site ($f = 2\Omega\sin\phi$ at latitude ϕ and earth's rotation $\Omega = 7.292.10^{-5}$ rad s^{-1}), and the roughness length z_0 is mostly determined by the characteristics and arrangements of the surface elements at the site of interest (see Section 2). The geostrophic wind speed G is determined by synoptic meteorology on a regular basis at any location.

However, the meteorological variables routinely calculated by operational meteorological models do not always provide all the necessary meteorological quantities required to determine all scaling parameters. Moreover, the values provided by NWP models for turbulence scaling parameters can sometimes be not suitable for dispersion calculation due to, e.g., changes of space scale and resolution of the considered air pollution phenomena. Thus, additional calculations and interpolation of data from routine meteorological stations may be necessary.

A few tests of the applicability of the simple scaling formulae of Appendix 1 for specific urban sites have so far yielded non-conclusive results due to the lack of real reference MH values (e.g., Berman *et al.*, 1997; Lena and Desiato, 1999). However, a comprehensive analysis of their applicability has not been

carried out yet. The main problem of such diagnostic methods is their assumption of horizontal homogeneity. Therefore, it is difficult to expect that they are applicable to city peripheries (with sudden changes of roughness), whereas they might be used in central (relatively homogeneous) areas of certain cities, because the physical mechanisms behind the MH formation are the same there as for other types of surface. Nevertheless, this weak agreement with measured urban MHs is not only due to the urban features since they do not yield very satisfactory results either for rural and/or homogeneous conditions (Seibert *et al.*, 2000; Baklanov, 2002; Zilitinkevich and Baklanov, 2002). Thus, for SBL cases, it is reasonable to use MH methods, which consider either vertical profiles or roughness and surface fluxes as input parameters, since, in the latter case, they can be used for urban conditions with corrections for the heat flux and surface roughness.

4.3.2. Approaches using free flow stability

Though the surface layer is well described by the classical MOST (Monin-Obukhov similarity theory) in nocturnal SBLs (i.e., flux-dominated, typical for mid-latitudes), and simple (local) pre-processors are expected to perform well, however, this traditional concept fails for long-lived SBLs occurring below the stably stratified free flow (common in Northern Europe). A new theory suggested by Zilitinkevich (2002) for third-order transport due to internal waves and non-local turbulence in the stably stratified surface layer shows that such pre-processors based on the classical MOST are not describing the long-lived SBL correctly. An extended (non-local) version of SBL theory including the Brunt-Väisälä frequency N, representative of the layer just above the ABL top, is needed to correctly describe the SBL. This extended theory also explains why it is possible that developed turbulence in SBL can exist at much larger Richardson numbers than the classical theory predicts ("upward" radiation of internal waves from SBL leaves more room for generation of turbulence by velocity shear). Therefore, Zilitinkevich *et al.* (2002) and Zilitinkevich and Baklanov (2002) suggested new diagnostic and prognostic formulations for the SBL height, which include the third-order transport due to internal waves and non-local turbulence in the stably stratified surface layer (see Eqs. 7 and 8 in Appendix 1). This formulation does not display the underestimation of MH in strong SBLs by the formulation of Zilitinkevich and Mironov (1996). Furthermore, Zilitinkevich and Esau (2003) have incorporated baroclinic effects into the above formulation.

An equivalent method was independently derived by Kitaigorodskii and Joffre (1988) based on an integrated formulation of the TKE equation that yields analytical formulae for the MH depending on the stability parameter $\mu_N = L_N/L$, where $L_N = u_*/N$ and L is the MO-length. Here again, N represents non-local effects through background stratification at the top of the ABL. Joffre *et al.* (2001) investigated the variability of the stable and unstable boundary layer height over a forest (i.e., roughness conditions comparable to those of a city). They found that under both stable and unstable conditions, a great deal of the variability of the mixing height is well described by the expressions of Kitaigorodskii and Joffre (1988) through the scales L_N and Lwhile the dimensionless parameter N/f acts a secondary explaining parameter. They also showed that this integral formulation yields better results than some of the above-mentioned simple algorithms. Joffre and Kangas (2002) derived more accurate values of the physical constants embedded in this Kitaigorodskii-Joffre model (see Appendix 1). They also showed that these expressions for h are not strongly sensitive to a wide variation of roughness conditions, so that they can probably be applied to urban conditions, provided that the surface fluxes are representative of the urban canopy.

The use of N in diagnostic formulation obviously implies some pre-knowledge of the MH itself, since N should represent a layer, say, 100-300 m deep, just above the MH. For this purpose, one can use either some climatological information of the local MH or actual $h-$estimates from a previous time step of the model or from a previous atmospheric sounding (radiosondes or remote sensing) representing similar atmospheric conditions. Then, taking into account the probable meteorological tendency, one can use an atmospheric layer safely above h. As the value of N does not vary in practice within a broad range, the exact value of N should not be too critical for the estimate of the MH. Furthermore, since N represents conditions above the UBL, which should be more spatially homogeneous than those close to the surface, then, even when the vertical temperature profile (in general a radiosounding) is not from exactly the urban site under consideration, this should not be of dramatic consequence on the accurate value of N. For the period before the night-time radiosounding (in Europe), this procedure should be carefully applied depending on the situation during the previous day.

For more accurate SBL height calculations within 1-D and 3-D models, respectively, the diagnostic and prognostic formulations of Zilitinkevich *et al.* (2002) are recommended. It is necessary to mention that diagnostic methods for estimating the urban MH are often not good enough due to the strong horizontal

non-homogeneity and temporal non-stationarity of the UBL and the non-local character of the urban MH formation. Nevertheless, the mechanisms involved in the formation of the daytime MH (or CBL) are better understood than the corresponding ones at night time. Therefore, it is strongly recommended that more emphasis should be given to improving the methods for the night time MH determination.

4.4. Internal boundary layer development over an urban area

In this Section we turn to the second category of MH-schemes based on a general method describing the growth of the IBL height following an abrupt change (smooth-to-rough) of surface roughness. Just a few authors have suggested such a method specifically for the urban MH.

Formulae for the IBL height were actively developed principally for coastal sites (e.g., Panovsky and Dutton, 1984; Walmsley, 1989; Garratt, 1990; Wright *et al.*, 1998). The same approach can be used for the height of the urban IBL, the so-called downwind 'urban plume' (see Fig. 4.1). For instance, Henderson-Sellers (1980) developed a simple model for the urban MH as a function of distance downwind into the city. Nkemdirim (1986) tested and further improved the Summers (1965) formulation for the urban MH:

$$h_\alpha = \left[\frac{2Q_{Hc}x_k}{\rho c_p \alpha U_a} \right]^{1/2} \tag{4.8}$$

where Q_{Hc} is the cumulative heat flux between x_0 and x_k; x_k being the downwind distance, α is the difference between the dry adiabatic lapse rate and the prevailing lapse rate at x_0, and Ua is the reference wind speed. The formulation was verified for the cities of New York and Calgary. It was shown that it could be used for a rough MH estimation, but only for wind velocities $U_a < 4 \ \mathrm{m\,s^{-1}}$.

Estimates of the height of the thermal IBL for Athens were compared to the ATHIBLEX data of Melas and Kambezidis (1992). The estimated IBL heights were derived from three slab methods: (i) Gamo *et al.* (1983), (ii) Venkatram (1986), (iii) Gryning and Batchvarova (1990), as well as from (iv) a simple empirical diagnostic method (as a function of the distance to the city along the wind direction), and (v) from one similarity model (Miyake, 1965). It was found

that the similarity model of Miyake (1965) failed to give any reasonable prediction, indicating that models should not be extended beyond their stability and fetch range. Relationships based on the slab models showed a high correlation with observations, but the thermal IBL heights were always under-estimated by the models unless both convective and mechanical turbulence were taken into account. The formulation proposed by Gryning and Batchvarova (1990) was found to be in good agreement with the measurements. Within the range of the local equilibrium concept, the thermal IBL height is assumed to grow with the downstream fetch x as x^p where the exponent p depends upon several IBL parameters.

In Gryning and Batchvarova (1996), the above mentioned zero-order scheme slab model was extended for the IBL over terrain with abrupt changes of surface for near neutral and unstable atmospheric conditions, yielding:

$$
\left\{ \frac{h^2}{(1+2A)\,h - 2B\kappa\,L} + \frac{Cu_*^2 T}{\gamma\,g\,[(1+A)\,h - B\kappa\,L]} \right\} \times
$$
$$
\times \left(\frac{\partial\,h}{\partial\,t} + u\frac{\partial\,h}{\partial\,x} + v\frac{\partial\,h}{\partial\,y} - w_s \right) = \frac{Q_0}{\gamma}
$$

$$(4.9)$$

where u and v are the horizontal components of the mean wind speed in the IBL in the x- and y-directions, γ - the potential temperature gradient, w_s - the mean vertical air motion above the boundary layer, Q_0 is the kinematic heat flux, and A, B and C empirical dimensionless constants. The vertical velocity can be estimated when the horizontal divergence of the large-scale flow is known as a function of height. Alternatively, Gryning and Batchvarova (1999) devised a method based on the rate of warming caused by subsidence of the free atmosphere that can be determined from successive radiosoundings. The constants most suitable for this model are discussed in Källstrand and Smedman (1997). The model includes coastline curvature and spatially varying winds and was solved numerically for the IBL height of an urban area with a coastline and showed good applicability (Batchvarova and Gryning, 1998; Batchvarova *et al.*, 1999; Gryning and Batchvarova, 2001).

Batchvarova *et al.* (1999) tested the ability of two quite different models to simulate the combined spatial and temporal variability of the IBL in an area of complex terrain and coastline during one day. The simple slab model (Eq. 4.9) of Gryning and Batchvarova (1996) and the Colorado State University Regional

Atmospheric Modelling System (CSU-RAMS) were tested against data gathered during the field study Pacific '93 of photochemical pollution in the Lower Fraser Valley of British Columbia, Canada, which includes urban areas. The data were obtained from tethered balloon flights, free flying balloon ascents, and down-looking lidar operated from an aircraft flown at roughly 3500 m above sea level. Both models simulated very well the temporal and spatial development of the IBL height over the Lower Fraser Valley, and reproduced many of the finer details revealed by the measurements.

Cleugh and Grimmond (2001) also assessed the validity of the simple CBL slab model for urban conditions. This was integrated forward in time to predict the MH, temperature and humidity using measured local-scale heat and water vapour fluxes for the Sacramento urban region, California. The prediction of the slab model for the well-mixed CBL height agreed fairly closely with the measured values. Of the four different CBL growth schemes used, the Tennekes and Driedonks (1981) model was found to give the best performance.

For the urban nocturnal ABLs it is also reasonable to consider the strong horizontal inhomogeneity and temporal non-stationarity of the UBL and the non-local character of UBL formation. For such cases Zilitinkevich and Baklanov (2002) suggested to calculate the stable ABL height h more accurately within 3-D models on the basis of a prognostic formulation and accounting for the horizontal transport through the advection term and the sub-grid scale horizontal motions through the horizontal diffusivity K_h:

$$\frac{\partial h}{\partial t} + \mathbf{V}\,\nabla h = -C_E|f|(h - h_{CQE}) + K_h\nabla^2 h \qquad (4.10)$$

where $\mathbf{V} = (u, v)$ is the horizontal velocity vector, C_E is a constant ($C_E \approx 1$), and h_{CQE} is the equilibrium MH, calculated from a diagnostic formulation (e.g., Zilitinkevich *et al.*, 2002).

4.5. Applications of NWP model outputs

4.5.1. Boundary layer depth in the NAME-model

The UK Met Office maintains a long range Lagrangian (random walk) model to simulate operational dispersion problems, including nuclear accidents, air quality forecasts, movement of radiatively active gases (CFCs), fumigations,

aerosol and PM_{10} formation, ozone episodes, and movements of volcanic ash plumes. NWP data (fields-files) are input to NAME from the Met Office Unified Model; these files include wind speed U, potential temperature θ, etc. at many vertical levels z at every grid-point. The correct magnitude of boundary layer depth is crucial for modelling the advection, dispersion and deposition to the ground, as reported by Maryon and Buckland (1994) and Maryon *et al.* (1999). They explained that at the time NAME was first developed, the sensitivity of the modelling to boundary layer depth was somewhat unexpected. It remains a reason for the importance assigned to establishing boundary layer depth in the urban lidar project introduced in Section 4.2.2 (Davies *et al.*, 2003).

NAME can use the boundary layer depth as calculated by the NWP model. This has a numerical value defined at each grid-point. Alternatively, NAME uses NWP data to derive boundary layer depth in two ways (Maryon and Best, 1992).

A gradient Richardson number is calculated for each model layer (see also 4.2.1): the height of the boundary layer is set equal to the height z of the bottom of the layer in which it exceeds a critical value of 1.3 (this value is based upon experience using operational NWP data). The concept being invoked here is well known: boundary layer turbulence is suppressed where the Richardson Number is sufficiently stable (as discussed in Sutton, 1953). Thus, stepping up through model layers, evaluate Ri and halt at $Ri > 1.3$, with Ri calculated from the vertical gradient of potential temperature and of wind speed (squared):

$$Ri = \frac{g\Delta\theta/\Delta z}{\bar{T}(\Delta u/\Delta z)^2} \tag{4.11}$$

where $\bar{T}$ is the mean temperature of the layer.

A parcel ascent method, essentially an adaptation of Holzworth (1964, 1967) by Maryon and Best (1992), to suit the needs of NWP data is used in the NAME dispersion model. A parcel of air is assumed to have the same temperature as the air near to the ground. For this the NWP model temperature from the first model level was more robust than the surface temperature (which can exhibit large variations). The parcel is allowed to rise, with adiabatic expansion, until neutrally buoyant (equal potential temperatures for the parcel and its surroundings). This defines the boundary layer depth. When NAME calculates the height where the dry adiabat meets the temperature profile, a

small temperature offset[5] (0.5-1.5 degrees) is added to the first layer temperature (cf. Holzworth, 1964, who used 5 degrees). The dry model was sufficient and computationally quicker to use than virtual potential temperature, which takes water vapour into account.

The gradient Richardson number method and parcel ascent method are both calculated in NAME, then the larger of the two boundary layer heights is selected. If the result is small, then it is reset to the minimum value, typically 80 metres. Although NAME does not have an explicit test for day or night:

- The Richardson Number method, which relies upon wind speed and potential temperature profiles, is adopted mostly at night (stable conditions).

- The parcel ascent method, which relies solely upon the potential temperature profile, is mostly adopted in daytime (unstable conditions).

However the exact selection depends upon the temperature and wind speed profiles that are received from the NWP model.

4.5.2. Boundary layer depth in the ADMS-model

The ADMS model is an important tool for environmental impact assessments of stacks and for local air quality management in towns and cities across the U.K. It uses non-Gaussian plumes whose spread is calculated from turbulence profiles modelled in the boundary layer.

The ADMS met pre-processor can accept a range of options, from which hourly values of the boundary layer parameters are calculated, if not already supplied amongst the input data. These parameters include the sensible heat flux Q_H, the friction velocity u_*, the MO-length L, the convective velocity scale w_*, and the boundary layer depth h. The meteorological pre-processor is documented in Thomson (2000).

In stable conditions, the heat flux $Q_H \leq 0$, and the method of Nieuwstadt (1981) is employed:

---

[5]For NAME in urban areas it may be necessary to re-examine the temperature off-set that is most appropriate. At present the model relies on the NWP generated temperature, with a fixed off-set, but with high resolution mesoscale modelling, modelled temperatures will increasingly reflect urban effects.

$$h = L\frac{0.3u_*}{|f|L}\frac{1.0}{1.0 + 1.9h/L} \tag{4.12}$$

This equation enables h to be calculated hour by hour from L and u_*. Under stable conditions, the model imposes a lower limit value for L as 1 m (rural) or 10 m (urban).

In neutral conditions, as L becomes very large,

$$h = \frac{0.3u_*}{|f|} \tag{4.13}$$

In connection with the very classical expression (4.13), it is noteworthy to mention that generally data seem to indicate much lower values of the coefficient, mostly between 0.05 and 0.2 (Joffre, 1985; Mahrt, 1981; Joffre *et al.*, 2001), depending on roughness and free flow stability N.

In unstable conditions, the rate of growth of the boundary layer must be solved. Using solar radiation (needed as source of the driving energy) from the sun's position in the sky, cloud cover (needed to modulate the solar input), and wind velocity, one can calculate the sensible heat flux Q_H, the friction velocity u_*, the MO-Length L, the convective velocity scale w_*, and the boundary layer depth h. The rate of growth of the daytime ABL is modelled each hour on the basis that a given part of the solar energy is an input to the convection. The energy reflected varies with the surface albedo (reflectivity). Energy used for evaporation may be described using a modified Priestley-Taylor parameter for moisture availability (ranging from 0.0 in desert, 0.5 urban, to 1.0 rural). The growth depends also on the lapse rate of the stable layer aloft. This lapse rate may be input if available. The depth of the boundary layer increases as the turbulence erodes the stable layer aloft. The model follows the schemes of Tennekes (1973), Tennekes and Driedonks (1981), and Driedonks (1982), taking values of the constants as in the latter. The solution for h at each hour during daytime is found by solving the rate of growth of the boundary layer in earlier hours, and varies with time according to conditions.

Near dawn, or dusk, the heat flux is changing rapidly, so an additional code is needed to ensure a smooth transition. The solutions for h are constrained into limit values of 50 m and 4000 m in ADMS.

4.6. Stability classes and the mixing height

All the parameterised methods introduced so far require the determination of z/L or Ri. Measurement of these parameters requires the use of eddy correlation techniques which are usually not available at routine meteorological stations. For environmental expertises on air pollution, knowledge of atmospheric stability is often still obtained from discrete stability classes which are determined on the basis of routine meteorological observations when ultrasonic anemometers are not available. Such expertises are usually undertaken for different kinds of medium or high stack plants, which are not often situated in densely built-up areas. As an example, the system to determine stability classes used in Austria is briefly introduced. Average local MHs calculated by a meteorological pre-processor can be rather easily assigned to these stability classes, generally yielding plausible results.

Such simple methods to assess stability from routine meteorological measurements are generally based on data representing rural conditions. However, their simplicity would call for their extension to be applicable to urban conditions as well. This section shows the limits of applying this widespread method to determine atmospheric stability to urban conditions. Comparison with or substitution by measured MO-length whenever available is strongly recommended for urban studies.

In Austria, a traditional discrete stability classification scheme with dispersion parameters developed by Reuter (1970) is used. Stability classes are determined as a function of half-hourly mean wind speed and a combination of sun elevation angle, cloud base height and cloud cover; alternatively, the radiation balance (net radiation) or the vertical temperature gradient is used in combination with the mean wind speed. Of these methods, only representatively measured vertical temperature gradients have the potential to reflect urban conditions properly, but these have so far not been realised in Austria as there are no meteorological towers in central city areas; cloudiness and net radiation are mostly not very different over an urban area compared to its rural surroundings. A three-dimensional statistics of stability classes contains the percentage frequency of each combination of wind direction (36 categories), wind speed (12 categories), and stability class (6 categories), e.g., over the whole year. The calculation of stability classes is necessary to determine the dispersion parameters σ_y and σ_z as discussed by Hanna and Chang (1992).

In practice, within the Reuter (1970) scheme, stability classes 2 to 7 can occur in Austria. Stability classes 2 and 3 occur during daytime in a well-mixed boundary layer, class 3 allowing also for cases of high wind velocity and moderate cloud cover. Class 4 is representative for cloudy and/or windy conditions including precipitation or fog and can occur day and night. Classes 5 to 7 occur at night, static stability increasing with class number.

In Austria, the most widespread method to determine stability classes is based on a so-called radiation index calculated from the wind speed and a combination of the three parameters: sun elevation angle, cloud cover and low cloud base height, and wind speed. At first, for the location of interest, hourly values of the sun elevation angle φ are determined for the whole year and are transformed into an index IN according to Table 4.1. Once IN is known, the radiation index can be determined according to Table 4.2.

If during daytime the radiation index according to Table 4.2 is less than one, it is set to 1, except for the case $h_c \leq 2000$ m and a cloud amount of 8 octas. The resulting classification scheme is shown in Table 4.3.

Table 4.1: Index IN depending on the sun elevation angle φ.

φ	$\leq 0°$	$0° < \varphi \leq 15\circ$	$15° < \varphi \leq 35°$	$35° < \varphi \leq 60°$	$\varphi > 60°$
IN	0	1	2	3	4

Table 4.2: Radiation index depending on the index IN, cloud amount, and the height h_c of the lowest clouds

	Night			Day		
Cloud amount	$0/8 - 3/8$	$4/8 - 7/8$	$8/8$	$0/8 - 4/8$	$5/8 - 7/8$	$8/8$
	Radiation index					
$h_c \leq 2000$ m	-2	-1	0	IN	$IN - 2$	0
$h_c > 2000$ m	-2	-1	-1	IN	$IN - 1$	$IN - 1$

Table 4.3: Stability classes defined on the radiation index (columns) and wind speed (rows, in m s^{-1})

	-2	-1	0	1	2	3	4
< 1.8	7	6	4	3	2	2	2
1.8 to 3.3	6	5	4	4	3	2	2
3.4 to 3.8	5	4	4	4	3	2	2
3.9 to 4.8	5	4	4	4	3	3	2
4.9 to 5.3	5	4	4	4	4	3	3
5.4 to 5.8	4	4	4	4	4	3	3
> 5.8	4	4	4	4	4	4	3

The stability classification scheme based on the radiation balance (net radiation) and the wind speed is shown in Table 4.4, while the one based on the vertical temperature gradient and the wind speed is displayed in Table 4.5.

For unknown reasons, the wind speed classification in Table 4.3 is not consistent with that in Tables 4.4 and 4.5; this leads to deviations in stability class statistics derived with different methods at the same site. The vertical temperature gradient is seldom used to derive stability classes. Temperature gradients on the basis of routine measurements taken at different elevations cannot be often determined representatively and with enough accuracy.

Table 4.4: Stability classes defined on the radiation balance (columns, in W m^{-2}) and wind speed (rows, in m s^{-1})

	< -28	-28 to -7	-6 to 54	55 to 109	110 to 244	245 to 415	> 415
< 2	7	6	4	3	2	2	2
2 to 2.9	6	5	4	4	3	2	2
3 to 3.9	5	4	4	4	3	2	2
4 to 4.9	5	4	4	4	3	3	2
5 to 6.9	5	4	4	4	4	3	3
> 6.9	4	4	4	4	4	4	4

Table 4.5: Stability classes defined on the vertical temperature gradient (columns, in °C/100 m) and wind speed (rows, in m s^{-1})

	>2	0.1 to 2	−0.6 to 0	−0.8 to −0.7	−1.1 to −0.9	−1.4 to −1.2	<−1.4
< 2	7	6	4	3	2	2	2
2 to 2.9	6	5	4	4	3	2	2
3 to 3.9	5	4	4	4	3	2	2
4 to 4.9	5	4	4	4	3	3	2
5 to 6.9	5	4	4	4	4	3	3
> 6.9	4	4	4	4	4	4	4

When eddy correlation techniques are not available to determine z/L, the determination of stability classes is crucial for regulatory modelling. Based on an at least one year time series of hourly meteorological observations, hourly values of stability classes by one of the three methods are computed. The observations have to be representative for the site of interest. While the network of wind data is quite dense in many parts of Central Europe, this is not the case for cloud amount, net radiation, or the vertical temperature gradient, which may cause problems to properly determine stability classes representative for a specific site. Consequently, on-site measurements of net radiation and wind are often used to get the necessary stability information, sometimes restricted to shorter time periods when pollution levels are expected to be highest. Time series of wind and stability data are then used to compute or forecast, e.g., yearly averages and frequency distributions of concentrations and the percentage of threshold exceedences by a given pollutant. If current concentrations are known, e.g., from measurements, then future changes of pollution levels can be estimated. There are some algorithms available to transform the Reuter's stability classes to more widespread ones such as those of Klug-Manier used in Germany or Pasquill–Gifford used in the USA.

For model calculations, a fixed value of the mixing height is frequently assigned to each stability class. Using the Austrian regulatory Gauss model, default values for summer are 2500, 2000, and 1100 m for classes 2 to 4, respectively, and 1100, 1100, and 800 m for winter. No mixing heights are needed in the model for classes 5 to 7 due to negligible vertical mixing in these situations.

Table 4.6: Average mixing heights, standard deviations (m above ground) and number of cases dependent on stability class (Table 4.3) for the area Linz, Austria. Results are for hourly values over a period of five years.

Stability class	Winter		Summer	
	Urban	Rural	Urban	Rural
2	1347/619 (712)	1146/734 (378)	2216/ > 1000 (3458)	1830/825 (2272)
3	1012/794 (2915)	859/714 (1485)	1731/179 (4580)	1507/ >1000 (3249)
4	480/338 (11686)	485/60 (14460)	1498/248 (7297)	1189/ >1000 (9837)
5	124/88 (1053)	202/293 (1475)	128/89 (539)	146/213 (1232)
6	55/48 (3078)	187/279 (1844)	52/46 (2956)	142/252 (2208)
7	35/13 (2231)	138/225 (1391)	37/15 (2870)	115/198 (2070)

Alternatively, a pre-processor can be used to derive average MHs dependent on the stability class. Here, hourly mixing heights were calculated with the meteorological pre-processor TAMOSP (Pechinger *et al.*, 2000). The energy budget was calculated according to Holtslag and Van Ulden (1983). The convective MH was calculated after Maul (1980) and Carson (1973) as in CALMET, the mechanical MH after Nieuwstadt and Tennekes (1981) as in the OML pre-processor. For the urban site, model land-use 1 (urban) was used with the following settings: roughness length 1 m, albedo 0.3, Bowen ratio 1.5, factor for evaluating the ground heat flux from global radiation 0.25 and leaf area index 0.2. For the rural site, model land use 2 (meadow, fields) was taken with the following parameter values: roughness length 0.25 m, albedo 0.15; Bowen ratio 0.5; factor for ground heat flux from global radiation 0.15; leaf area index 3. Results for the Austrian city of Linz are presented in Table 4.6 (Baumann-Stanzer *et al.*, 2004). Meteorological data were taken from the airport ("rural") or the station "Linz-Stadt" ("urban").

According to Table 4.6, a large number of stable conditions (classes 5 to 7) is

determined also for the urban site, as the urban effect in determining stability is only accounted for through the measured wind speed. This shows clearly the limit of the method when applied to central urban areas. As expected, however, MHs determined from TAMOSP with urban/rural settings are within the expected range and decrease with increasing stability class number under all conditions. In convective conditions (stability classes 2 and 3), the urban MH is on average clearly larger than the rural one, both in winter and summer, and the values are not far away from the default values given above. For stability class 4, which comprises all non-fair weather cases both day and night, larger average urban MH are calculated only in summer. Under night-time mechanical turbulence (classes 5 to 7), rural MH are on average larger, which can be attributed to higher windspeeds at the airport compared to the city. Apart from the parameter settings given above and from the different ground-based stations, TAMOSP does not include any other important effects like heat storage into and release from the urban fabric which might strongly alter especially the night-time stability and MHs. This simple standard procedure can therefore not be recommended for use in dense urban areas, at least not for night-time conditions (unless representative vertical temperature gradients are available, which is so far usually not the case).

4.7. Future Prospects for NWP models

The non-homogeneity in surface types and thermal properties within a city should be adequately modelled. In the context of NWP, one can thus raise the question whether the MH is still a valid concept. It seems that their practical usefulness in understanding episodes and as input values for the simpler types of pollution dispersion model renders the concept of MH useful, despite the recognised uncertainty in its definition. There is increasing interest in using numerical outputs from NWP models to generate formatted data that can be then easily input into environmental impact assessment or air quality forecast models, and where the MH is an important requirement, alongside the stability. However, within NWP models, simple closure models for the evaluation of the MH do not work well. Nocturnal stable conditions in urban areas present the greatest difficulty for modellers. The performance of these simple methods seems more acceptable for daytime than for nocturnal conditions (Baklanov and Mestayer, 2004).

Although modern NWP models can approach the necessary resolution for the urban scale, the parameterisations of urban effects in most of the existing operational models are absent or greatly simplified for this purpose, therefore it is very important to implement the 'urbanisation' of NWP models to make their results more suitable for urban MH calculation. Currently this work is realised within the EU project FUMAPEX (Baklanov, 2003; see also Section 3.5).

Nevertheless, one potentially promising method to estimate the MH or turbulence profiles for dispersion models is using output from meso-scale NWP models. There are several possible ways for this. First of all, it is possible to avoid using the MH concept in dispersion models that can directly use the eddy diffusivity profiles. This can be done using modern turbulence closures in meteorological models (using similarity hypothesis of the turbulent viscosity and diffusion) or directly in 3D atmospheric pollution models. Many advanced atmospheric dynamics and pollution models already follow this approach (e.g., Baklanov, 2000a; Zhang *et al.*, 2001; Kurbatskii, 2001). However, the complexity of prognostic turbulence closure schemes, the requirements for high grid spatial resolution and problems due to numerical diffusion in Eulerian models make this method too expensive for practical application for the time being. So, many dispersion models, especially regulatory models, are still not coupled to meteorological models. They are based on *in situ* measurements of meteorological characteristics and need the MH as an input parameter.

Several meso-meteorological models (so-called 'models with an unfixed upper boundary') calculate the ABL height from a separate prognostic MH-equation and then use it as the height of the simulation area. Such models were suggested by Penenko and Aloyan (1974, 1985). A simple version of this method was also realised by Arya and Byun (1987) and Byun and Arya (1990) for a 2-D numerical model of the UBL. Such a method can be very useful for next-generation models, especially if the meteorological models include urban effects. However, such models are much more expensive in computation time (Baklanov *et al.*, 2002).

More recently, output data from 3-D NWP models have been increasingly used for MH estimation based on different approaches, e.g.: turbulent kinetic energy models, k-ε models, sub-grid scale turbulent closure models (incl. LES mode), and second-order momentum turbulent closure models. The MH can be estimated at each model grid point from the vertical profile of indicators of turbulence, e.g.:

- The turbulent kinetic energy (TKE) or eddy decay,

- The Richardson-number method, or

- Various parameterisation methods or simple models (see Section 4.3).

The direct calculation of MH from the simulated TKE or turbulence profiles for the daytime UBL shows good and promising results (e.g., Batchvarova *et al.*, 1999). However, this approach is very sensitive to the turbulence closure scheme, and can thus be quite uncertain in practice. Zhang *et al.* (2001) showed that local closure schemes lead to considerable errors for the daytime MH as well. In spite of promising results for the CBL height, using the same method for the nocturnal MH (SBL) can yield considerable problems and large uncertainties for the MH estimation, e.g., from the TKE equation using a local closure. This was shown by Baklanov (2000b) with a new version of the DMI-HIRLAM model (Sass *et al.*, 2000; Nielsen and Sass, 2000) using the CBR-turbulence scheme (Cuxart *et al.*, 2000) to test the direct calculation of the ABL height from the TKE-profile by the eddy decay approach, which yielded considerable underestimation of the stable ABL height.

5. Recent experimental campaigns and data

We present in this Chapter a set of recent field campaigns providing relevant meteorological, turbulence and urban features data for European urban and sub-urban conditions. Such data can be used for testing and validating parameterisation schemes and models.

5.1. Basel, Switzerland

The Basel UrBan Boundary Layer Experiment BUBBLE (Rotach *et al.*, 2004a, b) was a long lasting and detailed experimental (full-scale and wind tunnel) and numerical modelling effort to better understand the (thermo)dynamics of the UBL. Its philosophy was mainly based on the notion that both, detailed near-surface turbulence observations *and* information on the full UBL, are required. Therefore, for a period of one year, a network of seven micrometeorological stations (three urban, one suburban and three rural reference sites) was operated in the City of Basel with 6 levels of turbulence observations up to more than twice the local building height. At these sites the full radiation balance (four components) was continuously measured. For the same period of one year, a wind-profiler near the city centre yielded the mean wind profile as well as some turbulence information with a 43 m vertical resolution every 1/2 hour. Also an essentially co-located aerosol lidar gave information on the aerosol distribution (vertical resolution: 10 m) in the lower urban atmosphere and hence allowed derivation of the 'Aerosol Mixing Height' (as a surrogate for the UBL height).

For a period of some five weeks in summer 2002 (IOP) a large number of additional observations was realised:

- More surface sites (profiles up to twice the obstacle height): one suburban and several rural stations (e.g., Christen *et al.*, 2003).
- Additional turbulence observations at one urban site (spatial heterogeneity, averaging, CO_2 exchange).
- Additional remote sensing: RASS (urban site), 2 sodar sites (rural), tethered balloon (urban).
- Detailed street canyon energetics (surface temperatures, radiative emissions and divergences, etc.).
- A tracer release experiment with near-roof level source and sampling (Rotach *et al.*, 2004a).

In addition to these full-scale observations, numerical (Roulet, 2002) and physical modelling (Feddersen *et al.*, 2003) is being pursued in order to optimally take advantage of all these different approaches to investigate the UBL. For further details on BUBBLE and first results see Rotach *et al.* (2004b).
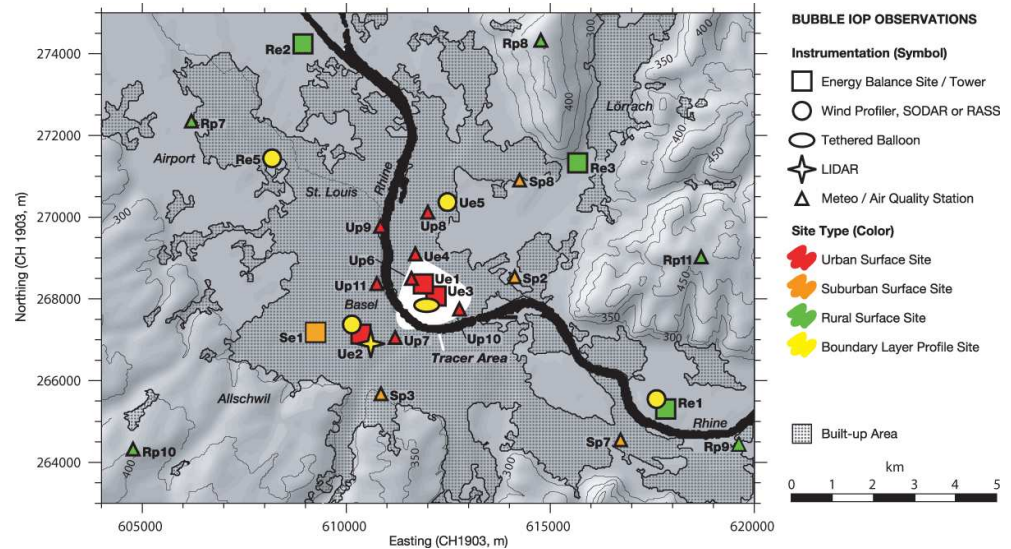

Figure 5.1: Map of the activities during the Basel Urban Boundary Layer Experiment (BUBBLE), in Basel, Switzerland 2001/2002. All surface sites are coded by three letters "Ab1", with A indicating the surface type: urban (U), suburban (S) or rural (R). The second letter indicates if the station is experimental (e) or if it is an operational and permanent (p) station. Five sites are outside the map subset. Topography is indicated in m above sea level. The built-up area includes urban, industrial, and higher density suburban areas (from Rotach et al., 2004a).

5.2. Greater Marseille area, France (UBL-ESCOMPTE)

The ESCOMPTE field campaign took place over an area of 120 km x 120 km, from June 4 to July 16, 2001. The set-up involved 20 stations, equipped for gas (ozone, nitrogen oxides, VOCs, etc.) and/or particle measurements, among which two on boats, and two in trucks. The surface energy budget was measured at 9 sites. The meteorological basic parameters were also measured at 5 complementary sites. Wind profiles were continuously measured at 12

sites by 7 sodars, 4 UHF and 4 VHF radars. Three lidars were also operated, as well as 4 radiosonde systems, and 7 aircrafts. Finally 33 constant-volume balloons were launched and tracked during the Intense Observation Periods (IOPs). As a complementary project, the UBL/CLU experiment documented the four-dimensional structure of the urban boundary layer in connection with the urban canopy energy exchanges with the atmosphere during a summer period of low wind and breeze conditions. The objectives were (1) to compare urban and rural atmospheric boundary layers, explore the influence of sea breeze on the UBL, and document the UBL turbulent fields, and (2) to construct a data base allowing testing of urban energy exchange schemes, surface temperature remote sensing from satellites, and high resolution meteorological and chemistry-transport models.

During the campaign, two types of intensive observation periods provided more comprehensive data:

(i) Five ESCOMPTE IOPs during situations of land-sea breeze and high insulation eventually mixed with a light Mistral during the IOPs 2a and 4. During these periods one airplane flew over Marseille to document the UBL, measuring the atmospheric composition and the wind and turbulence within or at the top of the boundary layer.

(ii) Four Infrared IOPs when a light airplane equipped with a thermal infrared mapping camera scanned the urban canopy at different times in the day. The influence of spatial resolution and sensor orientation on the surface temperature measurements were documented by flying successively over three urban districts in 8 different directions with respect to the sun, including the city centre measurement site that was monitored by an array of IR radio-thermometers.

After qualification/validation, the data have been included in the ESCOMPTE structured data base (`http://medias.obs-mip.fr/escompte`) which is freely accessible (Mestayer *et al.*, 2004).

In the urban area, the instrumentation was mainly deployed at five sites along the North-South axis of the city, roughly parallel to the bay shoreline (Fig. 5.2). Three urban/suburban stations (GLM, CAA, STJ) were equipped with micro-meteorological masts where the turbulent and radiation fluxes necessary to monitor the canopy surface energy budget were continuously measured: the masts rose some 12 to 20 m above the urban canopy level and the turbulent fluxes were measured at 2 levels. The other two sites (OBS, VAL) also included

turbulence instrumentation on 12 and 10 m-masts, respectively, as a ground reference for vertical profilers (see below).

The central site (CAA) was located in the rather uniform, dense part of the city centre. Surface energy balance fluxes were measured using eddy covariance instruments and radiometers, mounted on a pneumatic tower 20.7 m above roof level. Two scintillometers were also deployed to evaluate the integrated heat flux over the city centre, with $\sim$2 km optical paths oriented N-S and E-W, respectively. The site was also equipped with an array of up to 19 IR radio-thermometers, either fixed ones to monitor the surface temperature of selected elementary surfaces, or hand-held to evaluate surface temperature distributions during periods of intense observation. In this urban fragment, during some periods thermometers also monitored heat exchanges between the inside and the outside of buildings. At the suburban site STJ, two IR radio-thermometers were also operated to monitor the composite surface temperatures of the ensembles immediately North and South of the site.

An array of 20 T-RH sensors with continuous recorders, at a height of 6 m above the ground allowed monitoring the dependency of the urban heat island on meteorological conditions, district structure, and the distance to the sea (Figure 5.2). In addition, some T-RH transect measurements were occasionally obtained with a car equipped with T-RH ventilated sensors at $z = 2$ m.

The set-up included an array of four vertical sounders: two sodars at the suburban sites GLM and STJ, sounding the lower part of the ABL, a UHF-wind profiler radar (and a tethered balloon occasionally) measuring thermodynamic (and ozone) ABL profiles at the OBS site, close to the city centre, and a RASS-sodar sounding wind and temperature vertical profiles at the VAL site. At this site, located at the border of the city and overlooking most of the urban area two lidars were scanning the atmosphere horizontally and vertically up to a distance of about 10 km: a UV lidar measuring ozone concentrations, and a 10 μm Doppler lidar (called TWL, transportable wind lidar) measuring the radial wind. Both instruments were operated in parallel to generate tomographic observations of the aerosol content and the UBL structure in the scanned volume (Fig. 5.3). These sounders were also part of the larger array of 18 vertical sounders deployed in the ESCOMPTE set-up allowing to monitor the 3-D structure of the ABL over the regional domain. The data from the sounders have been composed with those obtained during the airplane flights over Marseille (Fig. 5.4) to provide in-depth description of the UBL/ABL structure.
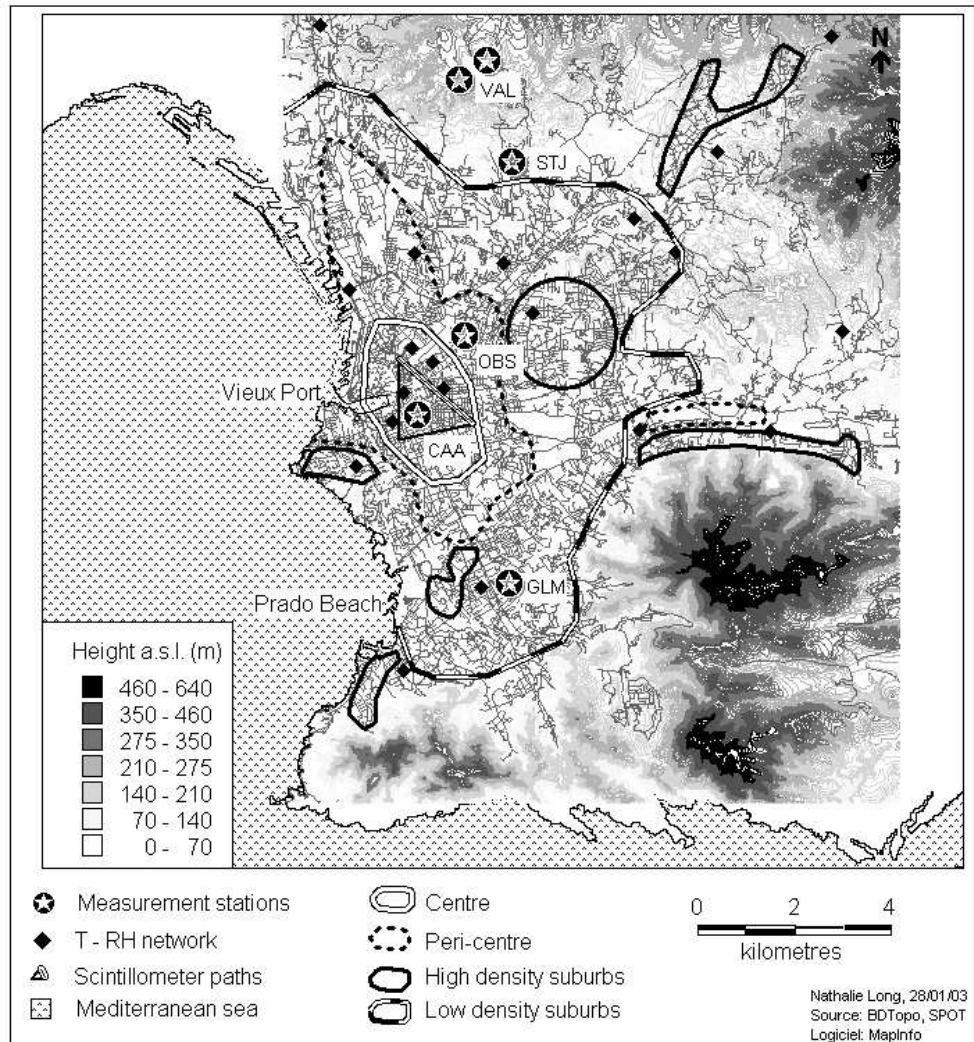
Figure 5.2: Map of Marseille city and its vicinity (analysed section of the BDTopo). The Etoile ridge lies immediately north of the map limit. The map indicates the limits of the main built-up area (Long, 2003), the stars – the positions of UBL/CLU measurement stations; the diamonds – the T-RH network, and the straight lines – the scintillometer paths.
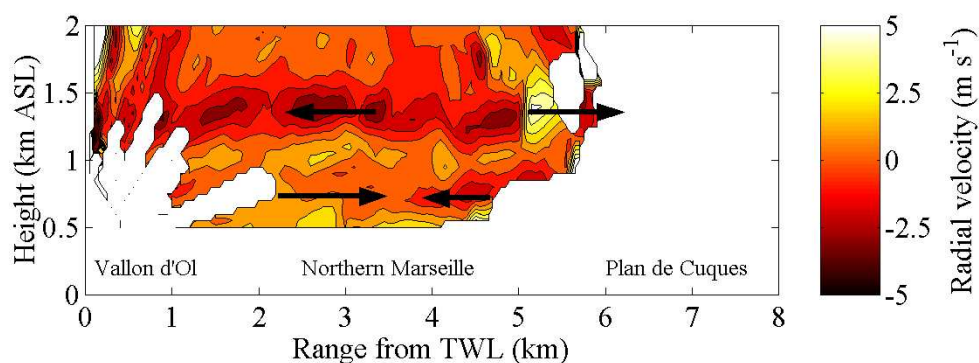
Figure 5.3: Vertical cross section of radial velocities with TWL pointing eastward towards land (azimuth 110°). The arrows indicate the flow circulation in the section (after Mestayer et al., 2003, 2004).
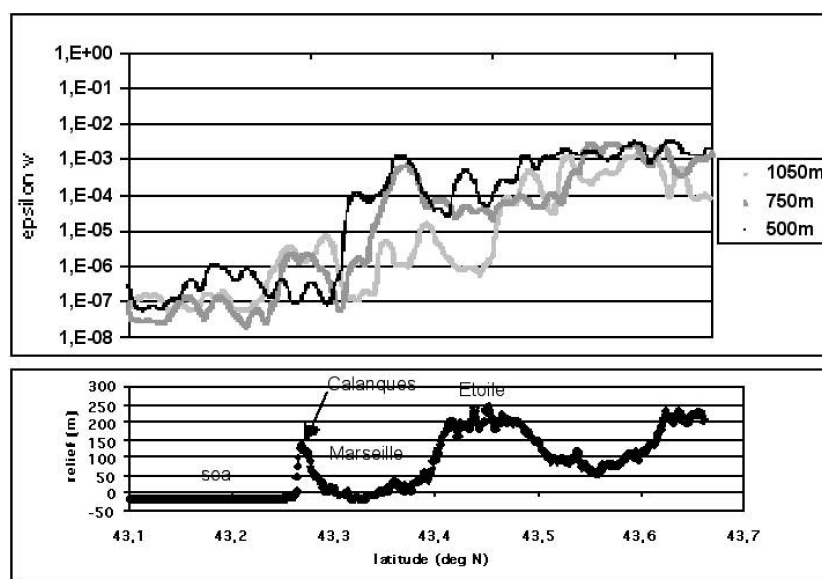
Figure 5.4: Dissipation rate of turbulent kinetic energy ($m^2 s^{-3}$) measured with the Merlin IV-aircraft (MeteoFrance) along the south-north legs at levels 1050, 750 and 500 m. The overflown relief is also represented with the sea on the left (south). The duration of the flight over the town, between the Calanques ridge to the south and the Etoile massif to the north, is 3 minutes. The energy spectrum high frequency tail is a relevant indicator of turbulence intensity in such inhomogeneous conditions (after Saïd et al., 2001).

The remote sensing part of the project includes analysis of visible and infrared data from satellite and from an airborne camera, compared to ground-based measurements. About 150 useable images from the Advanced Very High Resolution Radiometer (AVHRR) on board satellites NOAA-12, -14, and -16, with an average of 4 images/day, are under analysis. Sixty-six images from MODIS on board the TERRA satellite were also obtained from the NASA/EOSDIS data centre. Finally, a single high resolution ASTER image was obtained from NASA/JPL and NASDA on 27 May 2001. Airborne measurements include nadir surface temperatures from a PRT5 Barnes radiometer (8-14 μm spectral band) aboard the Merlin IV aircraft, and images from a thermal infrared (TIR) camera (INFRAMETRICS model 760, 7.5-13 μm spectral window) equipped with 80° wide-angle lenses and placed aboard a PA28 aircraft, inclined about 20° backward. Flying several crossing axes above the city allowed obtaining TIR measurements in a -60° to +60° range of zenith view angles in all azimuth directions, in order to characterize TIR directional effects as the difference between oblique and nadir measurements of radiative surface temperature.

Multi-spectral and panchromatic SPOT images were also analysed to obtain surface types coverage with a very high resolution. Specific statistical analysis of the 3-D data base BDTopo of IGN (the French national geographic institute), describing such urban objects as buildings, constructions, vegetation, etc., have been combined with satellite data to generate high resolution maps of the surface energy model input parameters such as urban land uses, roughness length, albedo, etc., and to characterise the district types (Fig. 5.2).

5.3. Birmingham, UK

The Birmingham field trials carried out in 1998, 1999 and 2000 were designed to measure the sensible heat flux and stability in order to improve air quality forecasting. Three urban experiments have been conducted at the Dunlop factory site within the city of Birmingham, U.K. (Ellis and Middleton, 2000a,b,c). Work on the roughness length, wind speeds and friction velocity of the site has been summarised for COST-715 WG1. With regard to WG2, the data set includes measured values for radiation, sensible heat flux, and stability (as the Monin-Obukhov length L). Instruments were operated on 15 m, 30 m, and 45 m masts for 4-week periods in 1998, 1999 and 2000 at the factory site. This site was involved in continuous tyre production, so significant amounts of energy were used. Synoptic observations were taken from the Coleshill station outside the city.

At Dunlop Tyre Ltd, a small grassed area of lawns located near the Tyre Testing area with modest trees to the Western end of the lawn was used. The lawn area free of small trees was just big enough to accept the guy ropes of the tallest mast, 45 m high, with guy ropes for smaller masts at 15 m (2 of) and 30 m fitted in amongst them. This also meant the masts were fairly close to factory buildings, as the lawn was surrounded by roadways and then factory buildings. One side was more open in aspect. The topography is generally fairly flat, apart from the many large factory buildings. Although the measurement site itself was over grass, the location as a whole was well within the city and largely surrounded by extensive areas of factories and housing. The masts were well above roof heights. Masts carried instruments so that values of the above variables were measured. On the other hand, the relief around Coleshill could be described as "gently rolling": there are no steep slopes nearby. The station is located in a field at a farm, with hedges, trees and farm buildings, and so it is less well exposed than an airport station would be. It is about 8.5 km from the Dunlop site (see Fig. 5.5).


Figure 5.5: Relative positions of Dunlop Tyres Ltd. and Coleshill synoptic station. Map shows an area of approximately 17.4 km × 10.9 km.

During the 2000 campaign, following discussions in COST-715, a sonic anemometer was also placed on a 15 m mast beside the Coleshill station, to measure sen-

sible heat flux, friction velocity and Monin-Obukhov stability simultaneously at both sites. In addition to the expected change in wind speed associated with increased surface roughness, a clear difference in heat flux at the two sites was observed. Just adding this one instrument to an existing standard observing station provides valuable measurements of variables that are very important in influencing dispersion near the ground: the friction velocity and MO-length L. Traditionally, these are not often routinely observed. Measurements remain an important research question for urban meteorology: how should they be done, and where sited. In the light of discussions within WG1 of COST-715, the data have been examined in several ways, especially in comparing the urban and rural measurements. The experiment was reviewed in Middleton *et al.* (2002).

Mean wind and direction, standard deviations of azimuth and elevation, and the three wind components were obtained. In the later study a fast hygrometer measured water vapour fluctuations for the latent heat flux. Monin-Obukhov length, friction velocity, turbulence intensity, and surface roughness length for momentum were estimated. At and below the surface, the mean temperatures on grass and concrete were measured. In the later study a downward IR-thermometer also gave a measure of surface temperature. Radiometers measured upward and downward components of short wave and long wave radiation. Humidity (via dew point), pressure, and rainfall were also recorded.

The primary stimulus to the experiment was the need to obtain measurements of heat flux and stability in a UK city. These were crucial to further improvements in the forecasting of urban air quality. The UK National air quality bulletin system at the time was using the BOXURB model, and during the period of the study has switched to a version of the NAME model. In either case a proper diagnosis of stability, especially at the morning and evening transition, which may coincide with a peak in emissions at rush-hour, was required. Applications of the data in verifying surface energy balance schemes and for use in urban mesoscale modelling were also of interest, although the mast height of 45 m was judged low at the time of the experiments for the purposes of mesoscale model verifications. The questions to be addressed included:

- What is a possible choice of the default limit to be set upon $1/L$ when modelling an urban area in stable conditions?

- How can urban thermal properties be easily parameterised?

- How should urban stability be allowed for in dispersion modelling?

- In what meteorological conditions and at what latitudes can urban conditions still go very stable?

In 1998 and 1999, the rural Coleshill data were restricted to the normal synoptic observations from a standard Met Office station, e.g., 10 m cup van/anemometer. In 2000, a 15 m mast with a sonic anemometer was placed alongside the station, to record the three wind components and temperature fluctuations. From these data were derived estimates for the turbulence, standard deviations of wind elevation and azimuth directions, sensible heat flux, friction velocity and Monin-Obukhov length.

5.4. Bologna, Italy

Bologna is located in the south-eastern border of the Po Valley basin, Italy, near the Apennines mountain chain. The terrain is characterised by a complex morphological structure with several small valleys leading to the flat land. The whole area is heavy industrialised and densely populated. In the flat Po Valley basin, calm wind is very frequent and strong temperature inversions are often observed near the ground, during the night and in the winter period, when the occurrence of a stable boundary layer is common. This SBL is related to heavy pollution episodes because the pollutants emitted at the ground level are capped inside.
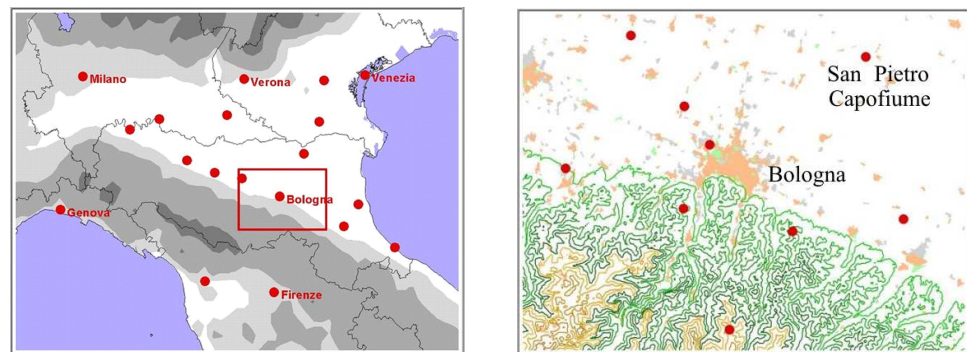

Figure 5.6: Left, the Po valley and the experimental area (highlighted by the red square, where dots represent the main cities). Right, the Bologna urban area (urban in orange and industrial in grey), orography (coloured level lines) and the 9 standard permanent meteorological stations (red dots).

During the sunny days, especially in summer, a thermal convective boundary layer (CBL) is common in the Po Valley. During summer anti-cyclonic conditions, the local circulation is completely driven by thermal contrasts (Tampieri and Trombetti, 1981). Near the coastline and at the exit of the valley in the plain, where the heterogeneities become more important, the growth of an internal boundary layer (IBL) is expected.

Because urban areas are the main cause for surface heterogeneities due to the large amount of the urbanised areas in the Po valley, an experimental study was performed to assess the influence of one of these urbanised surfaces, Bologna, on the structure of the ABL (Fig. 5.6). Bologna is the main urban area in the Emilia-Romagna region, with a metropolitan area of about half a million inhabitants. It is located close to hills with maximum heights around 300 m, where two small valleys enter the plain. Therefore, there is a combined effect of complex terrain features and urban influences on the ABL structure.

The Bologna experiment took place in 2001 and 2002 to investigate the surface fluxes and evaluate the surface energy budget and the mixing height, during typical summer and winter weather conditions. Turbulence and mixing height measurements were carried out by means of a sodar, a sonic anemometer and a high frequency hygrometer located on the top of a building in the Bologna city centre and at the rural synoptic meteorological station of San Pietro Capofiume, where standard vertical soundings (TEMP) are also performed. The sodar and sonic data cover periods ranging between 20 and 30 days, mainly during May-August 2001 and January-March 2002.

Moreover, to investigate the heat island effect, a temperature mapping experiment was made by positioning 21 thermometers in the town and in the suburban and rural surroundings. All the data were compared with data from 9 ground meteorological stations located inside the experimental area. The data cover periods of 20-30 days during winter (January-February 2001) and summer (May-June 2001). Figure 5.7 shows the location of instruments during the temperature mapping experiment (left) and during the surface fluxes and mixing height experiment (right).
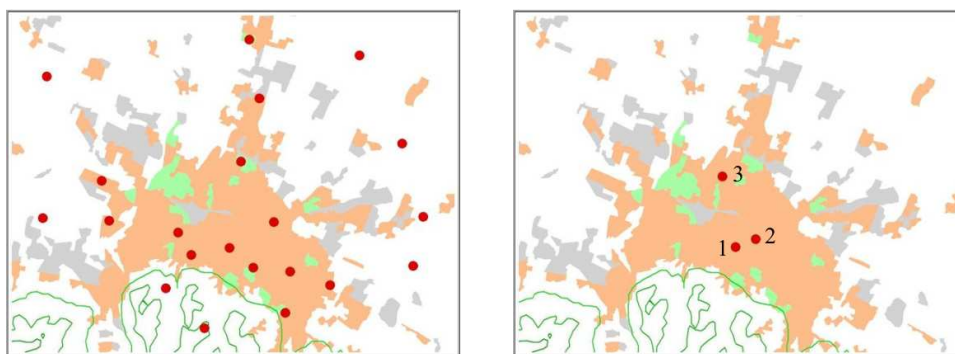
Figure 5.7: The location of instruments in the urban area during the "temperature mapping experiment" (left) and during the "surface fluxes-MH experiment" (right), numbers refer to the instrument locations: 1 – Palazzo Accursio, 2 – Torre della Specola, and 3 – CNR.

The 21 thermometers used for the temperature mapping were located mainly above the mean roof level inside the urban area, avoiding local obstacles and roofs irradiance, and at ground level on grass surface in the surroundings.

During the urban campaigns, sodar and sonic anemometers were placed over 2 historic towers (Torre della Specola 50 m and Palazzo Accursio 35 m) both higher than the surrounding buildings (12-18 m) and located in Bologna downtown at the centre of the urbanised surface. A third instrumented site was in the northern part of the city (CNR, 25 m) in a suburban area. During the campaigns, instruments were located at the rural site of San Pietro Capofiume, a meteorological observatory located about 25 km NNE from Bologna where a standard radiosonde is launched every day at 00:00 and 12:00 GMT. The site is about 11 m a.s.l. in a flat rural area, and well representative of typical Po valley conditions. The Bologna data-set is available from `http://envecity.fmi.fi/cost715/`, and contains all the data from the experiment.

The 30 minutes averages of the sonic anemometer time series were split into stable, neutral and convective periods on the basis of the Monin-Obukhov length L. The splitting was made to compare L with a threshold value L_{thr}. This threshold value was chosen empirically in order to minimise the mis-diagnosis of convective conditions during the night. After several tests, the threshold value was set to 100 m for urban and 50 m for rural conditions.

Table 5.1: Characteristics of the Bologna experiment: measurement campaigns, sites, periods and instruments.

sites	type	period	height over ground level (m)	instruments
2 hilly, 4 downstream hills, 4 downstream valleys, 11 flat	6 urban, 2 urban parks, 5 suburban, 8 rural	24 Jan - 19 Feb 2001 19 May - 23 Jun 2001	urban sites: 32, 25, 22, 18, 13, 8; parks: 10, 2; suburban sites: 18, 11, 10, 9, 9; rural sites: 4, 2, 2, 2, 2, 2, 2, 2	21 Gemini Tinytag Ultra and Tinytalk thermometers
Torre della Specola Palazzo d'Accursio San Pietro Capofiume San Pietro Capofiume Torre della Specola	urban urban rural rural urban	9 - 29 May 2001 27 Jun – 5 Jul 2001 6 – 27 July 2001 21 Jan – 4 Feb 2002 7 Feb – 4 Mar 2002	54 45 10 2.9 60	1 sonic anemometer (Solent Research Gill), 1 hygrometer (KH20), 1 hygro-thermometer (Rotronic 103A)
Torre della Specola Palazzo d'Accursio San Pietro Capofiume C.N.R. San Pietro Capofiume C.N.R.	urban urban rural suburban rural suburban	3 – 24 May 2001 25 Jun – 4 Jul 2001 9 – 26 Jul 2001 19 – 28 Sep 2001 18 Jan – 4 Feb 2002 5 Feb – 15 Mar 2002	50.8 35.8 0.8 24.8 0.8 24.8	1 sodar (Phase Array Sodar PA1 Remtech)
San Pietro Capofiume San Pietro Capofiume Torre della Specola	rural rural urban	10 Jul – 27 Jul 2001 21 Jan – 4 Feb 2002 7 Feb – 4 Mar 2002	1.8 1.8 52	1 pyranometer (Schenk), 1 pyrradiometer (Schenk)

The mixing height estimated using the signals measured by the sodar on the top of a building in Bologna city centre was chosen as the "reference" MH-value using the following method. In stable conditions, the MH is identified as a local minimum level of the structure parameter for temperature C_T^2, just above its first maximum from the surface (Klapisz and Weill, 1985):

$$\text{MH}_{\text{stable}} = z(C_T^2 = \text{min}). \tag{5.1}$$

Under convective conditions, because the maximum measurement level reached by the sodar was always below the MH, a similarity method based on profiles of the vertical standard deviation σ_w was applied, as suggested by Seibert *et al.* (1998). In these conditions, the σ_w-maximum level is taken as the third of the MH:

$$\text{MH}_{\text{convective}} = c\,z(\sigma_w = \text{max}) \tag{5.2}$$

with $c \approx 3$, an "empirical" factor suggested by F. Tampieri (*personal communication*). For neutral conditions the MH was not estimated from sodar measurements.

The MH and surface energy budget parameters from the Bologna experiment were also compared with simulations by the mass-consistent meteorological pre-processor CALMET-SMR running daily at the ARPA meteorological service (Deserti *et al.*, 2001). The CALMET pre-processor (Scire *et al.*, 1999) is based on the Holtslag and Van Ulden energy budget method.

Results on the surface energy budget parameters (u_* and L) and the MH from the Bologna experiment are reported in Sections 6.1.5 and 7.3.2, respectively.

5.5. Cracow, Poland

Two extensive measurement periods were simultaneously conducted in the framework of COST-715, in the cities of Cracow and Katowice, Poland (20–25.08.2002 and 10–8.06.2003) to investigate the city influence on the ABL, especially on the mixing height. Cracow is one of the biggest cities of Poland with about 1 000 000 inhabitants, while Katowice, distant from Cracow by 70 km, is also a large city in the centre of the Silesia industrial region.

The measurement site in Cracow is located in the city area: the Urban Meteorological Station (UMS) is Cracow Czyyny, located in the middle of the city between two main centres of urbanisation (the old centre of Cracow and the new industrial part Nowa Huta; Fig. 5.8). The area is flat, surrounded by numerous trees and bushes. The nearest great buildings are located at about 300 m, though smaller flat buildings are quite near (20 m). The station is located near the centre of the urban heat island, as identified on satellite images. The mean wind speed at UMS is about half of the values recorded at a station located outside the city.

During the COST-715 experiment, most of the remote sensing equipment was located in Cracow with two sodars located at the UMS: one monostatic with Doppler analyses of vertical wind components (covering the layer 30–1000 m), and one Doppler sodar for the determination of the vertical wind profile. Additionally, at the UMS in Cracow were operated an aerosol lidar, a tethered balloon (profiles of wind speed, temperature, humidity), one sonic anemometer mounted 2 m above the grass-covered surface, a system of three pyranometers
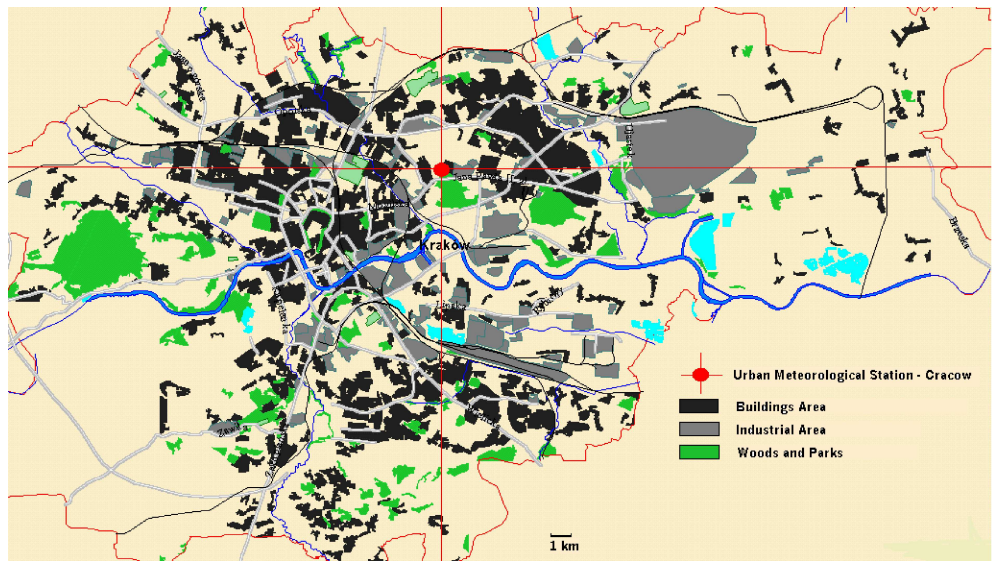
Figure 5.8: The Cracow area with indication of the main land use classes. The urban meteorological station site is marked by a red dot. The station is located near the old, historical airport not used now, covered by buildings.

and a semiconductor sensor to determine the heat flux. An automatic meteorological system measured temperature and wind speed every 6 s at heights of 2 and 10 m for the calculation of the Monin-Obukhov length L. A second measurement site was located in the urban part of Katowice (located at 70 km from Cracow) with one monostatic Doppler sodar. The two data sets were analysed separately, the data set of the "Katowice" monostatic sodar was used for preparing the MH determination method based on the concentration of Polonium (see Section 7.6).

These measurements were supplemented by standard meteorological measurements in both cities and with a network of meteorological stations in the surrounding rural areas. The evolution of meteorological conditions involved the following parameters: atmospheric pressure, air temperature, wind velocity, relative humidity, precipitation, solar radiation, cloudiness, visibility, and cloudbase.

The tracer measurements consisted of pumping ambient air together with all particles through a filter with adjusted flow rate. A special semiconductor PIPS CAM detector was placed above this filter so that alpha radiation emitted by

polonium ^{218}Po, which was separated out of the air stream and deposited on the filter, could be detected. The detector was part of an alpha spectroscopy system. Therefore, it was possible to distinguish alpha particle energy and identify isotopes collected on filters (Osrodka *et al.*, 2002). Two 24-hrs measurements of Polonium concentrations were performed on a former airfield in the centre of Cracow near the UMS from where meteorological data were also collected, during days with well-marked diurnal changes of MH (sunny, hot weather). In Katowice, Polonium concentration measurements near the surface and investigations of their relationship to the MH have been performed on an experimental basis since 1999. Now the Polish Institute of Meteorology and Water Management has data from 30 such experiments.

Measurements of radon ^{222}Rn concentrations in soil gas were performed at a depth of 1 meter using the Barasol probe. This probe is adjusted to permanent and long-term measurements. This device is equipped with a silicon detector of PIPS type. Results were averaged over period of 15 minutes.

The data set will be used for calibrating the formulae for the determination of the MH and the heat fluxes. The objectives of the campaigns were: (i) to verify the radiation balance models by comparison with measurements, (ii) to verify MH models by comparison with measurements, (iii) to implement the MH parameterisation model based on measurements of concentrations of Radon derivatives, and (iv) to apply a LES-model to the calculation of ABL turbulent flow characteristics (TKE, MH, roughness coefficient, u_*, radiation flux, etc.), in order to verify pollution dispersion parameterization in other widely used models (like Gaussian plume model, Gaussian cloud model).

The MH was determined in both Cracow and Katowice using the monostatic sodar. Physical parameter data of the boundary layer were collected in real time. However these results were averaged over 1-hr periods to harmonise them with polonium air concentration measurements. Results on the MH are reported in Sections 7.3.3, 7.4.2, and 7.6.

5.6. Helsinki, Finland

Mixing height estimates utilising data from the Kivenlahti radio tower (327 m high tower located in the western suburban area of Helsinki, in Espoo) are continuously compared with predictions from the NWP HIRLAM-model. One

objective of this work is to improve the parameterisation for urban turbulence and the MH in the UDM-FMI and HIRLAM models (e.g. Rantamäki *et al.,* 2003), especially under stable situations. These studies are continued as part of the FUMAPEX-project.

An extensive amount of ceilometer data and vertical soundings data from the Helsinki area is utilised to test the applicability of the ceilometer for mixing height determination. The typical problem for lidars, to be able to measure in the lowest few hundred meters due to inadequate optical overlap, is overcome with the Vaisala CT25K single-lens design (a pulsed diode, InGaAs, lidar-based ceilometer operating at 905 nm with a measurement range of 7.5 km), with which the highest signal-to-noise ratio is achieved at the lowest altitudes. This permits determining, e.g., the nocturnal boundary layer better than before. Furthermore, since in an urban environment the atmosphere is always more or less turbid, this will provide more detectable signal than in a clear atmosphere, hence providing a clear opportunity for using ceilometers for measuring and predicting urban pollution levels and the urban mixing height.

Measurements used in this study were carried out in 2002 at the test field of Vaisala Ltd, in the northern suburban area of Helsinki, using a Vaisala CT25K ceilometer pointing in a near-vertical direction. Routine soundings carried out every workday provided reference information, and all standard meteorological parameters including visibility and present weather were recorded continuously nearby (ref. `http://www.vaisala.com/weather`). Data were recorded at 15-second intervals and stored for later analysis. The surroundings are rural-suburban, 15 km north of downtown Helsinki and the southern coast of Finland. No major industry is present in the neighbourhood. The results of a meteorological pre-processing model FMI-MPP (Karppinen *et al.*, 1998) were also utilised in this study.

5.7. The CALRAS data set

As a result of the Mesoscale Alpine Programme MAP, the MAP data centre (`www.map.ethz.ch`) issued the comprehensive Alpine radiosonde data set CALRAS (*Comprehensive Alpine Radiosonde;* Häberli, 2001) for the period 1991–1999 with additional stations in Central Europe. The quality controlled, high resolution radiosoundings from CALRAS are also available for big cities in and around the Alpine area (Fig. 5.9).
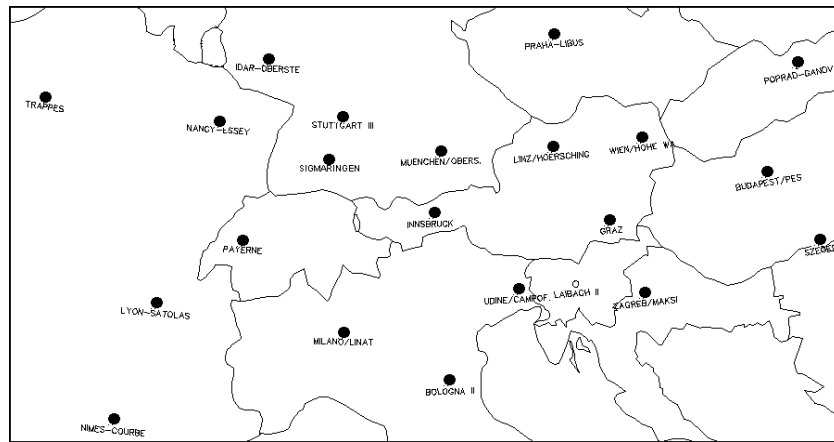
Figure 5.9: Radiosonde launching sites of the CALRAS data set 1991-1999.
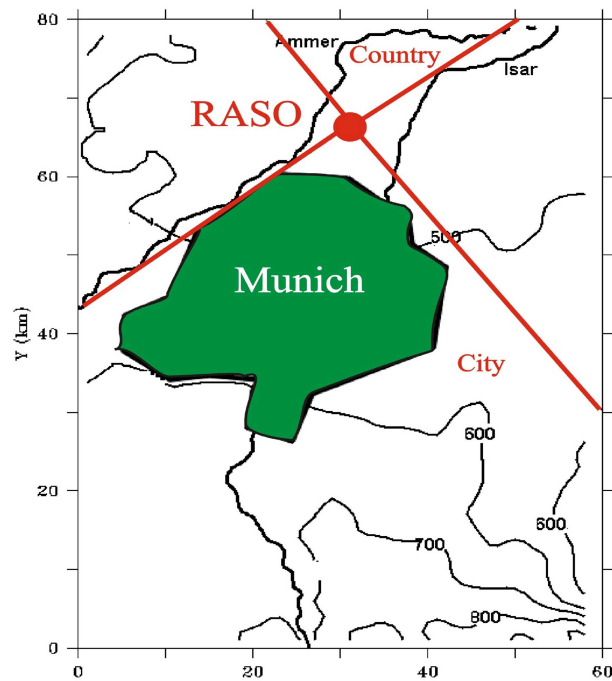
Figure 5.10: Urban area of Munich, position of the radiosonde site at the airport (RASO), topography (contour lines) and sectors of wind directions with urban/rural influence.

The project "Climatology of Alpine Boundary Layer Heights" used the CAL-RAS data set of the MAP upper air station network set up during the Special Observation Period between Sept. 7 and Nov. 15, 1999, to test a set of diagnostic schemes like the Heffter method, parcel methods, Richardson number methods, the humidity-jump method (see Section 4.2.1) and the height of the local wind maximum to derive the mixing height (Baumann-Stanzer and Groehn, 2004). In Section 7.2.1, the CALRAS data set for Munich will be used to compare different diagnostic schemes to derive MH both for day and night.

MHs are calculated for all cases when the radiosoundings sampled within the urban plume downwind of the city and for those cases when mainly rural areas upwind of the radiosonde site influence the profile. The observed wind direction at 500 m above ground is used to determine whether the radiosounding is mainly launched within the urban plume ("urban" profile) or whether the probed air has crossed the countryside before arriving at the sounding site ("rural" profile). This is indicated by the wind direction sectors for Munich in Fig. 5.10.

5.8. ATHIBLEX/MEDCAPHOT experiments in Athens

The MEDCAPHOT-TRACE experiment took place in the Greater Athens area (Fig. 5.11) for 30 days during the summer of 1994, and encompassed a variety of meteorological situations (Ziomas, 1998). The purpose was to study the chemical and meteorological evolution of ozone and related compounds under various synoptic and local meteorological conditions.

Meteorological measurements included: near surface wind measurements performed on small masts at 11 locations, turbulence measurements with two sonic anemometers at two sites (one within the city, at the National Observatory of Athens, NOA, 4 km inland from the shoreline station, the other one 13 km inland in a suburban area, Marousi), profiles of wind speed and direction, air temperature and humidity up to 500 m height with tethersondes at both sites; and regular radiosoundings performed twice a day at the old Athens Airport near the coastline. Besides, in addition to the 9 operating stations of the existing air pollution monitoring network, 18 new stations were operated within the Greater Athens area. Instrumentation for air quality consisted of ground-based air pollution measuring systems (gas analyzers and gas chromatographs), integrated-path air pollution measuring systems (DOAS), and ground-based laser remote sensing systems (lidar). These data were completed by 9 flights
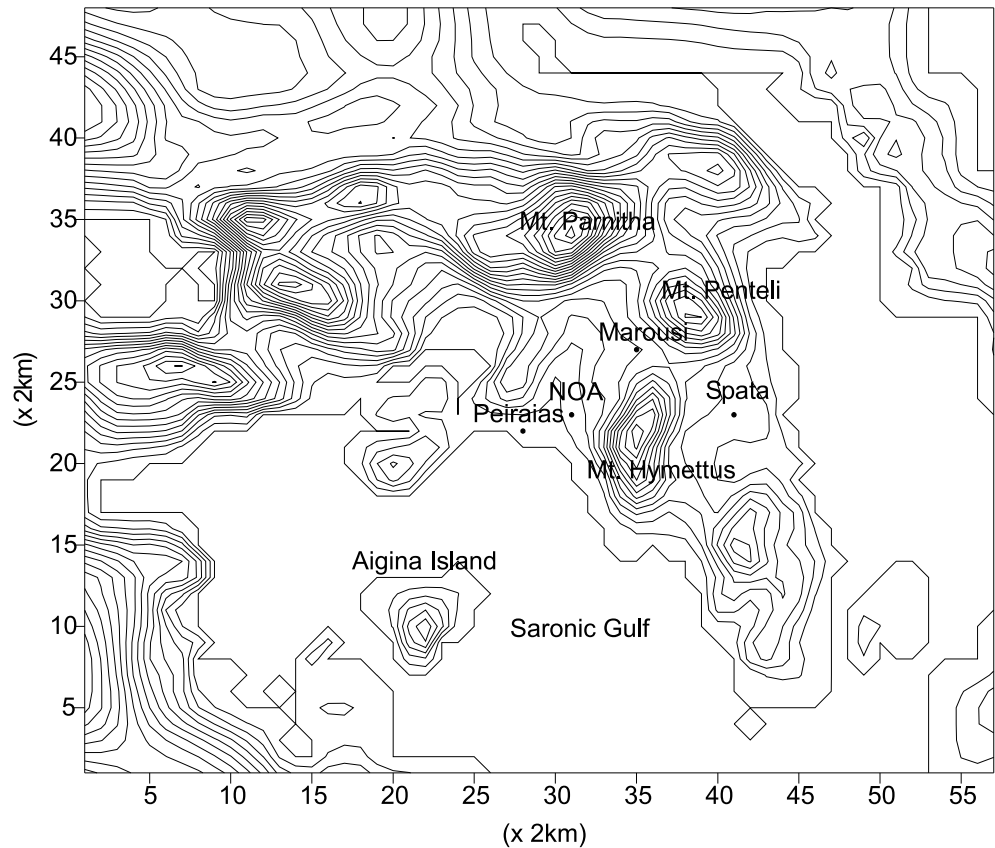
Figure 5.11: Topography contour lines with 50m intervals of the Attiki peninsula. The locations of the stations at the city center (NOA), Marousi, and Spata are also indicated.

of an aircraft measuring air pollution and meteorological parameters during a period of 10 days.

Atmospheric turbulence and vertical profiles of various meteorological parameters over the area (mainly at NOA and Marousi) were investigated by Batchvarova and Gryning (1998) who obtained the following useful information on urban and suburban characteristics:

- During prevailing synoptic winds (Northerlies), heat fluxes were 25% higher at NOA than at the Marousi station, while the difference in friction velocity was less than 15% (higher at NOA).

- During days with a pronounced sea breeze, the differences in heat fluxes were larger at the two sites compared with days with synoptic winds.

- The temperature amplitude at Marousi is larger for sea breeze days compared to northerly winds days, while at NOA there is no difference in air temperature amplitude for the two types of wind flow. During the sea breeze days, the temperature at Marousi is more than $2°C$ lower than the temperature at NOA during the night while it becomes $1°C$ higher during the day.

- The height of the internal boundary was also measured at NOA for several days. This was found not to exceed 400 m.

The collected data were re-examined by Dandou *et al.* (2004) using numerical simulations in order to advance our understanding of urban effects on meteorological parameters. The simulations were carried out with a modified version of MM5 where changes were introduced both in the thermal and the dynamical part.

5.9. Copenhagen, Denmark

Several experimental studies on the ABL structure and dispersion in the Copenhagen area and surroundings have been performed: the Copenhagen experiment (Gryning and Lyck, 1980), the Øresund experiment (Gryning, 1985), the Jægtvej study (Kemp and Palmgren, 2003), and the Jægersborg measurements (Rasmussen *et al.*, 1997; Baklanov and Kuchin, 2004).

The Copenhagen metropolitan area (Greater Copenhagen) was chosen particularly for the inter-comparison of methods and experimental studies on the mixing layer under urban conditions (Baklanov and Kuchin, 2004). Figure 5.12 presents a map of the Copenhagen Metropolitan area and its surroundings with the locations of the meteorological measurement stations of the Danish Meteorological Institute (DMI) and other Danish research institutes. The radiosounding station of Jægersborg (marked by a big red ellipse on the map) is used for the MH studies. This station is situated inside Greater Copenhagen and it can be considered as an urban (or semi-urban) site. It is situated on a small hill (40 meters above sea level) with a relatively homogeneous and

open surface ($\sim$ 100 m), and surrounded by urban areas from S, SW, and SE-directions; semi-urban and rural areas – from NW and N-directions, and by a forest park in the coastal area with the Øresund water surface upwind from the NE-direction. Therefore, all measurements from the radiosounding station were separated for analysis according to the wind direction from three corresponding sectors: 1) urban areas of central Copenhagen 2) rural and semi-urban areas, and 3) water and coastal forest. The sector separation is indicated by the black lines on the map in Fig. 5.12. The effective roughness for these sectors is 1) 1 m, 2) 0.31 m, 3) 0.2 m, respectively.

Several years statistics of radiosounding profiles from the Jægersborg station were analysed and included in the dataset. This station is included in the WMO database, but DMI radiosounding stations use a higher vertical resolution than the WMO standards, therefore, we will use the original data with the highest resolution. The Jægerborg station releases radiosondes twice a day: 12:00 and 24:00, local time (corresponding in winter to 11:00 UTC and 23:00 UTC). The vertical structure (from 2 m up to 5000 m) of the following meteorological values is measured: pressure, wind velocity, wind direction, air temperature and dew-point. From these data the vertical profiles of the potential (θ) and virtual (θ_v) temperature, relative humidity (q), and mixing ratio (r) can be calculated. The first lowest level measurements are performed at 2 meters for pressure, air temperature, and dew-point; and at 10 meters for wind velocity and direction by separate instruments at the moment of the radiosonde launching. The next level of a radiosonde measurement corresponds to 25–50 metres, and further measurements follow each 5 seconds with a vertical resolution of 25–50 m depending on the ascent velocity of the radiosonde.

Additionally, wind and temperature vertical profiles for the Copenhagen area are available from measurements by commercial aircrafts departing or landing at the Kastrup airport (situated almost inside of Greater Copenhagen, Fig. 5.12). Most of the airplanes are equipped with on-board sensors of pressure, temperature, wind velocity, and will be equipped soon with moisture sensors. In the framework of the EUMETNET-AMDAR Project (Aircraft Meteorological Data Reporting; E-AMDAR, 2002), in which DMI participates (see also Section 4.2.3), all meteorological data from the involved airplanes are transferred in the AMDAR communication system (AMDAR, 2003) and available operationally. The DMI-HIRLAM model already assimilates these data for the operational NWP. The quality of these data is comparable with the radiosounding data and will be increased in the future, besides the fact that aircraft measurements are much more frequent in time (excluding night-time).
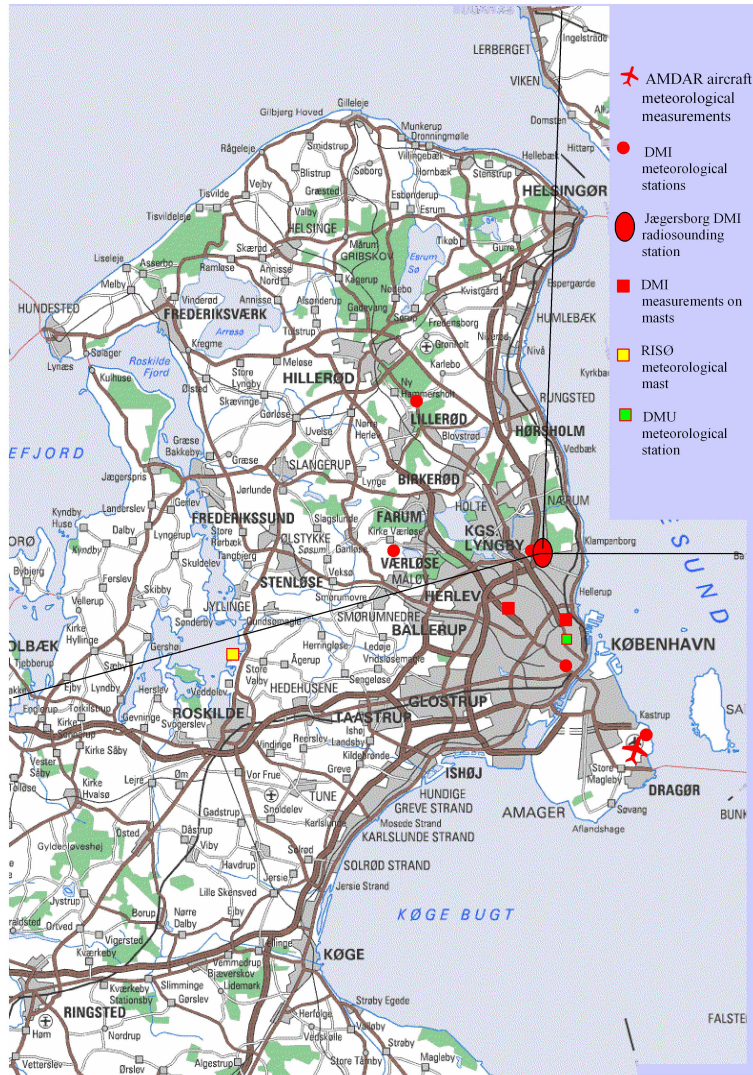
Figure 5.12: Map of the Copenhagen Metropolitan area and surroundings with the position of meteorological measurement stations. The radiosounding station Jægersborg is marked by a big red ellipse, the corresponding 3 sectors, considered in the report for the station, are separated by the black lines.

Finally, measurements from the Risø research meteorological mast (200 m high) outside of the Copenhagen urban area can be used as reference data for comparative studies of the urban effects on the ABL.

5.10. Hannover, Germany

In the framework of the project VALIUM (Validation of instruments for environmental policies) within the program AFO2000 (Atmospheric Research 2000) of the German Federal Ministry of Education and Research, long-term meteorological and air quality measurements were carried out in the street canyon "Göttinger Strasse" in the town of Hannover in Northern Germany from spring 2001 to spring 2003. This street canyon runs in front of the main building of the Lower Saxony Agency for Ecology (NLÖ). The horizontally averaged roughness length of the more or less urban area within a radius of 10 km is about 1 m. A CD with the professionally-made data bank VALIDATA containing the whole Hannover data set is freely available from the coordinator of the VALIUM project, Michael Schatzmann at the Meteorological Institute of the University of Hamburg, Germany.

In order to monitor the ambient flow conditions (wind profile and MH) near this street canyon a sodar was placed about 550 m upstream (with respect to the most frequent wind direction, which is Southwest) of the street canyon and the roof-top station (on top of the NLÖ building) was on the premises of a larger factory away from housing areas. An analysis of the mean wind profiles obtained in Hannover can be found in Emeis (2004). For comparison with the sodar data, a ceilometer (Räsänen *et al.*, 2000) was placed about 20 m above ground level on the roof of the NLÖ building. The distance to the roof-top station HRSW is about 30 m. Additionally a RASS (Vogt and Jaubert, 2004) was operated 150 m away from the roof-top station in the backyard of the NLÖ building. The intensity of the acoustic sound emission by the RASS had to be limited due to the people working in a near-by office building. Sodar, RASS, ceilometer, and roof-top stations were positioned along an almost straight line that is running from Southwest to Northeast. The end points of this 550 m long line are indicated by the two red dots in Fig. 5.13.

The sodar used was a METEK DSD3x7 mono-static Doppler sodar (Reitebuch and Emeis, 1998) having three antennas with seven sound transducers each (i.e., a device that serves both as a loudspeaker and as a microphone, depend-
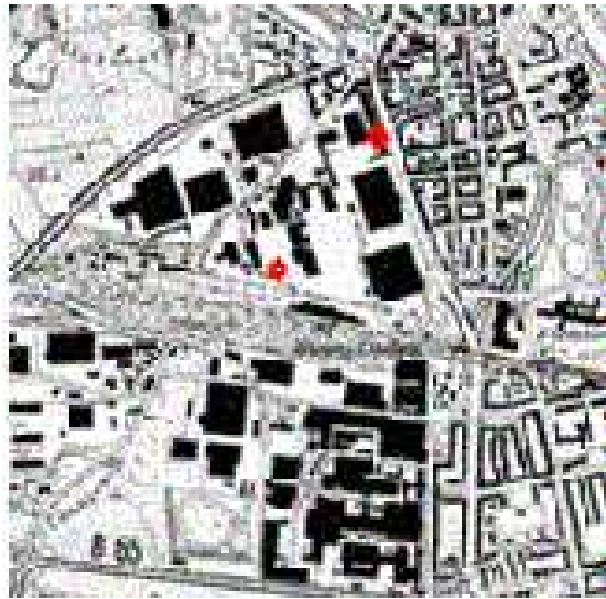
Figure 5.13: Map of central Hannover with the position of the measurement sites (see text for details)

ing on the phase of the measurement cycle), working at about 1500 Hz. The instrument is optimised for long-range detection up to 1300 m above ground in ideal conditions without external noise sources.

The sodar was operated from October 2001 until April 2003 with one and the same settings (with the exception of June and July 2002). The ceilometer was run from February 2002 until April 2003. The RASS was deployed to Hannover only for two shorter campaigns in spring and autumn 2002. The first time period during which all three remote sensing instruments were available was from April 26 to May 12, 2002. A second period was from October 19 to November 1, 2002. The results of the instrument inter-comparison are presented in Emeis *et al.* (2004). The ceilometer was made available by C. Münkel from the company Vaisala, the RASS by S. Vogt from the Institute for Meteorology and Climate Research of the "Forschungszentrum Karlsruhe".

6. Data validation of surface energy budget schemes and models

6.1 Results from field measurements

6.1.1 North America

In the last decade, a series of local-scale energy balance observations have been conducted at a restricted number of sites, largely, though not exclusively, residential areas in North America (see, for example, Grimmond and Oke, 1995, 1999a, 2000; Grimmond *et al.* 1996; Oke *et al.* 1998, 1999; Spronken-Smith, 1998; Feigenwinter *et al.*, 1999).

A Multi-city Urban Hydrometeorological Database (MUHD) has been generated to document local-scale surface heat flux variability in several North-American cities (Grimmond and Oke, in COST-715, 2002a). MUHD integrates surface energy balance observations, each 1 to 8 weeks in duration, conducted over a ten-year period. These surface energy balance data were collected primarily in summertime, with the exception of Mexico City (dry winter season). The urban land uses represented include central city, light industrial, and low or medium density residential. Sites were selected to represent different building densities (sometimes in the same city) and climates. Grimmond and Souch (1994) outlined the methods used to develop the surface cover information for the MUHD sites. For all sites, areas of similar surface cover and morphometry in a 2–5 km radius around each measurement site are mapped from aerial photographs, and detailed attributes such as building height and type, density, vegetation amount and type are documented. These databases are then coupled to the Flux Source Area model of Schmid (1994, 1997) to quantify the surface cover influencing local-scale surface energy balance observations taken using instruments mounted on tall towers ($> 2z_H$, the mean height of the surrounding roughness elements).

Some key characteristics of surface energy balance partitioning, derived from MUHD, are summarised in Table 6.1. In general, the radiation fluxes of cities show magnitudes and diurnal behaviour similar to those of rural surfaces (Oke *et al.*, 1998). As expected, areas with little vegetation have extremely small latent heat flux values. Of the residential sites, the neighbourhood in Vancouver had the lowest measured rates, due to an effective garden irrigation ban that was in force in 1992, an abnormally dry year (Oke *et al.*, 1998). The remaining residential areas have daytime peaks in evaporation ranging from

125 to 235 $W\,m^{-2}$; these are significant fluxes, sustained by garden irrigation and/or frequent rainfall (at least 20 to 40% of daytime Q^*). At all sites, more energy leaves the surface as sensible rather than latent heat flux; consequently the Bowen ratio values are greater than unity (Table 6.1). Storage heat flux was determined as a residual (Eq. 1 in Grimmond and Oke, 1999a). This is always a significant term in the surface energy balance in urban areas, and is considerably larger than for most natural systems, except water. In general, the storage sensible heat flux is most important at central city and light industrial sites (at least 50% of daytime Q^*), whereas turbulent sensible heat flux is most important at residential sites (40 to 60% of daytime Q^*).

Table 6.1: Ranges of average daily maximum values of net radiation and fluxes at the MUHD sites (after Grimmond and Oke, in COST-715, 2002a)

Parameter	Range ($W\,m^{-2}$)
Net all-wave radiation Q^*	$< 400 - 650$
Latent heat flux Q_E	$10 - 235$
Sensible heat flux Q_H	$120 - 310$
Storage heat flux G	$150 - 280$
Average daytime Bowen ratios Q_H/Q_E:	(Dimensionless)
Residential sites	$1.2 - 2$
During irrigation ban Vancouver	~ 2.8
Light industrial site	~ 4.4
Downtown	~ 9.8

An investigation of urban-rural energy balance differences for three North-American cities with different rural environments revealed contrasting heat and water balance regimes, some even being capable of completely inverting expected urban-rural difference (Oke and Grimmond, in COST-715, 2002a). The cities studied were Tucson, Arizona, with surrounding desert, Sacramento, California, with semi-arid grassland and irrigated farmland, and Vancouver, British Columbia, with surrounding moist farmland. Whereas urban-rural differences in net radiation are mostly less than $+/-50$ $W\,m^{-2}$, the Tucson results are distinctly different. Daytime urban Q^* in Tucson is as much as 125 $W\,m^{-2}$ greater than in the surrounding rural desert suggesting the city is a better absorber than the desert by day. This might be interpreted to be due to the lower albedo and/or lower surface temperature of the city, which in turn is related

to greater abundance of urban vegetation and irrigation. For all the cities, the storage heat flux is, as expected, greater than the rural values; the urban fabric sequesters more heat by day than the surrounding countryside. At night, the cities release greater amounts of heat from storage. For the turbulent sensible and latent heat fluxes, the station pairs with moist and wet rural sites (Vancouver and Sacramento) confirm conventional expectations, i.e. cities evaporate less and generate a greater sensible heat flux to the air than their rural surroundings. On the other hand, the semi-arid and desert pairs show the reverse. The source of urban moisture here is garden irrigation.

While offering much new insight into surface energy exchanges in urban environments, more data need to be collected to represent cities with different building materials and architectural styles, as well as for conditions with direct energy release from human activities (the anthropogenic heat flux, Q_F) is more significant. Moreover, the above results cannot be directly extrapolated to European cities due to land use, climatological and urban metabolism differences. There are several experimental studies of the urban surface energy budget for European cities (e.g. Klysik, 1996; Dupont *et al.*, 1999; Holmer and Eliasson, 1999), but they do not specifically analyse the different components of the surface energy budget in cities. Therefore, three new field campaigns, in Basel, Marseille and Birmingham, have been initiated, to more explicitly study processes in European cities.

6.1.2. Basel

6.1.2.1 Urban Radiation Balance

Albedo:

Recent European field campaigns showed that the surface albedo of most European urban surfaces is remarkably low. Long term albedo values in the city centre of Basel are around 10% (Christen *et al.*, 2003), 8% were reported from downtown Marseille (Roberts *et al.*, 2004) and around 9% from Lodz, Poland (Offerle *et al.*, 2003). It is found that the taller and denser the buildings, the lower the albedo. Dark materials and shading in narrow street canyons lower the albedo significantly and suggest that dense European city centres are better absorbers than most North American city surfaces, which are typically in the range 15–20% (Sailor and Fan, 2002).

Net Radiation:

Measurements in the city of Basel during BUBBLE (Section 5.1) showed that this higher short-wave energy input of the urban surfaces due to the low albedo is mostly counterbalanced by an increased loss through long-wave components. This finally results in nearly equal daily totals of the net all-wave radiation $Q*$ over urban, suburban, and rural surfaces. During daytime the city centre captures slightly more energy compared to the rural surfaces (approx. +5%). Reversely, during night, the city loses slightly more energy through long-wave emission and a dryer atmosphere than rural sites (Christen and Vogt, 2004).

6.1.2.2. Turbulent Flux Densities

During BUBBLE, a network of seven micrometeorological stations was operated in the city of Basel, Switzerland (Section 5.1, Fig. 5.1). Three urban sites provided turbulent flux densities and radiation data over dense urban surfaces. Together with a suburban site and three rural reference sites, this network allows the simultaneous comparison of the urban, suburban, and rural energy balance partitioning in a Central European city during a summertime period of one month. Figure 6.1 presents the diurnal courses of the surface energy balance of one urban, one suburban and one rural site, which were all operated simultaneously. The curves represent the average diurnal course including all weather conditions from clear-sky to completely overcast days.
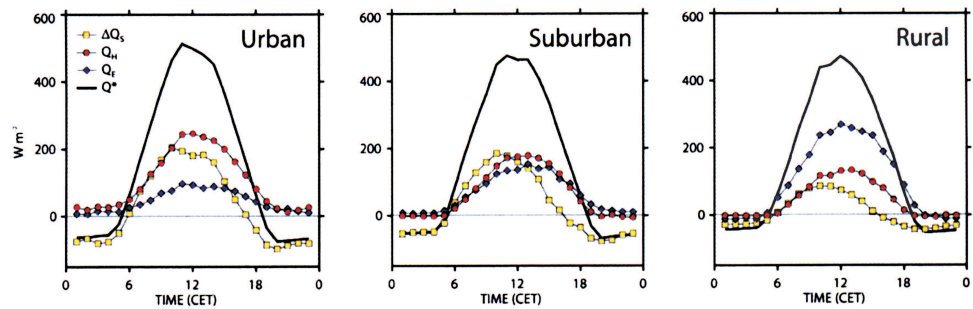
Figure 6.1: *Ensemble diurnal courses of the energy balance at three sites during BUB-BLE for an average day during the IOP from June 10 to July 10, 2002 (including all sky conditions) of an urban site (Basel-Sperrstrasse), a suburban site (Allschwil), and a rural site (Village-Neuf) (modified after Christen et al., 2003).*

It is not surprising, that the lower the vegetation aspect ratio, the less latent

heat flux density Q_E is observed. On the other hand, the sensible heat flux Q_H and storage heat flux ΔQ_S are increased in the city. The instrumented towers operated during BUBBLE provide insight into the vertical profile of Q_H down into street canyons. The largest gradients of the sensible heat flux, and therefore the strongest heat flux density divergences $\partial Q_H/\partial z$, are found around roof level and in the upper canyon part indicating that mainly the roof areas contribute to Q_H in a dense city. During midday only 20% of Q_H originate from the street canyon's floor, 70% of Q_H diverge between $0.8 < z/z_H < 1.4$. This indicates that for Q_H the blending height z^* is already reached at $1.5z_H$.

Similarly to other urban energy balance studies, all built-up sites in the city of Basel (3 urban, 1 suburban tower) show also a significantly increased magnitude of the storage heat flux densities ΔQ_S, an effect of the urban surface materials and higher complete aspect ratio. Daytime values of ΔQ_S are two to three times more intense in the city centre compared to rural sites and ΔQ_S shows a pronounced hysteresis in its diurnal course at all sites. The daily peak values are reached 1 to 2 hours before the maximum intensity of Q^* is recorded, and in the evening the urban surfaces start to release stored energy one to three hours before Q^* changes sign.

The huge daytime heat storage into buildings is counterbalanced by an extremely high nocturnal release of stored heat. The nocturnal release of ΔQ_S in the city centre of Basel is often higher in magnitude than the radiative loss. This leads to typical nocturnal ratios of $\Delta Q_S/Q^*$ between -0.9 and -1.3. In contrast to rural surfaces, where nocturnal sensible heat fluxes Q_H are directed towards the surface, over urban areas both turbulent flux densities transport energy away from the surface in the city centre of Basel. The nocturnal upward directed turbulent fluxes are observed all around the year as long-term measurements between 1994 and 2002 at the tower "Basel-Spalenring" show (Fig. 6.2, Christen and Vogt, 2004).

The nocturnal upward directed turbulent fluxes in dense urban areas determine the stability of the near surface air layer. Stable situations in the city centre are seldom observed ($< 10\%$ of all cases). Stable situations during night become more and more dominant (rural approx. 60%) with decreasing building intensity. Remote sensing instruments and tethered balloon measurements during BUBBLE show that this nocturnal unstable layer is only found very close to the urban surface. An elevated inversion layer is observed over the city, often at heights between 50 and 250 m (Rotach *et al.*, 2004a).

Sensible Heat Flux at Basel-Spalenring (Eddy Covariance, 1994-2002)
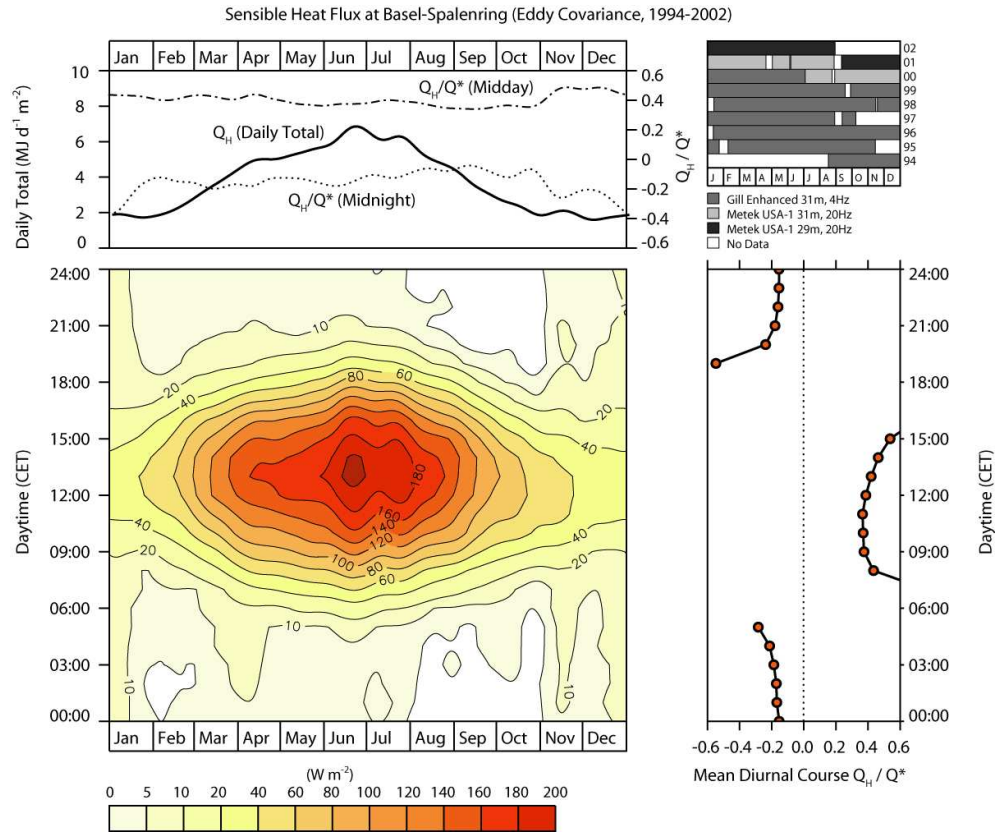
Figure 6.2: Measured sensible heat flux Q_H between 1994 and 2002 over the urban sur-
face at the long-term tower "Basel-Spalenring" using different eddy-covariance
systems. Main plot: The iso-flux diagram illustrates the climatologically aver-
aged values of the sensible heat flux ($W\ m^{-2}$) as a function of the hour and the
day of the year. This shows that during the night positive heat fluxes (i.e. away
from the surface) are measured all around the year. Right plot: mean diurnal
course of the fraction Q_H/Q^* as a function of hour of the day for the period
1994–2002. Upper left plot: Yearly course of the daily total values (full line) and
fraction Q_H/Q^* at Midday and Midnight. Upper right: Documentation of the
different eddy covariance systems that were operated at this site and contributed
to the climatologically averaged values (modified after Christen et al., 2003).

6.1.3. Marseille (UBL-Escompte)

Surface energy budget fluxes were measured for a total of 28 days (June 16 – July 14) at the city centre site. Preliminary results show that the turbulent sensible heat flux is the dominant mode of heat transfer away from the surface during the middle of the day. As found at other densely-developed urban sites in other cities the convective sensible heat flux remains positive throughout the night, sustained by large releases of heat stored in the urban fabric from the previous day (Oke, 1988; Grimmond and Oke, 1999a, 2002). As expected, given the absence of vegetation cover at this site and the dry conditions during the measurement period, the latent heat fluxes are small (Fig. 6.3). As found in other urban areas (Grimmond and Oke, 1999a), ΔQ_S peaks before solar noon and the flux turns negative a couple of hours before the net all-wave radiation (Q^*). Heat storage at this site has been investigated in detail (Roberts *et al.*, 2003).
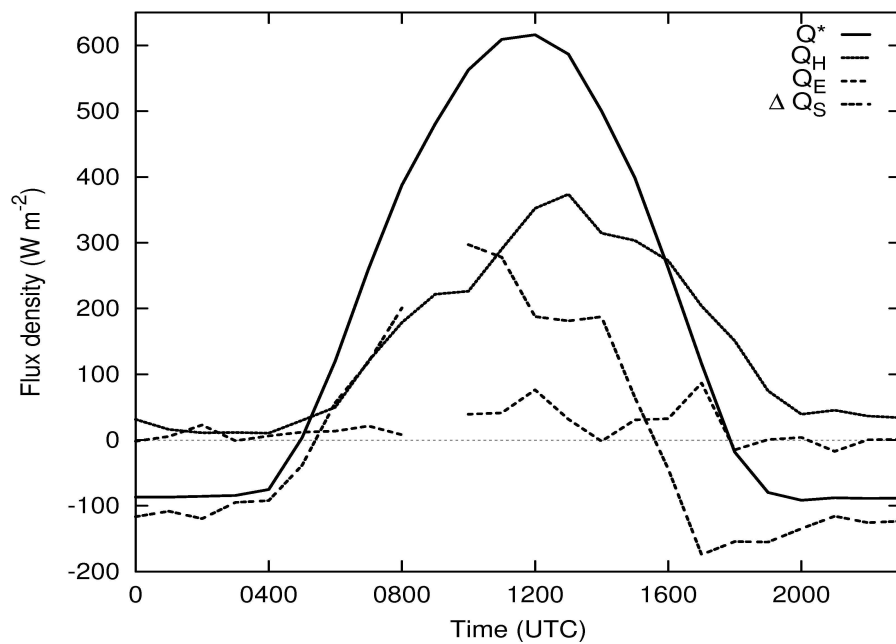

Figure 6.3: Observed surface energy balance fluxes for the six days of IOP 2a and b (days 172-178, June 21-26) at the Marseille city centre site, ensemble mean for the period including the storage heat flux determined as the residual of the observed terms.

The sensible heat fluxes were estimated using Large Aperture Scintillometers (LAS, see Section 5.2). Line-averaged Q_H from the LASs was computed over 15-min periods using two methods (McAneney *et al.*, 1995; De Bruin *et al.*, 1995). The first method combines the scintillometer derived temperature scale T_* with the friction velocity u_*, determined independently, to estimate $Q_H = -\rho c_p u_* T_*$, where ρ is the air density and c_p the specific heat of air at constant pressure. The second method assumes free convection and Q_H is computed directly from the measured structure parameter for temperature, C_T^2. The very good agreement found between both methods and the eddy covariance (EC) measurements on the CAA central mast illustrates the promising potential of scintillometry for urban areas where spatial heterogeneity is large (Lagouarde *et al.*, 2002).

6.1.4. Birmingham, UK

Figure 6.4 shows a clear difference in the hourly averaged heat fluxes over the 21 day period between the urban Dunlop tyre factory site and the rural Coleshill site (Middleton *et al.*, 2002). The urban heat flux at the Dunlop site (solid line) was on average larger during the day. At night the average remained practically zero (neutral) whilst the rural synoptic site (broken line) had a negative average heat flux (stable) reaching a minimum of -30 W m^{-2} at 20:00 UTC. The difference may be due to both the urban heat storage effect and anthropogenic energy. In terms of dispersion meteorological pre-processing, note that a difference in behaviour at night is very important. The mean hourly results showed that over the days studied, the urban heat flux (averaged for each hour) was very close to zero, and remained there, overnight. Meanwhile the rural site showed a negative average heat flux overnight. Diagnosis of stability on this basis would tend to give neutral at night at the factory, but more stable at the rural site. These results were from July/August 2000, the English summer; a long period of observations at a rural and an urban site would be needed to see what happens in all seasons of the year. In this study it was not possible however to have long term deployment of the sonic anemometers.

Figure 6.5 compares the values of reciprocal MO-Length, $1/L$ (plotted as $1000/L$) at the two measurement sites, with the urban data from Dunlop factory site in the vertical, and rural data from Coleshill in the horizontal. If the two sites had the same stability behaviour, apart from the natural occurrence of scatter, we might expect to see the points lying about a line $y = x$. This was not the case; in these data, different stabilities were observed at these two sites 8.5 km apart.
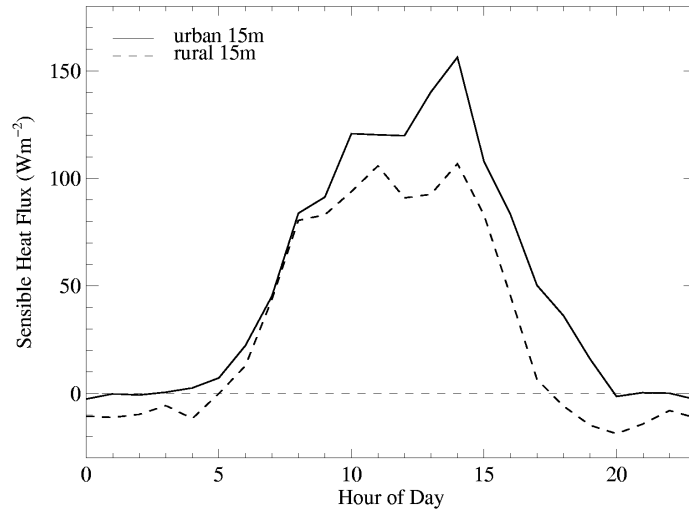
Figure 6.4: Comparison of sensible heat flux measured using sonic anemometers on 15 m masts at Coleshill synoptic station and at Dunlop Tyres Ltd factory site (plot by Nikki Ellis, personal communication). Results are averages by hour of day for the period from 10:00 UTC on 7 July 2000 to 17:00 UTC on 28 July 2000.
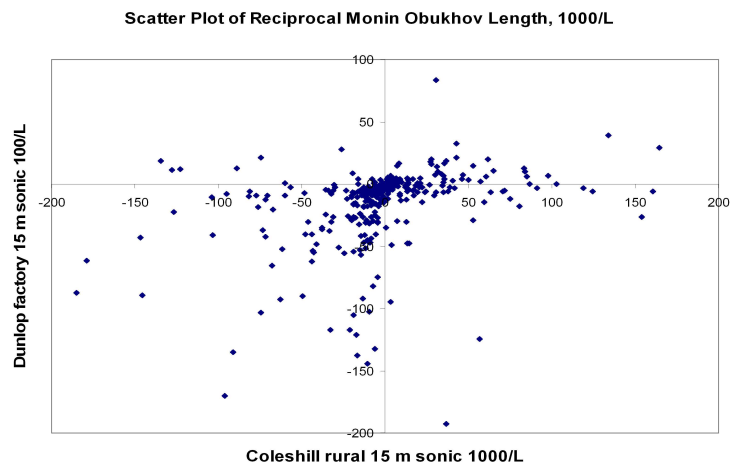

Figure 6.5: Comparison of static stability (1000/L) at Coleshill (rural, x-axis) and Dunlop factory (urban, y-axis).

Negative values (bottom left quadrant where both sites were unstable) are unstable, values clustered at origin are neutral, and positive values (top right quadrant has both sites stable) are stable. Notice that when Coleshill was stable, on the right side of the plot, the Dunlop values tended to fall nearer the horizontal axis, consistent with a bias to more neutral conditions in the urban area. Overall, there were relatively few stable cases (the somewhat few points above the horizontal axis with $1/L > 0$ were almost all showing $0 < 1000/L < 30$, i.e., $L > 33$ m) at the Dunlop site. Additional work is needed to confirm these indications of a limit to L of ~ 33 m for an urban site in the stable case, however.

The experiments have provided a useful set of urban data from three different times in the year for a UK city. Information on roughness lengths as well as the differences in wind speeds, temperatures and heat flux were reported in Ellis and Middleton (2000a).

6.1.5. Bologna

6.1.5.1. Surface fluxes

The turbulent fluxes were evaluated by the eddy covariance method with data collected by the ultrasonic anemometer. A streamlined processing method (Anfossi *et al.*, 1993) was applied to obtain the mean wind velocity and direction, the standard deviations of the longitudinal, lateral and vertical components of the wind (σ_u, σ_v, σ_w), the sensible heat flux, the friction velocity (u_*) and the Monin-Obukhov length (L).

The mean value of the sensible heat flux and of turbulence intensity, described as the ratio between standard deviations of the wind components and the friction velocity, are reported in Table 6.2. This shows that, on clear days, the diurnal sensible heat fluxes markedly increase with respect to the rural site, while the sensible heat flux is positive during nights in summer. In winter, the increased σ_w/u_* values reflect the enhanced turbulence in the urban area compared to the rural area.

6.1.5.2. The "urban effect" in Bologna

During the Bologna experiment, the heat island effect was mapped by deploying 21 thermometers in the town, the suburbs and rural surroundings. All the

Table 6.2: Mean value of some micrometeorological variables on clear days (mean cloud cover < 3 oktas) during the day (10:00–16:00) and at night (22:00–05:00) at an urban (Torre della Specola) and rural site (San Pietro Capofiume).

Season	Site	Night/Day	Sensible heat flux [W/m^2]	σ_u/u_*	σ_v/u_*	σ_w/u_*
summer	Urban	Night	17	3.6	1.9	0.7
		Day	191	6.9	5.8	1.5
	Rural	Night	−2	2.3	3.1	0.1
		Day	161	4.4	6.2	1.0
winter	Urban	Night	−2	3.0	2.1	0.6
		Day	59	2.3	2.8	1.2
	Rural	Night	−1	1.5	1.1	0.1
		Day	26	3.2	2.6	0.4

data were compared with data from 9 ground meteorological stations located inside the experimental area. The data cover periods of 20-30 days during winter (January–February 2001) and summer (May–June 2001). Analysing the interpolated temperature distributions enabled to put into evidence the heat effect of the urban area by subtracting the map based on all data from the map made up of rural data only (Deserti *et al.*, 2003). An example is shown in Fig. 6.6 with a clear distinctive urban heat island feature that is particularly strong (with mean differences of 5 °C between urban and rural sites) during winter nights and periods of synoptic calm and clear sky conditions. The heat island effect depends on cloud cover, and the heat island intensity was observed to be almost linearly inversely correlated with the mean nocturnal cloud cover, as observed at the city airport (Fig. 6.7).

The analysis of the sodar data revealed the existence of urban breeze regimes, combined with an attenuation of the wind intensity in the lowest levels, stronger in the urban than in the rural area. Sodar data (Fig. 6.8) show an attenuation of the wind in the lowest levels near the ground over the urban area during summer nights (left), while at the rural site the wind during the night is often stronger (right).

The vertical wind velocity distributions (Fig. 6.9) observed by sodar put into evidence intense vertical velocity during late spring and summer days (10–20 cm s^{-1}), in both urban (Specola and Accursio) and rural areas (SPC). Similar convective conditions (10 cm s^{-1}) were observed also in winter over the urban area (CNR), during the warmest hours of the day, in the first 200 m over the surface.
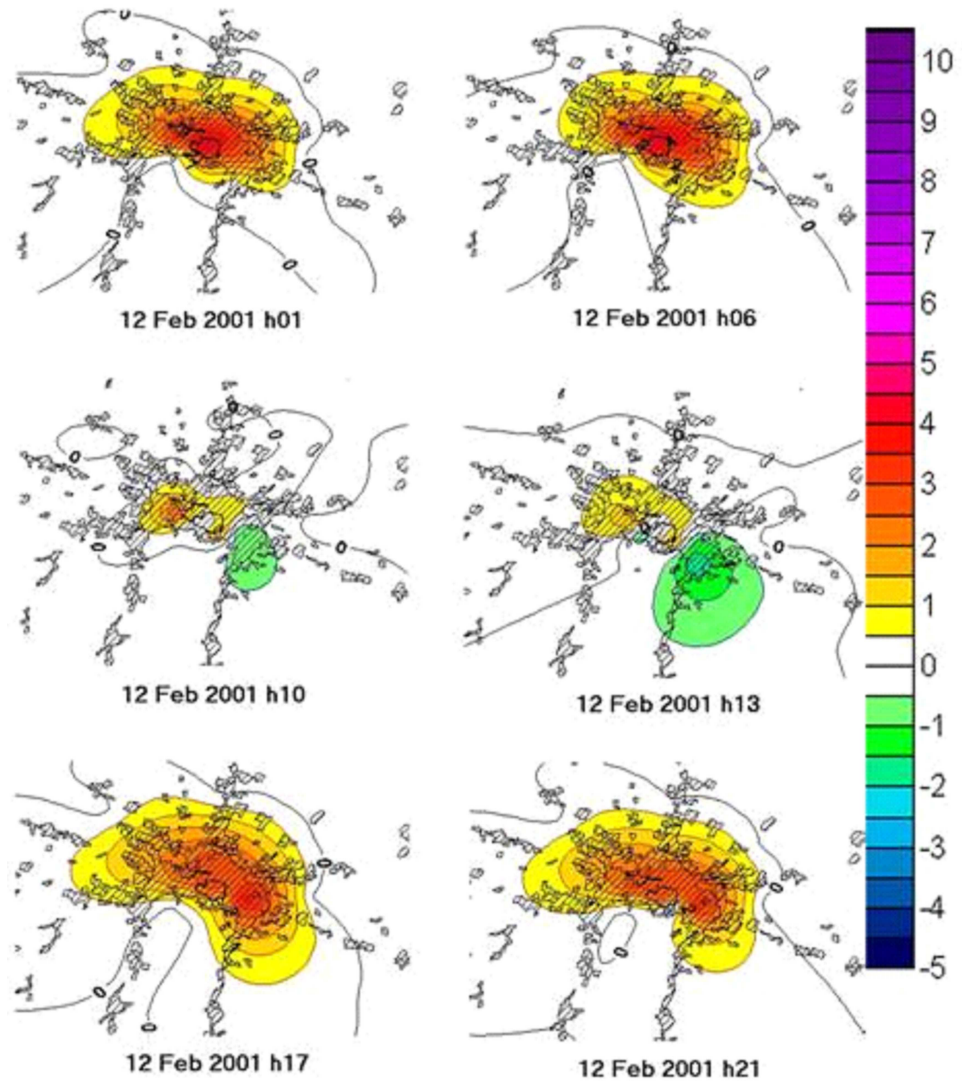
Figure 6.6: Evolution of the hourly heat island in Bologna on 12 February 2001 under
clear sky conditions. The map represents the difference between rural and urban
temperatures. The colour scale is in °C.
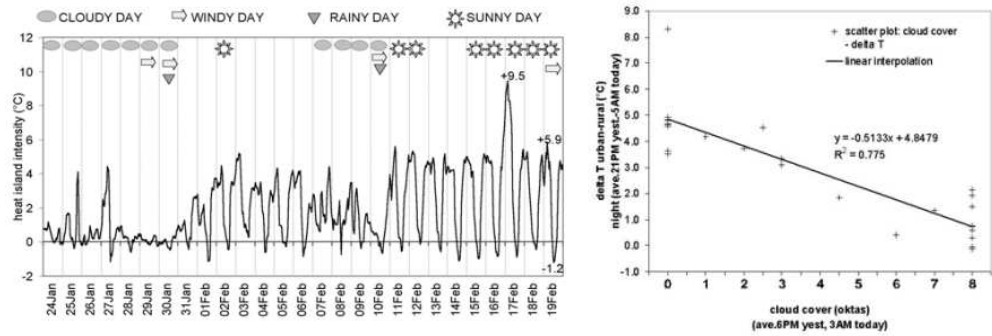
Figure 6.7: Left: meteorological conditions and heat island intensity during the winter phase of the "temperature mapping experiment". Right: relationship between the heat island and the mean nocturnal cloud cover, as observed in the city airport (Heat island intensity = T_{average} of urban sites – T_{average} of rural sites).
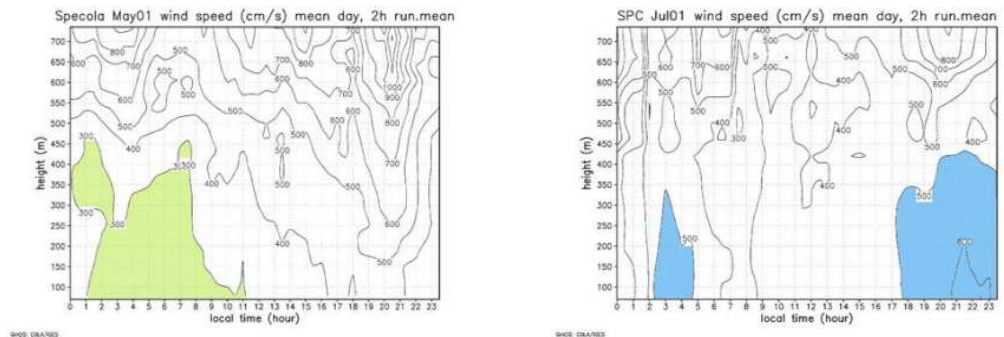
Figure 6.8: Vertical profiles of the horizontal wind velocity (cm/sec) observed by sodar at an urban site (left: Torre della Specola, averages per hour of day for the period 03–24 May, 2001) and at a rural site (right: San Pietro Capofiume, averages per hour of day for the period 03–26 July, 2001) during summer conditions.

Urban summer (Specola)   Urban summer (Accursio)

Rural summer (SPC)   Urban winter (CNR)
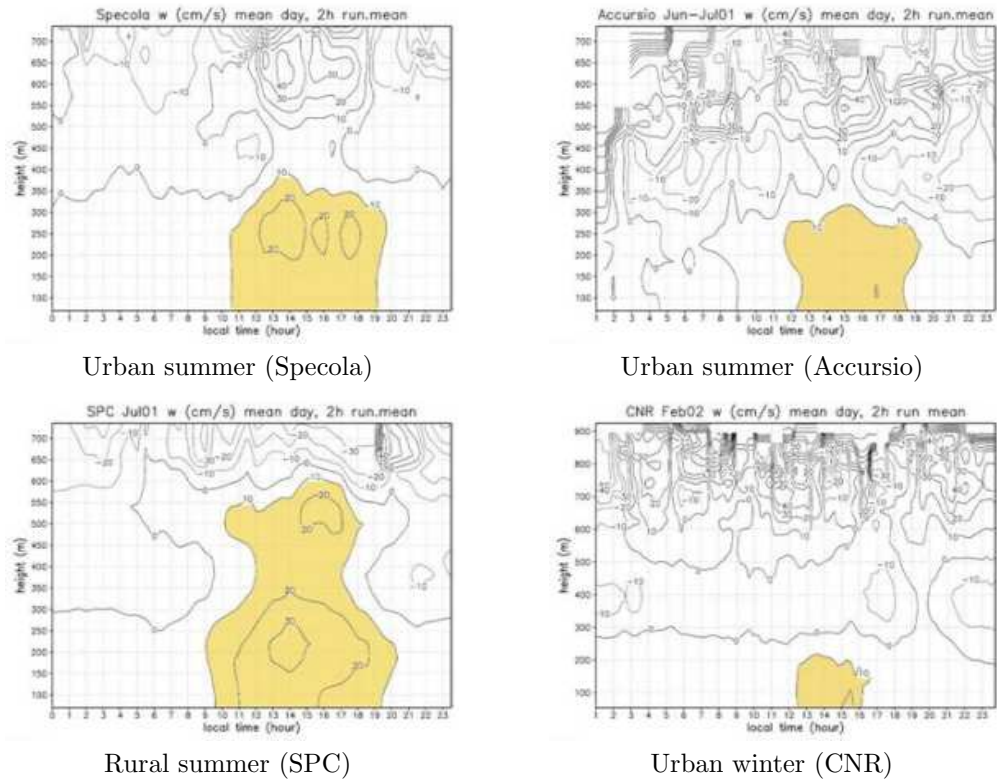
*Figure 6.9: Vertical profiles of the vertical wind velocity (cm/sec) observed by sodar in urban summer conditions (upper part), rural summer (lower left part) and urban winter (lower right part) conditions (averages per hour of day).*

6.2. Parameterisation and modelling

Though parameterisation schemes have been developed to estimate net radiation, sensible heat flux and other boundary layer parameters on a routine basis from hourly standard meteorological data (e.g., van Ulden and Holtslag, 1985; Berkowicz and Prahm, 1982), most of these models were developed and validated using data from flat, grass-covered environments and were limited to horizontally quasi-homogeneous conditions (see a review in COST-710, 1998). In urban areas, as shown in Sections 2, 3 and 6.1, there are marked differences in energy partitioning compared to rural conditions and there is still considerable uncertainty concerning the role of surface cover (e.g., the fractions of built-up areas/green space), city surroundings, and prevailing meteorological conditions. Nevertheless, very recently, some substantial improvements have been achieved

in including urban features specifically into pre-processors or parameterisation schemes. These schemes are described in Sections 3.2.1 to 3.2.5.

6.2.1. Results with the SM2-U soil model

Figure 6.10 (Dupont *et al.*, 2003) shows examples of simulations with the SM2-U soil model (Section 3.2.4) obtained for 4 typical European districts, city centre, residential, industrial-commercial, and high-rise building districts, with their average mixture of building densities, bare and paved soils, and vegetation cover over natural or semi-impervious surfaces. These simulations were obtained
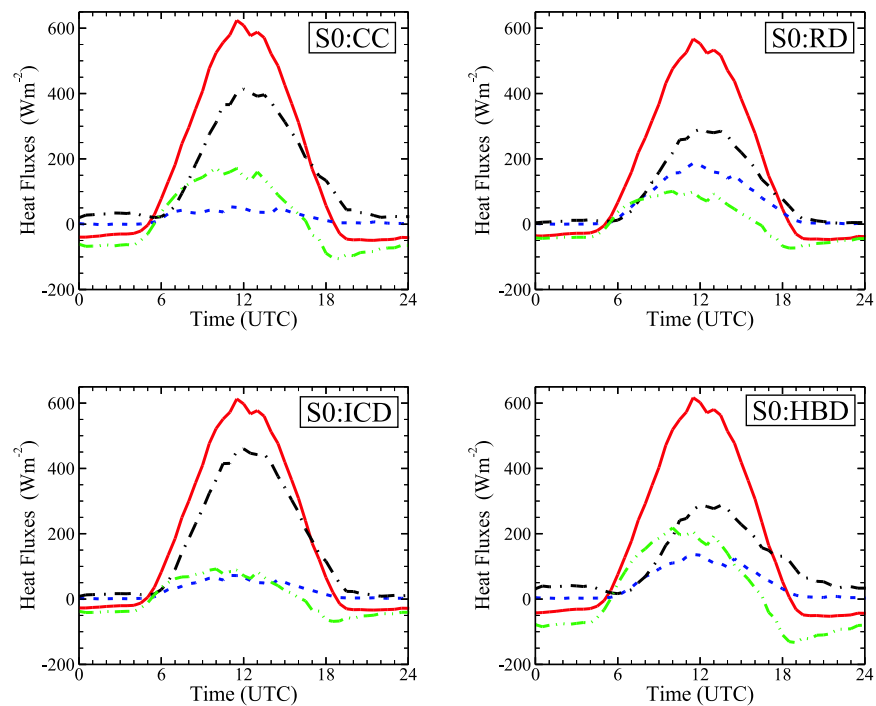
Figure 6.10: Energy budgets over four typical European urban districts (from Dupont et al., 2003): CC, city centre; RD, residential district; ICD, industrial-commercial district; HBD, high building district. The simulation corresponds to an average diurnal cycle in July in Nantes, France, and S0 indicates no surface-atmosphere feedback computation. The curves depict ——net radiation flux; —-, latent heat flux; –·–·–, sensible heat flux; and –··–··–, storage heat flux.

without feedback from the lower atmosphere. Feedback effects are currently studied in the ESCOMPTE simulations for Marseille and idealised cities. Figure 6.10 demonstrates the influence of building density and district structure not only on the magnitude of the heat fluxes but also on the phase lag between the energy budget components, which is a key factor in the urban heat island process: in the first half of the day a large amount of heat is diverted from the budget and provisionally stored in the artificial ground and building materials, at the expenses of the sensible heat, while in the evening and at night these materials, warmer than air, release the stored heat to provide the nocturnal positive sensible heat flux.

6.2.2. Results with the TEB/ISBA scheme

The meso-scale atmospheric model Meso-NH (Lafore *et al.*, 1998) has been used in combination with the TEB scheme (and the ISBA model for rural areas) to compute urban surface fluxes to investigate the influence of Paris on the atmospheric boundary layer for an anticyclonic summer day (Lemonsu *et al.*, in COST-715, 2002a). The TEB model parameterises both the urban surface layer and the roughness sublayer, so that the atmospheric model only "sees" a constant flux layer as its lower boundary. All the turbulent fluxes and the upward radiation flux are computed for each land cover type (e.g. sea, lake, natural and cultivated terrestrial surfaces, urban) by the appropriate scheme (TEB/ISBA) and then averaged in the atmospheric model grid mesh, in proportion to the area covered by each land cover type. The city is represented by generic buildings which have the same height and width, and all road orientations with the same probability. Surface cover information comes from the CORINE Land Cover database with a horizontal resolution of 250 m. Atmospheric data come from ECMWF analyses updated every 6 hours.

When the simulation output is compared to observations from 30 meteorological stations in and around Paris, and with atmospheric profiles from radiosondes, the urban heat island is simulated fairly well, though temperature is over-predicted, especially during the night (Fig. 6.11). Simulated surface energy balance fluxes are shown in Fig. 6.12. The enhanced storage heat flux documented in urban areas and the distinct diurnal hysteresis pattern (Grimmond *et al.*, 1991) are both reproduced well. During the night, storage heat release is enough to maintain a small positive turbulent sensible heat flux.
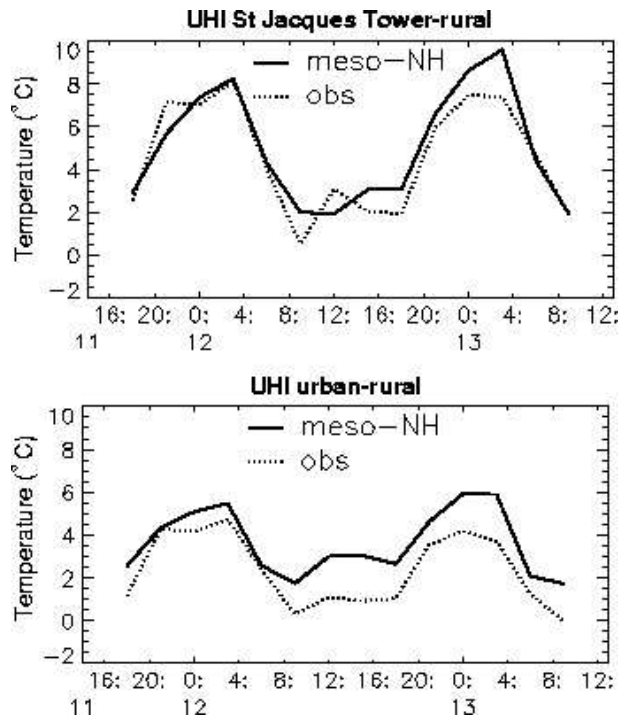
Figure 6.11: Observed and simulated urban heat island on 11-13 July, 1994. Top: between the centre of Paris and the surrounding countryside; bottom: between all dense urban area and countryside (from Lemonsu et al., in COST-715, 2002a).

The TEB scheme of Masson (2000) has been evaluated off-line using observations of local scale fluxes and surface temperatures during UBL-ESCOMPTE. In this study, TEB is used for built areas and the ISBA-scheme (Interaction Soil-Biosphere-Atmosphere; Noilhan and Planton, 1989) for vegetated areas. The two models are combined using the plan areas of built and vegetated surfaces with their respective weighting. A static modelling domain was defined for the area within 500-m radius centred on the city centre tower site. The TEB input parameters (surface cover fractions and geometric dimensions of the streets) were derived from analysis of aerial photographs (Grimmond *et al.*, 2002) and the data base of building heights. Thermal properties of materials were assigned based on published sources. Given the importance of traffic in the city centre, an anthropogenic heat flux was estimated following the method of Grimmond (1992). In off-line mode, the TEB-ISBA models are forced by observations of air temperature, humidity, wind speed, and incoming solar and long-wave radiation at the top of the tower. For Marseille, TEB-ISBA is be-
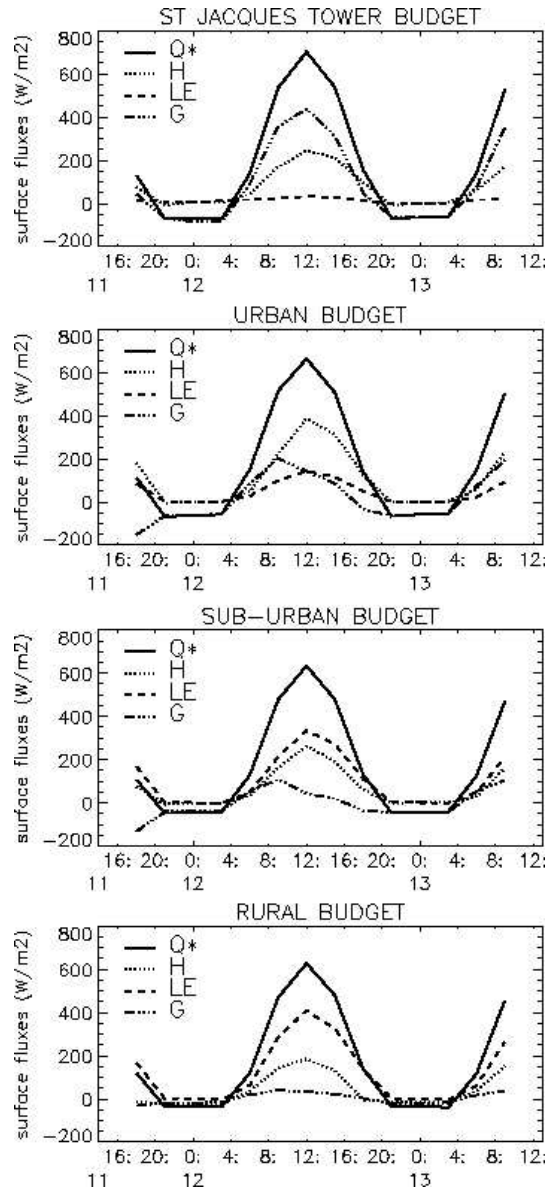
Figure 6.12: Comparison of surface fluxes at various sites in the City of Paris as calculated by MesoNH using the TEB scheme. The four panels refer to different sites representing specific type of areas. (from Lemonsu et al., in COST-715, 2002a). In this figure, H and LE refers to Q_H and Q_E of Eqs. (3.1-3.3), respectively.

ing evaluated using the measurements of air temperature from within the street canyons, the surface temperatures of roads, roofs and walls, and fluxes from the city centre tower (eddy covariances) and the LAS scintillometers. It is assumed that the amount of energy leaving the top of the canopy does not change with height, as in a classical "constant flux" atmospheric surface layer, which can be true only for a horizontal spatial average, since vertical and horizontal flux divergence prevails in the roughness sub-layer. Figure 6.13 shows a comparison of the 21-days averaged measured and simulated fluxes. Heat flux measurements at the mast and with the scintillometers show an excellent agreement while the energy fluxes appear well simulated. The model succeeds in producing a positive turbulent sensible heat flux at night, and the correct daily cycle of heat storage.

6.2.3. Results with the Finite Volume Model

The model has been run for an idealised 2-D case of an UBL with a flat terrain and a city of 10 km (building height 25 m, street width 25 m) surrounded by a rural area. The computations show that walls are the most active surfaces for momentum and turbulent kinetic energy, during day and night. For heat, on the other hand, streets and roofs are more active during daytime and walls during night-time.

Determining the impact of vertical and horizontal surfaces on the energy balance is very important in order to estimate the storage heat flux term correctly. To investigate this, Martilli *et al.* (2002) have compared their new surface exchange scheme ("Urb" in Fig. 6.14) to the "traditional" approach ("Trad"), in which the roughness length and the soil thermal properties are modified in order to simulate urban influences. Considering only the ground as an active surface with an increase in the roughness length and the soil thermal characteristics of the concrete ("Trad" in Fig. 6.14), there is a tendency to underestimate the magnitude of the storage heat flux during day- and night-time. On the other hand, there is quite a good agreement in the three-day simulation between the results obtained with the new parameterisation used in FVM and the Objective Hysteresis Model OHM (Grimmond *et al.*, 1991; Arnfield and Grimmond, 1998; Grimmond and Oke, 1999a).

The model of Martilli has been implemented, along with the SM2-U soil model (see Section 3.2.4), in the MM5 model by Otte *et al.* (2003) and tested with success for the area of Philadelphia.
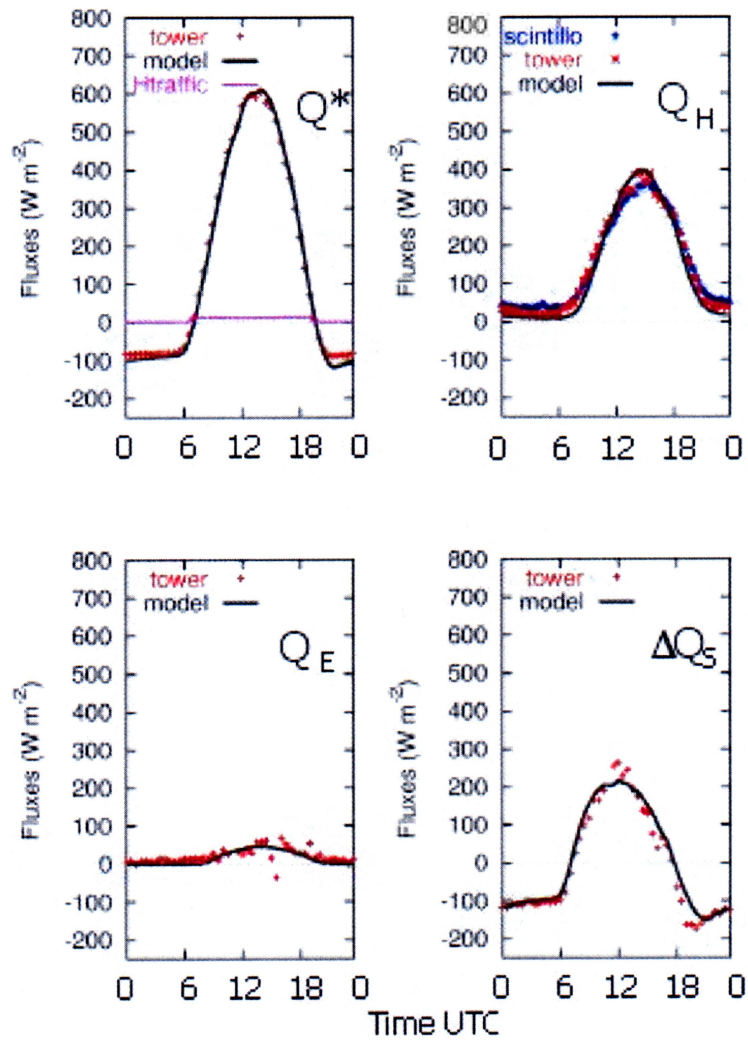
Figure 6.13: Comparison between observed and simulated surface energy balance fluxes in the city centre, averaged over 21 days. Red crosses – observed eddy covariance fluxes; continuous line – simulated fluxes using TEB, that are an average of the fluxes from roads, walls, roofs and natural surface cover. Blue stars in the turbulent sensible heat flux graph are calculated from the scintillometer data using the free-convection method (after Lemonsu et al., 2004)
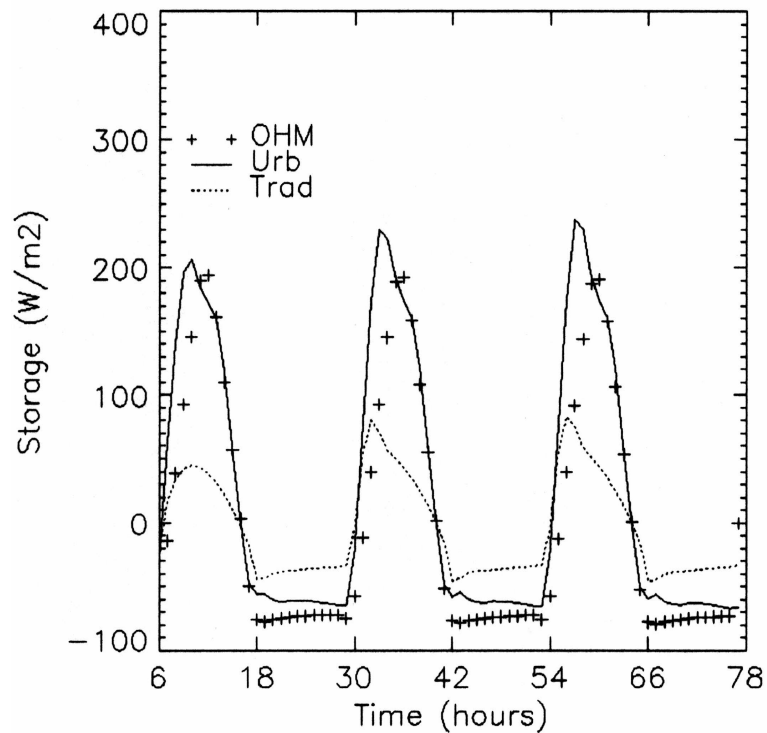
Figure 6.14: Comparison of different methods to estimate heat storage (from Martilli et al., in COST-715, 2002a). OHM refers to the Objective Hysteresis Model (Grimmond et al., 1991), 'Trad' and 'Urb' are defined in the text.

6.2.4. Results with the ARPS model for Paris

The scheme described in Section 3.2.5 was used within the ARPS model to simulate the surface energy balance of the central Paris area on a sunny day (see Section 8.4 for details on the set-up of that simulation). The modelled surface energy balance was compared to the Objective Hysteresis Model (OHM; Grimmond *et al.*, 1991). The OHM is based on an empirical formula relating the storage heat flux into buildings, ground substrate, among other things, to the net surface radiation. Figure 6.15 shows components of the simulated surface energy balance, together with values produced by the OHM method. The most striking feature of the energy balance is the magnitude of the storage heat flux, both during the day (positive) and at night-time (negative).
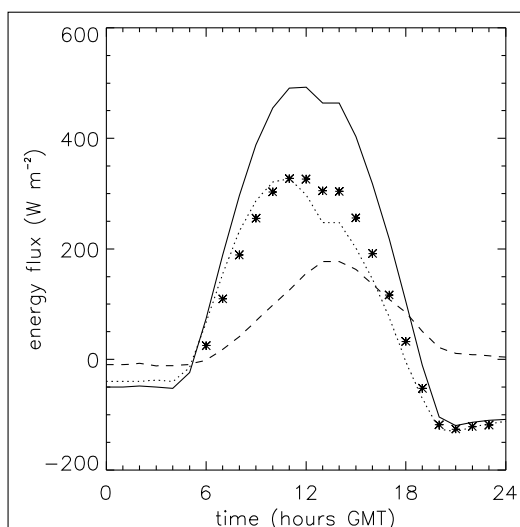
Figure 6.15: Simulated surface energy balance for the central part of Paris: net ra-
diation flux (solid line), storage heat flux (dotted line), and sensible heat flux
(dashed line). The asterisks represent the values calculated by the Objective
Hysteresis Model.

The consequences of this behaviour of the urban SEB are rather significant. Indeed, since the storage heat flux takes such a large share of the available radiant energy, relatively little is left during the daytime for the sensible heat flux towards the atmosphere (dashed line in Fig. 6.15). This leads to the apparently paradoxical conclusion that, even though at noon urban surface temperatures are about 10 to 15 degrees warmer than their surroundings, the heat they inject into the atmosphere is in fact only marginally higher. Practically, this means that the impact of vegetation changes on urban daytime atmospheric circulation patterns may be less important than anticipated. The situation is quite different though during the night, because, after sunset, the city starts liberating the enormous heat amount stored during the day. Therefore, heat flux values remain positive throughout the night over the city, whereas rural sensible heat flux values plunge towards negative values of a few tens of W m^{-2}. This confirms earlier findings that the main effect of cities on atmospheric structure and circulations is more prominent during the night than during the day.

6.2.5 Results with ADMS for Birmingham

The ADMS model was run assuming a rural site with roughness length set to 0.1 m via the user interface. This roughness length was chosen as the Coleshill site is a farm (see Section 5.3) and is less well exposed than an airport; there are some hedges, trees, and further away some farm buildings. With such value, the best straight line fit between the ADMS-modelled heat flux values and the observed fluxes at the Coleshill rural site ($Q_{Hmod} = 0.48Q_{Hobs} + 4.1$) went slightly above the origin with slope showing that during the daytime, the ADMS routine was underestimating the sensible heat flux (Fig. 6.16). Note that no attempt was made here to optimise the ADMS settings to match these data, the program was simply run from the usual format of synoptic data from the standard observations. Notice also that there is a large scatter in these results; it may be possible to find settings for the model which might improve the fit. Nevertheless these results suggest that it will be a useful piece of work to understand how the heat flux calculation might be improved, e.g., is there perhaps an explanation to be found in the estimation of the sensible heat flux, the partitioning into latent/sensible/ground fluxes, or even the adjustment of solar radiation for cloud cover.
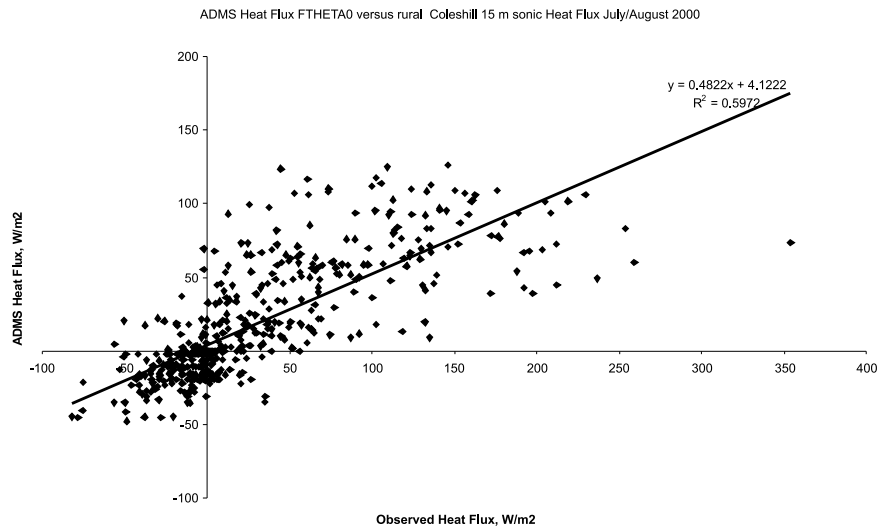

Figure 6.16: Scatter plot of the sensible heat flux measured at the Coleshill rural site against ADMS-modelled values with z_0 set to 0.1 m (rural).

ADMS HeatFlux FTHETA0 versus urban Dunlop 15 m sonic Heat Flux July/August 2000
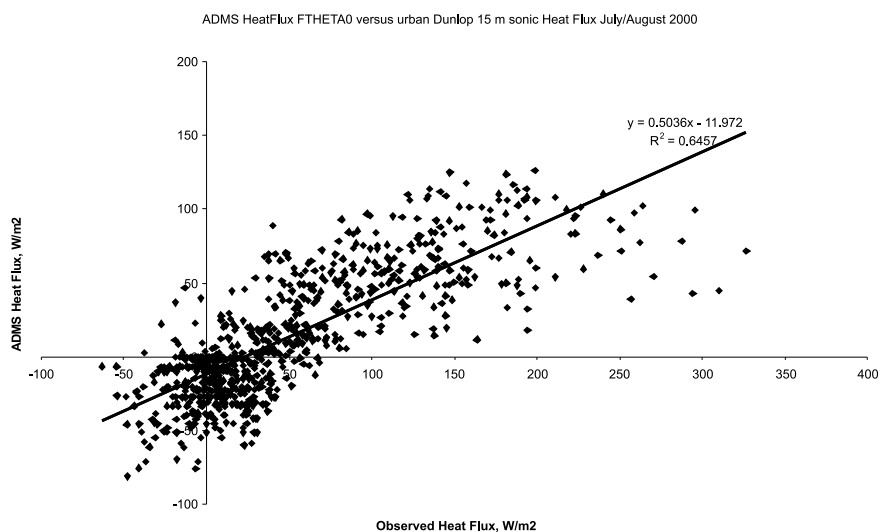
Figure 6.17: Scatter plot of the sensible heat flux measured at the Dunlop urban site against ADMS-modelled values with z_0 set to 1 m (urban).

For the comparison in Fig. 6.17, ADMS was given a roughness length of 1.0 m to represent urban effects. No provision is made to alter the modelled heat flux in any way, other than the change that accompanies the change in roughness length (increasing the setting for z_0 increases the values of the friction velocity and the sensible heat flux calculated by the met pre-processing). At this factory site, the model underestimated the heat flux with a very similar slope ($Q_{Hmod} = 0.50 Q_{Hobs} - 12.0$), again showing the lower estimates for sensible heat flux in the model when compared with the observations. However the intercept was now below the origin at -12 W m^{-2}, so the best fit line was off-set. There is some evidence of the heat flux in both graphs to have a non-linear behaviour tending to curve over a little and flatten off rather than growing to the larger values; also in both plots there was a similar scatter: correlation was similar with $r^2 \sim 0.6$ in either case. Notice that these urban results at the Dunlop factory have a significant number of positive values that were measured, but predicted to be negative by the model. This is likely to be an urban effect, since it was not present at Coleshill, where, in the previous Fig. 6.16, the intercept was numerically nearer to zero.

To summarise, in this application of the ADMS met-preprocessor with roughness lengths of 0.1 and 1.0 m respectively, there was under estimation of the

sensible heat flux by about a factor of 2 in rural and urban situations. The lines of best fit suggested for observed rural or urban fluxes of 100 Wm^{-2}, the model gave 52 W m^{-2} and 38 W m^{-2} respectively. Further investigation here is required, as roughness adjustment alone seems insufficient for modelling urban stability.

6.2.6. Cracow

Sensible heat flux measurements with the R. M. Young ultrasonic anemometer model 81000 were tested in the framework of the COST-715 measurement campaign at the Urban Meteorological Station in Cracow (see Section 5.5). The measurements were performed at a height of 2 m at the UMS site located in the middle of the urban heat island of Cracow. Sensible heat fluxes were calculated at 4 Hz and averaged over 30 minutes. The sensible heat flux was calculated directly from the formula:

$$Q_H = 1216 \; \overline{w'\theta'} \qquad (6.1)$$

where the factor 1216 is a conversion factor between kinematic unit (K m s^{-1}) and heat fluxes (W m^{-2}). The measurements were compared to formulae based on the Penman-Monteith resistance method with 3 different theoretical approaches (Smith, Holtslag-Van Ulden, Berkowicz-Prahm). These formulae are widely used for flat non-urban terrain. The input data for the formulae consisted of measurements of net radiation Rn (pyrradiometer Schenk model 8111 working in the 0.3-60 μm range with upward and downward oriented sensors), surface temperature as well as air temperature, relative humidity, and wind speed at the 2 m level.

The Smith Scheme:

This scheme (Smith, 1990) assumes that the energy partition between the sensible and the latent heat flux is proportional to the total net radiation with an additional dependence on sun elevation φ. Sensible heat flux is calculated by the Penman-Monteith resistance method (Monteith and Unsworth, 1990) with the aerodynamic resistance inversely proportional to wind speed. Surface resistance depends on temperature and sun elevation (Galinski and Thomson, 1995).

The calculations were made without any modification to the Smith's scheme with a height of $z = 3$ m and a coefficient $c_z = 188.9$. Wind speed U_z values were taken as 5-minutes mean values of the sonic anemometer wind speed. For calm wind conditions, a value of $U_z = 0.01$ m s^{-1} was used to eliminate infinite values of the aerodynamic resistance r_a. Heat flux values from the Smith scheme in daytime are compared to observed values in Fig. 6.18. The statistics for all three schemes are given in Table 6.3 at the end of Section 6.2.6.
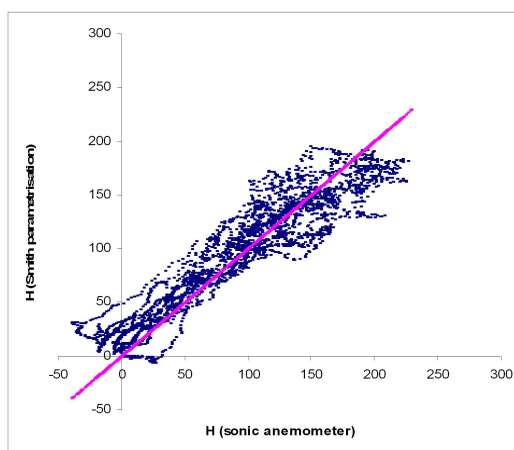
Figure 6.18: Scatter plot of calculated and observed values of daytime (sun elevation angle $\varphi > 10°$) sensible heat flux from the Smith heat flux scheme.

The Holtslag-Van Ulden Scheme:

This scheme assumes the energy partition between the sensible and latent heat fluxes with the available energy equal to 90% of the total net radiation Rn. The sensible heat flux is taken from the Penman-Monteith resistance method with empirical parameters α and β depending on the soil moisture conditions (Holtslag and Van Ulden, 1983; Van Ulden and Holtslag, 1985). For moist surfaces, $\alpha \approx 1$ and $\beta \approx 20$ W m^{-2} were found to be good estimates by Holtslag and Van Ulden. However, they led to a significant reduction of our Q_H values. The best fit between the calculated and measured values was found with $\alpha \approx 0.7$ probably because of the drought condition in June in Cracow.

A scatter plot of heat flux values from the Holtslag and Van Ulden daytime scheme against observed values is given in Fig. 6.19 and statistics are given in Table 6.3.
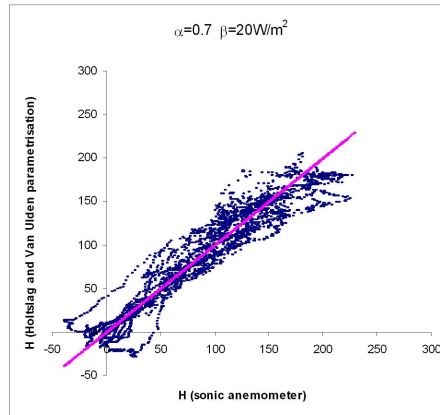
*Figure 6.19: Scatter plot of calculated and observed values of daytime (sun elevation
angle $\varphi > 10°$) sensible heat flux from the Holtslag-Van Ulden heat flux scheme
for $\alpha = 0.7$.*

Table 6.3. Heat flux statistics during daytime ($(\varphi > 10°)$ fro the three schemes of
Smith, Holtslag-van Ulden (HU, $\alpha = 0.7$) and Berkowicz-Prahm (BP): n = number of
values, $\bar{x}$ = mean observed (sonic anemometer) value, $\bar{y}$ = mean estimated value, s_x =
standard deviation of the observed value, s_y = standard deviation of the estimated
value, rms error and r = correlation coefficient).

	Smith	H-U	B-P
n	3340	3340	3340
$\bar{x}$	87.34	87.34	87.34
$\bar{y}$	91.23	85.55	62.92
s_x	64.41	64.41	64.41
s_y	54.50	61.61	48.41
$\bar{y} - \bar{x}$	3.88	-1.80	-24.43
rms	23.41	19.95	33.05
r	0.94	0.95	0.96

The Berkowicz-Prahm Scheme:

The ground heat flux Q_G is parameterized as $Q_H/3$. The aerodynamic resistance used by Berkowicz and Prahm, which is based on the Monin-Obukhov similarity theory is determined by means of iteration (Berkowicz and Prahm, 1982). They suggested taking the surface resistance inversely proportional to a function F. This function depends on the absolute net radiation and two terms A and D. These terms are determined from the "integrated hourly net radiation since last recorded rainfall".

A scatter plot of heat flux values from the Berkowicz and Prahm daytime scheme against observed values is given in Fig. 6.20 and statistics are given in Table 6.3. It seems possible, that the too low values of the sensible heat flux, obtained by the Berkowicz-Prahm iteration method, are caused by the assumed values of surface resistance.
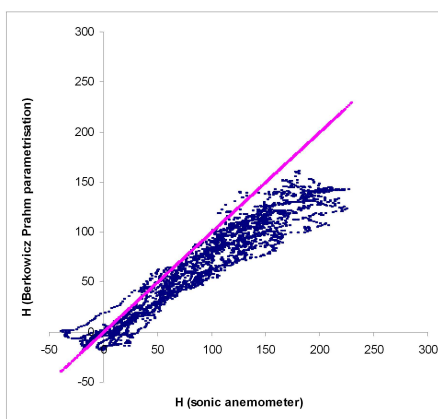
Figure 6.20. The scatter plot of the calculated and observed values of daytime ($\varphi > 10°$) sensible heat flux from the Berkowicz and Prahm heat flux scheme.

The results presented show overall good agreement between calculated and observed values of the sensible heat flux, for all the parameterisation schemes used. However it has to be noted that although these measurements were performed on a flat grass-covered former airfield in the middle of the city with the nearest buildings at 150 m, the low measurement height (2 m) implies a very close foot print more representative of semi-rural conditions than of characteristic urban conditions.

6.3. Implications of Surface Energy Balance results for NWP modelling for European cities

In the context of urban air quality modelling, a significant upgrading of models could be achieved through better representation of urban features in the land surface schemes, i.e., with appropriate values for albedo, thermal admittance, and roughness, as well as an adequate representation of water flow after rainfall. It seems that the most fundamental change lies in the parameterisation of the temperature roughness (section 3.4). A subsequent issue is about the adequate averaging/aggregation techniques used to represent the patchwork of various types of surfaces with their intrinsic characteristics at each model cell.

As mentioned in Section 3.5, modern nested NWP models can utilise land-use databases down to resolution of a hundred meters, and are approaching the horizontal resolution (down to 1–5 km) necessary to provide weather forecasts for the urban scale. Recent scientific developments on urban sub-layer atmospheric physics (see Chapter 3 and 6.2) together with the enhanced availability of high-resolution urban surface characteristics would in principle enhance the capability of NWP models to deliver high quality urban meteorological data once they have been "urbanised", i.e. include representative and critical urban features. The forthcoming Action COST-728 ("Enhancing Meso-scale Meteorological Modelling Capabilities for Air Pollution and Dispersion Applications") will also provide a suitable forum for such developments.

Enhancing our capabilities to simulate urban conditions will imply to improve the SEB schemes for urban areas in NWP models, since more and more urban air quality models use input meteorological fields from NWP. Generically, the following urban surface aspects should be implemented into improved urban-scale NWP models:

- Higher spatial (horizontal and vertical) grid resolution, e. g. using nesting techniques;

- Improved physiographic data and land-use classification;

- Calculation of the effective urban roughness;

- Calculation of urban heat fluxes;

- Sub-models for the urban canopy and soil layers;

- Assimilation of urban surface characteristics data into NWP models.

Within the FUMAPEX project, several operational and experimental NWP models (the Danish, Finnish and Norwegian HIRLAM, the Lokalmodell LM, MM5 and RAMS) were tested as to their capacity to simulate meteorological fields during different urban pollution episodes in three European cities: Helsinki, Oslo and Bologna (Helsinki and Oslo episodes are reported in Fay *et al.*, 2004; Neunhäuserer *et al.*, 2004). The initial city episode simulations were performed with the operational setup of the models, but also including higher resolution nested versions but without improved parameterisations. Both the model evaluation against observations and the model inter-comparison during pollution episodes clearly show the current limitations of even high-resolution mesoscale NWP models. Thus, it is expected that results would be improved once proper urban-adapted high-resolution surface and boundary layer parameterisations have been developed and implemented into NWP models.

The improvement of NWP models for urban areas by implementing different urban SEB schemes is currently realised by several national meteorological centres in Europe (HIRLAM/DMI; LM/DWD and AlMo/MeteoSwiss; MM5/DNMI, Univ. Hatfield, FMI; RAMS/CEAM, Arianet; TVM/Univ. Louvain, B;. FVM/EPFL, CH; SUBMESO/ECN, F; ALADIN and Meso-NH with TEB module/MeteoFrance (Masson, 2000; Section 3.2.2), but the operational stage is not reached yet. Such developments are in particular realised within FUMAPEX, which develops a strategy for the "urbanisation" of NWP models (Baklanov and Mestayer, 2004; Baklanov and Joffre, 2003). It includes the development of a new urban sub-layer module for NWP models, which includes four main submodels that can be chosen depending on the specific problem at hand, the model resolution or the city area:

1. Corrections to the surface roughness for urban areas (Baklanov and Joffre, 2003) and to the heat fluxes (by adding an extra urban heat flux, e.g., via heat/energy production/use in the city, heat storage capacity and albedo change) in the existing non-urban physical parameterisations of the surface layer in higher resolution NWP models with improved land-use classification. Furthermore, an analytical model for wind velocity and diffusivity profiles inside the urban canopy is suggested (Zilitinkevich and Baklanov, 2004).

2. The Full Force-Restore Soil submodel SM2-U for urban areas developed by Mestayer *et al.* (2004) and considered in Section 3.2.4.

3. The urban sub-layer model BEP (Martilli *et al.*, 2002; Hamdi and Schayes,

2004), which includes specific physical parameterisations of the urban surface exchange for the urban sub-layer implemented into (or after) the NWP model. This approach is considered in Section 3.2.3.

4. A combined module, including all non-overlapping mechanisms from the SM2-U and BEP models.

The first and simplest urban module includes corrections to urban roughness parameters, the incorporation of the displacement height, calculation of the effective roughness for momentum, heat and moisture, for anthropogenic and storage fluxes, for albedo, etc. (Baklanov and Mestayer, 2004). It is reasonable to use this method for relatively computionally cheap simulations and for low vertical resolution NWP models (first vertical level higher than 20 m), when more complicated methods for the urban sub-layer (BEP and SM2-U) would not considerably affect the results or would be too time-demanding for operational forecasting purposes. For such an approach, the flux aggregation technique of Hasager *et al.* (2002) can be very useful. This module has been implemented in the DMI-HIRLAM model only for non-urban areas for the moment. The approach can be still improved for urban canopies, however, experimental data are needed for verifying this parameterisation for urban areas.

The suggested improved modules computing the roughness parameters of urban areas for NWP systems include:

- Increased surface resolution and land-use databases for calculating the roughness length.

- Modified algorithms for urban roughness parameters based on the morphologic method (Mestayer and Bottema, in COST-715, 2002b).

- The effect of stratification on the surface roughness over very rough surfaces.

- Distinct roughness lengths for momentum, heat, and moisture.

The module implementation scheme for different NWP models is presented in Figure 6.21. It includes classification of urban land-use classes and calculation of corresponding physical parameters at the initial step and running one of the above-mentioned urban modules for each time step. It is not compulsory to
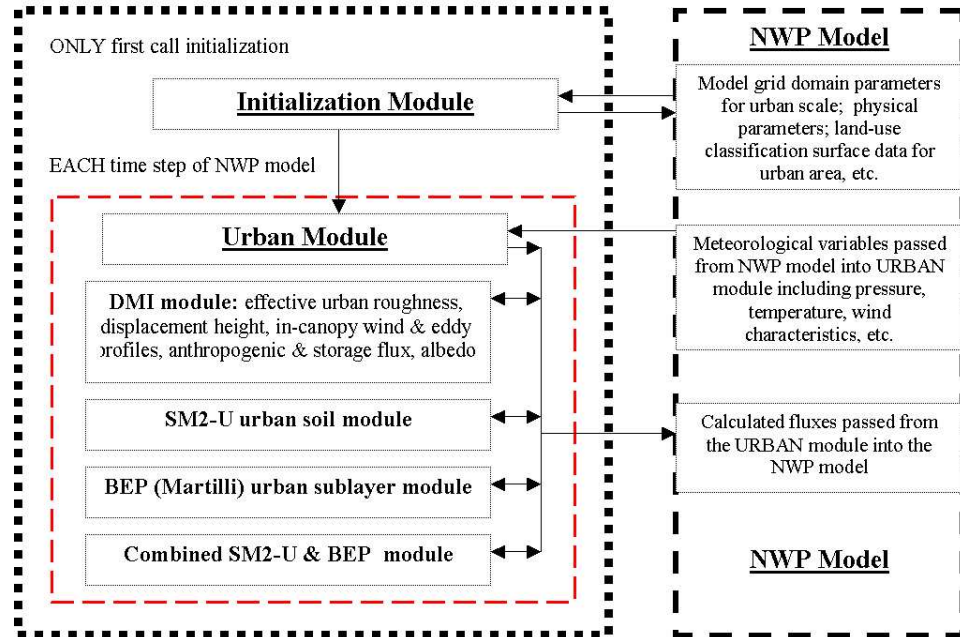
Figure 6.21: General scheme of the FUMAPEX system for NWP model urbanisation.

incorporate the module inside the NWP model code. It has a module structure and can be realised separately and called by the NWP model.

The implementation of distinct urban SEB models to improve the representation of urban meteorological fields for urban air quality models can be also achieved with an interface or post-processor module separated from the operational NWP model. In such case, the urban sublayer model will be run separately using ready NWP-data as a first approximation and will improve the meteorological fields in a layer close to the urban canopy and inside the canopy if a high resolution is possible. This configuation does not give any improvement of the NWP for urban areas and does not consider feedbacks. However, for urban air pollution modelling/forecasting and improvements of a UAQIFS, it can be useful and easier to realise because it does not request any modification of the operational NWP model (which is usually very difficult and time-consuming). Therefore, by following such an improving procedure in the FUMAPEX UAQIFS strategy, we can consider the models for the urban sublayer (and including several upper layers and surrounding areas) as interface modules between the NWP model and the UAP model (Finardi, 2004).

7. Data validation of mixing height schemes and models

This Chapter 7 focuses on results of studies mainly undertaken by COST-715 members during the last five years (see Chapter 5 for an overview of campaigns; a review of other experimental studies of the MH in urban areas is available from Baklanov, 2002). A variety of MH data achieved by different instrumentation (see Section 4.2) was available to the working group, and these have been compared with estimates of schemes, pre-processors and NWP models. Special attention has been paid to the different stability conditions, especially between day- and night-time. In spite of various limitations in the available data, which will lead to large uncertainties when statistical measures are applied, these comparisons enable us to analyse the effects of some of the urban specificities and to preliminarily assess different methods for estimating the MH for several types of urban areas.

7.1. Empirical evidence

There are several geographical distinctions for cities (e.g., flat terrain vs. mountain valleys, coastal vs. continental cities, northern vs. southern cities), the peculiarities of each type being able to affect the formation of the urban boundary layer. For example, the stably stratified nocturnal boundary layer (SBL) is not common in USA cities (Bornstein, 2001) and also not in many downtown areas of Central European cities like Marseille, Basel, Birmingham, mainly as a result of the large amounts of stored heat released at night (see Chapter 6); it could be an elevated nocturnal inversion layer only. However, especially for Northern European cities, the nocturnal SBL is very common (e.g., in Helsinki: see Railo, 1997). The temperature profiles in Fig. 7.1 show clearly the stably stratified nocturnal UBL in Northern European cities.

Figure 7.2 illustrates an example of the daily cycle of the aerosol concentration over Basel during the Basel Urban Boundary Layer Experiment BUBBLE (Rotach *et al.*, 2004b) together with the diagnosed aerosol mixed layer (AML) height, showing the typical development and decay of the convective boundary layer (CBL) all along the day. While the presented situation yields quite clear results concerning the AML height, a more complicated aerosol structure can sometimes be observed. During the night, elevated layers of high aerosol concentrations may be present in the residual layer, and sometimes up to three
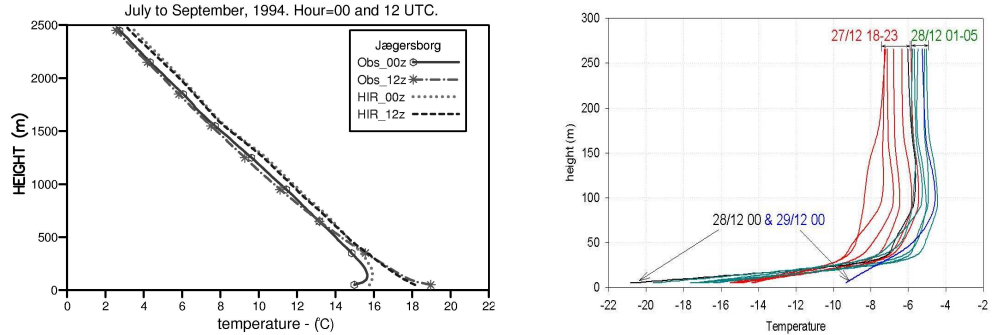
Figure 7.1: Temperature vertical profiles for North-European cities. Left: The 3-month mean measured (Obs) and modelled (HIR) profiles of temperature at 00 and 12 UTC for the radiosonde station Jægersborg in the metropolitan Copenhagen area (Rasmussen et al., 1999). Right: Evolution of a temperature inversion during an air quality episode in December 1995 for the Helsinki metropolitan area. The curves are numerical fits of the data measured at the Kivenlahti mast.
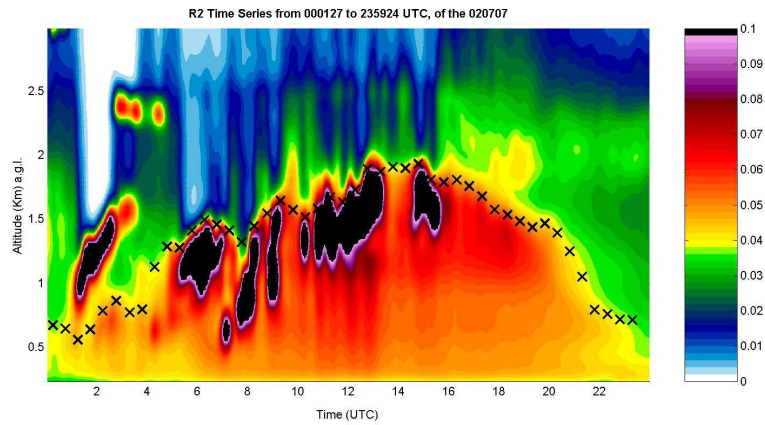
Figure 7.2: Lidar scans of the backscatter from the atmosphere on 7 July 2002 at a site in central Basel, Switzerland. The colour coding is proportional to the aerosol concentration (black=clouds). Crosses indicate the diagnosed Aerosol Mixed Layer height from the derivative of the logarithm of the range-corrected signal. Data courtesy Valentin Mitev and Giovanni Martucci, Neuchatel - Observatory

local minima in the derivative of the concentration profile are observed. Interestingly, quite often there is a pronounced local minimum in the derivative of the lidar signal at about 2.5-3 km (see also Fig. 7.2), most of the time well above the readily determined AML height. This example reflects the usual difficulties in interpreting data in order to estimate the MH, especially as there is no explicit definition.

7.2. Comparison of MH-schemes with radiosonde profiles

7.2.1. CALRAS data set: Munich

Based on the CALRAS dataset (see Section 5.7), Baumann-Stanzer and Piringer (2003) investigated the ability of routine radiosoundings to "see" urban effects on the mixing height when they are launched downwind of a city. In comparison to wind from predominantly rural sectors arriving at the radiosonde site, an increase in the average mixing height for the urban sector was to be expected. Their results for Munich are given in Table 7.1. The methods to diagnose MH from radiosoundings are explained in Section 4.2.1. The differences (to the advanced parcel method at daytime and to the bulk Richardson number method at night) are calculated on the basis of common data pairs given in the last line of the Tables. The humidity-jump method is calculated in convective conditions only which are determined by a positive w_* in the formula for the advanced parcel method.

The expected effect of increased MHs when the urban plume hits the radiosounding site is detected by all the methods applied. At daytime, five methods are available. In winter (Table 7.1a), the average "rural" MH is close within 100 m for all methods except the humidity-jump method; the parcel method and the humidity-jump method giving the lower and upper bounds, respectively. The "urban" MH is almost twice as large as the "rural" one for all methods applied. During daytime in summer (Table 7.1a), urban – rural differences are lower in percentage compared to winter, but still larger MH are calculated for all methods in the urban case. The Heffter and humidity-jump methods give the largest urban MH estimates, on average. For midnight radiosoundings at Munich (Table 7.1b), only two methods are available. There is again a significant increase in MHs under urban influence; especially with the Heffter method.

Table 7.1: Average MHs (in m above ground) for Munich diagnosed from radiosoundings by the Heffter (He), the bulk Richardson number (Ri), the parcel (Pa), advanced parcel (Apa) and humidity-jump methods (Hu).

a) daytime

winter rural

	He	Ri	Pa	APa	Hu
number of cases	142	138	91	91	74
mean	482	421	381	496	868
standard deviation	524	445	389	452	651
difference to APa	105	132	-115	0	358
number of data pairs	90	86	91		61

summer rural

	He	Ri	Pa	APa	Hu
number of cases	54	51	52	51	34
mean	1134	1290	857	1039	1109
standard deviation	681	826	568	561	706
difference to APa	204	464	-203	0	31
number of data pairs	48	44	51		32

winter urban

	He	Ri	Pa	APa	Hu
number of cases	116	117	88	88	61
mean	962	728	531	727	1347
standard deviation	635	606	358	433	766
difference to APa	385	255	-196	0	518
number of data pairs	81	82	88		52

summer urban

	He	Ri	Pa	APa	Hu
number of cases	210	203	230	230	132
mean	1506	1431	1021	1207	1516
standard deviation	550	623	482	469	637
difference to APa	333	324	-186	0	258
number of data pairs	206	199	230		132

b) night-time

winter rural

	He	Ri
number of cases	161	161
mean	120	181
standard deviation	184	83
difference to Ri	-60	0
number of data pairs	161	

summer rural

	He	Ri
number of cases	186	187
mean	78	177
standard deviation	76	106
difference to Ri	-99	0
number of data pairs	286	

winter urban

	He	Ri
number of cases	123	124
mean	564	241
standard deviation	572	148
difference to Ri	322	0
number of data pairs	123	

summer urban

	He	Ri
number of cases	192	195
mean	392	213
standard deviation	503	101
difference to Ri	182	0
number of data pairs	192	

The results of the MH statistics presented in Table 7.1 depend much on the methods used. On the one hand, the differences are due to the fact that the approaches use different meteorological parameters to deduce the MH: critical inversion (Heffter, 1980) and parcel methods are based on temperature, Richardson methods depend on wind and temperature while the humidity-jump approach relies only on humidity. On the other hand, the MH statistics summarise different numbers of cases as not all methods give results for all profiles: no single method works in all synoptic conditions.

Among the temperature-profile related methods available for daytime conditions, the Heffter method gives on average often the largest estimates, followed by the advanced parcel and the simple parcel method. When doing dispersion calculations, worst-case estimates of concentrations are best obtained using the simple parcel method in convective conditions. The average MHs with the Richardson number method are within the range of the temperature-based methods. The average MHs obtained by the humidity-jump method are comparable to the temperature-based methods in summer, but considerably larger in winter. Apparently, in summer under convective conditions, the capping inversion is often accompanied by a significant reduction in air moisture, whereas in winter a significant drop in humidity is frequently found at much larger heights than the capping inversion.

At night, the average Heffter MHs are lower than those of the Richardson number method for the rural and higher for the urban case. From the large differences seen especially in the "urban" case, the Heffter method apparently tends to over-estimate MH. Apparently, diagnostic formulations are difficult to recommend for night-time MH estimation.

7.2.2. Copenhagen

The mixing height was estimated from the radiosounding profile data for the Copenhagen area (see Section 5.9 and Fig. 5.9) for three pre-selected sectors of the wind direction. The following diagnostic MH methods were tested (see details in Baklanov and Kuchin, 2004). For the convective boundary layer (CBL, mostly daytime measurements): the bulk Richardson number method (RI), the simple parcel method (PAR), the advanced parcel method (PARADV), the humidity-jump method (HJMP) and the empirical method of Benkley and Schulman (BS, 1979). For the stable boundary layer (SBL, mostly nocturnal measurements): the bulk Richardson number method (RI), the maximum low-

level jet velocity method (VMAX), the humidity-jump method (HJMP) and several parameterisation methods from Appendix 1, in particular, the method of Arya (1981) and the empirical method of Benkley and Schulman (BS, 1979).

Radiosounding data from the year 2001 at the Jægersborg station (Fig. 5.9) were used for the study. Averaged annual vertical profiles for wind speed and potential temperature for the convective and the stable boundary layer are presented in Fig. 7.3. The profiles were calculated for three wind direction sectors: (i) under urban influence (black squares), (ii) under rural influence (yellow triangles), and (iii) under mixed sea/forest influence (red squares).

As seen from the CBL graphs, the wind velocity over the city and rural areas is similar (Fig. 7.3a), but near the ground it is lower for the urban sector, which can be explained by the urban canopy effect. For winds from the sea sector, the velocities are considerably lower and characterised by a velocity minimum at about 500 m. This minimum corresponds to the average level of the breeze wind direction change. The average potential temperature (Fig. 7.3b) for the urban sector is 1-2 degrees higher than the temperature for the rural sector and about 5 degrees higher than for the sea sector. The vertical temperature profile in the lowest levels of the urban sector is the most unstable.

For the SBL, the situation differs considerably. The average wind velocity (Fig. 7.3c) from the city sector is considerably higher than that of the rural and water surface sectors. Of course, this is not only due to urban effects, but also caused by the specific synoptic situations and characteristics of the northern and southern winds in the area. The potential temperature (Fig. 7.3d) over the city and rural areas above 700 m does not differ considerably, but below this level the temperature is lower for the urban sector. Note that the surface inversion in the urban sector is not less than that in the rural sector, and the elevated inversion (typical for southern large cities) does not appear to be typical for the Copenhagen area (at least for the considered urban sector). These results support the hypothesis that in Northern European cities the nocturnal SBL is very common, and their UBL structure differs from US cities (see Bornstein, 2001; Baklanov, 2002) as well as from Central and Southern European cities (this report). As the interpretation of sector (iii) is complex and uncertain due to the mix of a smooth sea surface and a rough forest cover, it will not be analysed further in the following discussion.

With respect to the winter SBL statistics, the situation is similar to the annual scale shown in Fig. 7.3, but the wind velocities for the urban and rural sectors
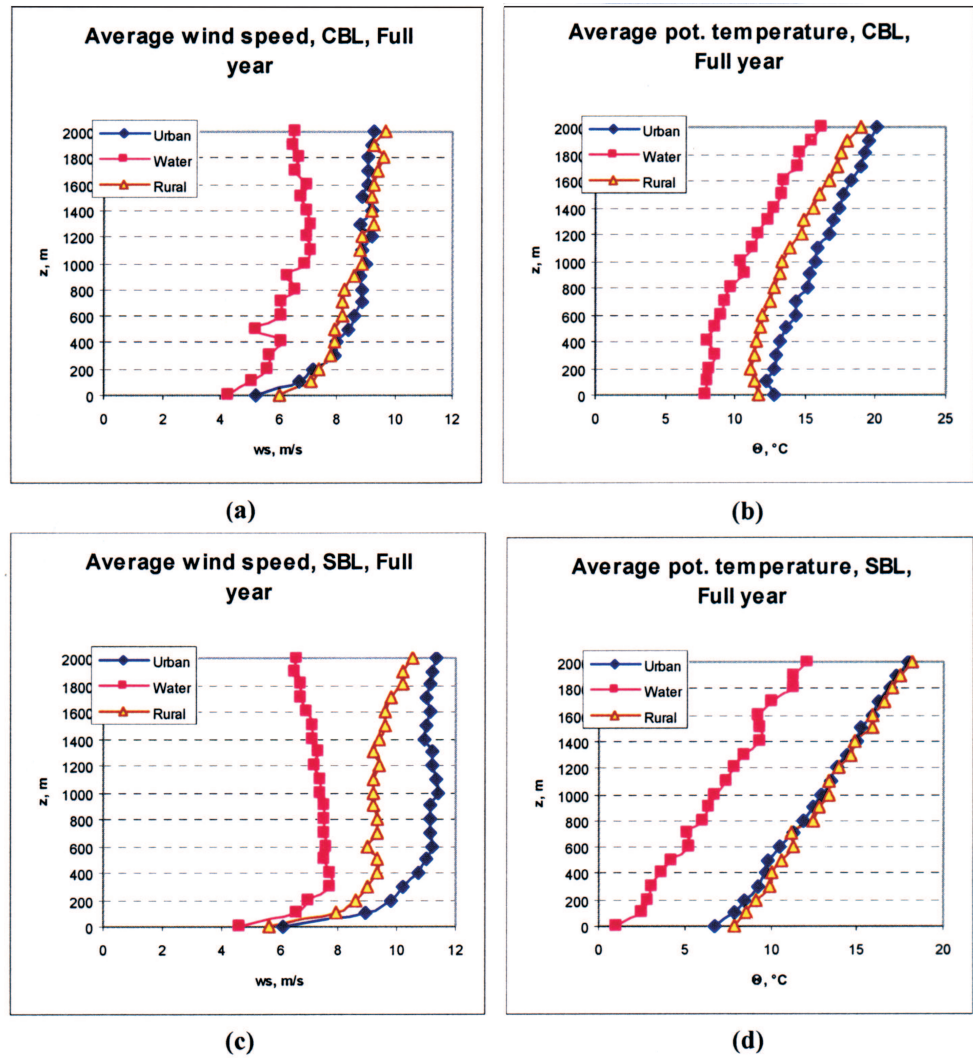
Figure 7.3: Mean annual vertical profiles for: (a,c) wind speed and (b,d) potential temperature during cases with CBL (a,b) and SBL (c,d) at the Jægersborg station in Copenhagen for wind directions from different sectors: under urban influence (blue squares), under rural influence (yellow triangles), and under sea/forest influence (red squares).

Table 7.2: Mixing heights for the Copenhagen area: mean value (in m), standard deviation (Std Dev) and number of profiles (n) for (i) urban, (ii) semi-urban and rural sectors. Left Panel, SBL: MH determined with the bulk Richardson (RI), Arya (1981) (AR81), Benkley-Schulman (BS), maximum low-level jet velocity (VMAX) and humidity-jump (HJMP) methods. Right Panel, CBL or neutral ABL: MH determined with the Richardson (RI), Parcel (PAR), advanced Parcel (PADV) and humidity-jump (HJMP) methods.

		S B L					**C B L**				
Sector	*Statistics*	*RI*	*AR81*	*BS*	*VMAX*	*HJMP*	*RI*	*BS*	*PAR*	*PADV*	*HJMP*
Urban (i)	*Mean*	261	783	764	593	456	799	918	718	900	532
	Std Dev	197	444	474	192	260	415	440	445	494	238
	n	114	114	114	114	44	61	61	61	61	29
Rural (ii)	*Mean*	189	451	595	552	462	965	920	898	1130	634
	Std. Dev	175	255	410	199	260	368	387	403	403	255
	n	122	122	121	122	59	80	80	80	80	21

are increased. Another important difference is that the potential temperature at the lowest levels in the urban sector is higher compared to the rural sector, and (most important) the surface inversion in the urban sector is less developed than for the rural sector. Probably, the urban heat flux (including the anthropogenic and storage heat fluxes) plays a more important role in the nocturnal UBL during the winter season.

Table 7.2 suggests that the effect of the urban sector on the average SBL MH values is significant for all the different methods considered (for the 2 wind sectors). The average MH values of the urban sector are *ca.* 100 m higher than the average rural MH. The bulk Richardson number method gives the lowest values of the MH in all the sectors (261/189 m). Of course, without direct measurements of the MH, no conclusion about the correct value of the MH can be made. However, based on a previous analysis of the bulk Ri-number method and a comparison with MH measurements by sodar (Zilitinkevich and Baklanov, 2002), it is expected that this method underestimates the MH for the SBL due to the fact that the critical value of the Ri-number is not a constant. Two other methods (AR81 and BS), based on surface level measurements only, probably strongly overestimate the urban MH (783 and 764 m for the urban sector). The VMAX method gives results in between. The HJMP method shows unexpectedly reasonable results. However, it is not recommended to use this method, because it is usually used only for neutral and convective conditions.

Figure 7.4 presents scatter plot diagrams of the MH for the SBL over the Copenhagen area for two wind sectors. They show a general wide spreading of the estimated MH values for the SBL cases. The correlation coefficients between the Ri-method and AR81 and BS methods are lower for the urban sector compared to the rural sector (Baklanov and Kuchin, 2004). This may be due to internal boundary layers caused by the coast line or the urban canopy. There is almost no correlation of VMAX and HJMP with the other methods.

(a)   (b)
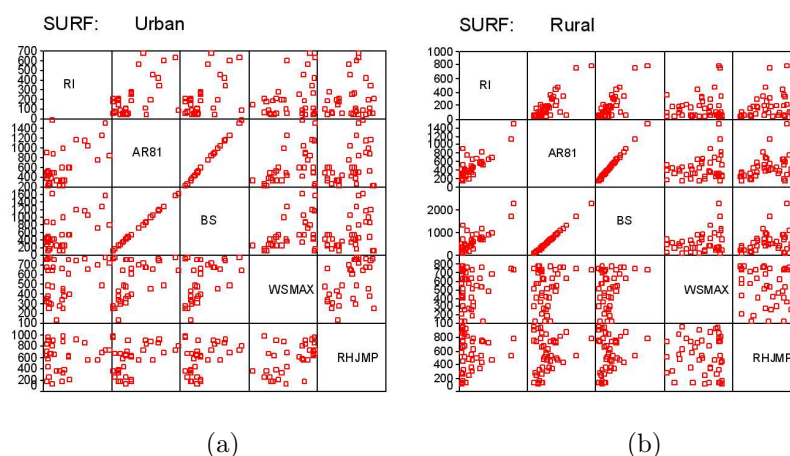
Figure 7.4: Matrix of scatter plots of the stable MH calculated from Jægersborg (Copenhagen) radio-sounding profiles by different methods: the bulk Richardson method (RI), Arya (1981) method (AR81), Benkley-Schulman method (BS), maximum low-level jet velocity method (WSMAX) and the humidity-jump method (RHJMP), for two different sectors: (a) urban, and (b) semi-urban and rural. The code names of the considered methods are mentioned in the diagonal boxes. The scatter-plots should be read in such a way that for each cell the y-axis scheme should be found on the same row while the x-axis scheme should be read from the same column as the cell (e.g., all scatter plots of the first row have the Ri-scheme values on the y-axis, all cells along the far-right column have the humidity-jump method values on their x-axis (thus, all scatter plots are repeated with the opposite correlation with respect to the diagonal cells). MH is presented on the scatter-plots in meters on identical scales for x and y (typed on the vertical axes from the left side only).

In contrast to the SBL cases, where urban effects were significant, for the CBL cases we cannot see any major effect of the urban surface on the MH values. The MH values are similar for the urban and rural sectors. In most cases we can even see the opposite effect with higher MHs in the rural/semi-urban than

in the urban sector. This, at first sight unexpected result, can be explained for the Copenhagen metropolitan area by its coastal position (see Fig. 5.9). For convective conditions, the anthropogenic heat flux does not play a dominant role compared to the sensible heat flux, so that see breeze effects, which are important for the rural sector, are stronger than the urban effects.

Most of the MH methods for the CBL show very good correlations for all sectors. The RI, PAR and adPAR methods have correlation coefficients from 0.90 up to 0.97. The exceptions are the BS and HJMP methods with very low correlation coefficients. This is not surprising since the Benkley-Schulman method, which uses the 10 m velocity as the only criterion, was not developed for convective conditions (we considered it just for a simple test of applicability of such simple methods).


(a)   (b)
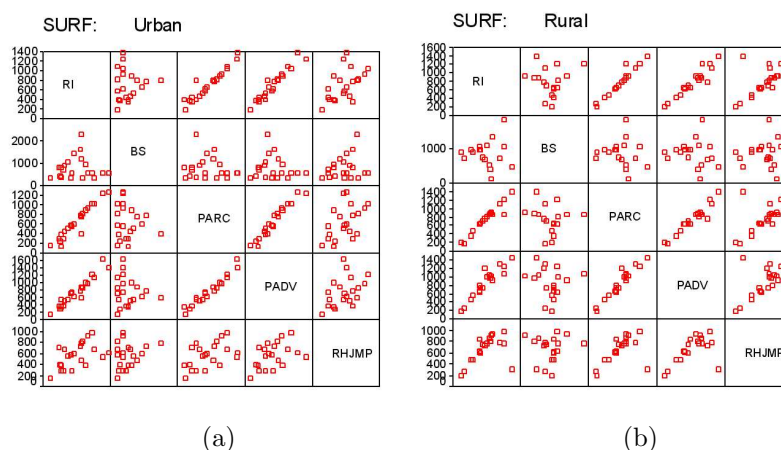
Figure 7.5: Matrix of scatter plots of the convective MH calculated from Jægers-borg (Copenhagen) radiosounding profiles by different methods: bulk Richardson method (RI), Benkley-Schulman method (BS), Parcel method (PARC), advanced Parcel method (PADV), and humidity-jump method (RHJMP) for different sectors: (a) urban, and (b) semi-urban and rural. For more explanations see caption of Figure 7.4.

Figure 7.5 presents scatter plots for the CBL for two opposite wind sectors. It shows that, in general, the spreading of estimated MH values for the CBL cases is relatively low for the RI, PAR and PARADV methods. The scatter plots for the BS and HJMP methods vs. other methods show a very high spread of data and almost no correlation. Therefore, the BS and HJMP methods cannot be recommended for practical use.

Thus, the analysis of a 1-yr statistics of radiosonde vertical profiles from the Jægersborg station (Copenhagen, Denmark) illustrated some effects of urban features on the MH in the Greater Copenhagen area and differences between urban and rural MHs. It appeared that the urban MH is considerably higher for the stably stratified (nocturnal) boundary layer cases in comparison with the 'non-urban' MH. Daytime (usually CBL) MH does not differ significantly in urban and 'non-urban' sectors. For convective conditions the anthropogenic heat flux does not play a dominating role and roughness features have the main effect. Therefore, an interaction of the sea breeze with urban effects and a combination of internal boundary layers drives the MH in CBL conditions over Copenhagen.

The results of this study for Copenhagen (Baklanov and Kuchin, 2004) support in general the conclusions from the CALRAS study (Section 7.2.1). The urban MH is considerably higher for (nocturnal) SBL cases in comparison with the 'non-urban' MH. On the other hand, daytime (usually CBL) MHs do not differ very much in urban and 'non-urban' sectors. This also supports the conclusions of Seibert *et al.* (2000) that it is more acceptable to apply standard methods for estimating the daytime MH than for the nocturnal MH. To minimise uncertainties, it is recommended to use a combination of the Richardson number and Parcel methods for diagnosing the MH from radiosounding profiles for both urban and non-urban CBL conditions.

7.2.3. Helsinki

Table 7.3 presents the basic statistics of the calculated MH with the scheme of Eq. (4.5) (see Section 4.2.1) using temperature profiles at either the suburban mast of Kivenlahti or radiosondes from the rural station of Jokioinen. Additionally, Table 7.3 presents calculated MH-values using three other schemes, namely:

(i) The classical Zilitinkevich (1972) scheme derived from scaling arguments:

$$h = c_2 \sqrt{\frac{u_* L}{f}} \qquad \text{with } c_2 = 0.35 \text{ according to Joffre (1981)} \qquad (7.1)$$

(ii) A simple scheme directly relating the Monin-Obukhov (MO) length L and the mixing height:

$$h = c_3 L \qquad \text{(with } c_3 = 2 \text{ from Kitaigorodskii \& Joffre (1988)} \qquad (7.2)$$

(iii) A scheme interpolating from near neutral to very stable conditions (Zilitinkevich, 1989):

$$h = \frac{u_*}{f}\left(\frac{1}{\Lambda} + \frac{\sqrt{\mu}}{\kappa C_h}\right), \ \mu = \kappa u_*/(fL), \ \Lambda_0 = 0.3 \quad \text{and} \quad C_h = 0.85 \qquad (7.3)$$

It should be noted that for the classical scheme (7.1) and for the simple MOST-scheme (7.2) there has been a very wide spread in the proposed constants. If we choose the constant c_2 in Eq. (7.1) to be 0.4 as proposed by Garratt (1982) and Brost and Wyngaard (1978) instead of the value 0.35, which was used in these calculations, we get identical mean values with the interpolation scheme of Eq. (7.3). Correspondingly, if we would like the mean value of the simple MOST-scheme to equal the mean of the Zilitinkevich interpolation scheme we would need to choose $c_3 = 0.9$.

Table 7.3: Statistical parameters associated with the use of the different MH-schemes.

	FMI Jokioinen	FMI Kivenlahti	Classical ($c_2 = 0.35$)	MO-simple ($c_3 = 2$)	Zilitinkevich interpolation
Mean	201	175	209	558	242
Standard Error	0.71	0.30	0.71	2.42	0.77
Median	164	175	165	385	97
Standard Deviation	153	64	153	524.18	166
Range	2450	239	1380	4948	1465
Minimum	50	33	22	52	27
Maximum	2500	272	1402	5000	1492
Number of cases	46951	46951	46951	46951	46951

The cross-correlation between these 5 different estimates are presented in Table 7.4, which show that the results from all three diagnostic mixing height formulae correlate nearly perfectly with each other and that the FMI-scheme for the Kivenlahti site has a moderate correlation with the diagnostic schemes. On the other hand, MH calculations using the Jokioinen-observatory data do not have any correlation with the diagnostic schemes and only a weak correlation with the MH estimates calculated with the same scheme but using the Kivenlahti data. This is obviously due to the fact that the FMI scheme does not use any information about the wind profile in estimating the MH, whereas all the other schemes utilise additionally wind speed information. This also explains

the good correlation between the three other schemes: since the physics of the schemes is nearly identical, results also are expected to be very similar.

Table 7.4: Correlation between the different mixing height schemes.

|	FMI-Jokioinen	FMI-Kivenlahti	Classical	MO-simple	Zilitinkevich
FMI-Jokioinen	1				
FMI-Kivenlahti	0.25	1			
Classical	0.07	0.40	1		
MOST-simple	0.09	0.47	0.98	1	
Zilitinkevich	0.07	0.37	0.998	0.97	1
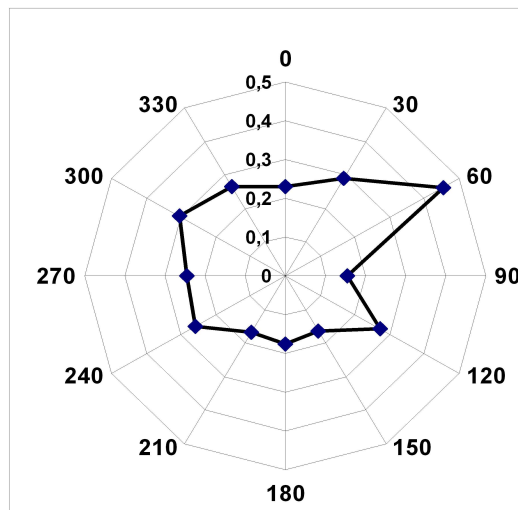
Figure 7.6: Correlation between the calculated mixing heights (FMI-scheme) using Jokioinen (radiosoundings) and Kivenlahti mast data.

The weak correlation between values calculated with the FMI-scheme using radiosonde profiles at Jokioinen and mast profiles at Kivenlahti was further investigated by dividing the data according to wind direction into 12 sectors. Figure 7.6 shows the partial correlations in each of the wind sectors. The correlation between the results from these two datasets is substantially dependent on wind direction, i.e., on the history of the air mass. The weakest correlation occurs for southerly winds (from the sea), which is to be expected, since

under such conditions Kivenlahti is substantially influenced by maritime air masses. The most urbanised area is located in the easterly direction from Kivenlahti, and the corresponding correlation also appears to be fairly low. For a non-homogeneous area, it is therefore advisable to include the information on measured wind speeds into the MH scheme used, as urban roughness greatly modulates the MH behaviour.

The clear dependence of the comparison on the wind direction suggests that for a non-homogeneous area it should be advisable to include the information on measured wind speeds in the FMI-scheme. The simplest way to include it in the stable mixing height formula (Eq. 4.5) is to use directly the measured difference of wind speeds ΔU between the two heights:

$$h = c\frac{\Delta U}{g_1 + 0.005}. \tag{7.4}$$

The value of the empirical constant is $c = 1.8$ K s m^{-1} and g_1 is the potential temperature gradient defined in equation 4.5.

If we evaluate the averages of calculated MHs in different wind direction sectors (Fig. 7.7), we note that the means of the two original FMI-schemes differ in the southerly wind sectors, which once again confirms the result that the effect of the sea is not observed in the Jokioinen soundings.
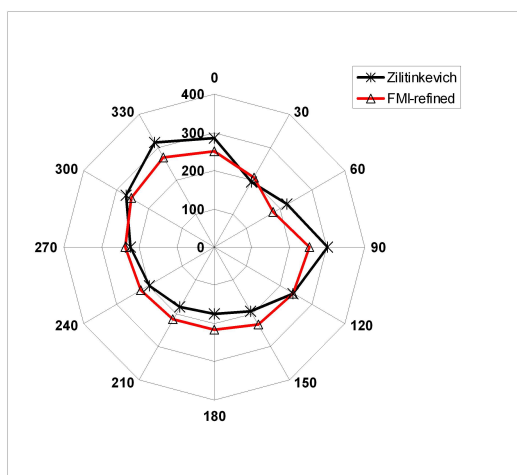

Figure 7.7: *The dependence of the mean of the calculated stable mixing height on wind direction based on 10-years data (1989-98, $n = 46951$) from the Kivenlahti mast.*

The Zilitinkevich interpolation scheme gives higher mixing heights than the simple inversion height-based FMI-scheme in the most urban and rough wind directions (Karppinen *et al.*, 1999) which clearly suggests that for rough and urban areas the different schemes give rather differing estimates for the height of the SBL. However, for the smooth, non-urban sectors, the averages of the calculated MHs are very similar. The modified FMI scheme gives very similar results with the Zilitinkevich interpolation scheme and also the correlation of the time-series of calculated MHs with the Zilitinkevich scheme is good (correlation = 0.90). However, all these simple diagnostic and empirical methods are observed to perform poorly especially in pollution episode situations (long-lived SBLs).

7.2.4. Lisbon

Midday MH values have been determined for Lisbon for the period April, 1st, 1999 to July, 31st, 2001 (28 months). The method used to estimate MH was to follow the dry adiabatic lapse rate from the maximum daily air temperature to its intersection with the vertical air temperature profile of the 12 UTC radiosounding at Lisbon airport, located in a suburban area. The results presented in Fig 7.8 shows the large day-to-day variability of the MH, which might be due to seasonal and synoptic conditions. The seasonal variability is on the other hand rather moderate due to the modulating effect of the nearby ocean.

Table 7.5 displays some statistics about midday MHs in Lisbon where the most frequent values occur from 800 m to 1400 m, but in December the more frequent classes range between 200 and 1000 m.

7.3. The mixing height diagnosed from sodar data

7.3.1. The long-term Hannover dataset

The MH has been detected from the sodar data of the Hannover experiment (Section 5.10) by employing two criteria. The first one diagnoses a sharp decrease of the acoustic backscatter intensity with height z. The height H_1 of this decrease usually indicates the top of a turbulent layer:

$$H_1 = z, \text{ if } R(z) < 88 \ dB \text{ and } R(z+1) < 86 \ dB \text{ and } R(z+2) < 84 \ dB \quad (7.5)$$

Here $R(z)$ denotes the acoustic backscatter intensity in the height z above

Lisbon; 1999/04/01 to 2001/07/31 (12h UTC sounding)
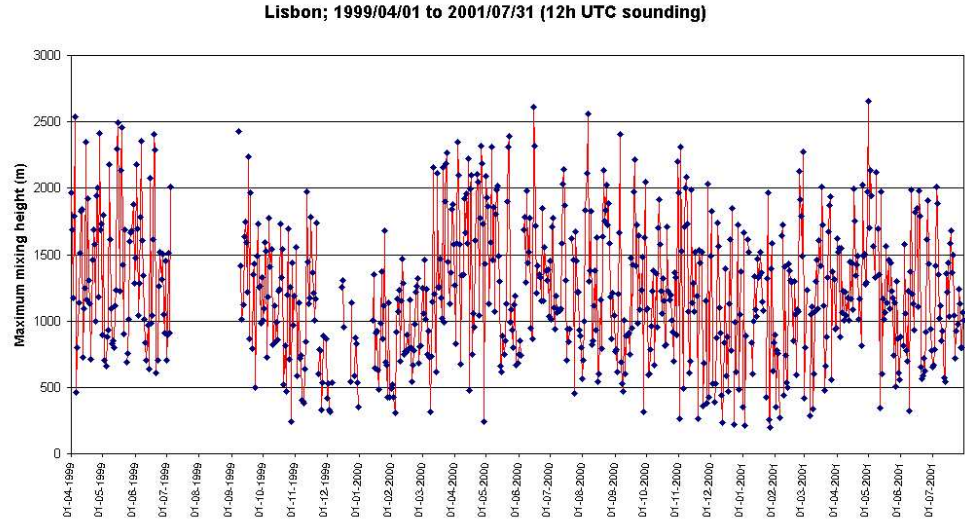
Figure 7.8: MHs at Lisbon, derived from 12 UTC radiosoundings.

Table 7.5: 12 UTC MH statistics for Lisbon.

Maximum mixing height statistics; Lisbon 1999/04/01 to 2001/07/31 (12h UTC sounding)											
	jan	feb	mar	apr	may	jun	jul	aug	sep	oct	nov	dec
n	44	56	60	90	90	85	66	31	51	62	55	43
average (m)	986	1017	1240	1465	1344	1312	1185	1353	1295	1143	1100	843
maximum (m)	1963	2272	2270	2541	2655	2612	2144	2562	2425	2199	2310	1848
minimum (m)	195	270	284	245	345	325	455	542	317	242	266	220
					Number of ocurrences in each class							
h<=200 m	0	0	0	0	0	0	0	0	0	0	0	0
200<h<=400	3	3	3	1	1	1	0	0	1	1	8	6
400<h<=600	4	8	3	2	2	2	3	3	3	3	4	12
600<h<=800	6	12	6	5	13	12	8	2	7	6	9	2
800<h<=1000	7	7	6	5	12	12	13	5	7	13	3	8
1000<h<=1200	8	7	11	17	16	10	14	4	4	13	10	4
1200<h<=1400	8	9	11	10	8	14	8	4	7	12	3	4
1400<h<=1600	4	4	6	16	9	10	9	1	8	7	7	2
1600<h<=1800	3	3	3	11	7	10	5	4	7	5	4	3
1800<h<=2000	1	1	5	11	9	7	2	4	2	1	3	2
2000<h<=2200	0	1	5	6	6	2	4	3	1	1	3	0
2200<h<=2400	0	1	1	4	4	3	0	0	2	0	1	0
2400<h<=2600	0	0	0	2	2	1	0	1	2	0	0	0
h>2600 m	0	0	0	0	1	1	0	0	0	0	0	0

ground. The dB values are derived from an arbitrary scale because the received backscatter intensities cannot be calibrated. The $R(z)$ values are therefore specific for the sodar used in this study. The second criterion looks for surface inversions and elevated inversions. It diagnoses (secondary) maxima of the backscatter intensity that are not related to high turbulence intensities. For elevated inversions we stipulate an increase in backscatter intensity below a certain height $z = H_2$ and a decrease above:

$$H_2 = z, \text{ if } \partial R/\partial z(z+1) < 0 \text{ and } \partial R/\partial z(z-1) > 0 \text{ and } \sigma_w < 0.70 \text{ m s}^{-1} \quad (7.6)$$

and for (usually nocturnal) surface inversions we demand:

$$H_2 = z, \text{ if } R(z) > 105 \ dB \text{ and } \sigma_w < 0.3 \text{ m s}^{-1} \quad (7.7)$$

The restriction to low σ_w values is necessary because high insolation leading to super-adiabatic temperature profiles near the ground also produces high backscatter intensities, but which are related with high turbulence intensities (high σ_w). The search for H_1 and H_2 is done separately. In both cases the search starts from below. If the criterion is fulfilled the search stops. If the search for H_2 detects a surface inversion it stops, too, and does not look for further elevated inversions. The MH is then defined:

$$MH = \min(H_1, H_2) \quad (7.8)$$

In case that neither H_1 nor H_2 is found, the MH cannot be determined from the sodar data. This happens, e.g., during the afternoon of warm and sunny days when the CBL top is higher than the range of the sodar. This does not necessarily mean that there is no inversion at all. More details can be found in Emeis and Türk (2004).

The results are presented for four selected months that are representative for the four seasons: April 2002 for spring, August 2002 for summer, November 2002 for autumn, and February 2003 for winter.

Figure 7.9 shows the frequency distribution of half-hourly values of MH from Eq. (7.8) for the four chosen months. The data have been separated for daytime (7 to 19 CET) and night-time (19 to 7 CET) conditions disregarding the seasons. This choice of an equal length for the daytime and the night-time period allows a direct inter-comparison of the frequency distributions for the nightly hours and the daytime hours in all months. Please note that in Hannover CET is only 21 min ahead of the mean local time. We identify three main regimes in the

frequency distributions. In the lowest height bins (roughly below 200 m) the frequency of nightly MH is higher. Here, surface inversions dominate. In the middle height bins (roughly from 200 m up to 600 m in February and November, up to 900 m in April, and up to 1200 m in August) the daytime MH is more frequent. Here, convective influences dominate. In the upper range of height bins (with the exception of August) we find equal frequencies of nightly and daytime MH due to very windy weather conditions. The rightmost columns give the frequency of half hours within which no MH could be detected. A failure in MH determination most frequently happens in April, August, and November, and is caused in most cases by thermal production of turbulence which leads to deep daytime convective boundary layers whose tops are out of range for the sodar. In November stormy weather leads to such high MH values.
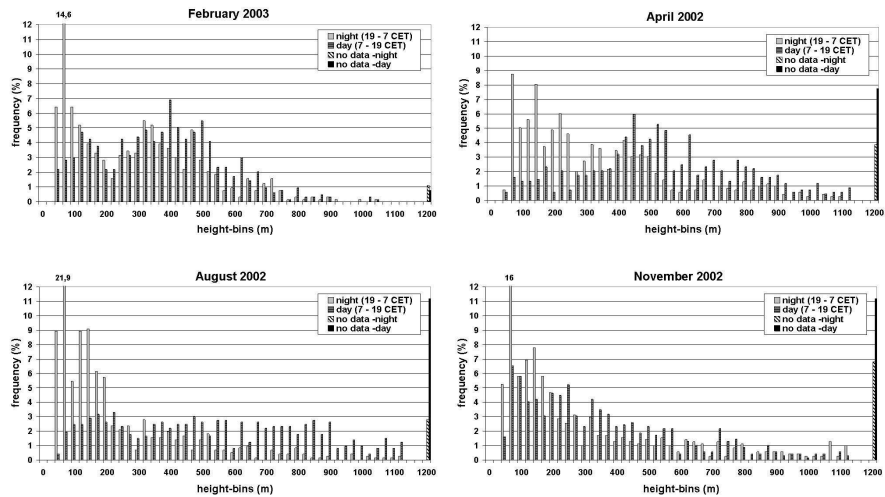
Figure 7.9: Frequency distribution of half-hourly values of MH, computed from Eq. (7.8), in %. Height bins are 25 m wide. The left column in each height bin is for night-time (19 to 7 CET); the right column is for daytime (7 to 19 CET). The columns in the height bin above 1200 m give the percentage of half hours in which no MH could be detected. Small numbers on top of columns indicate true value if the column exceeds the frame of the image.

In February 2003 (which was a cold winter month in Central Europe) the frequency of nightly MH shows two maxima, one at 75 m and one around 325 m. The first maximum is caused by low surface inversions in cold nights; the second maximum is due to two periods with a persistent elevated inversion between 250 and 450 m above ground. For the daytime the frequency peak from these persistent elevated inversions merges with the frequency peak from days with some convection which caused MH between 400 and 650 m. During the other three months the surface-based inversions dominate the night-time frequency distribution. Due to a larger number of days with the formation of a convective boundary layer in April and August the daytime frequency distribution is clearly shifted towards higher height bins compared to February and November. Due to the mostly mechanically produced turbulence in November the difference between the night-time and the daytime frequency distribution is smallest during this month.
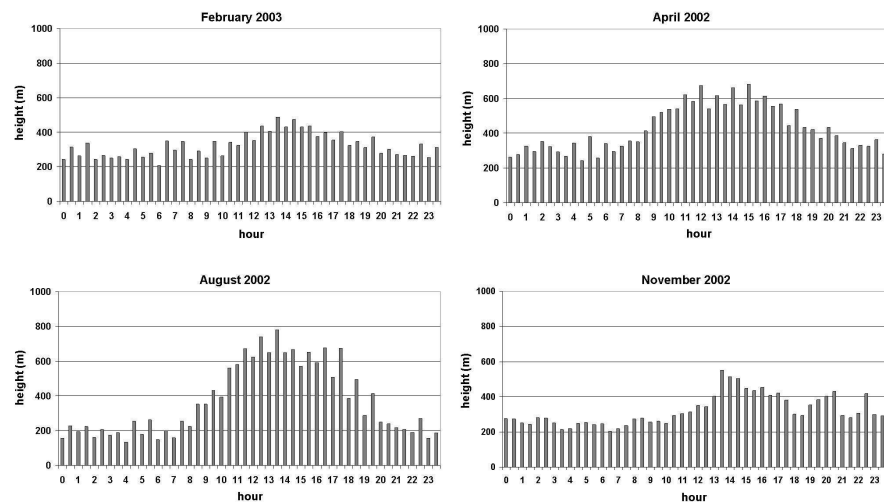

Figure 7.10: Mean daily course of MH (in m), computed from Eq. (7.8). The temporal resolution is one half hour.

Figure 7.10 shows the mean daily course of the MH determined from Eq. (7.8). The strongest diurnal variation is found in August 2002, the smallest diurnal

amplitude is observed in November 2002. This is caused by the amount of the incoming solar radiation which was highest in August (28 days with sunshine, among these were 19 days with more than four hours of sunshine). As February 2003 (22 days with sunshine, among these 12 with more than four hours of sunshine), April 2002 (22 days with sunshine, 14 with more than four hours) also had a large number of sunny days. They also exhibit a clear diurnal course but with smaller amplitude. November 2002 only had 15 days with some sunshine. Among these were only 6 days with more than four hours of sunshine. Dry air masses led to large differences between the daytime maximum temperature and the night-time minimum temperature in August 2002. This difference was regularly 10 degrees centigrade or even larger. In April 2002 this difference was only around 8 degrees. This strong diurnal course of near-surface temperatures led to the small MH values in August 2002 at night-time. The MH values are even lower than in April 2002.

The main results of the statistical evaluation of MH for Hannover are:

- It is possible to obtain long-term time series of MH with a sodar by an automated procedure.

- Three main regimes can be identified in the MH statistics: low nocturnal MH due to surface inversions, medium range daytime MH values indicating the top of a CBL, and quite high MHs which appear with equal frequencies at day and at night due to very windy weather.

- Monthly frequency distributions of MH and monthly mean daily courses of MH show a clear annual course. Surface inversions are found in all seasons, CBL development was most notable in spring and summer from the mean daily course of MH which had the greatest amplitude in these two seasons, and the windy weather was most pronounced in autumn.

- Specific meteorological characteristics of single months are distinctly mirrored in the MH statistics. This shows that the inter-annual variability can be diagnosed from this data set, too.

7.3.2. Comparison of mixing height formulae with sodar data, Bologna

An inter-comparison was carried out between various MH-formulae listed in Appendix 1 over Bologna. These formulae were calculated using "surface"

parameter turbulence data (u_*, L and w_*, from a sonic anemometer and a high frequency hygrometer) from the three urban measuring sites (Specola, Accursio and CNR) and from the rural site of San Pietro Capofiume (SPC) outside Bologna (see Section 5.4). The instruments were located above roof level at the urban sites and at ground level at the rural site. Radiosonde profiles from San Pietro Capofiume were used to determine N. The inter-comparison focuses on the differences between MH values calculated by these formulae under urban and rural conditions, and separately for stable (SBL), convective (CBL) and neutral (NBL) conditions.

A further comparison was made considering the MH estimated from sodar signals at the same locations. The sodars were located on the top of a building in Bologna city centre and at ground level at the rural station. Details on the data and methods applied to obtain MH values from the sodar profiles are provided in Section 5.4.

7.3.2.1. Intercomparison of various methods in Bologna

The comparison was performed by representing box plots for the various MH schemes for urban and rural conditions (Fig. 7.11). All the urban data, collected at three sites, were merged into the same box to obtain a sufficient number of data.

Figure 7.11 displays the expected increase of the MH from stable to unstable conditions. Furthermore, the urban MHs are higher than the rural ones for most methods. It can be noted that apart from the outliers, the range of MH values is 5000 m and 1000 m for unstable and stable conditions, respectively. Some of the methods sometimes yield unrealistic values, these occurrences and/or outliers are discussed for each method in the next sections. Nevertheless, one remarkable aspect of Fig. 7.11 is that there is a rather good internal consistency between the various schemes, though some are based on different theoretical background, whilst the sodar cluster of MH values clearly departs from the latter. This may be an indication that sodar data alone are definitively not appropriate for an accurate assessment of the MH even under stable conditions.

Box plots also give evidence that the various methods have different data frequency distributions. It appears that the median is near the lower quartile in
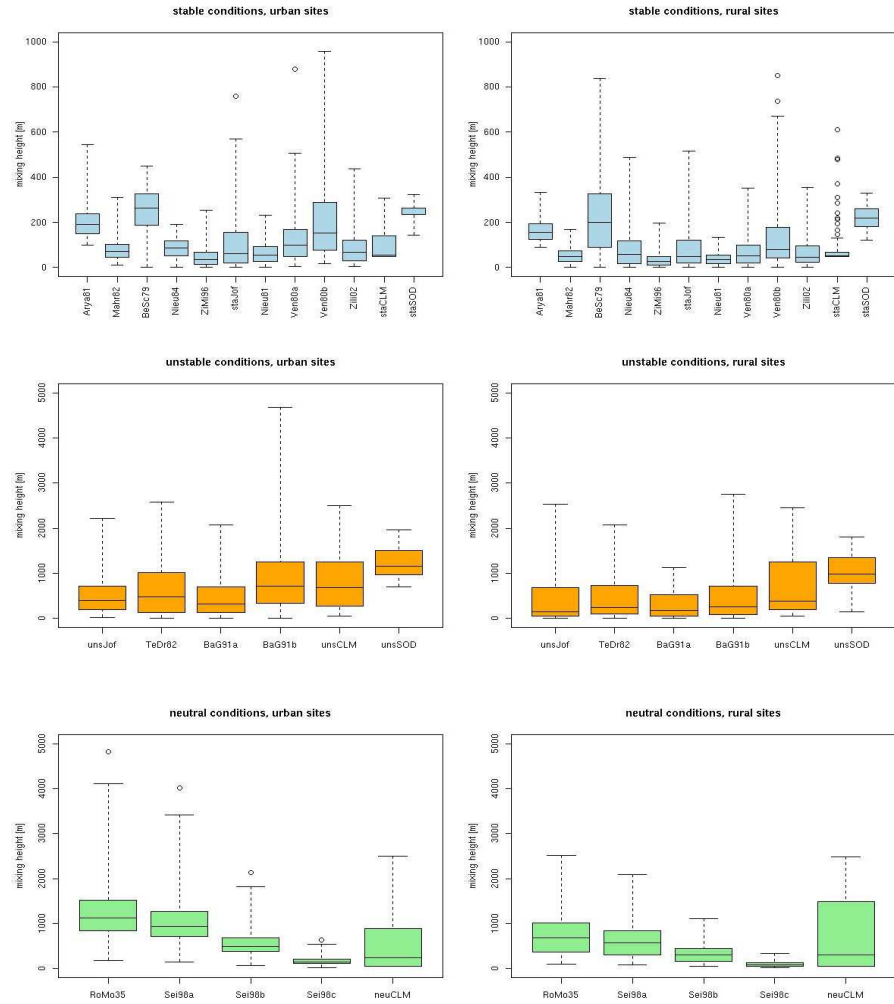
Figure 7.11: *Box-plot of the MH calculated by the different methods listed in Appendix 1 under stable (upper panel), unstable (mid panel) and neutral (lower panel) conditions at the three urban sites in Bologna (left) and at the rural site of S. Pietro Capofiume (right). Each box represents from bottom: 1st Quartile, Median and 3rd Quartile. The whiskers extend to the most extreme data points which are no more than 4 times the inter quartile range from the box. Open circles represent outliers. SOD refers to the sodar-estimated MH and CLM indicates the MH from the CALMET-SMR operational pre-processor.*

CBL ($n = 601$)   SBL ($n = 216$)
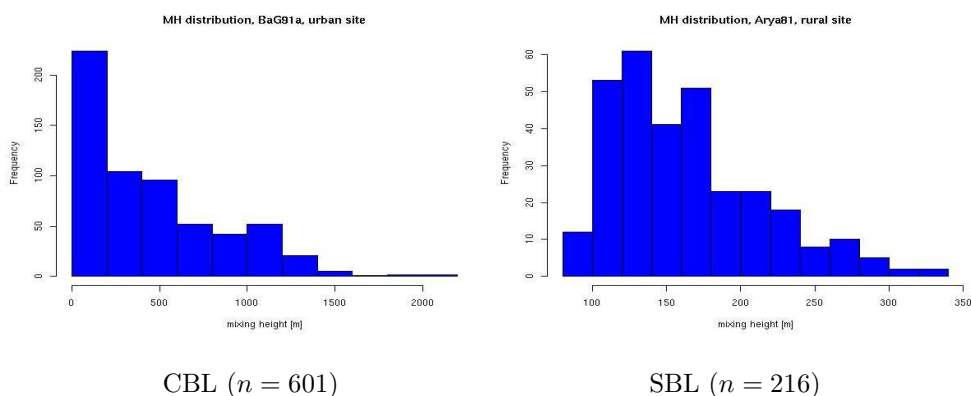
*Figure 7.12: Examples of typical frequency distributions for a convective formula at the urban sites (left) and for a stable formula at the rural site (right).*

most cases as can be seen in Fig. 7.12, which shows an example of typical frequency distributions for both the urban CBL (left) and rural SBL (right).

7.3.2.2. Sodar MH data vs. SBL diagnostic formulations

The inter-comparison between the various MH-estimates (from Appendix 1) and sodar estimates covers the period January-February 2002 in Bologna (urban) and the surroundings (rural). It should be noted that the first four schemes in the upper panel of Fig. 7.11 (stable conditions), are listed in Appendix 1 for neutral conditions but are tested here for stable conditions as was done for the Milan (Lena and Desiato, 1999) and Cabauw experiments (Zilitinkevich and Baklanov, 2002; Baklanov, 2001).

The number of data considered is in most cases around 200. The number of data drops to 30 (for Sodar, BeSc79 and Nieu84) because some of the input data needed by these formulae were missing during the campaign.

It can be seen from the box plots (Fig. 7.11) that the median value of the urban MH is always greater than the median value for rural conditions. The difference is more evident for the "Ven80b" formula (the difference between median urban and median rural is 73.5 m) and not relevant for the "staCLM" method (difference of 3 m). The MH estimated by sodar ("staSOD") is markedly greater for the urban case (difference of 14 m).

The box extremes (1st and 3rd quartile) show that some formulae provide MH estimations that range between ca. 80 and 300 m (Ven80b urban, and BeSc79 rural) while other formulae are characterized by a very narrow range of values (for examples ZiMi96, Mahr82 and Nieu8 ranges between around 10 and 70 m). The Ven80b formula gives some values greater than 2000 m (outside the range of the Figure) due to the method used to estimate N from radiosounding data. At the rural site, the CALMET pre-processor sometimes considers periods as convective that are classified as stable by the other methods, thus leading to a large number of outliers in Fig. 7.11.

BeSc79 and Nieu84 formulae gives very low values when the wind speed is very low. Such conditions often occur in the Po Valley where the measurements were made. The formulae ZiMi96, staJof, Nieu81, and Zili02 also give low MH in very stable conditions, when the measured L is very small (around 10^{-4} m), while Ven80a gives low values when u_* is small.

Since sodar-derived MH values can be considered independent from the MH estimates of the parametric methods using surface data, some statistical indexes such as the bias, root mean square error RMSE and the correlation coefficient were calculated from these two sets of MH-values. For the Bologna data set, these statistics were considered only for formulae for which at least 10 pairs of data were available. The number of data pairs in most cases is only about 20. The statistical comparison between the MH calculated by parametric formulae and the "independent" MH from sodar is shown in Table 7.6 for the urban and rural sites. Some previous similar comparisons, whereby the MH was also determined by sodar, with urban data in Milan (Lena and Desiato, 1999) and a rural data in Cabauw in the Netherlands (Vogelezang and Holtslag, 1996; Zilitinkevich and Baklanov, 2002; Baklanov, 2001) are also presented in Table 7.6.

Results in Table 7.6 show that all algorithms provide MH values that are poorly related with MH estimated by sodar both for urban and rural conditions. The bad correspondence between MH calculated by the various algorithms and MH estimated by sodar can be explained considering that, as described in Section 4.3, most of the algorithms for nocturnal conditions are very simple. On the other hand, sodar data have also known deficiencies, so that no firm conclusions can be drawn.

The results from the present study corroborated the results of Seibert *et al.* (1998) who found that the tested algorithms did not yield very satisfactory

Table 7.6: Comparative rural-urban evaluations of different SBL height equations versus some measurement datasets.

Formula code [Eq. #] cf Appendix 1	Urban, Bologna[4] (Feb. 2002)			Rural, Bologna [4] (Jan. 2002)			Urban, Milan [3] (May-Aug.1996)			Rural, Cabauw (years 1977-1979)		
	Bias	RMS error	Corr. coef.	Bias	RMS error	Corr. coef.	Bias	NMS error[5]	Corr. coef.	Bias	RMS error	Corr. coef.
Arya81b [1] [4]	–	–	–	–	–	–	−264	1.69	0.43	64.0	218	0.27
Ven80a [2]	−74	151	0.12	−210	263	−0.18	–	–	–	–	–	–
Ven80b [3]	−12	144	−0.01	−185	255	−0.21	–	–	–	–	–	–
Nieu81 [5]	−154	166	0.09	−224	270	−0.04	–	–	–	–	–	–
Zili72a [1]	–	–	–	–	–	–	−4.2	0.65	0.43	24.4	173	0.27
Arya81[2] [15]	−11	80	0.11	−111	192	−0.17	−72	1.69	0.43	103	86.3	0.48
Mahr82[2] [16]	−141	154	0.11	−215	264	−0.17	94	0.42	0.39	−24.4	18	0.48
BeSc79[2] [17]	–	–	–	−108	297	−0.34	52	0.25	0.39	208	264	0.48
Nieu84a[2] [18]	–	–	–	−227	318	−0.26	215	2.1	0.34	6.27	13.9	0.48
ZiMi96 [6]	−178	188	−0.01	−225	277	−0.18	–	–	–	−33.8	33.8	0.38
Zili02 [7]	−148	164	−0.03	−219	284	−0.17	–	–	–	6.21	19.2	0.60
staJof [9]	−108	173	−0.09	−212	281	−0.18	–	–	–	–	–	–

(1) Modified version of Zilitinkevich's (1972) formula with re-estimated constants.
(2) This equation was developed for neutral conditions, here used also for stable conditions.
(3) Based on the MH values from sodar data (see Lena and Desiato, 1999).
(4) Based on MH values from sodar data (see section 5.4) rural data refer both to summer and winter conditions, urban data refer to winter conditions.
(5) NMSE is the normalised mean square error.

results either, for rural and/or homogeneous conditions. Thus, the bad correspondence with the sodar derived MH is not very surprising and probably not just due to the urban features. A slight improvement, compared to urban conditions, can be noted for the formulation of Zilitinkevich *et al.* (2002, see Section 4.3.2) that performed much better than the other formulations against measurement data for the rural site of Cabauw.

7.3.2.3. Sodar data vs. CBL prognostic and diagnostic formulations

Four different methods (see Appendix 1) to estimate the convective MH were inter-compared and compared with MH-sodar estimates from Bologna and with

MH calculated from the CALMET-SMR pre-processor. The number of data considered is around 600. The number of data drops to 40 for the sodar method.

The box plot (Fig 7.11 mid-panel) shows that the difference between the urban MH median values and rural MH median values, range between 460 m for the "BaG91b" method and 142 m for the "BaG91a" method, while the median urban MH estimated by sodar is 164 m higher than at the rural site. The range of urban MH estimates is maximum for the "BaG91b" and "unsCLM" formulae and minimum for the "unsJof" and sodar methods. This behaviour is different at the rural site where the range of values from "unsJof" increases while the range of "BaG91b" decreases. The BaG91a and BaG91b formulae gives sometimes zero values, probably due to the method employed to estimate the potential temperature gradient γ above the ABL. Some formulae give sometimes very high values like 5000 m (e.g., BaG91b urban). These outliers can occur when the formula gives a strong increase of MH from one time step to the next (e.g., Arya81 around 12Z in the top panel of Fig. 7.14). To avoid these discontinuities in the time evolution of the MH, an upper limit to the incremental MH was set to 1000 m.

The typical increase of MH during daytime is illustrated in Fig. 7.13, which shows the mean daily course of MH calculated by the various algorithms during winter (left) and summer (right) at the rural (top) and urban sites (bottom). The expected daily course is more or less caught by all the formulae, however partly with large discrepancies that seem to increase in the course of the day. The Batchvarova and Gryning (1991) formula (BaG91a) has a slow growth during the morning and stays stationary during the afternoon. The second Batchvarova and Gryning (1991) formula (BaG91b) reaches high values at the urban sites and keeps growing during the afternoon, while at the rural site it stays stationary during the afternoon. The MH calculated by Tennekes and Driedonks' (1981) scheme grows during the first part of the afternoon not only at the urban but also at the rural site. Joffre and Kangas's (2002) mixing height often decreases during the afternoon and lead to irregular values. In all the conditions shown, the Tennekes and Driedonks formula is closest to the CALMET calculations, which shows the smoothest behaviour.

The discrepancies between the various methods can be better seen by directly comparing the time evolution of MH calculated by various methods. Figure 7.14 shows two summer days at the rural site (top) and a winter day at an urban site (bottom). All the days shown are sunny with low winds (the wind speed is < 3 m s^{-1} during the summer days and < 6 m s^{-1} during the winter
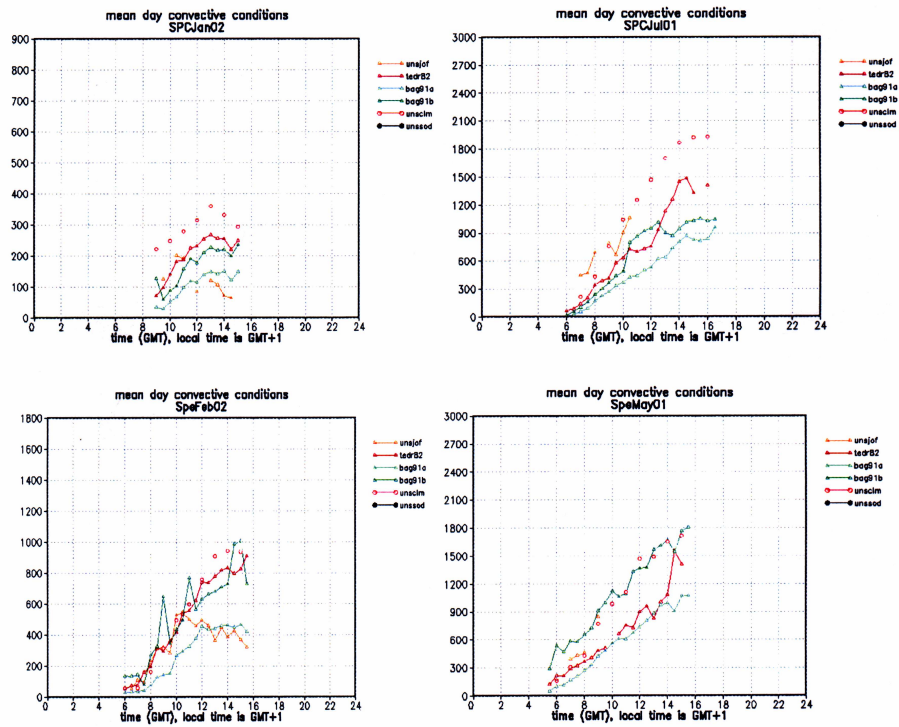
Figure 7.13: Mean daily course of the MH calculated with 5 different algorithms (orange
= Joffre and Kangas (2002); red = Tennekes and Driedonks (1973, 1982); green
= Batchvarova and Gryning (1991), their two different formulae; open red circles
= CALMET) during winter (left) and summer (right), at the SPC rural site (top)
and the Specola urban site (bottom). Note that the plots do not have the same
vertical scale. The sodar data are missing.

one) with prevailing convective conditions during the day. For summer condi-
tions, CALMET (dark red open circle in the plots) has often a strong growth
until 17.00 LST and a sudden decrease after sunset. The MH growth esti-
mated by the Tennekes-Driedonks' scheme (dark red triangle) and in particular
by Batchvarova-Gryning's formulae (dark and light green triangle) is weaker
in the afternoon. In summer, the MH evaluated by the sodar profiles (black
closed circles) stays closer to these three methods, rather than to CALMET val-
ues, whereas on the winter day shown, daytime CALMET and sodar estimates
are rather close. In this case, daytime MH estimates by Batchvarova-Gryning
and by Joffre-Kangas are considerably lower than those of the other methods
applied.
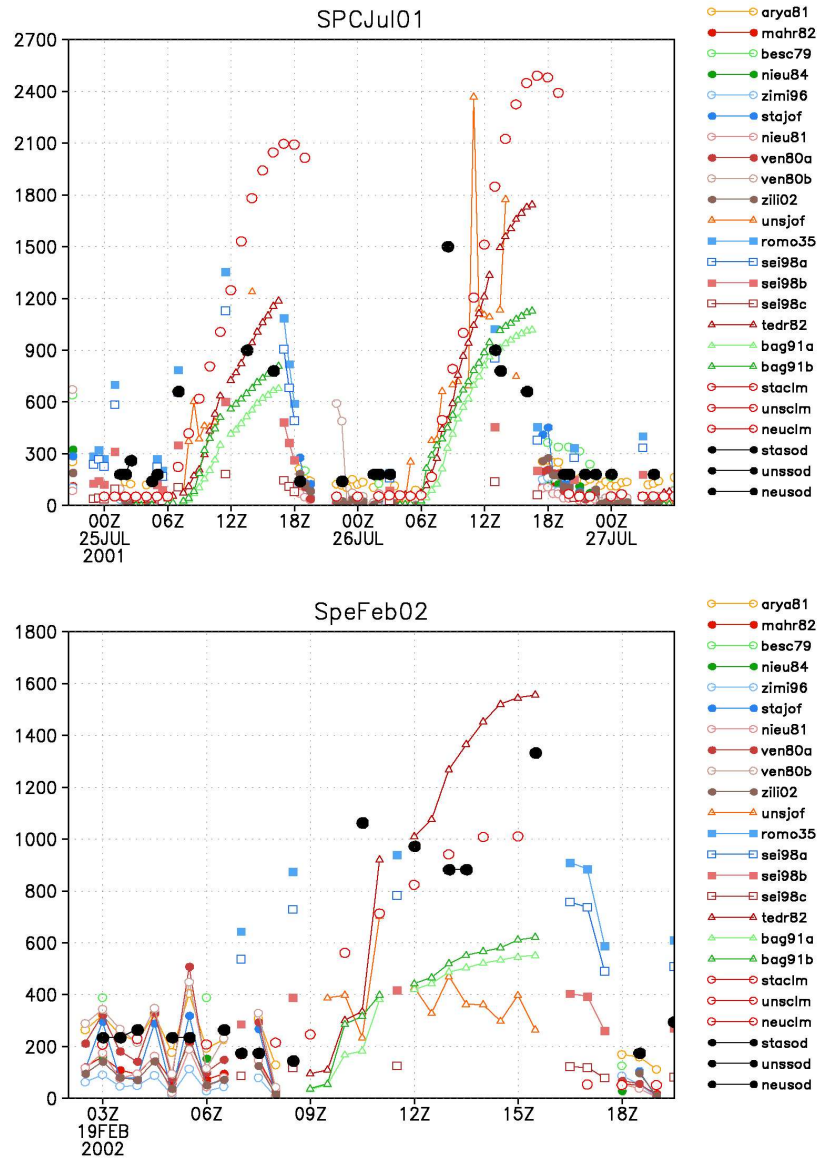
Figure 7.14: Temporal evolution of the MH estimated with different methods for Bologna. Top, two summer days at the rural site SPC; Bottom, a winter day at the Specola urban site. Open red circles = CALMET; close black circles = sodar; close blue squares = Rossby & Montgomery (1935); open blue squares = Seibert et al. (1998); dark green triangles = Gryning and Batchvarova (1991); light green triangles = Gryning and Batchvarova (1996); open red triangles = Joffre and Kangas (2002).

When comparing these various convective algorithms with sodar derived MH-values, they all show very poor correlation (correlation coefficients range between -0.3 and 0.1) and a negative bias (e.g., the sodar-derived MH is generally greater than MH estimated by the 5 formulae), with the only exception of CALMET in rural summer conditions (cf. Fig. 7.14, top panel). However, it is expected that the sodar is still less appropriate for determining the MH under unstable conditions than in stable conditions due to the fact that the daytime MH is frequently beyond the sodar vertical range.

7.3.2.4. Data vs. neutral ABL diagnostic formulations

Four different methods to estimate the neutral MH were inter-compared and compared with MH calculated from the CALMET-SMR pre-processor. The neutral ABL was not estimated from sodar data. All the tested "neutral" formulae simply differ by a multiplicative factor (see Appendix 1). The number of data considered is around 600 for the urban case and 200 for the rural case. The number of data drops respectively to 300 and 100 for the CALMET method.

The box plot (Fig 7.11, lower panel) shows that the difference between the urban MH median values and rural MH median values range between 435 m for the "RoMo35" method and 58 m for the "Sei98c" method. In contrast with these results, CALMET calculations provide rural MH values 55 m higher than urban ones. Apart from CALMET, the range of MH estimates in urban conditions is maximum for the "RoMo35" and minimum for the rural "Sei98c".

During late afternoon and evening hours, neutral conditions often occur due to the transition from unstable to stable conditions. Under such conditions, MH decreases through the evening. This typical course is illustrated in Fig. 7.15, where the hourly MH calculated by several methods at the Specola urban site in Bologna are shown for two late spring days (top) and one winter day (bottom). During the two late spring days (13–14 May) shown in the top panel of Fig. 7.15, the ABL was mostly neutral due to moderate wind conditions (wind speed between 5 and 9 m s^{-1} in Bologna), except for the period between 06:00 and 15:00 LST on May 14, when the ABL became convective. All the algorithms catch the transitions between the decreasing neutral ABL during the night and the increasing convective ABL after sunrise. During the moderate windy (wind speed about 6 m s^{-1}) 24 February 2002 (Fig. 7.15, bottom panel) the ABL was neutral for the whole period. The comparison in Fig. 7.15 shows that RoMo35 and Sei98a (blue closed and blue open squares) always give the highest MH,
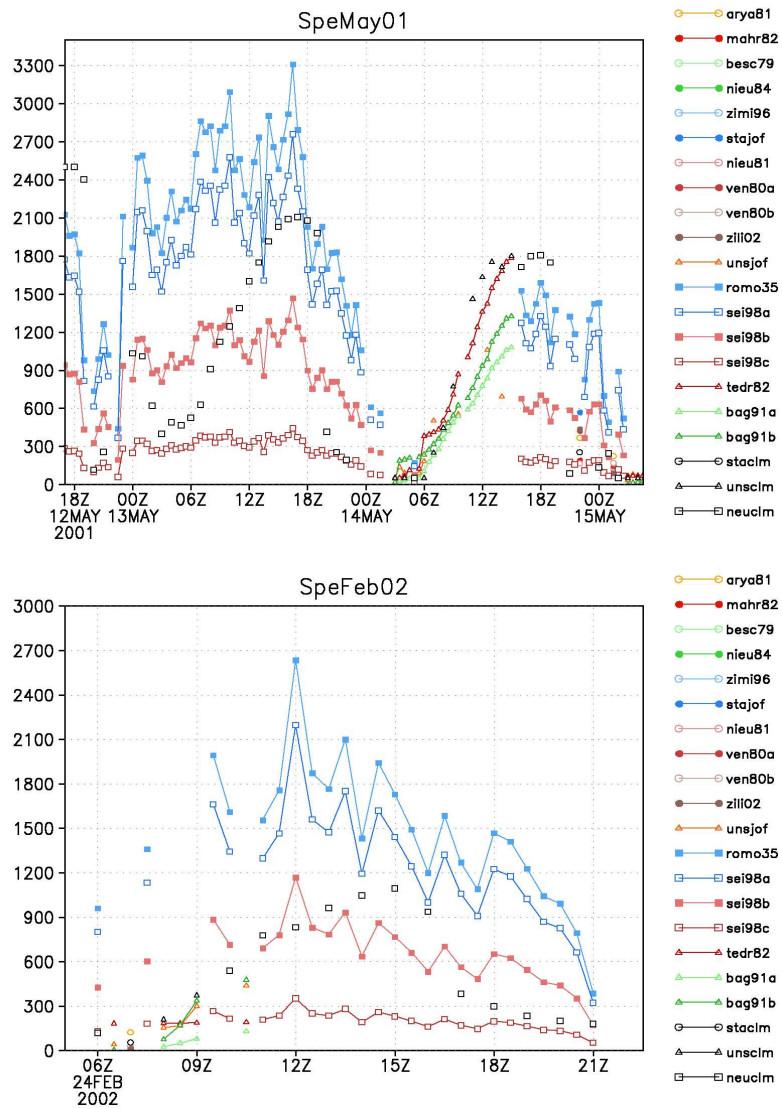
Figure 7.15: MH estimated with different methods during two late spring days at an urban site (Top) and a winter day at an urban site (Bottom). Neutral boundary layer: blue closed squares (Rossby & Montgomery, 1935), blue open squares (Sei98a), dark red closed squares (Sei98b), dark red open squares (Sei98c), where Sei = Seibert et al. (1998). Convective boundary layer: red close triangles (Tennekes & Driedonks, 1981), red open triangles (Joffre & Kangas, 2002), green close triangles (Batchvarova & Gryning, 1991), green open triangles (Gryning & Batchvarova, 1996), black open squares and triangles = CALMET-preprocessor.

while Sei98c (dark red open squares) the smallest MH. CALMET (black open squares) mainly shows a smoothed behaviour that is rather more sensitive to the thermal terms than to the mechanical ones.

7.3.3. Comparison between sodar and tethersonde data, Cracow

Two experiments were organised in the framework of COST-715 in August 2002 and June 2003 in Cracow, Poland, (see Section 5.5) for (i) determining the MH by tethered balloon equipped with instrumentation for wind speed, humidity, and temperatures of dry and wet thermometers and (ii) acoustic sounding of the atmosphere with a sodar. Both instruments were operated at the urban meteorological station. MH values deduced from the vertical profile of the tethersonde potential temperature were compared to those derived from the sodar echoes. In the cases when the temperature profiles for ascent and descent were different, a separate analysis was performed. We excluded those cases when the balloon sounding ceiling (ca. 1000 m) was lower than the MH derived from the sodar data.

Figure 7.16 clearly illustrates the development and structure of thermals along with typical processes from a 24-hr period sodar record between approximately 7:00 and 15:00GMT. During night-time, the structures are quite different as the thermals disappear and other motions and layering appear. The derivation of the MH by sodar is explained in Section 4.2.2.

7.3.3.1. Conditions at night

Ground-based inversion layers were observed every night during both experiments. The layers became visible in the sodar record near sunset and they disappeared about 1.5–2 hours after sunrise. Sometimes the ground-based inversion layer was accompanied by elevated inversion layers.

A comparison of the depth of ground-based inversion layers derived from sodar echoes and those derived from temperature profiles is presented in Fig. 7.17. Both methods give very similar values. The correlation coefficient for the case without elevated layers above the ground-based layer is 0.96 (number of cases $n = 41$) and for the case with elevated layers 0.93 ($n = 19$).
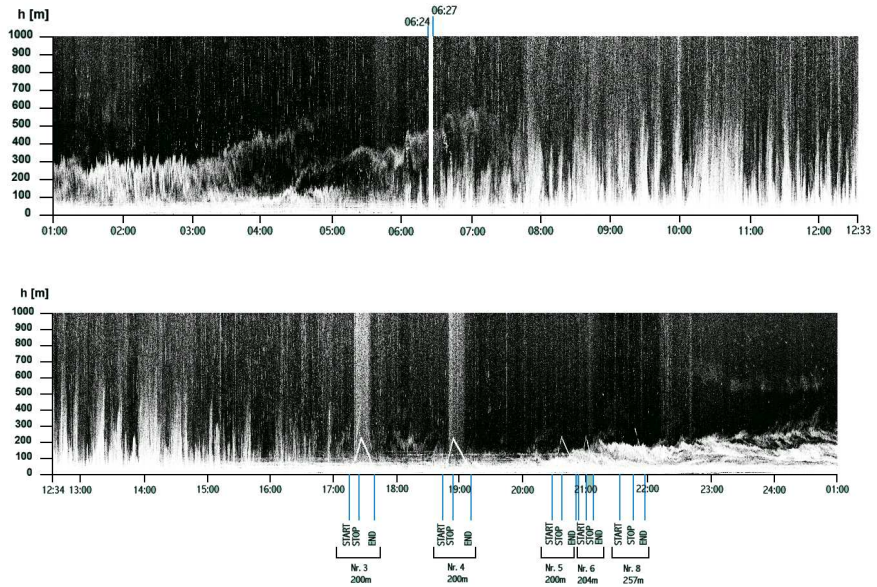
Figure 7.16: Diurnal record of vertical sodar echoes on June 10, 2003.
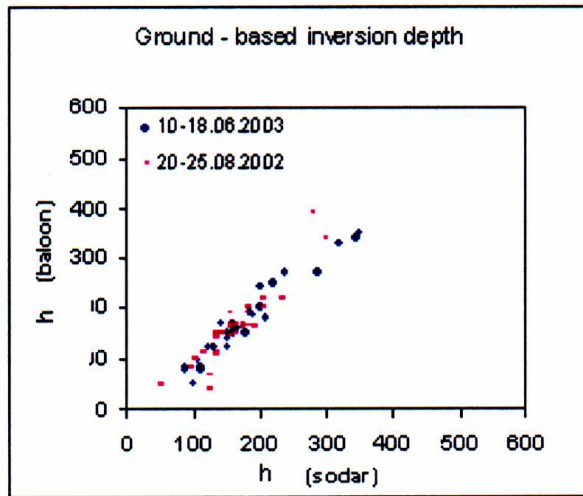
Figure 7.17: Comparison of ground-based inversion layer heights determined from sodar echoes (h-sodar) with those determined from the vertical profile of potential temperature (h-balloon).

7.3.3.2. Conditions during the morning and evening transitions

During the transition hours, the determination of the atmospheric stability is problematic, both for sodar and balloon data. The image of the sodar echoes is changing quickly, and the potential temperature gradient is near adiabatic, not favourable for sodar operation. In the morning, it is difficult to catch the moment at which the first convective structures appear, and their elevation is difficult to estimate before the ground-based inversion layer has clearly risen up.
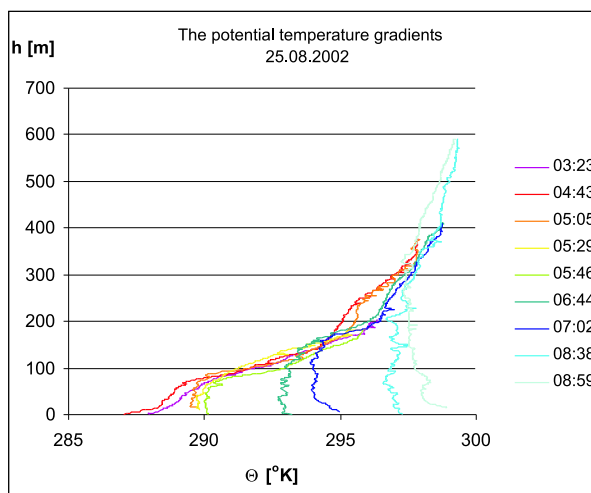

Figure 7.18: Temporal evolution of the potential temperature gradient during the morning transition with a ground-based inversion layer persisting up to 6 GMT, then becoming convection capped by an elevated inversion layer. The sun rose at 3:41 GMT.

In the evening, the weak decaying convection in the sodar record may be erroneously classified as a weak ground-based inversion layer. They are often accompanied by an adiabatic gradient of potential temperature. It can also happen that the sodar records still show convective structures while the temperature record of the balloon shows already a ground-based inversion up to several tens of meters (in the dead zone of the sodar).

Figure 7.18 displays the transition from stable (ground-based inversion layer) to unstable (convection with capping inversion layer), while Fig. 7.19 shows the opposite transition, as revealed by the behaviour of the balloon vertical potential temperature profiles.
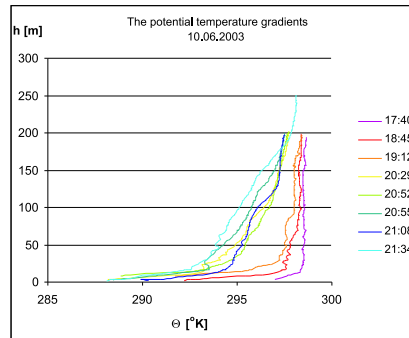
Figure 7.19: Temporal evolution of the potential temperature gradient during the evening transition with convection persisting up to 17.40 GMT, then leaving place for a ground-based inversion layer. Sunset occurs at 18.51 GMT.

7.3.3.3. Conditions during daytime

The warming-up of the surface after sunrise lifts and finally dissolves the ground-based inversion layer. The convective motions are initially limited by the elevated inversion layer which then disappears, whence thermals can rise higher. When the elevation of convective motions is limited by an elevated inversion layer below the vertical range of the sodar, the MH can be well deduced from the maximum in the acoustic backscatter, which is identified as the base of the elevated inversion layer. Figure 7.20 presents a comparison of MH values determined from sodar records and those determined from the potential temperature gradient of the balloon profile (correlation $= 0.96$, $n = 13$).
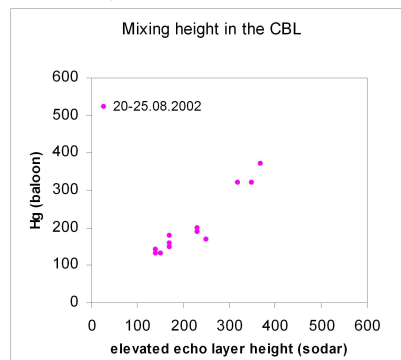

Figure 7.20: Comparison of MHs determined from sodar records and those determined from balloon soundings, for convective conditions capped by an elevated inversion layer.

Uncertainties arise when the elevated inversion layer disappears. The backscatter signal from the top of the convective structures may be weak enough to be unrecorded by the sodar. In addition, convection is only an indirect index of the mixing process, since mechanical mixing may be present in layers where thermal mixing does not occur.

In Cracow, the free-convective mixing layer height was determined on the basis of the maximum heights of the convective sodar echoes during a period of one hour. For noon and afternoon hours, this value is multiplied by 1.5 (for the older sodar version by 2.0). The idea of this procedure is based, among others, on the results of a series of experiments made in 1992 and 1993, when the SO_2 mixing layer height (i.e., the height up to which high concentrations of SO_2 are observed) was determined by a correlation spectrometer onboard an aircraft (Walczewski and Orkisz, 1994).
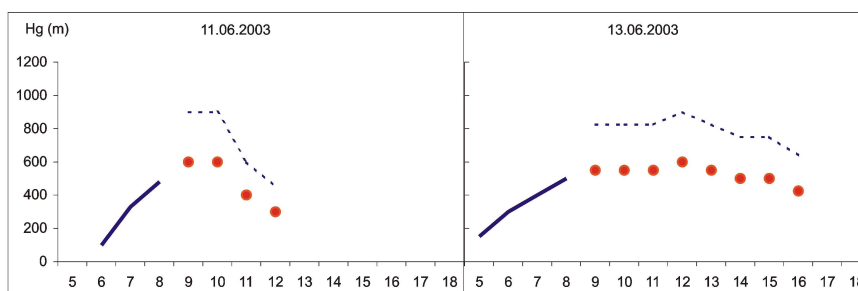

Figure 7.21: Selected mixing height time records determined by means of sodar observations during unstable conditions. The continuous line represents the base of an elevated inversion layer capping the convective cells. The dots indicate the height of free convection recorded by the sodar. The dashed line represents the estimated MH (maximum height of convective cells from sodar multiplied by a factor 1.5) for free convection conditions. Sunrise occurred at 2:27 GMT and sunset at 18:52 GMT. Free convection is starting at about 8 GMT. There was a storm over Cracow at 12 GMT on 11.06.2003.

Figure 7.21 displays an example of mixing height records determined by means of sodar observations versus time during a period of unstable conditions. After the growth of the mixing height and after the destruction of the elevated inversion by convective eddies, the height of convective cells stabilised at a nearly constant level. During the afternoon, a rather rapid drop of the convective MH occurs. Convective updrafts disappear about 2 hours before sunset. The results of this experiment show a reasonably good agreement between MH estimates from the sodar and those from tethered balloon measurements.

7.4. Comparison of numerical pre-processors and NWP models vs. data

7.4.1. Mixing height estimates from NWP/meteorological models

7.4.1.1. HIRLAM, Copenhagen

Methods for estimating the MH based on NWP output and different diagnostic methods, including the bulk Richardson number method, the Vogelezang and Holtslag's (1996) method, and the parcel methods were studied for the Copenhagen metropolitan area (Rasmussen *et al.*, 1997; Baklanov *et al.*, 2002; Baklanov and Kuchin, 2004). These and other methods were inter-compared (see Section 7.2.2), and MHs based on outputs from the DMI-HIRLAM NWP model profiles were compared with the corresponding MHs estimated from radiosonde data of the Jægersborg station in Copenhagen.
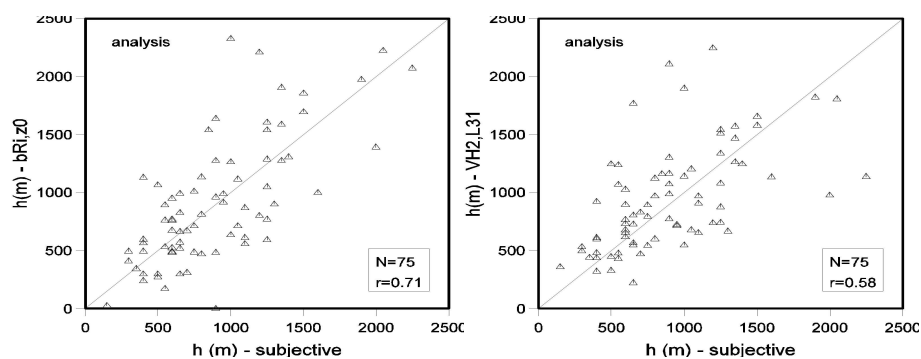
Figure 7.22: Scatter plots of the MH (determined by the parcel method) from radiosondes at Jægersborg, and the MH calculated from DMI-HIRLAM outputs by the bulk Richardson method (left panel) and the Vogelezang-Holtslag method (right panel).

The results shown in Fig. 7.22 for the period 1994-95 show that the agreement between MHs from measured radiosonde profiles and those from DMI-HIRLAM output profiles is fairly good in general. Moreover, MH estimates based on DMI-HIRLAM runs are in general of nearly the same quality as the estimates based on observed data. However, especially under unstable and convective conditions, there can be large errors in the temperature profiles generally caused by too a weak development of the boundary layer in these situations. For the nocturnal MH, results show a considerable underestimation of the MH by both

Ri-number methods and raise the need for improving the Ri-method (Zilitinke-vich and Baklanov, 2002).

The above comparison was performed for the operational DMI-HIRLAM version with a horizontal resolution of 15 km. Therefore, it was difficult to consider local effects due to urban or other heterogeneities of the surface. Model runs were also performed with the 1.4 km resolution experimental version of DMI-HIRLAM using a prognostic equation for the TKE, which included the advection terms and an adjustment of the roughness length for estimating the MH. This approach has the potential to simulate IBL features due to the sea coast-line transition and/or urban non-homogeneities (via the the roughness length and the prognostic TKE equation that includes the advection terms), but needs considerable improvements for SBL cases due to the used local-closure of the turbulence. Nevertheless, this experimental version of the DMI-HIRLAM used in the simulations, includes a simplified description of urban features (Baklanov *et al.*, 2002) and still leaves room for improvements.
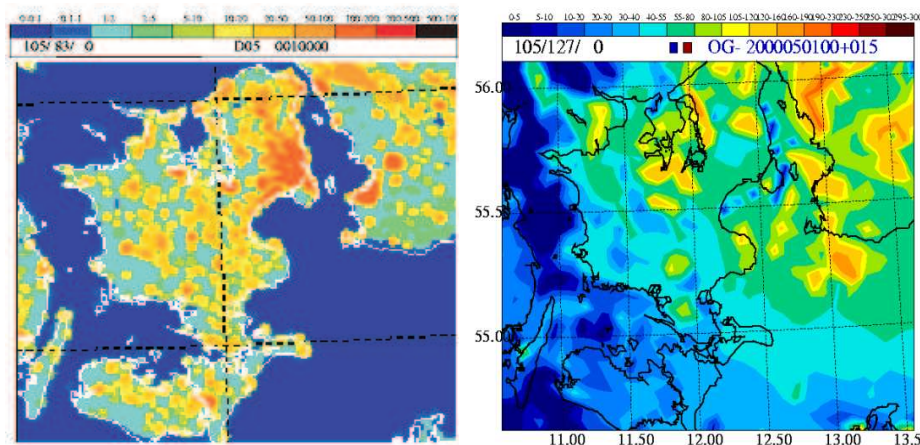
Figure 7.23: *The simulated roughness length (z_0, in cm) from the high resolution physiographic data (left panel) and operational forecasts of the mixing height (right panel, the palette values are given in 10m) with an experimental version of the DMI-HIRLAM model using the TKE decay method and a horizontal resolution of 1.4 km for the Sjælland Island with the Copenhagen metropolitan area (area of high roughness along the east coast of Sjælland).*

Figure 7.23 shows one example of the roughness length simulation (left panel) and the MH forecast using this approach (right panel) by the DMI-HIRLAM for the Sjælland Island where Copenhagen is located. In the considered meteo-

rological situation, the dominated wind direction over Sjælland is from the East and East-Southeast. We can see the downwind IBL growth from the sea surface of the Øresund strait to the land area and the Copenhagen city along the wind direction and the coast line. The prognostic TKE equation provides simulation of this effect, but, as it was mentioned above, the TKE decay algorithm for the MH (see Section 4.7) gives an underestimation of MH values over the cool sea surface. Therefore, in operational DMI dispersion models that are linked to DMI-HIRLAM, the bulk Ri-number method is preferably used utilising the profiles generated by the DMI-HIRLAM model.

7.4.1.2. MM5, Athens

The application of numerical meso-meteorological models to the estimation of the urban MH with respect to other simple MH schemes will be considered in this Section using the example of Athens city and its surroundings. The purpose was to evaluate the effects of different factors such as complex topography and strong changes in surface roughness (sea-land, urban-rural) on the evolution of the MH. The formation of the MH becomes a complicated process in those areas where these features coexist.

The work was based on applying the Penn State/NCAR Mesoscale Model MM5 (Anthes and Warner, 1978) model in three different configurations:

1. The MM5 model was applied in its original version with the high resolution non-local NCEP MRF (National Center for Environmental Prediction Medium Range Forecast Model) ABL scheme. This scheme is based on the Troen and Mahrt's (1986) representation for counter-gradients and K-profiles in the well-mixed CBL (Hong and Pan, 1996). In this version, urban areas are represented as bare soil with specific surface characteristics and physical parameters, such as roughness length, albedo etc. In this non local MRF scheme, the MH is given as a function of the critical bulk Richardson number.

2. A second simulation uses a modified ("urbanised") version of MM5 whereby urban features were introduced both in the thermal and the dynamical part (Dandou *et al.*, 2004). In particular, the urban heat storage was incorporated in the model following the Objective Hysterisis Model (OHM) of Grimmond *et al.* (1991) and anthropogenic heat effects for Athens were considered following Taha (1998). Also, the surface stress and heat flux

provided by the model were updated, with emphasis to rough surfaces under unstable conditions, according to Akylas *et al.* (2003). The whole scheme was supported by detailed information on land use cover derived from satellite image analysis.

3. In order to isolate the topographic influences on air motions in the city basin, another simulation was performed with the original version as well (case 1), but where Athens was replaced by dry cropland and pasture surface, as in the surrounding areas.

The MH is often higher in urban areas than in the rural case, especially during daytime hours. This is illustrated for Athens (Fig. 7.24) during the MED-CAPHOT experimental campaign. The modified version of MM5, which includes some urban effects, increases the MH for nocturnal conditions (due to anthropogenic heat and storage heat terms). During daytime, the values are a little smaller than those calculated by the original version and there is a delay of two hours until the maximum value is reached. On the other hand, the changes do not affect the MH-values for the non-urban site. For the case when the urban area of Athens is replaced by a dry cropland and pasture area, MH-values are much lower (300 m) compared to the ones from the original version; nevertheless, the maximum MH-values are still formed in the Athens basin due to the surrounding topographical features. This unrealistic run illustrates, as in case of Marseille, that in a complex situation, urban influences coexist with other mechanisms. Figure 7.25 shows the night-time spatial distribution of MH
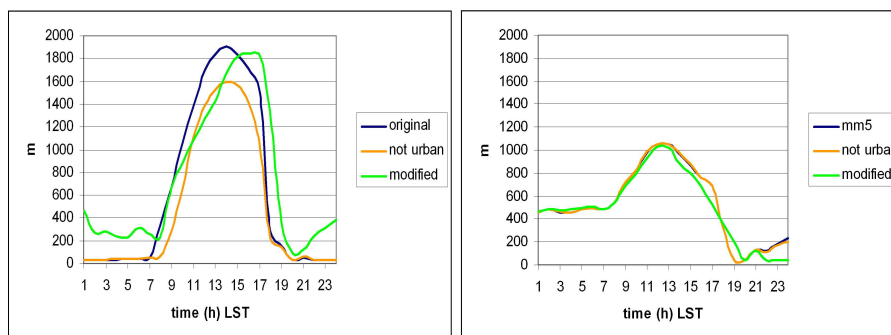

Figure 7.24: The diurnal variation of the mixing height (m) at the NOA station in the city centre of Athens (left) and the rural station of Spata (right), produced by the original MM5/MRF model (dark blue line), the urban area replaced by a dry cropland and pasture area (orange line) and the modified "urbanised" MM5/MRF model (green line) on 14.9.1994.
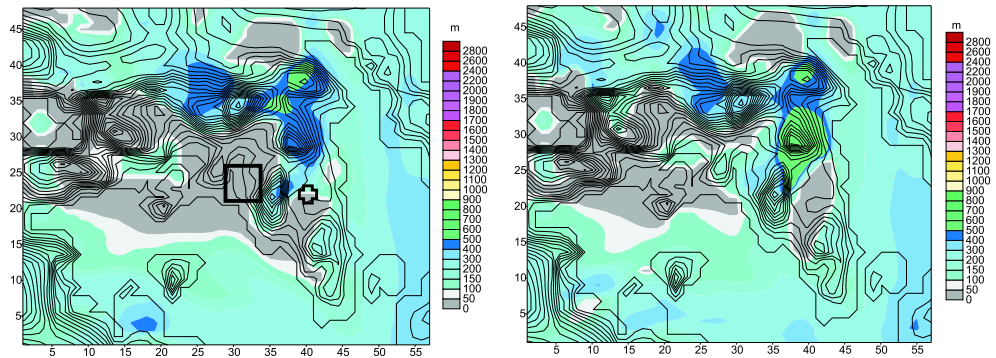
Figure 7.25: *Spatial distribution of the mixing height calculated by the original (left) and modified (right) MM5/MRF model, at 23:00 LST on 14.09.1994. The axes represent number of grid cells of 2 km each. Central Athens is indicated by a box and the rural Spata station is indicated by a cross in the middle of the left figure. The urban NOA station is inside the box.*

for the original case and the modified one, respectively. The increase of MH in the Athens area compared to the surroundings is clearly visible.
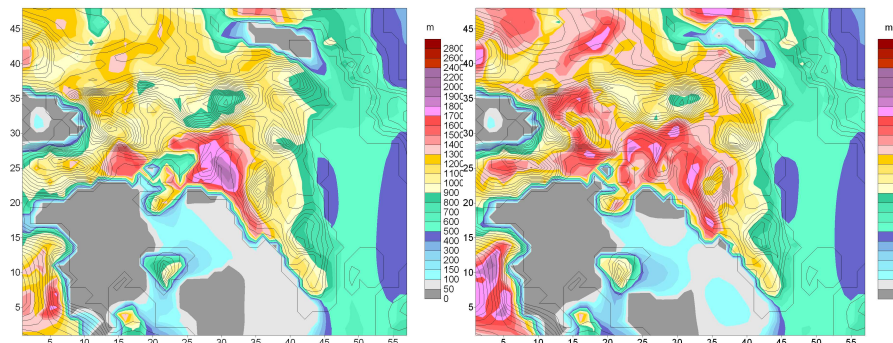
Figure 7.26: *Spatial distribution of the MH calculated by the original (left) and modified (right) MM5/MRF model, at 14:00 LST on 14.09.1994.*

During daytime, larger MH values are calculated by the modified version over a larger area, in contrast to the original model, corresponding to the urban expansion, as it has been observed on satellite images. Nevertheless, the maximum MH value is now substantially lower (Fig. 7.26), accompanied by a decrease of temperature and a reduction of momentum and heat flux (Dandou *et al.*, 2004). It is interesting to mention that only the modifications in the surface energy

balance have produced this much profound decrease of MH over the city area, explained by the absorbing role of the urban heat storage term. This arises from the fact that the changes in the dynamical part, introduced by Dandou *et al.* (2004), result in a substantial increase of MHs in areas where low winds under convective conditions prevail. This is apparent in the plain north of the mountainous area (Fig. 7.26b), where the MH is increased by more than 500 m in some areas.

a)

b)
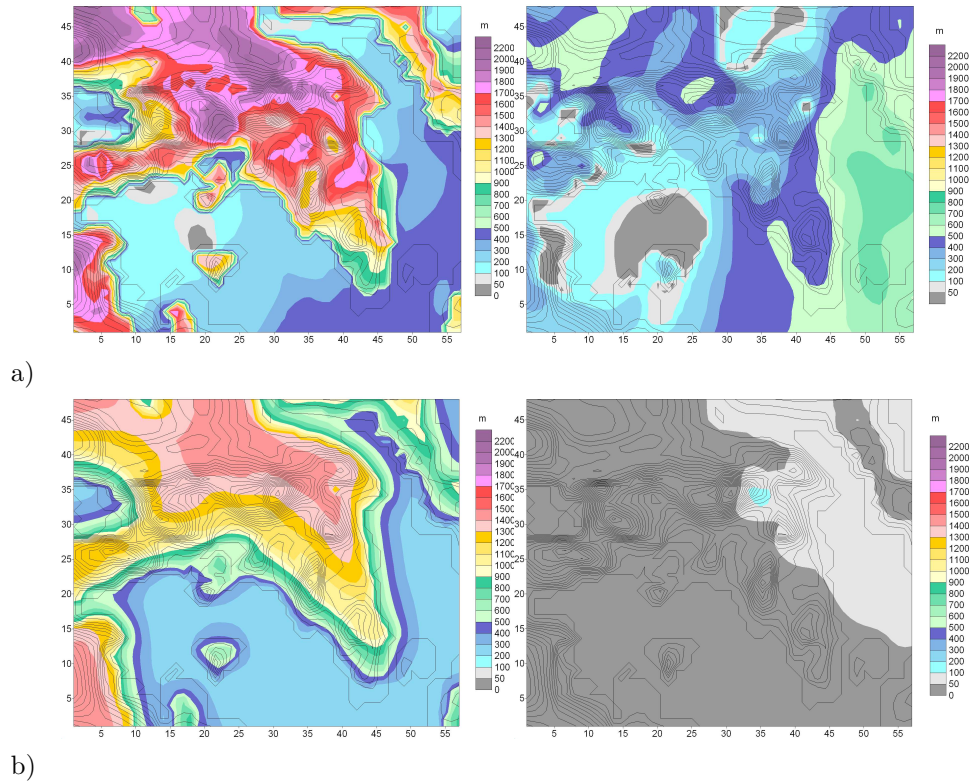
Figure 7.27: Spatial distribution of the MH calculated by: a) the CALMET diagnostic model; at 14:00 LST (left panels) and 23:00LST (right panels) and b) with the original MM5 using the MRF scheme also at 14:00 LST (left) and 23:00 LST (right) on 22.09.2002.

MHs were also calculated by CALMET, a frequently used diagnostic meteorological pre-processor that produces hourly 3D fields of various meteorological parameters, based on routine meteorological measurements (Scire *et al.*, 2000). Figure 7.27 shows the MH fields compared with those produced by the original MM5 version (configuration 1) for September 22, 2002, at 14:00 LST and

23:00 LST. The MH field, produced by CALMET, is unaffected by topographical effects, and its evolution depends only on the downwind distance from the roughness change (coast line).

In Figure 7.28, a comparison between the diurnal variation of the MH, produced either by the original MM5 model or by CALMET, is presented for the non-urban Penteli location and at the University campus, where measurements are available for 22.9.2002. The measured MH data were obtained by Asimakopoulos *et al.* (2004) in the framework of the EU-project ICAROS-NET during autumn 2002 at two sodar locations: one at a semi-urban background site (inside the University Campus) and the other one on the Penteli Mountain (PEN; 450 m height), which stands on the North-east of Athens. MM5 produces MH values closer to the sodar record than CALMET. Two different approaches were used to derive the MH by sodars. The sodar at PEN provided an automated way for determining the MH which is based on the estimation every half an hour of the vertical wind component power spectrum using a FFT technique. At the University of Athens, a Sodar-RASS, not equipped with this algorithm, was used manually, whereby the MH was determined by a visual inspection of the corresponding averaged profiles of the wind speed and direction and the acoustic echo returned signals (Asimakopoulos *et al.*, 2004).
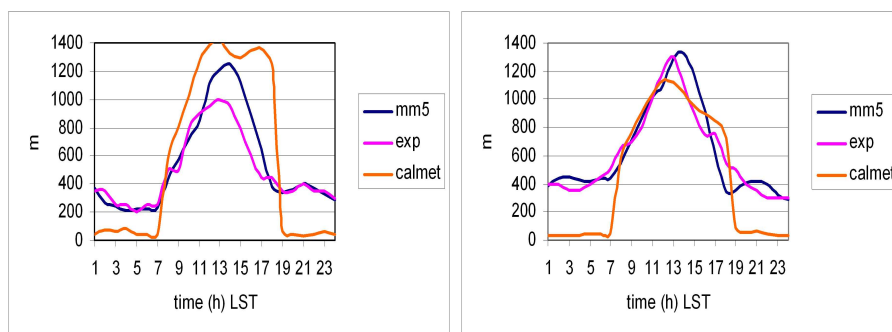
Figure 7.28: Comparison of the diurnal variation of MH (m) at Penteli (left) and the University campus (right) either by the original MM5 or CALMET and sodar measurements (see text) on 22.9.2002.

For the nocturnal MH, the CALMET pre-processor often disagrees with sodar data for both the urban and rural sites. In this first comparison, the modified (urbanised) MM5 version produces MHs closer to measurements than CALMET. During the night, the MHs calculated with MM5 almost coincide with the measurements, although these have been performed by the original version.

A probable explanation might be that the higher winds on this day produce a sufficiently large MH, which thereafter is expected to be less influenced by anthropogenic activities (see Dandou *et al.*, 2004, for further details).

7.4.2 Comparison of MHs estimated by the CALMET pre-processor with sodar data in Cracow

Mixing heights calculated with the CALMET pre-processor (Scire *et al.*, 2000) for the urban meteorological station Cracow-Czyzyny were compared to those derived from a monostatic sodar (SAMOS-4C sodar of Polish production) situated at the urban meteorological station in Cracow (Section 5.5). Data were available for April, June, September and December 2001. Inputs to CALMET were generated by the mesoscale meteorological model ALADIN. New urban features were implemented in CALMET to represent the city of Cracow. The anthropogenic heat was added to the input data of CALMET. The anthropogenic heat depends on the urban class (55 W m^{-2} for city centre, 30 W m^{-2} for city periphery areas, and 15 W m^{-2} for other urban-suburban areas). Additionally, the night-time minimum MH was changed from 50 to 80 meters. These changes improved the CALMET results slightly.

The ceiling of the sodar soundings is 1000 m (elevated layers are recorded up to this height), with a dead zone about 30 m above ground level. The scheme for determining the MH has been developed on the basis of comparisons between sodar echoes and the heights of dust layers observed with a lidar (Bielak *et al.*, 1997; Walczewski, 1997, 1998; Walczewski *et al.*, 1999). The MH was determined as:

- The height of the ground-based inversion layer (in presence of this layer), or of the top of the multi-layer structure connected to the ground based inversion;

- The height of the capping inversion, when the elevated inversion tops the convective cells beneath (morning evolution of the CBL);

- The height of the maximum range of convective plumes multiplied by a factor 1.5 in condition of a well-developed CBL until the maximum height is reached (see also Section 7.3.2.3). Then the estimated MH is allowed to decay to just 80% of this maximum near the end of the day when the stable layer re-appears and is clearly diagnosed.

The mixing height data set derived from the sodar can thus be divided into two groups: direct measurements (night stable case, morning evolution of a capping inversion layer), and estimates (MHs in strong convection). Both types of results are shown in Figs. 7.29 and 7.30 for April 2001 as an example. The described improvement of the parameterizations of the CALMET input and the sodar algorithm lead to a better correlation of both data sets.
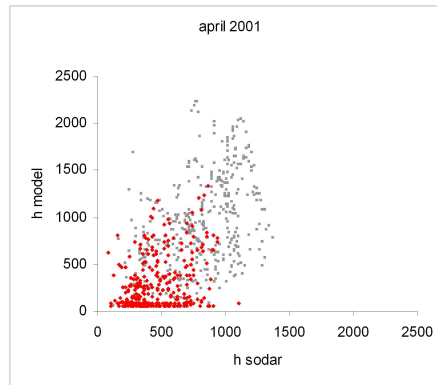
Figure 7.29: Scatter plot for the MH taken from sodar measurements versus calculated values with the CALMET pre-processor (using outputs from the meso-meteorological ALADIN model) for April 2001. Grey dots illustrate day cases, while red dots the night cases.
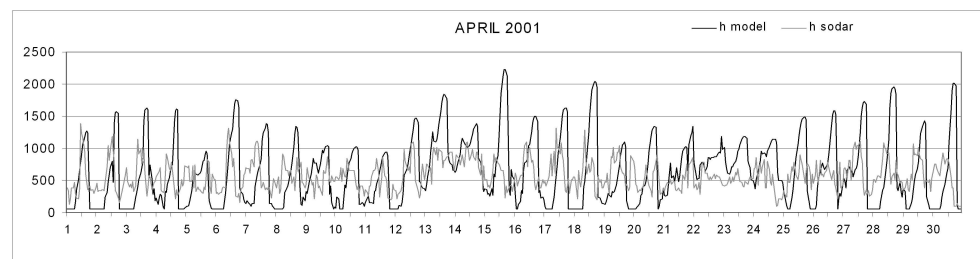
Figure 7.30: Comparative time series of MH variability extracted from the sodar measurements and calculated by the CALMET pre-processor (using outputs from the mesoscale ALADIN model) for April 2001.

As a conclusion of this analysis, there are large and partly systematic differences in MHs from CALMET and the sodar data. CALMET is apparently able to reproduce the expected daily cycle of MH as known, e.g., from textbooks (e.g., Stull, 1988). However, values during daytime are higher than those derived

from aircraft vertical temperature profiles, which were used to calibrate the sodar categorisation scheme for CBL conditions. At night-time, MHs from sodar are generally higher than those calculated by CALMET. Apparently, CALMET under-estimates the MH in many cases at night-time. The sodar MH values show too much short-term variation which is not realistic; more importantly, the continuous MH record by the sodar is possible only because of the subjective analysis given above.

7.4.3 Sensitivity study for London with the ADMS met-processor

The ADMS Model (details: `www.cerc.co.uk`) is a regulatory model with applications in the U.K. and elsewhere for assessing local air quality and for environmental impact assessments. It contains a meteorological pre-processor which uses synoptic observations to calculate the MO stability. The pre-processor is flexible in design, able to accept standard observations such as wind speed and cloud cover, or it can accept values of L, for example. It is a representative state of the art regulatory model. The model offers other facilities for data input, including the use of two roughness lengths. This means the value of the roughness at the anemometer position may be different from that where the dispersion is to be calculated. This option is designed for the usual situation where the data are from an airport but the air pollution must be calculated in the city. We explore here the effects of this urbanising option, and a related one that restricts the conditions from going too stable, representing some urban effect on stability (discussed in some detail in Chapter 3).

Using the ADMS model pre-processor, MHs for 6th–27th July 2003 have been calculated (as part of an urban lidar study, see Section 4.2.2) for the following cases, plotted as three time series in Fig. 7.31:

1. Uniform rural conditions ($z_0 = 0.1$ m assumed everywhere): green.

2. Uniform urban conditions ($z_0 = 1.0$ m assumed everywhere): pink.

3. Transition from rural conditions ($z_0 = 0.1$ m at anemometer site) to urban conditions ($z_0 = 1.0$ m over the urban site) for dispersion met pre-processor calculations: blue.

Figure 7.31 shows that for all the days tested, a uniformly rural roughness gave the lowest values of MH, whilst the uniformly urban roughness gave the largest
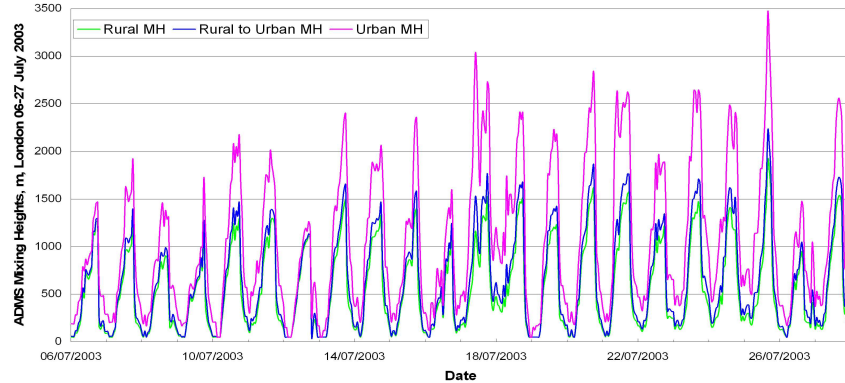
Figure 7.31: ADMS mixing heights using London Heathrow observations, 6–27 July 2003. Cases (1): rural roughness $z_0 = 0.1$ m (green); (2): urban roughness $z_0 = 1.0$ m (pink); (3): rural roughness $z_0 = 0.1$ m at airport with urban roughness at city $z_0 = 1.0$ m (blue).

values of MH. On the windier days the values of the 'urban' MH exceeded 2500 m, and this was judged somewhat unlikely. Therefore the transition case is of great interest; it was intended to be more physically representative, and does indeed yield values of MH which are increased only moderately over the uniformly rural case. This is judged to be more realistic, but field data are needed to validate these results.

Counter-intuitively perhaps, the errors in MH for dispersion calculations might be larger when an urban roughness is assumed everywhere rather than if a rural roughness were used everywhere including within the city. This is because at the anemometer site, too great a roughness would mean the model mis-interprets the effective strength of the wind. In short, if Case 3 seems physically most appropriate for urban dispersion, Case 1 might be the next best option, and Case 2 the least appropriate. Overall these few results shown here indicate that in estimating an urban mixing height, the manner in which the roughness length parameter z_0 is used to represent site conditions merits careful attention and field validation. The dual roughness option seems to have most merit here.

The model also has a stability limit, and Case 3 above was then re-calculated with a limit imposed on the MO-length L, where in stable conditions
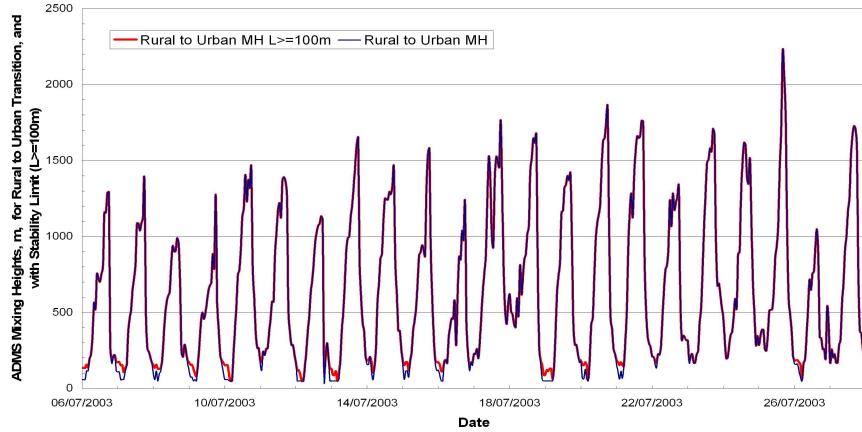
Figure 7.32: ADMS mixing heights using London Heathrow observations, 6–27 July 2003, using Case 3: rural roughness $z_0 = 0.1$ m at airport with urban roughness at city $z_0 = 1.0$ m (blue); and Case 4, same as Case 3 but with stability limit $L \geq 100$ m (red). A change appears at stable night-time; elsewhere the data coincide.
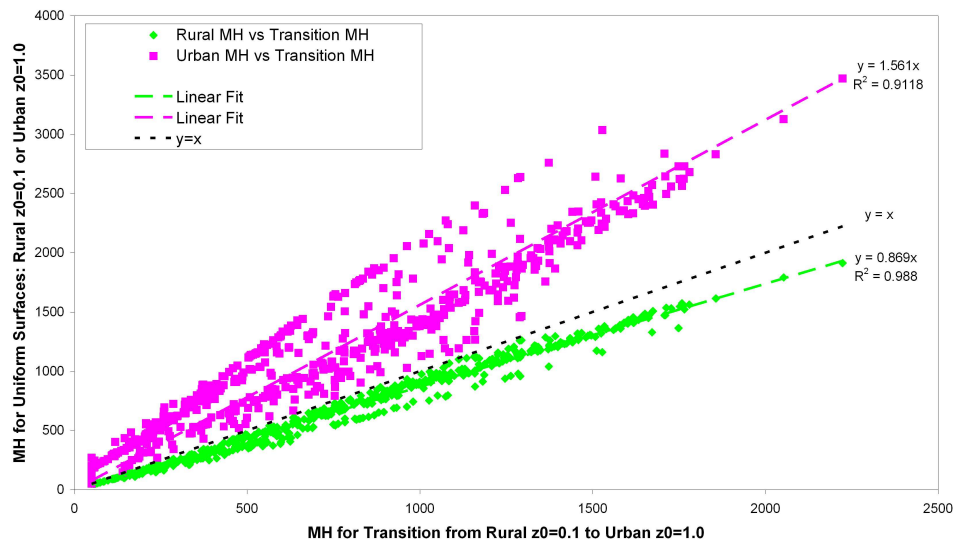

Figure 7.33: Comparisons of ADMS mixing heights using London Heathrow observations, 6–27 July 2003. Green: Case 1 versus Case 3 ('rural' versus 'rural to urban' transition); Pink: Case 2 versus Case 3 ('urban' versus 'rural to urban' transition).

$L \geq 100$ m, to simulate the fact that urban atmospheres tend to be less stable than rural ones, as plotted in Figure 7.32:

4. Transition from rural conditions ($z_0 = 0.1$ m) to urban conditions ($z_0 = 1.0$ m) with stability limit imposed (red), and with no limit (Case 3 blue).

In Figure 7.32, for much of the time, the mixing heights were equal, both with and without the limit on stability. This limit prevents diagnosis of the most stable situations, so only operates in such conditions. During some nights here, the effect of less stable nights was to make the calculated MH slightly larger (red line with limit appears overnight above blue line without limit). Similar minor changes observed in Cases 1 & 2 when the limit was applied are not plotted here.

Finally, the results from Cases 1–3 were compared directly using the scatter plot Figure 7.33. Here the transition Case 3 is plotted horizontally and serves as our reference data for comparison purposes. The uniform Cases 1 and 2 were plotted vertically. All the data points for 01–31 July 2003 are drawn in Figure 7.33 and the best fit lines through the origin show the all 'rural' results (green) are ∼10% smaller, whilst the all 'urban' results (pink) were ∼ 56% greater, than the rural-urban transition Case. This is the kind of shift in magnitude that merits field investigation.

In conclusion, the greatest sensitivity seen here was that an increased z_0 at the anemometer site is to make the urban mixing height much larger, and care should be taken to ensure that a proper roughness is used for the site where meteorological data are observed. A modest increase in the shallow overnight MH was produced when L was constrained to prevent it being diagnosed as very stable. These sensitivities merit further field investigation.

7.5. The mixing height derived from other remote sensing devices

7.5.1. Comparison between ceilometer and radiosonde data

First results of the radiosonde–ceilometer comparison from Helsinki (Section 5.6) show that under clear sky conditions the MHs determined from ceilometer based aerosol profiles, utilising a slightly modified method of Steyn *et al.* (1999) and CBL-height estimates based on radiosounding data (with the Holzworth

method) are in quite good agreement. The analysis included *ca.* 60 convective cases obtained during 2002. The rejected cases in Figs. 7.34 corresponded to very low aerosol concentrations in the mixed layer that led to a very weak aerosol backscatter signal in the lowest layer. Similar analysis for stable conditions has been conducted. The number of cases during 2002, where the ceilometer is able to determine the stable mixing height is quite limited due to frequent cloudy conditions.
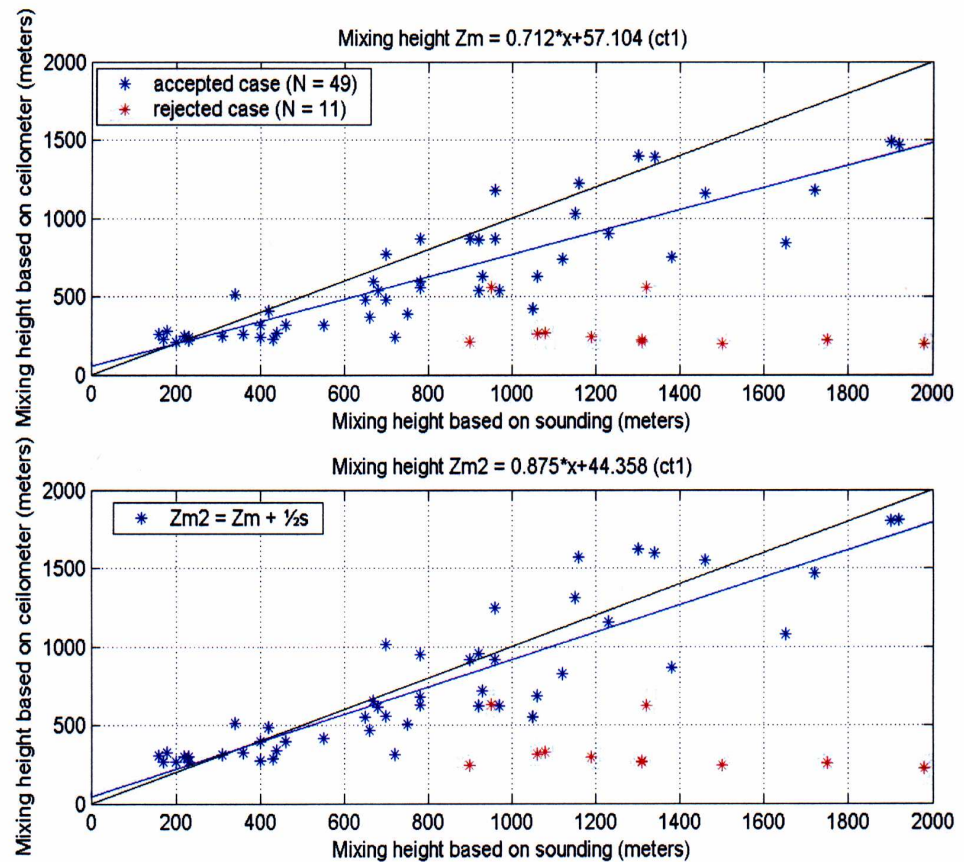
*Figure 7.34: Comparison of MHs estimated from radiosoundings and ceilometer aerosol profiles in Helsinki, 2002. a) ceilometer based mixing height Zm defined as the height of the midpoint of the entrainment layer, b) ceilometer based mixing height $Zm2$ defined as the height of the top of the entrainment zone (s is the depth of the entrainment zone).*

Thus, the ceilometer can be a useful instrument for determining the MH but,

again, it cannot be used automically without a careful assessment of the prevailing conditions (clouds, surface backscattering, initial guess), which otherwise could lead to spurious values.

7.5.2. Comparison between UHF profiler and RASS data

Observations of the ABL vertical structure over the ESCOMPTE regional area (see Section 5.2) included data from 7 sodars, 7 radars and 5 lidars, among which 3, 1 and 2 (sometimes 3), respectively, were within the Marseille urban area. The data analyses combine these observations, with those from the airplanes, keeping coherence with the SEB measurements within and outside of the city. Since the first efforts concentrate on the comparison of observations with the various types of sensor (Fig. 7.35) and on validating methods to combine them in order to obtain 3-D fields and evaluate spatial divergences, the first analyses are still very preliminary. Observations show the sometimes contradictory influences of several different factors: synoptic flow regime (especially the northerly Mistral wind), sea breeze systems at both local and regional scales, topography, and the urban canopy/surfaces. In such a geographical situation, the urban influence was never observed in isolation.

The direct comparison of the sea breeze systems over the urban and non-urban areas shows that: (1) the local city breeze is easily smeared out by a larger scale breeze system that develops at the daytime scale and, (2) that the influence of the city on the MH is complex, with sometimes some periodic UBL growth – destruction cycles within the day, with a period of about 1.5 hours; this is probably linked to both the large urban sensible heat flux and also to the large share of the energy balance that is diverted to the canopy heat storage during the first half of the day.

Elevated stratified layers were also observed to persist during some nights over the urban area. Also, observation of relatively homogeneous ozone concentrations in the lowest layer at night may indicate a weakly stable low level stratification or even an unstable layer due to the weak but positive nocturnal sensible heat flux in the city.
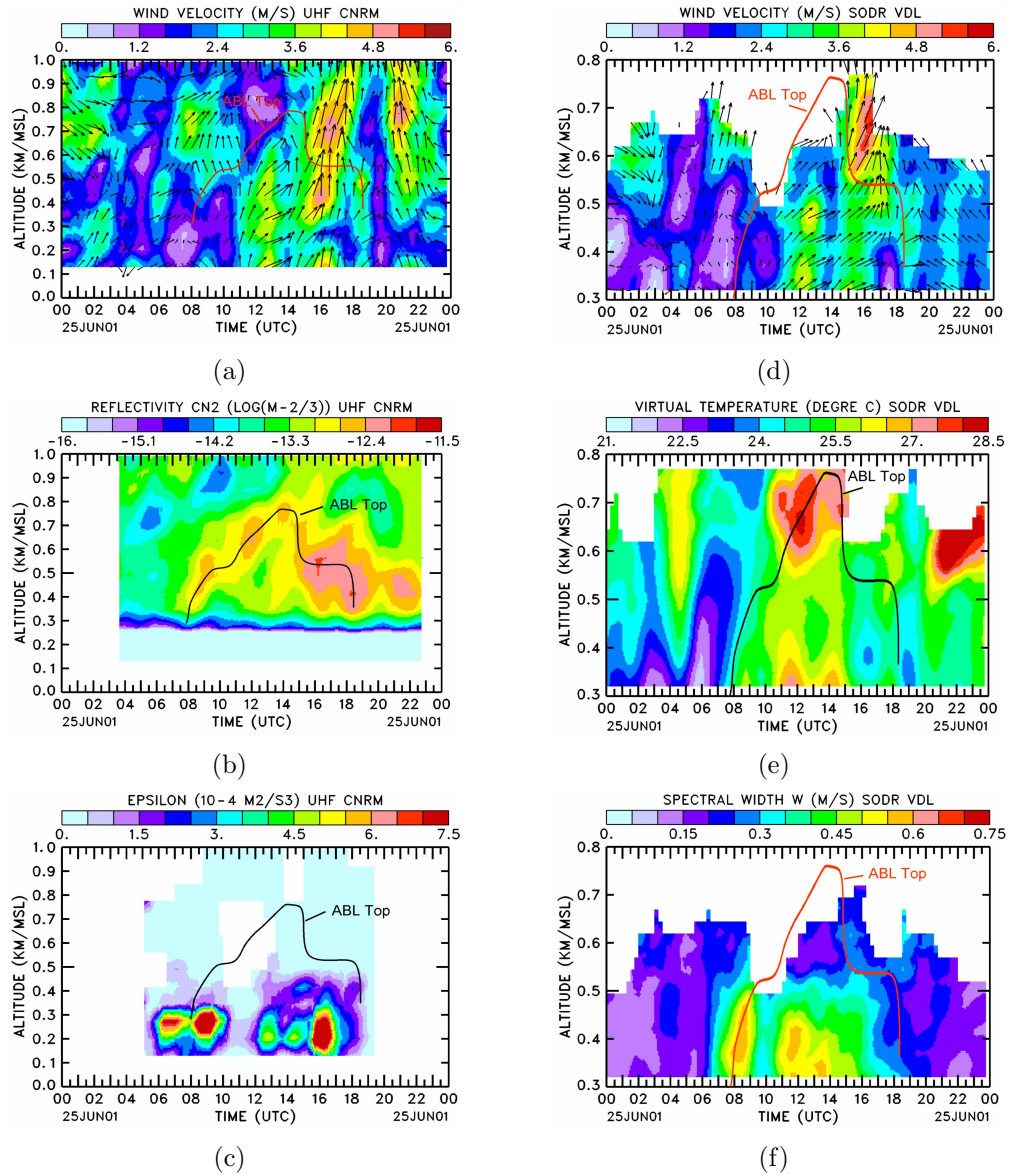
Figure 7.35: Time-height sections of UHF profiler at the Observatoire (left) and sodar-RASS at Vallon Dol (right): (a, d) Horizontal wind velocity (b), C_n^2 reflectivity, (e) virtual temperature, (c) dissipation rate of turbulent kinetic energy ε, and (f) sodar Doppler spectral width. The superimposed line is the top of the ABL as deduced from the maximum UHF reflectivity.

7.6. The mixing height deduced from tracer gas concentrations

7.6.1. Radon concentrations and meteorological elements

Tracer gas concentrations in the atmosphere have been used to estimate quantities such as turbulent diffusivity and the mixing height (Section 4.2.4). The influence of meteorological conditions on the variability of radon concentration in the soil gas was investigated in Katowice by Osrodska *et al.* (2002). They found that radon concentrations in the lower atmosphere could be empirically related to meteorological factors such as: air temperature, wind speed and total rainfall, integrated into a specific index IM. In some cases, however, estimated ^{222}Rn radon concentrations were systematically higher than observed radon values due to the influence of other meteorological factors not included in the index IM, e.g., in situations influencing the physical properties of the ground such as snow cover or a frozen soil. Therefore, the above mentioned regression relationship cannot be applied during winter periods (Osrodka *et al.*, 2003).

7.6.2 Polonium and the mixing layer.

In another study, the dependence of polonium ^{218}Po activity on the vertical thermal stratification shows up in the increased accumulation during nocturnal inversion and decreases when the atmosphere becomes unstable. During the period 2001-2002, several measurements of alpha radiation emitted in the radioactive transformation of ^{222}Rn into ^{218}Po in air were performed during the warm season (May-August) in Cracow and Katowice. Some of these polonium concentration measurements were performed during field campaigns realised in the framework of COST-715. Days with well determined daily profiles of the mixing layer (hot season and sunny weather) were identified by the index IM (see previous Section).

The analysis of polonium concentrations and MHs yielded a clear anti-correlation (r between 0.69–0.83 for Katowice and 0.42–0.73 for Cracow at the confidence level $p = 0.05$) but depending on meteorological conditions and associated radon concentration in the soil gas (Fig. 7.36).
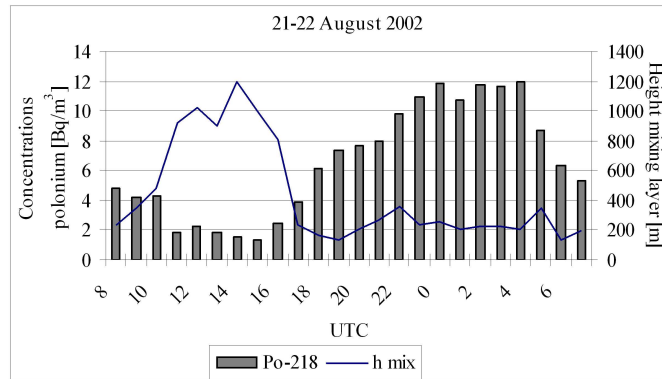
Figure 7.36: Relationship between polonium ^{218}Po concentrations and the mixing height in Cracow (21–22.08.2002).
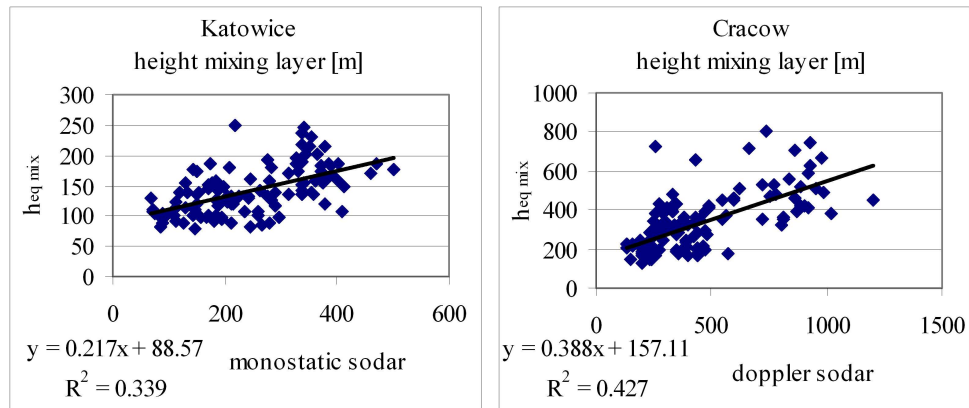
Figure 7.37: Comparison between the mixing layer height ($h_{eq_{mix}}$) calculated using Eq. (4.6) and observed by a monostatic sodar (Katowice) and a Doppler sodar (Cracow).

Applying the empirical power law (Equation 4.6) to these measurements yielded a statistically significant relationship (at $p = 0.05$) between polonium concentration (C_{Po}) in air and an "equivalent mixing layer height" ($h_{eq_{mix}}$) with the following empirical coefficient $B = 206.6$ for Katowice and 565.0 for Cracow.

This coefficient depends on specific local features of the radon release and meteorology. The results from Katowice and Cracow (Fig. 7.37) show a weak dependence with considerable scatter. Nevertheless, this method needs to be improved and verified against measurements in other cities. Radon emissions depend on many factors, e.g., strongly depending on precipitation and soil moisture. Therefore, it is unlikely that any simple dependence between Po concentration and the MH can be universal and useful. The large difference between values of B for Katowice (206.6) and Cracow (565.0) illustrates the uncertainties embedded in the method.

8. Satellite remote sensing to estimate surface fluxes and canopy characteristics

8.1. Challenges and possibilities

As discussed elsewhere in this report, the correct specification of the urban surface energy balance is of paramount importance in the context of urban atmospheric dispersion studies. Whereas most approaches to estimate the components of the surface energy balance are based on modelling, satellite-based measurements present a potentially interesting source, either for directly estimating heat fluxes, or for estimating land surface characteristics that can serve as input or validation variable in models.

Remote sensing of urban surfaces has gained considerable attention in recent years, as shown e.g. by some Special Issues in leading remote-sensing journals entirely devoted to this topic (Carlson, 2003; Gamba *et al.*, 2003). However, while quite some efforts have been concentrated on the improved characterisation of cities in the context of spatial planning and urban growth monitoring, very little research has been conducted on estimating urban heat fluxes from space. This is not surprising, as urban surfaces present particular difficulties when it comes to extracting useful and accurate information from the satellite signal.

In the remainder of this Chapter, an overview is given of methods for the determination of the urban surface energy balance from space. Section 8.2 gives an overview of satellite platforms and instruments with any potential in sensing the surface energy balance of cities. In Section 8.3, a brief description is given of direct methods to infer surface heat fluxes from remotely sensed surface temperature, emphasising difficulties related to the urban environment. Section 8.4 deals with satellite-based methods to retrieve land surface parameters for use in models. Finally, Section 8.5 describes a new instrument that claims to provide estimates of the MH, after which this Chapter is closed with an outlook on future developments.

8.2. Satellite remote sensing platforms and instruments

Earth observation instruments onboard satellite platforms come in different categories. Main characteristics are the instrument's spatial resolution, its tem-

poral sampling scheme, and the wave-bands in which the measurements are performed. Table 8.1 lists a few platforms and instruments that are relevant in the context of measuring the urban energy balance from space. All instruments in the list are carried on polar orbiting satellites, i.e., they circle the globe in a plane that is almost (but not entirely) perpendicular to the Earth's equatorial plane, most of them at an altitude of 700 to 800 km. The only exception is the Meteosat Second Generation (MSG) geostationary platform, located at an altitude of approximately 36000 km over a fixed spot in the frame of the rotating Earth. A detailed account of satellite orbits and instruments can be found in Kidder and Vonder Haar (1995).

Table 8.1: Overview of current satellite instruments. The "wavebands" column uses the following abbreviations: VIS=visible, PAN=Panchromatic, RED=red, NIR=near-infrared, TIR=thermal infrared.

Platform-instrument	Spatial resolution	Temporal resolution	Wave bands
NOAA-AVHRR	1 km	1 day	RED/NIR, TIR
Meteosat MSG-SEVIRI	1–3 km	15 min	RED/NIR, TIR
SPOT – VEGETATION	1.15–1.7 km	1 day	RED/NIR
SPOT 4 – HRVIR	20 m	26 days	RED/NIR
	10 m		PAN
SPOT 5 – HRG	10 m	26 days	RED/NIR
	2.5–5 m		PAN
HRS	10 m		VIS stereo
EOS-MODIS	250 m–1 km	1–3 days	RED/NIR, TIR
ENVISAT-MERIS	300 m	1–3 days	RED/NIR
DMSP-OLS	1 km	1 day	VIS
Landsat-ETM+	30-60 m	16 days	RED/NIR, TIR
IKONOS	4 m (2 m)	programmed	RED/NIR
(IKONOS-3)	1 m (0.5 m)		PAN
PLEIADES – HR (2006-09)	70–80 cm	26 days (5 days progr.)	PAN, RED/NIR
Quickbird	2.5 m	programmed	RED/NIR
	61 cm		PAN

The wavebands in the rightmost column of Table 8.1 are only those that are considered useful in the context of urban surface energy balance measurements. Some of the instruments have more wave bands than those mentioned, e.g.,MSG

possesses twelve channels in the visible, mid- and thermal infrared portions of the spectrum. For some of the sensors mentioned in Table 8.1, the spatial resolution is the one that applies to multi-spectral imagery. Certain instruments (Landsat, Spot, Ikonos, Quickbird) achieve spatial resolutions that are higher by about a factor of four in panchromatic mode, which is a broadband channel that covers most of the visible radiation. This higher resolution comes at the cost of the loss of spectral information.

Due to the relatively small scale of cities, one would be inclined to systematically use high-resolution imagery. However, as can be seen in table 8.1, this implies a low return frequency. As an example, imagery of the Landsat-7 instrument has a spatial resolution ranging between 15 m (panchromatic) and 60 m (thermal), but returns to the same spot on Earth only every 16 days. Accounting for cloudiness, mid-latitude areas can count on a few cloud-free images per year at best.

Whereas instrument accuracy of satellite sensors is generally more than adequate for Earth observation applications, most of the error on the geophysically relevant signal results from interference with the atmosphere, such as absorption by water vapour and scattering by aerosols. Taking that into account, typical errors on satellite-based surface temperature are of the order of a few degrees K, and the relative error on surface reflectance is roughly estimated to be of the order of 20 %.

A useful quantity in the general context of the land surface energy balance is the Normalised Difference Vegetation Index (NDVI), defined as

$$NDVI = \frac{R_{NIR} - R_{RED}}{R_{NIR} + R_{RED}}. \tag{8.1}$$

R_{NIR} and R_{RED} denote the surface reflectance in the near infrared and red portions of the electromagnetic spectrum, respectively. The $NDVI$ exploits the fact that green vegetation exhibits a much larger reflectivity in the NIR as compared to the RED band, yielding high values, whereas bare soil or urban surfaces exhibit much lower values. Although the reflectances themselves exhibit variability with viewing angle, the $NDVI$ is much less sensitive to such effects because it is a ratio. Though the $NDVI$ is a good indicator of the vegetation presence and activity, which may be used for mapping the land uses but also for determining such parameters as the average roughness length, as an expression such as Gupta *et al.*'s (2002) correlation:

$$z_0 = \exp(-5.5 + 5.8 NDVI) \tag{8.2}$$

yields very low roughness lengths (order cm), which is clearly not representative of cities. This formula may be representative for natural surfaces, but not at all for cities. It must be noted that for determining vegetation occupancy, a large number of other vegetation indices have been proposed, such as the Soil-Adjusted Vegetation Index (SAVI) designed to minimize the effect of the soil background.

8.3. Remote sensing of the surface sensible heat flux

An extensive body of literature on the subject of inferring components of the surface energy balance from space exists (Sellers *et al.*, 1990; Choudhury, 1991; Eymard and Taconet, 1995; Greenland, 1994; Diak *et al.*, 2004). However, most research in this field deals exclusively with rural or natural surfaces, the focus being on methods to infer evapo-transpiration for purposes of agricultural or ecosystems management.

It is only in recent years that thermal remote sensing has been employed in the context of the urban surface energy balance. Zhang *et al.* (1998) used Landsat Thematic Mapper (TM) data in conjunction with routine meteorological data and a bulk transfer approach to infer patterns of sensible and latent heat fluxes over the city of Osaka. A bulk transfer equation was also employed by Voogt and Grimmond (2000), using remotely sensed surface temperature from airborne and ground-based observing platforms, and obtaining valuable information on the ratio z_{0t}/z_0 (see Section 3.4) in the process. Yang (2000) used a 1-D model of the atmospheric boundary layer together with remotely sensed surface temperature from the AVHRR instrument onboard the NOAA-11 platform to infer the energy balance components, employing the method developed by Carlson *et al.* (1981). Hafner and Kidder (1999) used a similar approach on the city of Atlanta, though using a full 3-D mesoscale meteorological model instead, in order to account for horizontal heterogeneity of the atmosphere. More details regarding the use of remote sensing for obtaining information on the urban surface energy balance is provided in a recent review paper by Voogt and Oke (2003).

The most relevant component of the urban surface energy balance is the sensible heat flux. The most straightforward method to obtain the sensible heat flux Q_H at the surface-atmosphere interface consists of the implementation of MOST-based bulk formula (3.7) defined in Section 3.2.5:

$$(Q_H/\rho c_p) = (T_0 - T_a)/(r_a + r_b) \tag{3.7}$$

where the aerodynamic and laminar "resistances" are defined by Eq. (3.8). In principle, the sensible heat flux can be calculated with Eq. (3.7), using remotely sensed surface temperature together with ground-based measurements of temperature and wind speed, and supplying values for both roughness lengths used in Eq. (3.8). Unfortunately, applying the approach described above is problematic, especially for cities. Indeed, Eq. (3.7) is potentially prone to large errors, stemming mainly from errors on the input parameters required in this equation.

To start, satellite-retrieved surface temperatures carry errors due to atmospheric absorption and surface emissivity. Even after applying corrections for these effects, the remaining error is of the order of a few degrees (Vázquez *et al.*, 1997). A related difficulty is that T_0 is a rather ambiguous quantity. In Eq. (3.7), it represents the *aerodynamic* temperature, i.e., in principle the temperature of the first air molecules immediately above the surface, or more pragmatically the temperature value that yields the correct heat flux when using (3.7). However, the *radiative* temperature as observed from space may be quite different, and also depends on satellite view angle or solar position, which is clearly undesirable as these are not properties of the surface but rather of the "experimental set-up". Owing to their strong heterogeneity, cities suffer more from this problem than most natural surfaces: in particular the "surface" is not unambiguously defined. Roth *et al.* (1989) stress the difference between the "active" urban surface, which includes horizontal and vertical solid surfaces exchanging heat with the atmosphere, and the "satellite-sensed" surface that tends to over-emphasize the role of roofs and tree tops, while in meso-scale atmospheric models the "surface" may be a roughly horizontal immaterial surface above the canopy. In addition, in the urban canopy the coupling between surface temperature (controlled by the surface energy balance) and air temperature, say at mean roof level or above the roughness sub-layer, (dependent upon the flux divergence in and above the air canopy volume) is far from simple, as seen above, due to the surface folded shape and to micro-scale advection.

Another problem is related to incomplete knowledge of the appropriate surface layer values of U_a and T_a, both required in Eq. (3.7). Often, one has to rely on measurements of these quantities from routine meteorological observations from a nearby station. However, owing to the large spatial heterogeneity typical of the urban environment, an error of several degrees is to be expected on T_a, and a

relative error of up to several tens of percent on U_a. Especially this last error will induce an error of a similar magnitude on the heat flux. An additional problem is caused by the fact that wind and temperature measurements required for Eq. (3.7) are often carried out within the roughness sub-layer or in sheltered locations, thus invalidating similarity theory altogether.
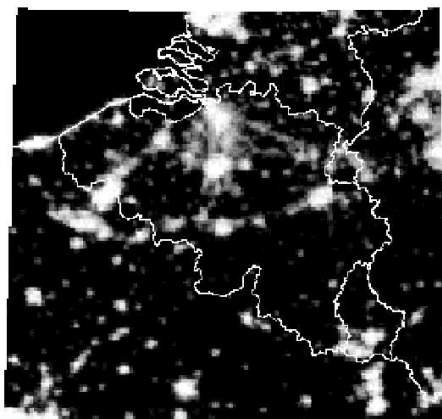
Figure 8.1: City lights of Belgium observed with the OLS instrument onboard the DMSP platform.

Finally, the most serious problem resides in the insufficient knowledge of the laminar resistance r_b. Indeed, very limited information is available on the ratio z_0/z_{0t} which, for cities, is expected to be significantly larger than for homogenous vegetated surfaces. Studies are starting to emerge in which estimates for this ratio are provided and that yield encouraging results (see Sections 3.2.5 and 3.4 and Voogt and Grimmond, 2000), but more research is required.

Alternative T_s-based retrieval techniques exist, some of them combined with the NDVI, and others making use of temporal changes of surface temperature, which is available from geostationary satellites. Even though the latter's horizontal resolution is too coarse to be of use in urban applications, there exist spatial disaggregation techniques that combine information from geostationary platforms with high- or medium-resolution imagery such as from, e.g., Landsat or MODIS instruments. A recent review of these and other methods is provided by Diak *et al.* (2004).

Finally, we should mention an instrument with some potential in retrieving the anthropogenic heat flux, i.e., the Operational Line Scan (OLS) instrument onboard platforms of the Defense Meteorological Satellite Program (DMSP).

Employing a very sensitive sensor, it is capable of observing night-time city lights (Fig. 8.1), and there are reports of relations between OLS-based measurements and energy consumption (Elvidge *et al.*, 1997).

8.4. Remote sensing of surface parameters

As shown in the previous Sections, the direct retrieval of the sensible heat flux over urban surfaces is problematic for a variety of reasons. An alternative way of obtaining the components of the urban surface energy balance consists of modelling. Here, satellite remote sensing can contribute significantly, as it offers the possibility of retrieving land surface parameters that have a crucial impact on the energy balance. In the remainder of this Section it will be described how remote sensing from space can contribute to modelling the energy balance in a mesoscale meteorological model operating at urban to regional scales. A review on retrieving land surface parameters from space is provided by Hall *et al.* (1995), though the focus there is on rural and natural surfaces.

Note that certain surface parameters can be obtained from land-use maps. A good example is the CORINE map, covering Europe and containing 44 land-use categories that can be associated with certain surface parameters, essentially those that do not change much over time (albedo, emissivity, roughness length). (Note that the CORINE map itself has been established largely based on high-resolution satellite imagery.)

Among the parameters that change over time, green vegetation abundance (or green vegetation cover fraction) is important. This quantity can be estimated from a vegetation index such as the NDVI (defined above). Green vegetation cover relates well to the NDVI, and most often a simple linear relationship is assumed (Wittich and Hansing, 1995; Gutman and Ignatov, 1998). Figure 8.2 shows an application of the use of NDVI imagery (from the SPOT-VEGETATION instrument, see Table 8.1) to retrieve green vegetation fractional cover, subsequently employed as input to a land surface scheme embedded in a mesoscale meteorological model performing simulations for the Paris area. In order to demonstrate the usefulness of remote sensing imagery in an atmospheric model, a brief description is given of a one day simulation over Paris. In this simulation, satellite data were used not only for the specification of surface characteristics, but also for a model validation exercise in which simulated and remotely sensed surface temperatures were compared.

A simulation at one kilometre resolution was performed for the larger area of Paris on a 100×100 km^2 domain (Fig. 8.2) with the meteorological model ARPS including the new urbanised land surface module described in Section 3.2.5. The day chosen was 15 May 1998, because of the clear skies occurring over the study area that day, thus allowing the retrieval of surface temperature from space, which is part of the validation exercise as explained below. The synoptic weather conditions were accounted for by nesting the simulation domain in output from the European Centre for Medium-Range Weather Forecasting (ECMWF) operational model, using intermediate domains with spatial resolutions of 20 and 5 km, respectively, to bridge the gap with the ECMWF data available on a 0.5° grid. Terrain data were obtained from various sources and interpolated to the model grid. Orography was taken from the EDC Digital Elevation Model (`http://edcdaac.usgs.gov/gtopo30/gtopo30.html`) at 30 arc-second resolution, and land use type was derived from CORINE digital raster maps at 250 m (Heymann *et al.*, 1994). Vegetation cover fraction was derived from 1-km imagery generated by the VEGETATION instrument (`http://www.vgt.vito.be`) onboard the SPOT satellite platform, making use of the Normalised Difference Vegetation Index (NDVI) as described above.

The simulated surface temperature was compared to thermal imagery from the Advanced Very High Resolution Radiometer (AVHRR) imagery onboard the NOAA-14 platform, obtained from the Deutschen Zentrum für Luft- und Raumfahrt (DLR; data available through: `http://isis.dlr.de`). The result is shown in Fig. 8.3, using the DLR's Land Surface Temperature (LST) product, which is corrected for atmospheric and surface emissivity effects. Even though there are differences between simulation and observation, the overall extent and magnitude of the urban-induced temperature anomaly is well reproduced. More importantly, the urban-rural temperature difference is rather well captured by the model.
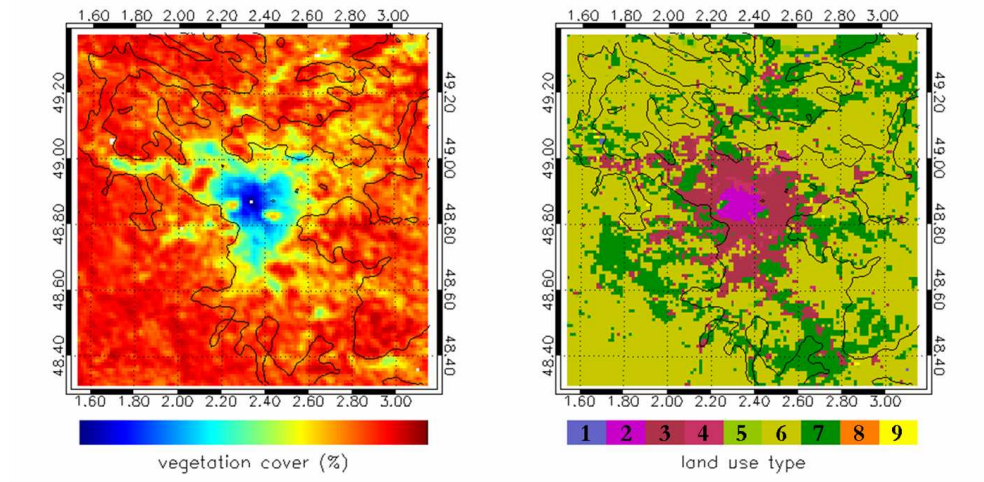
Figure 8.2: Paris simulation domain. The left panel shows green vegetation cover, and the right panel land use type. The numbers in the land use type legend respectively correspond to water (1), continuous urban (2), discontinuous urban (3), industrial (4), pasture (5), crops (6), forest (7), snow (8), and shrubs (9).
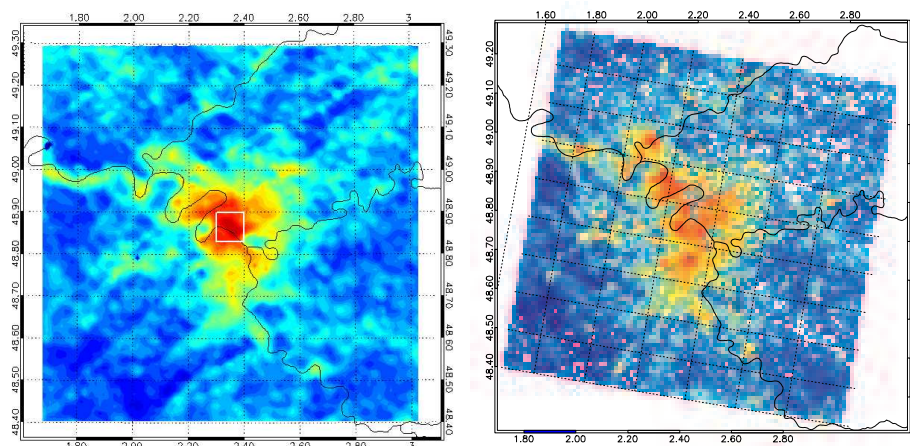
Figure 8.3: Simulated (left panel) and remotely sensed (right panel) land surface temperatures for the Paris area at 14:00 GMT on 15 May 1998. The colour code ranges from 298 K (dark blue) to 318 K (dark red). The white frame in the left panel indicates the location for which the energy balance model is evaluated (see Section 6.2.4). The white grid cells in the satellite image correspond to missing values. Note that the satellite image has to be rotated slightly anti-clockwise to match the simulation domain.

8.5. Remote sensing of the mixing height

The Geoscience Laser Altimeter System (GLAS) instrument on the Ice, Cloud, and land Elevation Satellite (ICESat, launched on 12 January 2003) provides estimates of the so-called planetary boundary layer (PBL) height along global measurements of polar ice sheet elevation and roughness, cloud and atmospheric properties, land topography, vegetation canopy heights, ocean surface topography, and surface reflectivity (Zwally *et al.*, 2003; `http://nsidc.org/data/gla08.html`). GLAS has a 1064 nm laser channel for surface altimetry and dense cloud heights, and a 532 nm lidar channel for the vertical distribution of clouds and aerosols (top and bottom heights of elevated aerosols from -1.5 km to 20.5 km at 4 sec sampling rate, and from 20.5 km to 41 km at 20 sec sampling rate). The PBL height is determined at a 4 sec sampling rate from the 532 nm channel only. The PBL height is the lowest layer that can be resolved with the ground as its bottom. Thus, one can assume the equivalence between the estimated PBL height and the mixing height discussed in this report. In the GLAS procedure, the MH thickness (top minus ground height) cannot exceed 6 km. If the layer top is greater than 6 km above the local ground height, it is not identified as the MH top. The MH top is first searched by using a 4 sec average profile. If the top is found at that resolution, then the MH top is located from each of the 20 (5 Hz) shots that make up that 4 sec period.

Each MH top retrieval is given a confidence rating similar to the elevated aerosol layer flag. The values run from "1" (lowest) to "13" (highest) confidence of a good MH height retrieval. The MH quality flag is computed from the ratio of the average signal (attenuated, calibrated backscatter) within the MH to the average signal 500 m above the MH. Normally, the backscatter increases significantly at the top of the MH and remains higher within the MH unless it is attenuated by a cloud, extremely dense dust, or smoke; thus, the quality flag is proportional to the magnitude of the gradient of scattering at the MH top. The larger this gradient, the easier it is to find the MH top and hence the higher confidence in its detection.

However, these measurements still require a dedicated and specific validation against various ground-based estimates of the MH.

8.6 Future developments and requirements to use the full potential of satellite imagery

As outlined above, the direct approach based on the bulk transfer equations using remotely sensed surface temperature in conjunction with routine meteorological data is prone to large errors, and may not be the ideal way of inferring surface fluxes over cities except under very controlled circumstances, e.g., identifying the source area for sensible heat flux as was done by Voogt and Grimmond (2000). Another problem associated with the bulk-transfer method is that it is only applicable under clear-sky conditions, hence seriously limiting the temporal continuity of any such scheme, at best delivering sporadic results.

A more promising approach for routine applications is based on the combination of atmospheric modelling and remote sensing of relevant urban surface parameters. These parameters include vegetation fraction cover, soil moisture, albedo, temperature roughness, and the soil's heat capacity and thermal conductivity – the latter two possibly combined as the thermal admittance. Satellite measurements of these parameters are also limited to cloud-free viewing conditions, but as most of the parameters do not change rapidly over time that does not pose a large problem. (An exception is perhaps soil moisture, but other – microwave based – sensors are more appropriate to retrieve this quantity as clouds become transparant at wavelengths in the microwave range.)

Some recently launched satellite instruments already have the potential of improving estimates of certain of these parameters. The MODIS and MERIS instruments, both with a spatial resolution (pixel size) of the order of a few hundred metres, will yield NDVI maps with a higher resolution than what can be obtained from the AVHRR and VEGETATION instruments, both with a resolution of the order of a kilometre. The main result of the improved spatial resolution is that cities are better defined, especially at their edges. Indeed, owing to the positional inaccuracy of satellite pixels – of the order of one to a few pixels – imagery composed of, say, 300-m pixels, will yield an 'effective' image resolution of the order of a kilometre.

Another recent instrument with a potential in urban surface climate applications is the SEVIRI instrument onboard the Meteosat Second Generation (MSG) platform. Its main advantage is the high temporal sampling frequency of one image every 15 minutes that allows constructing the diurnal surface temperature cycle with great detail. Whereas Meteosat platforms have been in use

for decades, the MSG platforms is the first to carry an instrument with a spatial resolution in the thermal infrared of around 3 km, compared to 8 km for the older instruments. Obviously, this increase of resolution is quite relevant for most cities. Time series of MSG imagery could be used in schemes that follow the philosophy of Carlson *et al.* (1981), with the advantage of disposing of almost a hundred samples (images) per day, compared to a few samples when using imagery from AVHRR imagery at different overfly times (see, e.g., Hafner and Kidder, 1999). As a result of this dense sampling, the amplitude and phase of the diurnal cycle are much better represented, which should yield better estimates of, e.g., thermal admittance. Another advantage of MSG imagery is that one can use the diurnal amplitude of the surface temperature rather than the latter's absolute value. Errors related to surface emissivity or atmospheric transmissivity then disappear or are very strongly reduced. However, it is not possible to get rid of the angular dependence of the retrieved surface temperature. This angular dependence, which is caused by the solar-versus-viewing geometry, may give rise to an error of several degrees Celsius. Currently, studies are being carried out to correct for such angular effects (Lagouarde *et al.*, 2004).

One of the main difficulties one is confronted with when retrieving the surface energy balance of a city from space is the lack of appropriate ground truth to (in-)validate a given approach. Owing to cities' strong spatial heterogeneity, it is difficult or even impossible to compare ground-based measurements – which are necessarily representative of relatively small areas – with satellite-based measurements containing pixels covering areas of the order of about one to ten square kilometres.

9. Conclusions and recommendations

9.1. General remarks

The underpinning purpose of the COST-715 Action (*"Meteorology Applied to Urban Air Pollution Problems"*) was to review, assess and contribute to the development of methods for providing this meteorological information specifically for urban pollution dispersion and transport models. The urban situation is a major issue as pollution levels are generally highest in urban areas where the vast majority of European citizens live (ca. 70%). The critical meteorological challenges as to routine observations, modelling and pre-processing methods should be tested against a new generation of dedicated measurements. Besides, long-term monitoring data can be used to raise awareness of decision-makers in order to define and assess protection measures (e.g., legislative, technical, social). One of the main benefits of meso-scale models is that they enable predictions of air pollution episodes to be made. Urban meso-scale models also enable a better scientific interpretation of observational data due to their higher resolution and their more comprehensive physics.

Another related incentive for COST-715 was the expressed or potential requirements of pollution protection agencies in European countries to be able to forecast and explain why high pollution levels have occurred on a specific day. Although a pollution episode is expressed in terms of chemical concentrations exceeding a specific threshold value, predicting and describing the meteorological situation before, during and after the episode is crucial to the interpretation. The full report of COST-715 (2004) addresses the various issues of science, applications and data of urban meteorology for air pollution applications.

This report from Working Group 2 of the COST Action 715 should be considered a working document on a newly stimulated field of research. The breadth of issues is considerable. Hence it represents work in progress in various European countries and contains some repetition. On the other hand, this report does not aim at being exhaustive but at synthesising previous and ongoing works by the authors and some cooperating colleagues. Besides, more information, results and analyses are available in the proceedings of the 3 workshops convened by Working Group 2 (see Section 1).

Nevertheless, this work contributed to the coordination and tasks sharing between the involved research groups as the COST framework is very suitable

for European coordination and harmonization and as an exploratorium of actions for new and emerging problems. This Action brought together several groups that had no previous cooperation and thus generated new synergies between various expertises. There was not much relevant high-quality data before this Action so that its launching was timely as model resolution and physical parameterisation were improving. Furthermore, COST-715 stimulated several major field campaigns in European cities (Basel, Marseille, Bologna, Birmingham, Cracow) and an EU-funded project for developing urban air quality information and forecasting systems (FUMAPEX).

The following Sections summarise the scientific conclusions of this work (for the surface energy balance based on an analysis in Piringer et al., 2002) including the identification of gaps in our knowledge, make some recommendations as to further work, data collection and field experiments, and try to assess the limitations of current modelling tools in the scope of air quality applications in urban areas. These conclusions are destined to both the scientific community and other end-users of scientific knowledge and data dealing with urban meteorology and air pollution (e.g., city managers and planners, environmental authorities, engineering consultants).

9.2 Improvement of existing pre-processors, schemes and models for the surface energy budget

Available observations of urban heat fluxes demonstrate significant perturbation of surface energy balance partitioning compared to the rural surroundings. Thus, this will imply specific parameterisation schemes and models to properly estimate the surface energy budget under urban conditions.

9.2.1. Understanding of physical processes

The most distinguishing features of the urban surface energy budget are the generally (but not always) higher Bowen ratio and the anthropogenic heat flux. Regarding parameters that characterise urban surfaces, the uncertainties on the surface temperature (that affects emissivity) and the high ratio z_0/z_{0t} stand out as typical. The following aspects still deserve further work.

- Understanding the behaviour of vertical turbulent flux profiles in the

roughness sub-layer, due to high roughness elements requires more study, both in the field and with models.

- The influence of the breakdown of the MOST (Monin-Obukhov Similarity Theory) assumptions due to horizontal and vertical flux divergences generated by urban heterogeneity in roughness and thermodynamic properties requires further assessment study.

- The applicability of the concept of effective roughness length and other surface parameters for aggregation of surface fluxes should be developed further and tested for urban areas with adequate experimental data. The use of satellite-based remote sensing for these latter should be further investigated.

- It appears extremely important to assess separately the aerodynamic roughness length, z_0, and the scalar roughness lengths for temperature, z_{0t}, and for moisture, z_{0q}, in city-scale models.

- There is a hysteresis in the diurnal cycles, with phase lags between the SEB components due to heat being diverted from the budget and provisionally stored in the building materials during daytime at the expenses of the sensible heat, while the stored heat is released in the evening and at night.

- The state of rural soil moisture, and therefore soil thermal admittance is a very important determinant of city heat island effects; the state of the surrounding countryside therefore must be considered in any such studies.

- Horizontal inhomogeneity of the canopy means that the diffusivities for heat and water vapour differ, (i.e., $K_E \neq K_H$). This is because while all surfaces are sources of sensible heat, not all urban surfaces are sources of water vapour (Roth and Oke, 1995).

9.2.2. Implementing improved knowledge: modelling tools and regulatory applications

For applications in connection with dispersion modelling, often no detailed surface exchange parameterisation can (computationally) be afforded. As an alternative, a meteorological pre-processor that has been modified for urban surfaces (LUMPS, Section 3.2.1) is available. Turbulent fluxes (and hence stability) obtained from this scheme apply to heights sufficiently far from the urban fabric.

A detailed validation, especially using data from European cities, would complement already existing North American studies and is much encouraged.

- A number of European groups run meso-scale models with sub-models of fluxes for urban areas. These models are not operational yet, but advances are encouraging. Preliminary simulations indicate that the influence of the urban canopy, building energy flows and thermal properties, along with effective albedo reduction by radiative trapping between canyon walls is important and needs to be explicitly modelled.

- Existing operational NWP models are undergoing strong increase in their spatial resolution so that they start to be able to distinguish certain urban features. However, their sub-surface, surface, and boundary layer formulations are still similar for urban and rural areas. Thus, dedicated efforts to bridge this gap should be undertaken with accompanying verification against appropriate data.

- Nevertheless, NWP models are not primarily developed for air pollution modelling. A revision of conventional methods to transform their outputs to be suitable inputs for urban and mesoscale air quality models is required in the framework of Urban Air Quality Information and Forecast Systems (UAQIFS). Such developments will also provide information to city managers regarding other emergency or stressing issues (e.g., urban runoff and flooding, icing and snow accumulation, high urban winds or gusts, heat or cold stress, accidental toxic emissions, potential terrorist actions).

9.3. Improvement of existing pre-processors, schemes and models for the mixing height

Useful background information has been provided by the COST-710 Action (COST-710, 1998; Seibert *et al.*, 2000). However, WG2 of COST-715 aimed at a more specific assessment of the MH for urban areas, especially taking into consideration the particular surface turbulent transfers, horizontal non-homogeneity and the vertical structure of the boundary layer over urban areas.

9.3.1. Understanding of physical processes

The urban boundary layer (UBL), in comparison with 'rural' homogeneous ABLs, is characterised by greatly enhanced mixing, resulting from both the large surface roughness and increased surface heating, and by horizontal non-homogeneity of the MH and other meteorological fields due to variations in surface roughness and heating from rural to central city areas. So, it is reasonable to consider the UBL as a specific case of the ABL over a non-homogeneous terrain. This relates, first of all, to abrupt changes of the surface roughness and the urban surface heat fluxes.

- Specific methods for MH determination in urban areas can be distinguished in two categories: (i) with a local correction of the heat fluxes due to urban effects (more appropriate for large cities), and (ii) with estimations of the internal boundary layer (IBL) height growth (more relevant for small cities and transition zones).

- When modelling the MH, the mechanisms involved in the formation of the daytime MH are better understood than the corresponding ones at night-time. It is therefore strongly recommended that more emphasis should be given to improving the methods for the night-time MH determination.

- Nevertheless, for SBL cases, it is reasonable to use MH methods, which consider either vertical profiles or roughness and surface fluxes as input parameters, since, in the latter case, they can be used for urban conditions with corrections for the heat flux and surface roughness.

- Inter-comparisons of various diagnostic MH-formulations against estimated MH data (mainly from sodar and radiosounding) led to rather unsatisfactory results, due to large scatter and bias and low correlation. However, it is very important to acknowledge that the MH-estimates cannot be considered as the empirical "truth" as they have their own theoretical and practical limitations, especially when profiles are not analysed individually but through an automatic algorithm or threshold procedure (critical Ri, first maximum echo level, etc.).

- On the basis of the data analysis performed during COST 715, it is difficult to recommend any formulae above another. Such goal can be achieved only through detailed analysis of individual profiles using in parallel different profiling techniques. Nevertheless, general suggestions, concerning

the applicability of 'rural' methods of the MH estimation for urban areas, are the following.

- ○ Routine radiosonde measurements and AMDAR data can be used for estimation of the MH in urbanised areas provided such stations are close to cities and the wind fetch is from the city. For more accurate results, finer vertical resolution is required, especially during stable conditions.

- ○ Standard SBL methods are less successful for the nocturnal UBL because they assume a negative surface heat flux. On the other hand, standard CBL formulae are more applicable to the estimation of the daytime MH (Seibert *et al.*, 2000).

- ○ Uncertainties in diagnosing the CBL MH from radiosounding profiles for urban and non-urban conditions can be minimised by using a combination of the Ri and Parcel methods.

- ○ The nocturnal UBL forms when anthropogenic/urban heat fluxes are zero or positive, in contrast to the negative 'non-urban' surface heat fluxes (see e.g. Fig. 6.4), and hence, the applicability of standard methods for the SBL estimation in urban areas is less promising.

- ○ For estimation of the daytime MH, applying standard rural methods is more acceptable than for the nocturnal MH, provided they allow for the urban heat storage as well as changed surface characteristics.

- ○ For the convective UBL the simple *slab models* (e.g. Gryning and Batchvarova, 2001) were found to perform quite well.

- ○ The determination of the SBL height needs further developments and verifications versus urban data. As a variant of the methods for stable MH estimation, the new Zilitinkevich *et al.* (2002) parameterisation can be suggested in combination with a prognostic equation for the horizontal advection and diffusion terms (Zilitinkevich and Baklanov, 2002).

- Significant new experience, information and data have been gained during recent field experiments, such as BUBBLE (in Basel, Section 5.1), UBL-ESCOMPTE (in Marseille, Section 5.2), in Birmingham (Section 5.3), Bologna (Section 5.4), and Cracow (Section 5.5), all of them generated or stimulated by the COST-715 activity.

- Though very simple and cheap, sodar data should be considered with great care and without extrapolating beyond the physical range of acoustic signals.

- Sodars and sodar-RASS determine MH from thermal characteristics of the ABL, lidars and ceilometers from the aerosol content profile. As long as aerosols are a good tracer of the mixing-layer, ceilometers are probably the simplest means to monitor MH (Emeis *et al.* 2004). Current ceilometers may need software upgrades to improve the information retrieved from the raw back-scattered signal.

- The effect of climatic differences on the urban MH has to be investigated more thoroughly. There are significant differences between, e.g., Northern and Southern European cities in this respect.

9.3.2. Schemes and regulatory models

- WG2 recommends that the MH is a useful concept in the context of simpler regulatory dispersion models, although not a very accurate one.

- No direct evaluation of the MH is necessary regarding the dispersion of traffic-originated pollution within the roughness sub-layer (e.g., within a street canyon). On the other hand, at the urban and meso-scales, the MH is an important parameter for practically all air pollution applications.

- Concerning numerical weather prediction (NWP) models, it is not so clear whether the MH is sufficiently accurate to be useful at the present stage of development of knowledge.

- Meso-meteorological and NWP models with modern high-order non-local turbulence closures give promising results (especially for the CBL), however currently the urban effects in such models are not included or included with great simplifications (Baklanov *et al.*, 2002).

- Therefore, it is very important to test different MH schemes not specifically designed for the urban environment against urban MH or IBL schemes for different data sets (for nocturnal conditions first of all) from different urban sites to gain insight in the possible improvements. It would also be of use to know which of the parameterisations are most sensitive to changes of which environmental variables.

Nevertheless, more specific definitions of the MH for urban areas and adapted for various empirical devices are needed. Though useful background information

was provided by the COST-710 Action, horizontal heterogeneity and the vertical structure of the ABL over urban areas have also to be taken into consideration to interpret data and derive MH-schemes.

9.4. Improving data availability and quality for research and applications

9.4.1. Data gaps

Classification of urban zones are so far not harmonised and may present biases depending on the geographical location of cities used for current schemes. Efforts should be dedicated to develop more universal, or at least regionally representative, classifications based on morphometry, land use and climatology using digital land use datasets based on maps or aerial photos.

Values of urban surface parameters (e.g., albedo, thermal admittance, and roughness) for each specific class defined above should be derived in order to be implemented in new generation models for a better representation of urban features in land surface models, as well as an adequate representation of water flow after rainfall. Nevertheless, it appears that the most fundamental change lies in the parameterisation of the temperature roughness.

A subsequent issue is about the adequate averaging/aggregation techniques for each parameter in order to represent the patchwork of various types of surfaces with their intrinsic characteristics at each model cell.

The present challenge is to provide new generation meteorological models with input values averaged at the hectometric scale (100-250 m). This implies creating algorithms to: (i) efficiently average the values of individual elements/facets in real situations/geometries (e.g., provide an effective albedo from the set of brick walls, glass windows, tile roofs, etc., individual albedo and canopy geometry in the computer cell), and/or (ii) to disaggregate kilometric scale values, obtained from global surveys, using high resolution land use classifications. Averaging/aggregation algorithms will combine results from micro-scale microclimatic simulations and very high resolution satellite observations.

One of the key aims of European environmental policy is to improve air quality in European cities and urban areas. The framework Directive on air quality assessment and management was adopted by the Council of Ministers of the

European Union in September 1996. It has led to daughter Directives on several air pollutants (NO_x, O_3, CO, PM, etc.) for which assessments of air quality in certain areas (mainly large urban areas with high populations) will be required. Remedial plans may need to be drawn up in areas of poor air quality. To undertake these tasks, reliable air pollution models are necessary to supplement, and sometimes replace, measurements and also to investigate future emission scenarios. These models will need accurate meteorological and chemical input variables consistently applied within EU Member States.

Characterising and predicting air quality in urban areas is a tremendous task that cannot be accomplished solely by monitoring chemical and meteorological descriptors at a few sites. The complexity of the urban environment sets special requirements for siting observation equipment in order to provide representative values of a given urban zone that are not much affected by close disturbing buildings or pollution source. Both the interpretation of atmospheric conditions and pollution level between measuring sites and forecasting ahead meteorological and air quality conditions require models. Models able to accurately represent meteorological and pollution conditions in the layers close to the surface require data inputs and/or parameterisation (i.e., pre-processors) on urban wind, turbulence profiles, surface heat flux and mixing height. New advanced models start to have the necessary resolution to be able to grasp small-scale features typical of urban areas, i.e. the so-called γ-mesoscale models (1–10 km, 0.5–3 hours). On the other hand, this induces new requirements for observational arrangements in terms of parameters, resolution and frequency.

9.4.2. Monitoring strategy for required parameters

As explained in the previous Section, meteorological and chemical monitoring in an urban environment requires special care, procedures and strategy.

— Siting criteria for urban stations are urgently needed. Sites should be characterised with the help of aerial photos, local surveys, maps, building dimensions, GIS (Geographical Information System), and urban databases.

— Measurement of surface fluxes at meteorological stations is desirable, but so far such measurements have only been realised in research programs of limited duration. Urban meteorological masts should extend above the roughness sub-layer into the inertial sub-layer and above. The heights of these layers vary with conditions and fetch (2 to 5 times the building

height). For central urban areas with relatively tall buildings, the above requirements may be unrealistic for practical purposes. Therefore, the urban roughness sub-layer should be investigated in more detail, specifically with regard to defining appropriate and practical guidelines for the siting of meteorological instruments in urban areas.

— Satellites can in principle be used to measure the urban surface energy balance, but there are significant issues concerning the ability to estimate the appropriate interface temperature.

— The use of thermal remote sensing to infer the surface heat flux is prone to potentially large errors, which become even more pronounced in the case of urban environments. This is due to uncertainties regarding T_s itself, as well as ancillary parameters (especially the large ratio z_0/z_{0t}). Techniques based on temporal changes of surface temperature could alleviate some of those problems. Notwithstanding these difficulties, it would be more than worthwhile testing some thermally-based algorithms with respect to their applicability on cities.

— Another approach that deserves further attention is the use of land surface models with remotely sensed input parameters, such as vegetation fraction cover. Comparison of results obtained with thermally-based and SVAT-based methodologies could also lead to a better understanding of the urban energy balance.

— A careful choice of the scaling velocity is required when simulating urban field studies in a wind tunnel.

— The full range of sensible heat flux and stability, so important for air pollution models, needs measurements in more cities to see whether models have a proper climatology of these parameters for urban situations.

— More climatological evidence on the urban MH, its daily and yearly course as well as differences according to typical climatic/geographic conditions, is needed.

— Ground-based remote sensing devices have good potential to determine the MH, but there is no unique remote sensing tool at present, which can determine operationally MH in all meteorological conditions. The instrumental requirements in order to estimate the MH may be different for day- and night-time. During daytime, a larger vertical range in combination with a coarser vertical resolution is required compared to night-time.

A combination of sodar-RASS and ceilometer, located at a representative site in the city, might be promising to capture MH in the majority of cases.

— Local air quality management relies heavily on the dispersion regime over several years being modelled in a statistically representative manner. National Meteorological Services should assist by upgrading synoptic data developed in the 50's to include at least heat flux and/or stability (e.g., through air temperature difference measurements between 2 different heights or direct assessment of the Monin-Obukhov length).

National Meteorological Services should also continue developing NWP models so that they are better able to develop long term archives of numerical weather data to support research studies, comparisons with urban field campaigns, and analyses of severe air pollution episodes after they have occurred (to identify causes and locate responsible emission sources, and to develop control policies able to avoid future such episodes).

9.4.3. Need and planning of future field campaigns

In the mid-1990's when the COST-715 Action was being planned, there were relatively few measurements in Europe from field campaigns to measure urban boundary layers. At that time the most comprehensive sets of measurements were those garnered for North America by Tim Oke and Sue Grimmond. As discussed in some detail in Chapter 5, several major campaigns have been performed during the period of COST-715 in Europe, some of them directly stimulated or instigated by COST-715 (BUBBLE, ESCOMPTE-UBL, Birmingham, Cracow, Bologna). These field campaigns have provided substantial new data sets, but the complexity of urban meteorology is such that gaps in knowledge remain and new campaigns, based on an analysis of critical gaps in knowledge and data will have to be planned and organised. Towards this, there is already a current extensive campaign CAPITOUL organised by MeteoFrance that will gather a variety of data during one year until March 2005 with 40 measuring sites in the conurbation of Toulouse in South-west France. These data will be used to test the SEB scheme TEB (see Section 3.2.2) for urban meteorological forecasts with a 2-km resolution (Masson *et al.*, 2004a,b).

There is the need for carrying out urban field campaigns in the future, as measurements provide the validation data that enable new modelling techniques

to be tested and then improved. Campaigns provide data from which insights may be drawn in order to devise simpler models and parameterizations for complex models. The existing measurements have limitations which arise due to inescapable constraints on field programmes in cities, including:

- Availability of suitable and representative instrument sites, allowing for security, power, data transmissions, neighbour comfortability, public safety, accessibility, and planning permission;

- Height and positioning of sensors to meet the needs of the researchers, such as adequate height, so that the appropriate surface type is within the upwind fetch and observational foot-print for the sensor;

- Duration of instrument deployment and data capture rates during the campaign, as few campaigns can be long term, yet measurements are needed in all seasons of the year;

- Sufficient sensors to deploy a number of reference instruments at well exposed rural sites so that influences due to the city can be differentiated from the daily and diurnal changes in prevailing meteorological situation;

- Planning and resourcing so that intense meteorological campaigns are suitably combined with related studies, especially in pollutant monitoring, tracer dispersion studies, and possible surveys of health characteristics in the local populace: weather (e.g. excess temperature in cities) as well as air pollution (e.g. fine particles or ozone) influence people's well-being;

- Capabilities of existing instruments and the opportunities offered by new technologies: cup anemometers have been superseded in many studies by ultrasonic anemometers, so that fluxes and stability are directly measured, and remote sensing offers new ways to solve old problems: for instance, by scintillometers (for data linked to heat flux), by fixed back-scatter lidar (aerosol concentrations and mixing heights), by scanning pulsed Doppler lidar (velocity and turbulence profiles, mixing heights), infra-red thermometers (e.g. for surface black-body temperatures), by sodar (a long established technique for convective mixing heights and wind profiles), RASS (an improvement on sodar).

- In the perspective of the potential of satellite-borne remote sensing methods to infer surface properties and parameters, more work should be allocated to the validation of remote sensing algorithms, which is still one of

the main difficulties for testing their applicability. Ideally, ground-based observations should be used for the inter-comparison, but few data sets are available at this time. Therefore, when considering future field experiments for urbanised regions, a satellite remote sensing component ought to be included, to test and further develop some of the methods described above.

Urban campaigns are needed so that the gaps in knowledge discussed above may be addressed and the numerical models improved. Advances in experiments will come by applying a number of techniques together, so the fundamental need is to plan large co-operative campaigns which apply a wide variety of measuring and modelling approaches. There is a real need for long measurement runs, so a variety of conditions are sampled, and that instrumental techniques can be compared against each other. There is also a need to bring together the expertise of different groups in different European countries to study the techniques they have used and to make recommendations regarding their deployment and use, methods of data capture and signal processing, and the derivation of dispersion model and urban boundary layer parameters from the remote sensing products. Remote sensing platforms for urban science include ground or building mounted sensors, aircraft and satellites. There is also a need to see how such data can be either used within numerical models, or used to validate calculated variables within these models.

Despite recent advances, there remain significant gaps in our understanding of and data sets for urban meteorology. It is therefore recommended that:

- Urban field campaigns should combine the latest technology sensors with more traditional instruments, and resourcing should be sufficient for long runs of data, for multiple sites, and to include good reference stations for the urban hinterland (e.g. rural, sea). A variety of geographical situations merit study;

- Campaigns are costly, and it follows that pollutant and tracer studies should be dovetailed into the urban campaigns. Good examples have been noted in this report (above). Some tracer and chemistry studies would benefit from a larger meteorological component, both measured and modelled;

- The multi-disciplinarity and variety of facets of the problematic call for a co-operative study across Europe to address the design of urban cam-

paigns, to review the capabilities of existing remote sensing technologies and their suitability for urban deployment, to evaluate their compatibility with the numerical modelling requirements, to identify suitable locations for study, to develop experiments for filling gaps in knowledge and to compare instrumentation. Such co-operation could be partly supported under the auspices of COST, with respect of its flexibility and basic philosophy of coordination through cooperation on researchers' terms.

The next steps will be to plan and organise pluri-disciplinary observations of urban characteristics and issues in the perspective of urban studies and management within the frame of urban science.

Appendix 1: Some formulations for estimating the MH

Reference [code]	SBL height equations
1. Zilitinkevich (1972)	$$h = c_2 \left(\frac{u_* L}{f} \right)^{1/2}$$ $c_2 \approx 0.4$ (varies from 0.13 to 0.72 according to different authors)
2. Venkatram (1980) [Ven80a]	$$h = 2300 u_*^{1.5}$$
3. Venkatram (1980) [Ven80b] [(2)]	$$h = u_* \sqrt{\frac{2}{fN}}$$
4. Arya (1981) (after Zilitinkevich, 1972)	$$h = a \left(\frac{u_* L}{f} \right)^{1/2} + b; \quad a = 0.43, b = 29.3$$
5. Nieuwstadt (1981) [Nieu81]	$$h = L \frac{0.3 u_*}{|f|L} \frac{1.0}{1.0 + 1.9h/L}$$
6. Zilitinkevich & Mironov (1996) [ZiMi96]	$$\left(\frac{fh}{0.5 u_*} \right)^2 + \frac{h}{10L} + \frac{Nh}{20 u_*} + \frac{h|f|^{1/2}}{(u_* L)^{1/2}} + \frac{h|Nf|^{1/2}}{1.7 u_*} = 1$$
7. Zilitinkevich *et al.* (2002) [Zili02] [(1)]	$$h = \frac{C_R u_*}{|f|} \left[\left(1 + C_h \frac{w_h}{u_*} \right) \bigg/ \left(1 + \frac{C_R^2 u_* (1 + C_{uN} NL/u_*)}{C_S^2 L|f|} \right) \right]^{1/2}$$ with: $C_R = 0.4$, $C_S = 0.74$, $C_{uN} = 0.25$ and $C_h = 0.3$.
8. Zilitinkevich & Baklanov (2002)	$$\frac{\partial h}{\partial t} + \mathbf{V} \cdot \nabla h = -C_E |f|(h - h_{CQE}) + K_h \nabla^2 h \quad \text{with} \quad C_E \approx 1$$
9. Joffre and Kangas (2002) [staJof]	$$h = \frac{b'}{2a'} \mu_N \left\{ -1 + \left[1 + \frac{4a'm'}{b'^2} \mu_N^{-2} \right]^{1/2} \right\} L_N$$ with: $a' = 0.12$; $b' = 2.85$; $m' = 24$ (very rough surface)

Where u_{10} is the wind speed at 10 m height; $\mathbf{V} = (u, v)$ is the horizontal velocity vector, K_h is the horizontal diffusivity, h_{CQE} is the equilibrium MH calculated from a diagnostic formulation (e.g., Zilitinkevich *et al.*, 2002), $\mu_N = L_N/L$, $L_N = u_*/N$ (N

is the Brunt-Väisälä frequency), f is the Coriolis parameter, and w_h is the large-scale vertical velocity at the SBL upper boundary.

(1) In the Bologna experiment, formula 6 was applied supposing $w_h \approx 0$.

(2) In the Bologna experiment was also tested the Venkatram (1980) formula using only the friction velocity $h = 2300u_*^{1.5}$. This formula is referred to as Ven80a.

Reference [code]	CBL height equations
10. Tennekes (1973); Tennekes and Driedonks (1981) [TeDr82]	$\dfrac{dh}{dt} = \dfrac{S}{\Delta\theta}$; where $S = A\overline{(w'\theta')}_0 + \dfrac{Bu_*^3}{\beta h}$ $\dfrac{d\Delta\theta}{dt} = \dfrac{\gamma S}{\Delta\theta} - \dfrac{\overline{(w'\theta')_0}}{h} - \dfrac{S}{h}$; where: $A = 0.2$; $B = 5$.
11a. Batchvarova and Gryning (1991) [BaG91a]	$\dfrac{\partial h}{\partial t} = (1 + 2A)\dfrac{\overline{(w'\theta')_0}}{\gamma h} + 2B\dfrac{u_*^3}{\gamma\beta h^2}$, where: $A = 0.2$, $B = 2.5$
11b. Batchvarova and Gryning (1991) [BaG91b] [3]	$\dfrac{\partial h}{\partial t} = \overline{(w'\theta')}_0 \left[\dfrac{\gamma h^2}{(1 + 2A)h - 2kBL_*} + \dfrac{Cu_*^2}{\beta(1 + A)h - kBL_*} \right]^{-1}$ where: $A = 0.2$; $B = 2.5$; $C = 8$.
12. Gryning and Batchvarova (1996)	$\left\{ \dfrac{h^2}{(1 + 2A)h - 2B\kappa L} + \dfrac{Cu_*^2}{\gamma\beta[(1 + A)h - B\kappa L]} \right\} \cdot$ $\cdot \left(\dfrac{\partial h}{\partial t} + u\dfrac{\partial h}{\partial x} + v\dfrac{\partial h}{\partial y} - w_s \right) = \dfrac{\overline{(w'\theta')}_0}{\gamma},$ with $A = 0.2$, $B = 5$, $C = 1.3$
13. Joffre and Kangas (2002) [unsJof]	$h = \dfrac{b''}{2a''}\mu_N \left\{ 1 + \left[1 + \dfrac{4a''m''}{b''^2}\mu_N^{-2} \right]^{1/2} \right\} L_N$ with $a'' = 0.1$; $b'' = -0.85$; $m'' = 12$

Where γ is the potential temperature gradient above the ABL ($N^{\cdot 2} = \beta\gamma$), $\beta = g/T_0$ the buoyancy parameter, $\Delta\theta$ the temperature jump in the entrainment layer at the ABL top, $\overline{(w'\theta')}_0$-the surface sensible heat flux ($= Q_H/\rho c_p$), w_s the vertical synoptic velocity above the ABL. Equation (13) was derived for moderate unstable conditions (both buoyant and mechanical production of turbulence) but not for convective conditions.

(3) In the Bologna experiment formula 12 was applied supposing $w_s \approx 0$ and neglecting the horizontal advection term $u\dfrac{\partial h}{\partial x} + v\dfrac{\partial h}{\partial y}$, the constants were set as: $A = 0.2$, $B = 2.5$, $C = 8$, after Georgieva *et al.* (2003).

Reference [code]	Neutral ABL height equations
14. Rossby & Montgomery (1935) [RoMo35] [4]	$h = c_N \dfrac{u_*}{\|f\|}$, where: $c_N = 0.3$ ($c_N = 0.04 - 0.3$ according to Seibert *et al.*, 1998)
15. Arya (1981) [Arya81] [5]	$h = 0.089 \dfrac{u_*}{f} + 85.1$
16. Mahrt (1982) [Mahr82] [5]	$h = 0.06 \dfrac{u_*}{f}$
17. Benkley & Schulman (1979) [BeSc79] [5]	$h = 125 u_{10}$
18. Nieuwstadt (1984a,b) [Nieu84] [5]	$h = 28 u_{10}^{3/2}$

Developed for neutral conditions, Eq.(14–18) have been used also for stable conditions by some authors.

(4) In the Bologna experiment c_N was set equal to 0.25, 0.133 and 0.04 as suggested by Seibert *et al.* (1998), these formulae are referred respectively with Sei98a, Sei98b, Sei98c codes.

(5) In the Bologna experiment, formulae (14–18) have been applied also to the SBL.

Acknowledgements

References

Akylas, E., Y. Tsakos, M Tombrou and D. P. Lalas, 2003: Considerations on minimum friction velocity. *Quart. J. Roy. Meteorol. Soc.,* **129**, 1929–1943.

Allegrini, I., Febo A., Pasini A., and Schiarini, 1994: Monitoring of the nocturnal mixed layer by means of particulate radon progeny measurement. *J. Geophys. Res.,* **99**(D9), 18,765–18, 777.

AMDAR, 2003: International AMDAR Program: Aircraft Meteorological Data Relay, WMO, AMDAR Panel, 7 p.

Anfossi, D., Cassardo, C., Ferrero E., Longhetto, A., Sacchetti, D., Brusasca, G., Colombo V., Marzorati, A., Morselli, M. G., Rocchetti, F., Tinarelli, G., 1993: On the analysis of ultrasonic anemometer data. Internal Report ICG/CNR N.282/93, CNR, Torino (It), 62 p.

Angevine, W., 2003: Wind profiler, Applications. Lecture material for: *Short Course on the Fundamentals of Boundary Layer Wind and Temperature Profiling using Radar and Acoustic Techniques,* AMS Annual Meeting, Feburary 8–9, 2003 Long Beach, CA, `http://www.etl.noaa.gov/ams_measurement/short_course_2003.htm`

Anquetin, S., Chollet, J. P., Coppalle, A., Mestayer, P., and Sini, J. F., 1999: The Urban Atmosphere Model SUBMESO, *Proceedings EUROTRAC Symp. '98,* P.M. Borrel & P. Borrel (Eds.), WIT Press.

Anthes, R. A. and T. T. Warner, 1978: The development of hydrodynamic models suitable for air pollution and other meteorological studies. *Mon. Wea. Rev.,* **106**, 1045–1078.

Arnfield, A. J. and Grimmond, C. S.: 1998, 'An urban canyon energy budget model and its application to urban storage heat flux modelling', *Energy and Building,* **27**, 61–68.

Arya, S. P. S., 1981: Parameterizing the height of the stable atmospheric boundary layer, *J. Appl. Meteorol.* **20**, 1192–1202.

Arya, S. P. S. and Byun, D. W., 1987: Rate equations for the planetary boundary-layer depth (urban vs rural). In: *Modeling the urban boundary-layer.* American Meteorological Society, Boston, 215–251.

Asimakopoulos, D.N., Helmis C.G., and Michopoulos J., 2004: Evaluation of Sodar methods for the determination of the atmospheric boundary layer mixing height. *Meteorology and Atmospheric Physics,* **85**, 85–92.

Baklanov, A., 2000a: Application of CFD methods for modelling in air pollution problems: possibilities and gaps. *Environmental Monitoring and Assessment,* **65**: 181–190.

Baklanov, A., 2000b: Possible improvements in the DMI-HIRLAM for parameterisations of long-lived stably stratified boundary layer. *DMI Internal Report*, No. 00–15, 15 p.

Baklanov, A., 2001: Parameterisation of SBL height in atmospheric pollution models. *Air Pollution Modelling and its Application XV.* C. Borrego and G. Schayes (Eds.), Kluwer Academic / Plenum Publishers, New York, 415–424.

Baklanov, A., 2002. The mixing height in urban areas –a review. In Piringer M. & Kukkonen J. (Eds.), Proceedings of the Workshop "Mixing height and inversions in urban areas", Toulouse, France, 3–4 October 2001, COST report EUR 20451, 9–28.

Baklanov, A. (Ed.), 2003: FUMAPEX Integrated Systems for Forecasting Urban Meteorology, Air Pollution and Population Exposure – Project Kick-off Meeting and First Progress Report. DMI Sci. Report 03–12, ISSN 0905–3263. April 2003, 140 p., `http://www.dmi.dk/f+u/publikation/vidrap/2003/Sr03-12.pdf`

Baklanov, A. and S. Joffre (Eds.), 2003: Improved Models for Computing the Roughness Parameters of Urban Areas. D4.4 FUMAPEX Report, November 2003. DMI Sci. Report 03-19, ISBNnr.: 87-7478-495-1, 51 p.

Baklanov, A. *et al.*, 2004: The mixing height in urban areas – new experimental and modelling results. To be submitted to *Boundary-Layer Meteorol.*

Baklanov, A. and A. Kuchin, 2004: The mixing height in urban areas: comparative study for Copenhagen. *Atmos. Chem. Phys. Discus..* **4**, 2839–2866.

Baklanov, A. and P. Mestayer (Editors), 2004: Improvement of parameterisation of urban atmospheric processes and urban physiographic data classification. WP4 FUMAPEX Progress Report, April 2004. DMI Scientific Report.

Baklanov, A., A. Rasmussen, B. Fay, E. Berge, and S. Finardi, 2002: Potential and shortcomings of numerical weather prediction models in providing meteorological data for urban air pollution forecasting. *Water, Air and Soil Poll.: Focus,* **2**(5–6), 43–60.

Batchvarova, E. and Gryning, S.-E., 1991: Applied model for the growth of the daytime mixed layer. *Boundary-Layer Meteorol.*, **56**(3), 261–274.

Batchvarova, E. and Gryning, S.-E., 1998: Wind Climatology, Atmospheric Turbulence and Internal Boundary-Layer Development in Athens During the MEDCAPHOT-Trace Experiment, *Atmos. Environ.* **32**, 2055–2069.

Batchvarova, E., Cai, X., Gryning, S.-E., and Steyn, D., 1999: Modelling internal boundary-layer development in a region with a complex coastline. *Boundary-Layer Meteorol.*, **90**, 1–20.

Baumann K., and M. Piringer, 2001: Two-years of boundary layer measurements with a Sodar – statistics and applications. *Physics and Chemistry of the Earth*, Part B. **26**/3, 205–211.

Baumann-Stanzer, K., and M. Piringer, 2003: Diagnostic mixing heights with and without urban fetch. R. Sokhi and J. Brechler, Eds., Proc. of the 4th Intern. Conf. on Urban Air Quality, Charles University Prague, 25–27 March 2003, 412–415.

Baumann-Stanzer, K. and I. Groehn, 2004: Alpine radiosoundings – feasible for mixing height determination? *Meteorol. Z.* **13**, 1–12.

Baumann-Stanzer, K., W. Knauder, and M. Piringer, 2004: Assessment of meteorological input for dispersion modelling in Linz, Austria. Proceedings of the 4th EMS Conference, 27–30 September 2004, Nice, France.

Benkley, C.W. and Schulman, L.L., 1979: Estimating mixing depths from historical meteorological data, *J. Appl. Meteorol.,* **18**, 772–780.

Berkowicz, R. and Prahm, L.P., 1982: Sensible heat flux estimated from routine meteorological data by the resistance method. *J. Appl. Meteorol.*, **21**, 1845–1864.

Berman, S., Ku, J.-Y., Zhang, J. and Rao, S. T., 1997: Uncertainties in estimating the mixing depth: comparing three mixing-depth models with profiler measurements. *Atmos. Environ.*, **31**(18), 3023–3039.

Beyrich, F., 1997: Mixing height estimation from sodar data – a critical discussion. *Atmos. Environ.*, **31,** 3941–3954.

Bielak, A., Burzyski, J., Kaszowski, W., Walczewski, J. 1997: Some parametrisation formulae for mixing height compared with joint Sodar and Lidar observations. EURASAP Wokshop Proceedings 1–3 October 1997, Riso National Laboratory.

Boone, A., Calvet, J.C., and Noilhan, J., 1999: Inclusion of a Third Soil Layer in a Land Surface Scheme using the Force-Restore Method. *J. Appl. Meteorol.,* **38**, 1611–1630.

Bornstein, R.D., 2001: Currently used parameterisations in numerical models. *Workshop on Urban Boundary Layer Parameterisations.* COST 715, Zürich, May 24–25 2001.

Brost, R.A. and J.C. Wyngaard, 1978: A model study of the stably stratified planetary boundary layer. *J. Atmos. Sci.*, **35**, 1427–1440.

Brutsaert, W., 1975: The roughness length for water vapor, sensible heat, and other scalars. *J. Atmos. Sci.* **32**, 2028–2031.

Brutsaert, W., 1982: *Evaporation into the atmosphere.* D. Reidel, Hingham, Mass, 299 p.

Brutsaert, W., and Sugita, M., 1996: Sensible heat transfer parameterisation for surfaces with anisothermal dense vegetation. *J. Atmos. Sci.*, **53**: 209–216.

Byun, D. W. and Arya, S. P. S., 1990: A two-dimensional mesoscale numerical model of an urban mixed layer. I: Model formulation, surface energy budget, and mixed layer dynamics. *Atmos. Environ.,* **24**(4): 829–844.

Carlson, T.N., J.K. Dodd, S.G. Benjamin, and J.N. Cooper, 1981: Satellite estimation of surface energy balance, moisture availability and thermal inertia. *J. Appl. Meteorol.*, **20**, 67–87.

Carlson, T., 2003: Preface - Applications of remote sensing to urban problems. *Remote Sensing Environ.*, **86**, 273–274.

Carson, D.J., 1973: The development of a dry inversion-capped convectively unstable boundary layer. *Quart. J. Roy. Meteorol. Soc.*, **99**, 450–467.

Caughey, S.J., 1982: Observed characteristics of the atmospheric boundary layer. In: Nieuwstadt, F.T.M. and van Dop, H. (Eds.), *Atmospheric Turbulence and Air Pollution Modelling*. Reidel Publ. Co., Dordrecht (NL), 107–158.

Changnon, S.A., Jr (Ed.), 1981: *METROMEX: A Review and Summary.* Meteor. Monographs, **18**, No. 40, Amer. Meteor. Soc., Boston, 181 p.

Choudhury, B.J., 1991: Multispectral satellite data in the context of land surface heat balance. *Reviews of Geophysics*, **29**, 127–236.

Christen, A, Bernhofer C, Parlow E, Rotach MW, Vogt R. 2003. Partitioning of turbulent fluxes over different urban surfaces. *Proceedings of the Fifth International Conference on Urban Climate*, September 1–5 2003, Lodz, Poland.

Christen, A. and R. Vogt, 2004: The Energy and Radiation Balance of a Central European City. *Int. J. Climatol.* **24**, 1395–1421.

Cleugh, HA, Oke T.R., 1986: Suburban-rural energy balance comparisons for Vancouver, B.C. *Boundary-Layer Meteorol.* **36**, 351–369.

Cleugh, H. A. and Grimmond, C. S. B., 2001: Modelling regional scale surface energy exchanges and CBL growth in heterogeneous, urban-rural landscape. *Boundary-Layer Meteorology*, **98**, 1–31.

Collier, C.G., Bozier K.E., Davies F., Holt A.R., Middleton D.R., Pearson G.N., Siemens S., Willetts D.V., Upton G.J.G., and Young R.I., 2004: Dual Doppler lidar measurements for improving dispersion models. Paper in preparation, for submission to *Bull. Amer. Meteorol. Soc.*

COST-76, 2003: *Development of VHF/UHF wind profilers and vertical sounders for use in European observing systems.* Final Report: Dibbern, J., W. Monna, J. Nash and G. Peters (Eds.), European Commission, Report EUR 20614, Luxembourg, 433 p.

COST-710: 1998: *Harmonisation of pre-processing of meteorological data for atmospheric dispersion models.* Final report: Fisher, B. et al. (Ed.), European Commission, Report EUR 18195, Luxembourg, 431 p.

COST-715: 2002a: *Surface energy balance in urban areas'.* Piringer, M. (Ed.), Extended abstracts of an Expert Meeting. WG-2 COST Action 715, Antwerp, Belgium, 12 April 2000. European Commission. Report EUR 19447, Luxembourg, 103 p.

COST-715, 2002b: *Urban Boundary Layer Parameterisations.* Rotach M. W, Fisher B. and M. Piringer (Eds.) Extended abstracts of the Workshop, Zurich, 24–25 May, 2001, COST-715 Action. European Commission, Report EUR 20355, Luxembourg, 118 p.

COST-715, 2002c: *Mixing height and inversions in urban areas*, Piringer, M. and Kukkonen, J. (Eds.), Proceedings of the Workshop, 3–4 October, 2001, Toulouse, F. COST Action 715, European Commission, Report EUR 20451, Luxembourg, 113 p.

COST-715, 2004: *Meteorology applied to urban air pollution problems.* Final report. Fisher, B., S. Joffre, J. Kukkonen, M. Piringer, M. Rotach, and M. Schatzmann (Eds.), European Commission. (*in print*)

Cuxart, J., Bougeault, P., and Redelsperger, J.-L., 2000: A turbulence scheme allowing for mesoscale and large eddy simulations, *Quart. J. Roy. Meteorol. Soc.,* **126**, 1–30.

Dandou, A., Tombrou M., Akylas E., Soulakellis N. and E. Bossioli, 2004 'Urban parameterisation schemes into MM5 model'. Submitted to *J. Geophys. Res.*

Davies, F., Collier C.G., Holt A., Middleton D.R., Pearson G.N., Siemen S., Willetts D.V., and Young R.I., 2003: Boundary layer measurements of model parameters using dual Doppler Lidar at Malvern, UK. ISB52 Project Report July 2003, www.qinetiq.com

Davies, F., Middleton D.R. and Pearson G.N., 2004: Observations of boundary layer depth over an urban/rural transition. Presented at 5th Symposium on the Urban Environment, Vancouver, Canada, August 2004.

De Bruin, H.A.R., Van den Hurk, and B.J.J.M., Kohsiek, W., 1995: The Scintillation Method Tested Over a Dry Vineyard Area, *Boundary-Layer Meteorol.,* **76**, 25–40.

De Ridder, K., 2003: Horizontal scale of roughness variations for realistic landscapes. *Boundary-Layer Meteorol.,* **109**, 49–57.

De Ridder, K., J. Neirynck, and C. Mensink, 2004: Parameterising forest edge deposition using effective roughness length. *Agric. For. Meteorol.,* **123**, 1–11.

De Ridder, K., and G. Schayes, 1997: The IAGL land surface model. *J. Appl. Meteorol.,* **36**, 167–182.

Deserti, M., Cacciamani, C., Golinelli, M., Kerschbaumer, A., Leoncini, G., Savoia, E., Selvini, A., Paccagnella, T., and Tibaldi, S., 2001: Operational meteorological pre-processing at Emilia-Romagna ARPA Meteorological Service as a part of a decision support system for Air Quality Management. *Intern. J. Environ. Poll.,* **16** (1–6), 571–582.

Deserti, M, Bonafè, G., Minguzzi E., Tagliazucca M., and Trivellone G., 2003: The urban atmospheric boundary layer: experimental campaigns in Bologna (Italy). Procceddings of the 4th International Conference on Urban Air Quality - Measurement, Modelling and Management, 25–28 March 2003 Charles University Prague, Czech Republic) 404–407.

Diak, G.R., J.R. Mecikalski, M.C. Anderson, J.M. Norman, W.P. Kustas, R.D. Torn, and R.L. DeWolf, 2004: Estimating land surface energy budgets from space. *Bull. Amer. Metor. Soc.*, **85**, 65–78.

Driedonks, A.G.M, 1982: Models and observations of the growth of the atmospheric boundary layer. *Boundary-Layer Meteorol.*, **23**, 283–306.

Driedonks, A.G.M., and Tennekes, H., 1984: Entrainment effects in the well-mixed atmospheric boundary layer. *Boundary-Layer Meteorol.*, **30**, 75–105.

Dupont, S., 2001, Modélisation dynamique et thermodynamique de la canopée urbaine: réalisation du modèle de sols urbains pour SUBMESO. Doctoral thesis, University of Nantes, France, 319 p.

Dupont, E., Menut, L., Carissimo, B., Pelon, J. and Flamant, P.: 1999: Comparison between the atmospheric boundary layer in Paris and its rural suburbs during the ECLAP experiment. *Atmos. Environ.,* **33**, 979–994.

Dupont, S., Calmet, I., Mestayer, P.G. and Leroyer, S., 2003: Parameterisation of the Urban Energy Budget with the SM2-U Model For The Urban Boundary Layer Simulation. *Boundary-Layer Meteorol.*, in revision.

Dupont, S., T.L. Otte, J.K. and S. Ching, 2004: Simulation of Meteorological Fields within and above Urban and Rural Canopies with a Mesoscale Model (MM5). *Boundary-Layer Meteorol.*, **113**, 111–158.

E-AMDAR, 2002: EUMETNET-AMDAR Project: Aircraft Meteorological Data Reporting, `http://www.metoffice.com/research/interproj/amdar/index.html`

Ellefsen, R. 1991. Mapping and measuring buildings in the canopy boundary layer in ten U.S. cities. *Energ. Buildings.* **15–16** (3–4): 1025–1049.

Ellis, N.L. and Middleton, D.R., 2000a: Field measurements and modelling of urban meteorology in Birmingham, UK. Met Office Turbulence and Diffusion Note No 268. Met Office, London Rd, Bracknell, Berkshire RG12 2SZ, UK.

Ellis, N.L. and Middleton, D.R., 2000b: Field Measurements and Modelling of Surface Fluxes in Birmingham, UK. In 'Surface energy balance in urban areas'. Proceedings COST-715 Expert Meeting, Antwerp, Belgium, 12 April 2000. Piringer M. (Ed.). Report EUR 19447, 66–75.

Ellis, N. L. and Middleton, D. R., 2000c: Field measurements and modelling of urban meteorology in Birmingham, UK', *Proc. 3rd AMS Symposium on Urban Environment*, Davis, CA., 14–18 August 2000, American Meteorological Society, Boston, MA, 108–109.

Elvidge, C.D., K.E. Baugh, E.A. Kihn, H.W., Kroehl, E.R. Davis and C.W. Davis, 1997: Relation between satelite observed visible-near infrared emissions, population, economic activity, and electric power consumption. *Intern. J. Remote Sensing*, **18**, 1373–1379.

Emeis, S., 2004: Vertical wind profiles over an urban area. *Meteorol. Z.*, **13** (5), 353–359.

Emeis, S., Ch. Münkel, S. Vogt, W. J. Müller, and K. Schäfer, 2004: Atmospheric boundary-layer structure from simultaneous SODAR, RASS, and ceilometer measurements. *Atmos. Environ.* **38**, 273–286.

Emeis, S., and M. Türk, 2004: Frequency distributions of the mixing height over an urban area from SODAR data. *Meteorol. Z.*, **13**, 361–367.

Eymard, L., and O. Taconet, 1995: The methods for infering surface fluxes from satellite data, and their use for atmosphere model validation. *Intern. J. Remote Sensing*, **16**, 1907–1930.

Fay, B. (Ed.), 2004: Analysis of comparison study of air pollution episodes for Helsinki. D3.3 FUMAPEX Report, DWD, Germany.

Feddersen, B.; Leitl, B.; Rotach, M.W. and Schatzmann, M., 2003: Wind tunnel investigation of the spatial variability of turbulence characteristics in the urban area of Basel City, Switzerland. *WorkshopProceedings PHYSMOD2003*, September 3–5, 2003, Prato, Italy, Firenze University Press, 23–25.

Fehrenbach, U., Scherer D., and Parlow E., 2001: Automated classification of planning objectives for the consideration of climate and air quality in urban and regional planning for the example of the region of Basel/Switzerland. *Atmos. Environ.*, **35** (32), 5605–5615.

Feigenwinter, C., Vogt, R. and Parlow, E., 1999: Vertical structure of selected turbulence characteristics above an urban canopy, *Theoret. Appl. Climatol.*, **62**, 51–63.

Fiedler, F., and H.A. Panofsky, 1972: The Geostrophic Drag Coefficient and the 'Effective' Roughness Length. *Quart. J. Roy. Meteor. Soc.*, **98**, 213–220.

Finardi, S. (Ed.), 2004: Guidelines for the construction of the interfaces from operational NWP models to UAP models. FUMAPEX Report for D5.1, Arianet, Italy, January 2004, 47 p.

Fujinami, N. and Esaka S., 1988: A simple model for estimating the mixing depth from the diurnal variation of atmospheric ^{222}Rn concentrations. *Radiat. Prot. Dos.*, **24**, 89–91.

Galinski, A.E. and Thomson, D.J., 1995: Comparison of three schemes for predicting surface sensible heat flux. *Boundary-Layer Meteorol.*, **72**, 345–370.

Gamba, P., J.A. Benediktsson and G. Wilkinson, 2003. Foreword to the special issue on urban remote sensing by satellite. *IEEE Transactions on Geoscience and Remote Sensing*, **41**, 1903–1906.

Gamo, M., S. Yamamoto, O. Yokoyama and H. Yoshikado, 1983: Structure of the free convective internal boundary layer during the sea breeze. *J. Meteor. Soc. of Japan*, **61**, 110–124.

Garratt, J.R., 1982: Observations in the nocturnal boundary layer. *Boundary-layer Meteorol.*, **22**, 21–48.

Garratt, J.R., 1990: The Internal Boundary Layer - A Review. *Boundary-Layer Meteorol.* **50**, 171–203.

Garratt, J.R., 1992: *The Atmospheric Boundary Layer.* Cambridge University Press, Cambridge (UK), 316 p.

Garratt, J.R. and B.B. Hicks, 1973: Momentum, heat and water vapour transfer to and from natural and artificial surfaces. *Quart. J. Roy.Meteorol. Soc.*, **99**, 680–687.

Garrett, A.J., 1981: Comparison of observed mixed layer depth to model estimates using observed temperature and winds, and MOS forecasts. *J. Appl. Meteorol.* **20**, 1277–1283.

Gastellu-Etchegorry, J.P., Martin E. and Gascon, F, 2004: DART: a 3-D model for simulating satellite images and surface radiation budget. *Intern. J. Remote Sensing*, **25** (1), 73–96.

Georgieva, E., Canepa E., Bonafè G. and Minguzzi E., 2003: Evaluation of ABLE mixing heigth algorithms against observed and modelled data for the Po Valley Italy. Paper presented at: *26th NATO/CCMS International Technical Meeting on Air Pollution Modelling and its Application*, Istanbul, Turkey, 26–30 May, 2003.

Greenland, D., 1994: Use of satellite-based sensing in land surface climatology. *Progress in Physical Geography*, **18**, 1–15.

Grimmond, C.S.B., 1992: The Suburban Energy Balance: Methodological Considerations and Results for a Mid-latitude West Coast City under Winter and Spring Conditions. *Intern. J. Climatol.*, **12**, 481–497.

Grimmond, C.S.B., Cleugh, H.A. and Oke, T.R., 1991: An objective urban heat storage model and its comparison with other schemes. *Atmos. Environ.*, **25B**, 311–326.

Grimmond, C.S.B. and Oke, T.R., 1995: Comparison of heat fluxes from summertime observations in the suburbs of four North American cities. *J. Appl. Meteorol.* **34**, 873–889.

Grimmond, C.S.B. and Oke, T.R., 1999a: Heat storage in urban areas: Local-scale observations and evaluation of a simple model. *J. Appl. Meteorol.* **38**, 922–940.

Grimmond, C.S.B. and Oke, T.R. 1999b: Aerodynamic properties of urban areas derived from analysis of surface form. *J. Appl. Meteorol.* **38** (9), 1262–1292.

Grimmond, C.S.B. and Oke, T.R.: 2000: A local-scale urban meteorological pre-processing scheme (LUMPS). *Proceedings of the COST 715 Workshop "Preparation of Meteorological Input Data for Urban Site Studies"* (Ed.: M. Schatzmann, J. Brechler, B. Fisher),Prague, Czech Republic, June 15, 2000, 73–83.

Grimmond, C.S.B. and Oke, T.R., 2002: Turbulent heat fluxes in urban areas: Observations and local-scale urban meteorological parameterization scheme (LUMPS). *J. Appl. Meteorol.* **41**, 792–810.

Grimmond, C.S.B. and Souch, C., 1994: Surface description for urban climate studies: a GIS based methodology. *Geocarto International* **9**, 47–59.

Grimmond, C.S.B., Souch, C. and Hubble, M., 1996: The influence of tree cover on summertime energy balance fluxes, San Gabriel Valley, Los Angeles. *Climate Research* **6**, 45–57.

Grimmond, C.S.B., Salmond, J., Offerle, B.D. and Oke, T.R., 2002: Local-Scale Surface Flux Measurements at a Downtown Site in Marseille during the ESCOMPTE Field Campaign. Proceedings 4th Conf.on Urban Environment, Norfolk, USA, 20–24 May 2002, American Meteorological Society, 45 Beacon St., Boston, Ma, 21–22.

Groleau, D., Fragnaud F., Rosant J.M., 2003: Simulation of the radiative behavior of an urban quarter of Marseille with the Solene model. Fifth International Conference on Urban Climate, Lodz, Pologne, 1–5 September 2003.

Gryning, S-E. and Lyck, E. (1980) Medium-range dispersion experiments downwind from a shoreline in near neutral conditions. *Atmos. Environ.* **14**, 923–931.

Gryning, 1985: The Øresund experiment – A Nordic Mesoscale Discpersion Experiment over a Land-Water-Land Area. *Bull. Amer. Meteor. Soc.* **66**, 1403–1407.

Gryning, S-E. and E. Batchvarova, 1990: Analytical model for the growth of the coastal internal boundary layer during onshore flow. *Quart. J. Royal Meteorol. Soc.* **116** (491), 187–203.

Gryning, S-E. and E. Batchvarova, 1996: A model for the height of the internal boundary layer over an area with an irregular coastline. *Boundary-Layer Meteorology* **78**, 405–413.

Gryning, S-E. and E. Batchvarova, 1999: Regional heat flux over the NOPEX area estimated from the evolution of the mixed layer. *Agric. For. Meteorol.* **98–99**, 159–168.

Gryning, S-E. and E. Batchvarova, 2001: Mixing height in urban areas: will 'rural' parameterisations work? *COST-Action 715 Workshop on Urban Boundary Layer Parameterisations.* Zürich, May 24–25 2001, 99–109.

Gryning, S-E. and E. Batchvarova, 2002: Marine boundary layer and turbulent fluxes over the Baltic Sea: Measurements and modelling. *Boundary-Layer Meteorology* **103**, 29–47.

Gryning, S-E. and E. Batchvarova, 2003: Marine atmospheric boundary layer height estimated from NWP model output. *Int. J. Environ. Pollut.* **20**, 147–153.

Guedalia, D., Allet C. and J. Fontan, 1974: Vertical exchange measurements in the lower troposphere using ThB (Pb-212) and Radon (Rn-212). *J. Appl. Meteorol.* 13 p. 27-39.

Guilloteau, E., 1998: Optimized Computation of Transfer Coefficients in Surface Layer with different Momentum and Heat Roughness Lengths. *Boundary-Layer Meteorology* **87**, 147–160.

Gupta, R.K., T.S. Prasad and D. Vijayan, 2002: Estimation of roughness length and sensible heat flux from WiFS and NOAA AVHRR data. *Adv. Space Res.* **29** (1), 33–38.

Gutman, G., and A. Ignatov, 1998: The derivation of the green vegetation fraction from NOAA/AVHRR data for use in numerical weather prediction models. *Intern. J. Remote Sensing* **19**, 1533–1543.

Häberli, C., 2001: Möglichkeiten und Grenzen einer Klimatologie der Troposphäre und unteren Stratosphäre über den Alpen. (Possibilities and limits of a climatology of the troposphere and lower stratosphere over the Alps) In: *Preprints Deutsch – Österreich – Schweizerische Meteorologen – (DACH–) Tagung*, 79.

Hafner, J., and Kidder, S.Q., 1999: Urban heat island modeling in conjunction with satellite-derived surface/soil parameters. *J. Appl. Meteorol.* **38**, 448–465.

Hall, F.G., J.R. Townshend, and E.T. Engman, 1995: Status of remote sensing algorithms for estimation of land surface state parameters. *Remote Sens. Environ.* **51**, 138–156.

Hamdi, M. and G. Schayes, 2004: Improving the Martilli's urban boundary layer scheme: off-line validation over different urban surfaces. FUMAPEX WP4 report. Université catholique de Louvain, Belgium, 15 p.

Hanna, S. R. and J. C. Chang, 1992: Boundary-layer parameterizations for applied dispersion modeling over urban areas. *Boundary-Layer Meteorology* **58** (3), 229–259.

Hasager, C.B., and Jensen N.O., 1999: Surface-Flux Aggregation in Heterogeneous Terrain. *Quart. J. Roy. Meteorol. Soc.* **125**, 2075–2102.

Hasager, C. B., Nielsen, N. W., H. Soegaard, Boegh, E., Christensen, J.H, Jensen N. O., M. S. Rasmussen, P. Astrup, E. Dellwik, 2002: SAT-MAP-CLIMATE Project Results. *Riso National Laboratory Report, Riso-R-1350(EN),* Roskilde, Denmark, Aug 2002, ISBN-87-550-3079-3, 71 p.

Hasager, C. B. Nielsen, N. W., Boegh, E., Jensen, N. O., Christensen, J. H., Dellwik,E. and Soegaard, H., 2003: Effective roughnesses calculated from satellite-derived land cover maps and hedge information and used in a weather forecasting model. *Boundary-Layer Meteorology* **109**, 227–254.

Heffter, J. L., 1980: Transport layer depth calculations. In *Proc. 2nd Joint Conference on Applications of Air Pollution Modelling*, Amer. Meteorol. Soc., 787–791.

Henderson-Sellers, A., 1980: A simple numerical simulation of urban mixing depths. *J. Appl. Meteorol.* **19**, 215–218.

Heymann, Y., Steenmans, Ch., Croisille, G. and Bossard, M., 1994: *Corine land cover – Technical guide.* Office for Official Publications of the European Communities, Luxembourg.

Holmer, B. and Eliasson, I., 1999: Urban-rural vapour pressure differences and their role in the development of urban heat islands. *Intern. J. Climatol.,* **19**, 989–1009.

Holtslag, A.A.M. and Van Ulden, A.P., 1983: A simple scheme for daytime estimates of the surface fluxes from routine weather data, *J. Appl. Meteorol.* **22**, 517–529.

Holzworth, C.G., 1964: Estimates of mean maximum mixing depths in the continguous United States. *Mon. Wea. Rev.* **92**, 235-242.

Holzworth, C.C., 1967: Mixing depths, wind speeds and air pollution potential for selected locations in the United States. *J. Appl. Meteorol.,* **6**, 1039–1044.

Hong, S-Y. and H.-L. Pan, 1996: Nonlocal boundary layer vertical diffusion in a medium-range forecast model. *Mon. Wea. Rev.* **124**, 2322–2339.

Jensen, N. O., Hasager, C.-B. and Larsen, S.-E., 2002: Aggregation of momentum and temperature roughness based on satellite data. EGS XXVII General Assembly, Nice, France, 21–26 April, *Geophys. Research. Abstracts.*

Joffre, S. M., 1981: The Physics of the Mechanically-Driven Atmospheric Boundary Layer as an Example of Air-Sea Ice Interactions. University of Helsinki, Dept. of Meteorology, *Report No* **20**, 75 p.

Joffre, S. M., 1985: The Structure of the Marine Atmospheric Boundary Layer: A Review from the Point of View of Diffusivity, Transport and Deposition Processes. Finnish Meteorological Inst., Helsinki, *Technical Report No.* **29**, 119 p.

Joffre, S. M., 1988a: Modelling the Dry Deposition Velocity of Highly Soluble Gases to the Sea Surface. *Atmos. Environ.,* **22**(6), 1137–1146.

Joffre, S. M., 1988b: Parameterization and Assessment of Processes Affecting the Long-Range Transport of Airborne Pollutants over the Sea. Finnish Meteorological Inst. *Contribution No.* **1**, 49 p.

Joffre, S. and M. Kangas, 2002: Determination and scaling of the atmospheric boundary layer height under various stability conditions over a rough surface. In: Rotach M., Fisher B., Piringer M. (Eds.), COST Action 715 Workshop on Urban Boundary Layer Parameterisations (Zurich, 24–25 May 2001). Office for Official Publications of the European Communities, EUR 20355, 111–118.

Joffre, S. M., M. Kangas, M. Heikinheimo, and S. A. Kitaigorodskii, 2001: Variability of the stable and unstable atmospheric boundary layer height and its scales over a boreal forest. *Boundary-Layer Meteorology* **99** (3), 429–450.

Kallos, G., 1998: Regional/Mesoscale Models. *Urban air pollution – European aspects* (Part. IV., Chap. 11.), Kluwer Acad. Publ., Dordrecht, Boston, London, 177–196.

Kanda, M., Moriwaki R., Roth M., Oke T. 2002. Area-averaged sensible heat flux and a new method to determine zero plane displacement length over an urban surface using scintillometry. *Boundary-Layer Meteorology* **105** (1), 177–193.

Karppinen, A., J. Kukkonen, G. Nordlund, E. Rantakrans, and I. Valkama, (1998). A dispersion modelling system for urban air pollution. Finnish Meteorological Institute, *Publications on Air Quality* **28**, Helsinki, 58 p.

Karppinen, A., Joffre S.M., Kukkonen J. and P. Bremer, 1999: Evaluation of inversion strengths and mixing heights during extremely stable atmospheric stratification. In: 7th Intern. Conference on Harmonisation within Atmospheric Dispersion Modelling for Regulatory Purposes, Rouen (F), 11–14 Oct. 1999.

Kataoka, T., Yunoki E., Shimizu M., Mori T., Tsukamoto O., Ohhashi Y., Sahashi K., Maitani T., Miyashita K., Fujikawa Y., and Kudo A., 1998: Diurnal variation in radon concentration and mixing-layer depths. *Boundary-Layer Meteorology* **89**, 225–250.

Källstrand, B. and Smedman, A.-S., 1997: A case study of the near-neutral coastal boundary layer growth: aircraft measurements compared with different model estimates. *Boundary-Layer Meteorology* **85**, 1–33.

Kemp, K. and F. Palmgren, 2003: Air Quality Monitoring Programme, Annual Summary for 2002. 36 p. NERI Technical Report Nr. 450.

Kidder, S.Q., and T.H. Vonder Haar, 1995: *Satellite meteorology.* Academic Press, San Diego, 466 pp.

Kitaigorodskii, S. A. and S. M. Joffre, 1988: In search of a simple scaling for the height of the stratified atmospheric boundary layer. *Tellus*, **40A** (5), 419–433.

Klapisz, B., and Weill, A., 1985. Modélisation semi-empirique de la couche limite nocturne. Application au calcul du profil d'indice de refraction. *Ann. Telecomm.* **40**, 672–679.

Klysik, K., 1996: Spatial and seasonal distribution of anthropogenic heat emissions in Lodz, Poland. *Atmos. Environ.* **30**, 3397–3404.

Krajny, E., Osrodka L., Skowronek K., Skubacz M., and Wojtylak M., 2004:Diurnal variation of the mixing-layer height and polonium concentration in the air. Proceedings 9^{rmth} IC "HARMO'04", IMK-IFU, Karlsruhe, Vol. 2, 133–136.

Kuchin, A. and Baklanov, A., 2002: Experimental study of the PBL structure in Arctic conditions and verification of PBL height estimation methods. Proceedings Intern. Conference ENVIROMIS-2002, Tomsk, Russia, 58 p.

Kurbatskii, A.F., 2001: Computational modelling of the turbulent penetrative convection above the urban heat island in a stably stratified environment. *J. Appl. Meteorol.* **40**, 1848–1761.

Lafore, J., Stein, J., Ascencio, N., Bougeault, P., Ducrocq, V., Duron, J., Fischer, C., Héreil, P., Mascart, P., Masson, V., Pinty, J.P., Redelsperger, J.L., Richard, E., and Vila-Guerau de Arellano, J.: 1998: The Meso-NH Atmospheric Simulation System. Part I: Adiabatic Formulation and Control Simulations. *Annales Geophysicae* **16**, 90–109.

Lagouarde, J-P., Moreau P., Solliec F., Groleau D., Irvine M., Bonnefond J-M. and Voogt J., 2002: Etude expérimentale et modélisation des effets directionnels dans l'IRT en zone urbaine. Atelier de Modélisation de l'Atmosphère 2002, Météo France, Toulouse, 17–19 Dec. 2002. 111–114.

Lagouarde, J-P., P. Moreau, M. Irvine, J.-M. Bonnefond, J. Voogt, and Solliec, F. 2004: Airborne experimental measurements of the angular variations in surface temperature over urban areas, case study of Marseille (France). *Rem. Sens. of Environ.*, in press.

Lefebre, F., Lewyckyj, N., Mensink, C., Geyskens, F. and De Ridder, K., 2004 : Calculation of regional-scale benzene concentrations in the Antwerp urban area by means of a coupled traffic flow – atmospheric dispersion model, *Atmos. Environ.* (*submitted*).

Lemonsu, A., C. S. B. Grimmond and V. Masson, 2004: Modelling the surface energy balance of an old Mediterranean city core. *J. Appl. Meteorol.* **43**, 312–327.

Lena, F. and Desiato, F., 1999: Intercomparison of nocturnal mixing height estimate methods for urban air pollution modelling. *Atmos. Environ.* **33** (15), 2385–2393.

Lokoshchenko, M.A., 2002: Long-term Sodar Observations in Moscow and a New Approach to Potential Mixing Determination by Radiosonde Data. *J. Atmos. Oceanic Technol.* **19**, 1151–1162.

Long, N., 2003: Analyses Morphologiques et Aérodynamiques du Tissus Urbain: Application à la Micro-Climatologie de Marseille pendant la Campagne ESCOMPTE. Doctoral thesis (in French), Université des Sciences et Techniques de Lille, France.

Long, N., Mestayer P.G. and Kergomard C., 2003: Urban database analysis for mapping morphology and aerodynamic parameters: the case of St Jerome suburban area, in Marseille during ESCOMPTE. *Proceedings of the Fifth International Conference on Urban Climate*, September 1–5 2003, Lodz, Poland.

Lyra, R., A. Druilhet, B. Benech and C. Bouka Biona, 1992: Dynamics above a dense equatorial rain forest from the surface boundary layer to the free atmosphere. *J. Geophys. Res.*, **97** (12), 953–12, 965.

Mahrt, L., 1981: Modelling the depth of the stable boundary layer. *Boundary-Layer Meteorology* **21**, 3–19.

Mahrt, L., 1982: Momentum balance of gravity flows, *J. Atmos. Sci.* **39**, 2701–2711.

Mahrt L., and Ek M., 1993: Spatial Variability of Turbulent Fluxes and Roughness Lengths in HAPEX-MOBILHY. *Boundary-Layer Meteor.*, **65**, 381–400.

Martilli, A., Clappier, A. and Rotach, M.W., 2002: An urban surface exchange parameterisation for mesoscale models. *Boundary-Layer Meteorology* **104**, 261–304.

Maryon, R.H., and Best, M.J., 1992. *'NAME', 'ATMES' and the boundary layer problem*, UK Met. Office (APR) Turbulence and Diffusion Note, No. 204.

Maryon, R.H., and Buckland, A.T., 1994: Diffusion in a Lagrangian multiple particle model: a sensitivity study. *Atmos. Environ.* **28** (12), 2019–2038.

Maryon, R.H.Ryall, D.B. and Malcolm, A.L., 1999: *The NAME 4 dispersion model: science documentation.* Turbulence and Diffusion Note, No. 262, Met Office, FitzRoy Road, Exeter Devon EX1 3PB, U.K.

Masson, V., 2000: A Physically-based scheme for the urban energy budget in atmospheric models, *Boundary-Layer Meteorology* **94**, 357–397.

Masson, V., G. Pigeon, P. Durand, L. Gomes, C. Lac, A.Butet, 2004a: Observation of an urban plume during CAPITOUL experiment. In: 5th conference on the urban environment. Vancouver, August 2004. Paper 1.2, 4 p.

Masson, V., G. Pigeon, P. Durand, L. Gomes, J. Salmond,J.-P. Lagouarde, J. Voogt, T. Oke, C. Lac, C. Liousse, D. Maro, 2004b: The Canopy and Aerosol Particles Interaction in Toulouse Urban Layer (CAPITOUL) experiment: First results. In: 5th Conference on the urban environment. Vancouver, August 2004. Paper 1.5, 3 p.

Maul P.R., 1980: Atmospheric transport of sulfur compound pollutants. Central Electricity Generating Bureau MID/SSD/80/0026/R. Nottingham, England.

McAneney, K.J., Green, A.E. and Astill, M.S., 1995: Large-aperture Scintillometry: the Homogeneous Case. *Agric. For. Meteorology* **76**, 149–162.

Melas, D., and Kambezidis, H. D., 1992: The depth of the internal boundary layer over an urban area under sea-breeze conditions. *Boundary-Layer Meteorology* **61** (3), 247–264.

Mestayer, P.G., 1998: Urban Scale Models. In: *Urban air pollution - European aspects* (Part. IV, Chap. 11.), Kluwer Acad. Public., Dordrecht, Boston, London, 197–222.

Mestayer, P., R. Almbauer and O. Tchepel, 2003: Urban Field Campaigns, Air quality in cities. N. Moussiopoulos (Ed.) Springer Verlag Berlin Heidelberg (ISBN3-540-00842-x), 51–89.

Mestayer, P. G., Durand P., Augustin P., Bastin S., Bonnefond J. M., Bénech B., Campistron B., Coppalle A.,Delbarre H., Dousset B., Drobinski P., Druilhet A., Fréjafon E., Grimmond C. S. B., Groleau D., Irvine M., Kergomard C., Kermadi S., Lagouarde J-P., Lemonsu A., Lohou F., Long N., Masson V., Moppert C., Noilhan J., Offerle B., Oke T. R., Pigeon G., Puygrenier V., Roberts S., Rosant J. M., Saïd F., Salmond J., Talbaut M. and Voogt J., 2004: The Urban Boundary Layer Field Experiment over Marseille UBL/CLU-ESCOMPTE: Experimental Set-up and First Results. *Boundary-Layer Meteorology* (in print).

Middleton, D. R., N. L. Morrison, G. G. Rooney and D. J. Thomson, 2002: A comparison of dispersion model met pre-processing with urban flux measurements from Birmingham U.K. Presented at the 8th International Conference on Harmonisation within Atmospheric Dispersion Modelling For Regulatory Purposes, Sofia, Bulgaria, 14–17 October 2002, 226 p.

Middleton, D.R., and F.A. Davies, 2004: Evaluation of Dispersion Model Parameters by Dual Doppler Lidars over West London, U.K. Papers presented at 9th Workshop on Harmonisation within Atmospheric Dispersion Modelling for Regulatory Purposes. Garmisch- Partenkirchen, Germany, 1–4 June 2004. (*Submitted to IJEP*).

Miyake, M., 1965: Transformation of the ABL over inhomogeneous surfaces. Sci. Report Contract (NR 307-252) 477(24).

Monteith, J.L., and Unsworth, M.H., 1990: *Principles of Environmental Physics.* 2nd Edition, Arnold.

Mölder, M., and Lindroth A., 1999: Thermal Roughness Length of a Boreal Forest. *Agricultural and Forest Meteorology*, **98–99**, 659–670.

Münkel, C., S. Emeis, W.J. Müller, K. Schäfer, 2002: Observation of aerosol in the mixing layer by a ground-based LIDAR ceilometer. In: K. Schäfer, O. Lado-Bordowsky, A. Comeron, R.H. Picard (Eds.), *Remote Sensing of Clouds and the Atmosphere* VII, Proceedings of SPIE, Bellingham, WA, USA, 9th International Symposium on Remote Sensing, 24–27 Sept. 2002, Agia Pelagia, Crete, Greece, Vol. 4882, 344–352.

Nazaroff, W.W., 1988: *Radon and its decay products in indoor air,* John Wiley & Sons, Inc.

Nazaroff, W. W., 1992: Radon transport from soil to air. *Reviews of Geophysics*, **30(2)**, 137–160.

Neunhäuserer, L, Fay B., Baklanov A., Bjergene N., Kukkonen J., Palau J.L., Perez-Landa G., Rantamaki M., Rasmussen A., Valkama I., 2004: Evaluation and comparison of operational NWP and mesoscale meteorological models for forecasting urban air pollution episodes - Helsinki case study. 9th Intern. Conference on Harmonisation within Atmospheric Dispersion Modelling for Regulatory Purposes, 1–4 June 2004, Garmisch-Partenkirchen, Germany.

Nielsen, N-W. and B.H. Sass, 2000: A lower boundary condition for the mixing length in the CBR turbulence scheme. *HIRLAM Newsletter*, **35**, 128–136.

Nieuwstadt, F.T.M., 1981. The steady state height and resistance laws of the nocturnal boundary layer: theory compared with Cabauw observations. *Boundary-Layer Meteorol.* **20**, 3–17.

Nieuwstadt, F. T. M., 1984a: Some aspects of the turbulent stable boundary layer. *Boundary-Layer Meteorology*, **30**, 31–55.

Nieuwstadt, F. T. M., 1984b: The turbulent structure of the stable, nocturnal boundary layer. *J. Atmos. Sci.* **41**, 2202–2216.

Nieuwstadt, F. T. M. and H. Tennekes, 1981: A rate equation for the nocturnal boundary layer. *J. Atmos. Sci.* **38**, 1418–1428.

Nkemdirim, L.C. (1986). Mixing depths and wind speed in an urban airshed: a note on the limits to a relationship. *Atmos. Environ.* **20**(9), 1829–1830.

Noilhan, J. and Planton, S., 1989: A Simple Parameterization of the Land Surface Processes for Meteorological Models. *Mon. Wea. Rev.* **117**, 536–549.

Offerle, B., Grimmond C.S.B. and Oke T.R., 2003: Parameterization of Net All-Wave Radiation for Urban Areas. *J. Appl. Meteorol.* **42** (8), 1157–1173.

Oke, T.R., 1981. Canyon geometry and the nocturnal heat island: comparison of scale model and field observations. *J. Climatol.,* **1** (3), 1–16.

Oke, T.R., 1987: '*Boundary Layer Climates*, 2nd edition, *Routledge*, London, 435 p.

Oke, T.R., 1988: The Urban Energy Balance. *Progress in Phys. Geog.* **12**, 471–508.

Oke, T.R., Grimmond, C.S.B. and Spronken-Smith, R., 1998: On the confounding role of rural wetness in assessing urban effects on climate. *Preprints of the AMS Second Urban Environment Symposium*, 59–62.

Oke, T.R., Spronken-Smith, R., Jauregui, E. and Grimmond, C.S.B., 1999: Recent energy balance observations in Mexico City. *Atmos. Environ.* **33**, 3919–3930.

Ośródka L, Skubacz K., Skowronek J., Krajny E., Wojtylak M., 2002: Radon concentration in the atmosphere as an indicator of the height of the mixing layer in the region of mining activity. In: Development and Application of Computer Techniques to Environmental Studies IX, WIT Press, Vol. 7, 109–116.

Ośródka, L., Krajny E., Wojtylak M., Skubacz K. and Skowronek J., 2003: Estimation of the height of the mixing layer using polonium concentrations in the atmosphere. An attempt of modelling. In: Air Pollution XI, Series: Advances in Air Pollution, Eds. C.A. Brebbia and F. Patania, WIT Press, Vol. 13, 23–31.

Otte, T. L., A. Lacser, and S. Dupont, 2003: Implementation of an Urban Canopy Parameterization in MM5. *J. Appl. Meteorol.*, to appear.

Panovsky, H.A., and J.A. Dutton, 1984: *Atmospheric Turbulence.* Wiley, NY, 397 p.

Pechinger, U., K. Baumann, M. Langer, E. Polreich, and H. Scheifinger, 2000: Entwicklung eines Modellpaketes für die Berechnung der Ozonbelastung: Abschnitt Meteorologie. Final report to the Austrian Ministry of Science and Transport, Vienna. 124 p.

Penenko, V.V. and A.E. Aloyan, 1974: Numerical method for some meso-meteorological problems with free top of atmospheric mass. *Trudy ZapSibNII*, Novosibirsk, 14, 52–66. (in Russian)

Penenko, V.V. and A.E. Aloyan, 1985: Models and Methods for Environmental Problems. *Nauka*, Novosibirsk, 256 p. (49–55) (in Russian)

Piringer, M., K. Baumann, 1999a: Investigating the mixing height over the city of Vienna, Austria. *International Congress of Biometeorology and Intern. Conf. on Urban Climatology ICB/ICUC*, Sydney, Australia, 8–12 Nov. 1999, Program and Abstract Book, ICUC 16.2, 130 p.

Piringer, M. and K. Baumann, 1999b: Modification of a valley wind system by an urban area – experimental results. *Meteorol. Atmos. Phys.*, **71**, 117–125.

Piringer, M., C. S. B. Grimmond, S. M. Joffre, P. Mestayer, D. R. Middleton, M. W. Rotach, A. Baklanov, K. De Ridder, J. Ferreira, E. Guilloteau, A. Karppinen, A. Martilli, V. Masson, and M. Tombrou, 2002: Investigating the Surface Energy Balance in Urban Areas – Recent Advances and Future Needs. *Water, Air and Soil Poll.*: Focus **2**, 1–16.

Porstendörfer, J., Butterweck, G. & Reineking, A., 1991: Diurnal variation of the concentrations of radon and its shorts-lived daughters in the atmosphere near the ground. *Atmos. Environ.*, **25A(3/4)**, 709–713.

Railo, M., Editor (1997). *Urban Episodes. Problems and Action Plans*: Paris, Berlin, Helsinki, Turku. *IImansuojelu.* Helsinki, Special Issue. **6**, 29 pp.

Rantamäki, M., Pohjola, M., Kukkonen J. and Karppinen, A., 2003: Evaluation of the HIRLAM model against meteorological data during an air pollution episode in southern Finland 27–29 December 1995. In: Sokhi, R.S. and Brechler, J. (Eds.), Proceedings of the Fourth International Conference on Urban Air Quality - Measurement, Modelling and Management, Charles University, Prague, Czech Republic, 25–27 March 2003. University of Hertfordshire, Hatfield, United Kingdom, 420–423.

Rasmussen, A., J.H. Sørensen and Nielsen, N.W., 1997: Validation of Mixing Height Determined from Vertical Profiles of Wind and Temperature from the DMI-HIRLAM NWP Model in Comparison with Radiosoundings. EURASAP Workshop Proc. on the determination of the mixing height – current progress and problems,Risø-R-997(EN), 101–105.

Rasmussen, A., J.H. Sørensen, N.W. Nielsen and B. Amstrup, 1999: Uncertainty of Meteorological Parameters from DMI-HIRLAM. *Report RODOS* (WG2) TN(99)12.

Räsänen, J., J. Lönnqvist and A.K. Piironen, 2000: Urban boundary layer measurements with a commercial ceilometer. Proc. 3rd Symp. on Urban Environment, Aug. 15–18, 2000, Davis CA, Amer. Meteorol. Soc., Boston, 34–35.

Reitebuch, O. and S. Emeis, 1998: SODAR-measurements for atmospheric research and environmental monitoring. *Meteorologische Z.*, N.F., **7**, 11–14.

Remtech, 1994: Doppler Sodar Operating Manual. Technical Report DT94/003.

Reuter, H., 1970: Die Ausbreitungsbedingungen von Luftverunreinigungen in Abhängigkeit von meteorologischen Parametern. *Arch. Met. Geoph. Biokl.* A, **19**, 173–186.

Roberts, S.M., Oke, T.R., Voogt, J.A., Grimmond, C.S.B., and Lemonsu, A., 2003: Energy Storage in a European City Center'. In CD proceedings, *5th International Conference on Urban Climate*, Lodz, Poland, 1–5 Sept. 2003, O.12.1, 4 p.

Roberts, S.M., Oke T.R., Lemonsu A., Grimmond C.S.B., Jackson P., 2004: Sensitivity of surface atmosphere energy exchanges within urban areas derived from simulations. *84th AMS Annual Meeting, Symposium on Planning, Nowcasting, and Forecasting in the Urban Zone.* Seattle, January 10–16 2004.

Rogers, R.R., M.-F. Lamoureux, L. Bissonnette and R.M. Peters, 1997: Quantitative interpretation of laser ceilometer intensity profiles . *J. Atmos. Ocean. Tech.*, **14**, 396–411.

Rossby, C.G. and Montgomery R.B., 1935: The layer of frictional influence in wind and ocean currents. *Pap. Phys. Oceanogr. Meteorol.*, **3**(3), 1–101.

Rotach, M.W., 2001: Simulation of urban-scale dispersion using a Lagrangian stochastic dispersion model, *Boundary-Layer Meteorol.,* **99**, 379–410.

Rotach, M.W., Fisher, B. and Piringer, M., 2002: COST 715 Workshop on Urban Boundary Layer Parameterizations. *Bull. Amer. Meteorol. Soc.*, **83** (10), 1501–1504.

Rotach, M.W., Gryning. S-.E., Batchvarova, E., Christen, A. and Vogt, R., 2004a: Pollutant dispersion close to an urban surface - the BUBBLE tracer experiment. *Metorol. Atm. Phys.* **87** (1–3), 39–56.

Rotach, M.W., Vogt R., Bernhofer C., Batchvarova E., Christen A., Clappier A., Feddersen B., Gryning S-E., Martucci G., Mayer H., Mitev V., Oke T.R, Parlow E., Richner H., Roth M., Roulet YA., Ruffieux D., Salmond J., Schatzmann M., and Voogt J., 2004b: BUBBLE – a Major Effort in Urban Boundary Layer Meteorology. Accepted to *Theoretical and Applied Climatology.*

Roth, M. and Oke, T.R., 1995: Relative efficiencies of turbulent transfer of heat, mass and momentum over a patchy urban surface, *J. Atmos. Sci.* **52**, 1864–1874.

Roth, M., T.R. Oke, W.J. Emery., 1989: Satellite-derived urban heat islands from three coastal cities and the utilization of such data in urban climatology. *Intern. J. Remote Sensing*, **10**, 1699–1720.

Roulet, Y-A., 2002: Integration of urban effects in a mesoscale dynamical model over the region of Basel (Switzerland) as a part of the BUBBLE experiment. *Preprints 4th Symposium on the Urban Environment*, 20–24 May 2002 in Norfolk, VA, 13–14.

Said, F., B. Campistron, A. Coppalle, A. Dabas, Ph. Drobinsky, E. Fréjafon, E. Gizard, A. Mériaux and P. Mestayer, 2001: Influence of sea breeze and relief on the mixing height during ESCOMPTE in the Marseille area. *COST-715 Workshop 'Mixing heights and inversions in urban areas'*, Meteo-France, Toulouse, 3–5.10.2001.

Sailor, D.J. and Fan H., 2002: Modeling the diurnal variability of effective albedo for cities. *Atmos. Environ.* **36** (4), 713–725.

Sass, B.H., Nielsen, N.W., Jørgensen, J.U., Amstrup, B., and Kmit, M., 2000: The operational HIRLAM system. *DMI Technical report* 00–26. `http://www.dmi.dk/f+u/publikation/tekrap/2000/Tr00-26.pdf`.

Schlünzen, H. and J.J. Katzfey, 2003: Relevance of sub-grid-scale land-use effects for mesoscale models. *Tellus* **55A** (3), 232–246.

Schmid, H.P., 1994: Source areas for scalars and scalar fluxes, *Boundary-Layer Meteorol.* **67**, 293–318.

Schmid, H.P., 1997: Experimental design for flux measurements: matching scales of observations and fluxes. *Agriculture and Forest Meteorology* **87**, 179–200.

Scire J.S., Robe F.R., Fernau M.E., and Yamartino R.J., 1999, A User's Guide for the CALMET meteorological model (version 5.0) Earth Tech Inc., Internal Report.

Scire, J.S., Yamartino, R.J., and Fernau, M.E., 2000: A user's guide for the CALMET meteorological model. Earth Tech, Concord, MA., `http://www.src.com`.

Seibert, P., Beyrich F., Gryning S-E., Joffre S., Rasmussen A. and Ph. Tercier, 1998. Mixing height determination for dispersion modelling. Report of Working Group 2. In: "Harmonization in the Preprocessing of meteorological data for atmospheric dispersion models", COST Action 710, CEC Publication EUR 18195, 145–265.

Seibert, P., Beyrich, F., Gryning, S-E., Joffre, S., Rasmussen, A. and Tercier, Ph., 2000: Review and Intercomparison of Operational Methods for the Determination of the Mixing Height. *Atmos. Environ.* **34** (7), 1001–1027.

Sellers, P.J., S.I. Rasool, and H.-J. Bolle, 1990: A review of satellite data algorithms for studies of the land surface. *Bulletin of the American Meteorological Society*, **71**, 1429–1447.

Smith, F. B., 1990: "Atmospheric Structure" unpublished note presented at Air Pollution Modelling for Environmental Impact Assessment, International Centre for Theoretical Physics, Trieste, June 1990.

Sørensen, J.H., Rasmussen, A. and Svensmark, H., 1996: Forecast of Atmospheric Boundary-Layer Height for ETEX Real-time Dispersion Modelling. *Phys. Chem. Earth*, **21** (5–6), 435–439.

Spronken-Smith, R.A., 1998: Comparison of summer and wintertime energy fluxes over a suburban neighbourhood. *Preprints of the Second Urban Environment Symposium*, Christchurch, New Zealand, American Meteorological Society, 243–246.

Spronken-Smith, R.A., 2002: Comparison of summer- and winter-time suburban energy fluxes in Christchurch, New Zealand. *Intern. J. Climatol.* **22** (8), 979–992.

Steyn, D.G., M. Baldi ja R.M. Hoff, 1999: The detection of mixed layer depth and entrainment zone thickness from lidar backscatter profiles. *J. Atmos. Ocean. Technol.* **16**, 953–959.

Stull, R.B., 1988: *An Introduction to Boundary layer Meteorology.* Amospheric Sciences Library, Kluwer Academic Publ., Dordrecht, The Netherlands, 666 p.

Stull, R.B., 1991: Static Stability – An Update. *Bull. Amer. Meteorol. Soc.* **72**, 1521–1529.

Summers, P. W., 1965: An urban heat island model: its role in air pollution problems with applications to Montreal. *First Canadian Conf. on Micrometeorology.* Toronto, CMOS, 22 p.

Sutton, O.G., 1953: *Micrometeorology.* McGraw-Hill, 333 p.

Taha, H., 1998: Modifying a Mesoscale Meteorological Model to Better Incorporate Urban Heat Storage: A Bulk-Parameterization Approach. *J. Appl. Meteor.* **38**, 466–473.

Taha, H. and Bornstein, R.: 2000, 'Urbanization of meteorological models and implications on simulated heat islands and air quality', In: R. J. de Dear, J. D. Kalma, T. R. Oke and A. Auliciems, Eds.: *Biometeorology and Urban Climatology at the Turn of the Millenium.* Selected Papers from the Conference ICB-ICUC '99, Sydney, Australia, 8–12 Nov. 1999, 431–435.

Tampieri, F. and Trombetti F., 1981: Summer Daily Circulation in the Po Valley, Italy. *Geophys. Astrophys. Fluid Dynamics*, **17**, 97–112.

Taylor, G.I., 1931: Effects of variation in density on the stability of superimposed streams of fluids, *Proc. R. Soc. (London), Ser. A*, **132**, 499–523.

Taylor, P., 1987: Comments and further analysis on the effective roughness length for use in numerical 3D models. *Boundary-Layer Metorol.*, **39**, 403–418.

Tennekes, H., 1973: a model for the dynamics of the inversion above a convective boundary layer. *J. Atmos Sci.* **30**, 550–567.

Tennekes, H. and A. G. M. Driedonks: 1981: Basic entrainment equations for the atmospheric boundary layer. *Boundary-Layer Meteorol.* **20** (4), 515–531.

Thomson, D.J., 2000: The Met Input Module ADMS 3 Documentation Paper Number P/05/01J/00. The Met Office, FitzRoy Road, Exeter Devon EX1 3PB, U.K.

Troen, I. and L. Mahrt, 1986: A simple model for the atmospheric boundary layer: Sensitivity to surface evaporation. *Boundary-Layer Meteorol.* **37**, 129–148.

Van Ulden, A. P. and Holtslag A. A. M., 1985: Estimation of Atmospheric Boundary Layer Parameters for Diffusion Applications. *J. Climate Appl. Meteorol.* **24**, 1196–1207.

Vázquez, D.P., Reyes, F.J.O. and Arboledas, L.A., 1997: A comparative study of algorithms for estimating land surface temperature from AVHRR Data. *Remote Sens. Environ.* **62**, 215-222.

Venkatram A., 1980: Estimating the Monin-Obukhov length in the stable boundary layer for dispersion calculations, *Boundary-Layer Meteorol.* **18**, 481.

Venkatram, A., 1986: An examination of methods to estimate the height of the coastal internal boundary layer. *Boundary-Layer Meteor.* **36**, 149–156.

Vogelezang, D.H.P. and Holtslag, A.A.M., 1996: Evolution and model impacts of the alternative boundary layer formulations. *Boundary-Layer Meteorol.* **81**, 245-269.

Vogt, S. and G. Jaubert, 2004: Foehn in the Rhine valley as seen by a wind-profiler-RASS system and comparison with the nonhydrostatic model MESO-NH. *Meteorol. Z.,* **13**, 165–174.

Voogt, J.A. and Grimmond, C.S.B., 2000: Modeling surface sensible heat flux using surface radiative temperatures in a simple urban area. *J. Appl. Meteor.* **39**, 1679–1699.

Voogt, JA, and Oke T.R., 1997: Complete surface temperatures. *J. Appl. Meteorol.* **36** (9), 1117–1132.

Voogt, J.A., and Oke, T.R., 2003: Thermal remote sensing of urban climates. *Remote Sens. Environ.* **86**, 370–384.

Walczewski, J., 1997: Some aspects of estimation of mixing height using vertical sodar records. EURASAP Workshop Proc., 1–3 Oct. 1997, Riso Nat. Lab., Roskilde, Denmark, 91–94.

Walczewski, J, 1998: Sodar data as a basis for an empirical model of diurnal and annual variability of mean mixing height. *Proc., 9*[th] *Intern. Symp. On Acoustic Remote Sensing – ISARS'98*, Destrreich. Beitraege zu Meteorologie und Geophys., No 17, Vienna 1998, 235–238.

Walczewski, J., Bielak A. and Kaszowski W., 1999: Aerosol layers in the atmosphere observed by vertical-sounding lidar as an indication of mixing layer height – comparison with acoustic sounding data. *Optica Applicata*, Vol. XXIX, No. 4, 449–459.

Walczewski, J. and Orkisz K., 1994: Application of correlation spectrometer for determination of $S0_2$ mixing height in the atmosphere in the convective conditions. (In Polish, abstract in English). Reports of the Institute of Meteorology and Water Management, Vol. 17(38), No. 3, 71–80.

Walmsley, J.L., 1989: Internal boundary-layer height formulae – a comparison with atmospheric data. *Boundary-Layer Meteor.*, **47**, 251–262.

Wittich, K.-P., and O. Hansing, 1995: Area-averaged vegetative cover fraction estimated from satellite data. *Intern. J. Biometeorol.* **38**, 209–215.

Wotawa, G., A. Stohl, H. Kromp-Kolb, 1996: Parameterization of the planetary boundary layer over Europe: A data comparsion between the observation-based OML preprocessor and ECMWF model data. *Contrib. Atmos. Phys.* **69**, 273–284.

Wright, S.D., Elliot, L., Ingham, D.B. and Hewson, M.J.C., 1998: The adaptation of the atmospheric boundary layer to a change in surface roughness. *Boundary-Layer Meteorol.* **89**, 175–195

Xue, M., K. K. Droegemeier, and V. Wong, 2000: The Advanced Regional Prediction System (ARPS) - A multiscale nonhydrostatic atmospheric simulation and prediction tool. Part I: Model dynamics and verification. *Meteor. Atmos. Physics.*, **75**, 161–193.

Xue, M., K. K. Droegemeier, V. Wong, A. Shapiro, K. Brewster, F. Carr, D. Weber, Y. Liu, and D.-H. Wang, 2001: The Advanced Regional Prediction System (ARPS) - A multiscale nonhydrostatic atmospheric simulation and prediction tool. Part II: Model physics and applications. *Meteor. Atmos. Physics.* **76**, 134–165.

Yang, L., 2000: Integration of a numerical model and remotely sensed data to study urban/rural land surface climate processes. *Computers and Geosciences*, **26**, 451–468.

Zhang, X., Y. Aono, and Monji, N., 1998: Spatial variability of urban surface heat fluxes estimated from Landsat TM data under summer and winter conditions. *J. Agric. Meteorol.* **54**, 1–11.

Zhang, K., Mao, H., Civerolo, K., Berman, S., Ku, Y.-Y., Rao, S. T., Doddridge, B., Philbrick, C. R., Clark, R., 2001: Numerical investigation of boundary layer evolution and nocturnal low-level jets: local versus non-local PBL schemes. *Environ. Fluid Mechanics*, **1**, 171–208.

Zilitinkevich S.S., 1970: Dynamics of the Atmospheric Boundary Layer. Godrometizdat, Leningrad, USSR, (in Russian).

Zilitinkevich, S.S., 1972: On the determination of the height of the Ekman boundary layer. *Boundary-Layer Meteorol.* **3**, 141–145.

Zilitinkevich, S.S., 1989:Velocity profiles, the resistance law and the dissipation rate of mean flow kinetic energy in a neutrally and stably stratified planetary boundary layer. *Boundary-Layer Meteorol.* **46**, 367–387.

Zilitinkevich, S., 2002: Third-order transport due to internal waves and non-local turbulence in the stably stratified surface layer. *Quart. J. Roy. Meteorol. Soc.* **128**, 913–925.

Zilitinkevich, S. and A. Baklanov, 2002: Calculation of the height of stable boundary layers in practical applications. *Boundary-Layer Meteorol.* **105** (3), 389–409.

Zilitinkevich, S., A. Baklanov (2004) A simple model of turbulent mixing and wind profile within urban canopy. *Manuscript to be submitted.*

Zilitinkevich, S., A. Baklanov, J. Rost, A.-S. Smedman, V. Lykosov and P. Calanca, 2002: Diagnostic and prognostic equations for the depth of the stably stratified Ekman boundary layer. *Quart. J. Roy. Meteorol. Soc.* **128**, 25–46.

Zilitinkevich, S.S., and Deardorff, J.W., 1974: Similarity theory for the planetary boundary layer of time-dependent height. *J. Atmos. Sci.*, **31**, 1449–1452.

Zilitinkevich, S. S. and Esau, I. N., 2003: The effect of baroclinicity on the equilibrium depth of neutral and stable planetary boundary layers. *Quart, J. Roy. Met. Soc.* **129**, 3339–3356.

Zilitinkevich, S. and Mironov, D., 1996: A multi-limit formulation for the equilibrium depth of a stably stratified boundary layer. *Boundary-Layer Meteorology* **81** (3–4), 325–351.

Ziomas, I.C., 1998: The Mediterranean campaign of photochemical tracers-transport and chemical evolution (MED-CAPHOT-TRACE): an outline. *Atmos. Environ.* **32**, 2045–2053.

Zwally, H.J., R. Schutz, S. Palm, W. Hart, D. Hlavka, J. Spinhirne, and E. Welton, 2003: *GLAS/ICESat L1B Global Backscatter Data V001* (November 2003). Boulder, CO: National Snow and Ice Data Center. Digital media.

THE URBAN SURFACE ENERGY BUDGET AND MIXING HEIGHT IN EUROPEAN CITIES: DATA, MODELS AND CHALLENGES FOR URBAN METEOROLOGY AND AIR QUALITY

**Final Report of Working Group 2
of COST-715 Action**

EDITORS: Martin Piringer and Sylvain Joffre

Lead Authors:
Alexander Baklanov, Jerzy Burzynski,
Andreas Christen, Marco
Deserti, Koen De Ridder, Stefan
Emeis, Sylvain Joffre, Ari
Karppinen, Patrice Mestayer,
Douglas Middleton, Martin Piringer,
and Maria Tombrou

Contributions by:
Kathrin Baumann-Stanzer, Giovanni
Bonafè, Angela Dandou,
Sylvain Dupont, Nicola Ellis, Sue
Grimmond, Emmanuel
Guilloteau, Alberto Martilli, Valéry
Masson, Tim Oke, Victor
Prior, Mathias Rotach, and Roland
Vogt

cost